

© 2015 Subha Mukherjee

MECHANISTIC AND SYNTHETIC STUDIES ON THE PROCHLOROSIN AND
CYTOLYSIN FAMILIES OF LANTHIPEPTIDES

BY

SUBHA MUKHERJEE

DISSERTATION

Submitted in partial fulfillment of the requirements
for the degree of Doctor of Philosophy in Chemistry
in the Graduate College of the
University of Illinois at Urbana-Champaign, 2015

Urbana, Illinois

Doctoral Committee:

Professor Wilfred A. van der Donk, Chair

Professor Martin D. Burke

Professor William W. Metcalf

Professor Huimin Zhao

ABSTRACT

Peptides are an attractive class of therapeutics, occupying a niche between small molecules and biologics. Research in the van der Donk lab focuses on lanthipeptides, a class of ribosomally synthesized and post-translationally modified peptides (RiPPs) that commonly feature antibacterial activity and contain the characteristic thioether residues lanthionine (Lan) and methyllanthionine (MeLan). Installation of thioether crosslinks in lanthipeptide biosynthesis is carried out by designated synthetases and involves dehydration of Ser/Thr residues and cyclization via Michael-type addition.

The remarkably broad substrate scope of the synthetase ProcM inspired us to explore its mechanism in detail (chapter 2). My studies on ProcM revealed the directionality of dehydration, the order of cyclization, and that, despite the impressive substrate scope, none of the cyclizations are non-enzymatic. In collaboration, we established the irreversibility of the Michael-type addition and proposed that the topology of the thioether rings is under kinetic control. Solid phase peptide synthesis (SPPS) was used to generate the substrates to study ProcM, and is also a flexible tool to access non-native lanthipeptide analogues. Interestingly, a lanthipeptide, cytolysin S (CylL_S"), exhibited cytolytic activity in synergy with cytolysin L (CylL_L"). Given that a thioether crosslink in CylL_S" has an unusual LL-stereochemistry, the synthesis of a diastereomer of CylL_S" with the more common DL-stereochemistry was achieved by SPPS (chapter 3). We probed whether the cytolytic activity depended on the LL-stereochemistry observed in CylL_S". Surprisingly, the unusual LL-stereochemistry was found to be important for the antibacterial activity, but not necessary for the hemolytic activity of CylL_S". I have also synthesized another hydrophobic lanthipeptide analogue, the portion of microbisporicin that contains the A and B ring (chapter 4). We established that this motif is not recognized by the

halogenase MibH, and that the C terminus of microbisporicin is necessary for the chlorination by MibH.

During my graduate studies, I had the opportunity to collaborate in a different area of research in our laboratory, the phosphonates. My efforts in the syntheses of various substrates and intermediates were instrumental in elucidating the biosynthetic pathways of dehydrophos, fosfazinomycin, and rhizocticin (chapter 5).

For my wife and my parents

ACKNOWLEDGEMENT

My research towards my dissertation would not have been possible without the help of many individuals, to whom I am greatly indebted. First, I would like to thank Professor Wilfred van der Donk for accepting me as a 2010 graduate student in his laboratory. I learned immensely under his guidance on aspects of critical thinking, analyses, writing, and presentation skills. Over the years, he has encouraged me in my projects, and polished me into a better scientist.

During my early years of graduate studies, several senior members in the laboratory have trained me – Dr. Noah Bindman and Dr. Patrick Knerr primed me with the synthesis techniques used in our laboratory. Dr. Yanshiang Shi, Dr. Ayse Okesli, Dr. Gabrielle Thibodeaux, and Dr. John Hung patiently answered all my questions regarding microbiology and biochemistry experiments. I am also thankful to Dr. Rebecca Splain, Dr. Lindsay Repka, Dr. Christopher Thibodeaux, Dr. Mark Walker, and Manuel Ortega for proof reading my various write-ups during my stay at Illinois. I thank Dr. Yi Yu, Dr. Despina Bougioukou, Dr. Jiangtao Gao, and Dr. Svetlana Borisova for their fantastic collaborations. I would also thank Xiling Zhao, Dr. Weixin Tang, Dr. Neha Garg, Chantal Gonzalo, Kenton Hetrick, Dr. Xiao Yang, and Dr. Zedu Huang, for valuable discussions. I thank all the van der land members for their efforts in maintaining this large laboratory as a smooth running, productive, and fun-filled workplace.

I thank my committee members Professor Martin Burke, Professor Huimin Zhao, and Professor William Metcalf for offering critical comments and constructive criticism during my preliminary examination and original research proposal, which have helped me tremendously in getting better at work.

I would also thank Dr. Alexander Ulanov of the metabolomics center for assisting me with the GC/MS experiments; Dr. Dean Olson and Dr. Tracie Hubert for their assistance in using the NMR instruments; Dr. Furong Sun, Dr. Haijun Yao, and Dr. Kevin Tucker for their support in using the mass spectrometry facility. I would thank NIH and HHMI for funding.

No words can express my feeling of thankfulness and love for my wife, Priya, who understands me and always motivates me to dream big. She has been there through many ups and downs in my life, and has been a part of my journey at Chabana. I would like to thank my parents for their unconditional love and support throughout my formative years. I thank them for instilling the values of ethics and integrity in my life, and helping me to grow up to be an honest person.

TABLE OF CONTENTS

LIST OF FIGURES	x
LIST OF SCHEMES.....	xiii
CHAPTER 1: PEPTIDE THERAPEUTICS AND LANTHIPEPTIDES	1
1.1. PEPTIDES AS THERAPEUTICS	1
1.1.1. Advantages of Peptide-Therapeutics	1
1.1.2. Overcoming Challenges of Peptide Therapeutics	3
1.1.3. Notable Peptide Therapeutics	4
1.2. ANTIMICROBIAL DRUGS: NEED OF THE HOUR.....	6
1.2.1. Mechanism of Antimicrobial Resistance.....	6
1.2.2. <i>ESKAPE</i> Pathogens: Current Threats by Resistant Microbes	7
1.2.3. Peptides as Antimicrobial Agents.....	8
1.3. RIBOSOMALLY SYNTHESIZED AND POST-TRANSLATIONALLY MODIFIED NATURAL PRODUCTS	10
1.4. LANTHIPEPTIDES	14
1.4.1. Lanthipeptide Biosynthesis.....	14
1.4.2. Modes of Action of Lanthipeptides	19
1.5. CONCLUSION AND OUTLOOK	21
1.6. REFERENCES	22
CHAPTER 2: MECHANISTIC INVESTIGATION OF THE SUBSTRATE-TOLERANT LANTHIPEPTIDE SYNTHETASE PROCM.....	30
2.1. INTRODUCTION.....	30
2.2. RESULTS AND DISCUSSION	33
2.2.1. Choice of Substrates to Study ProcM.....	33
2.2.2. ProcM Dehydrates the ProcA2.8 Precursor Peptide in C-to-N-Terminal Fashion	34
2.2.3. ProcM Dehydrates ProcA3.3 Precursor Peptide in C-to-N-Terminal Fashion	40
2.2.4. Directionality of Cyclization by ProcM	44
2.2.5. Substrate Design to Probe Non-Enzymatic Cyclization in Prochlorosin Maturation ..	47
2.2.6. Efficient Cyclization of ProcA2.8 Requires ProcM	50
2.2.7. Ring Formation in ProcA3.3 Requires ProcM	52
2.2.8. Reversibility of Thioether Ring Formation: Studies on D–H Exchange.....	56
2.2.9. ProcM-Cyclized ProcA3.3 Undergoes Enzymatic D–H Exchange	57
2.2.10. D–H Exchange Is Not Observed in ProcA2.8 Substrates with Ser Mutated to Thr..	59
2.2.11. Exchange in ProcA3.3 Involves the B-Ring.....	60
2.2.12. Mutations of Three Zn(II) Binding Cys Ligands in ProcM	64
2.2.13. Differences in Enzymatic Activity between WT-ProcM and ProcM-C971H.....	65
2.2.14. Product Distribution in ProcA3.3 Modified by WT-ProcM or ProcM-C971H	69
2.2.15. Thioether Formation in ProcA3.3 Is Not Reversible.....	72
2.2.16. Oligomerization State of ProcM.....	75
2.3. CONCLUSIONS AND OUTLOOK	78
2.4. EXPERIMENTAL	80
2.4.1. Characterization of Small Molecules and Peptides	80
2.4.2. Small Molecule Synthesis: Materials and Methods	81
2.4.3. Synthesis of Compound 2.6 to Introduce C-Terminal Alkyne.....	82
2.4.4. Scheme for the Synthesis of Azide Building Block 2.8	83

2.4.5. Scheme for the Synthesis of Azide Building Block 2.9	83
2.4.6. Synthesis of Benzothiazolyl-Ethyl Disulfide 2.37	83
2.4.7. Scheme for Synthesis of Cys(<i>o</i> -NO ₂ Bn) Building Blocks 2.38 and 2.39 for SPPS....	84
2.4.8. Scheme for Synthesis of [2,3,3- ² H]-Ser Building Block 2.40 for SPPS	84
2.4.9. Scheme for Synthesis of Protected [2,3- ² H]-Thr Building Block 2.41 for SPPS.....	84
2.4.10. Solid Phase Peptide Synthesis (SPPS)	87
2.4.11. Generation of the Alkyne Modified ProcA3.2 Leader Peptide	96
2.4.12. Iodoacetamide Capping of the Free Cys Generated During EPL.....	97
2.4.13. Generation of ProcA2.8 Leader-AlaAla-MESNa Thioester	98
2.4.14. Copper Catalyzed Azide–Alkyne Cycloaddition (CuAAC) - ‘Click Chemistry’	99
2.4.15. Peptides Generated by Native Chemical Ligation.....	105
2.4.16. Purification of ProcM	106
2.4.17. Purification of ProcM in D ₂ O Containing Buffer.....	107
2.4.18. General Procedure for Heterologous Expression of Precursor Peptides	107
2.4.19. General Procedure for Selective Thioether Formation by ProcM.....	111
2.4.20. General Procedure for Probing Enzymatic vs. Non-Enzymatic Cyclization	112
2.4.21. General Procedure for the Incorporation of Deuterium in the ProcM Product	112
2.4.22. General Procedure for D–H Exchange Assays.....	113
2.4.23. General Procedure for Trapping Partially Dehydrated Peptides Containing Deuterium Labeled Ser/Thr to Probe Directionality of Dehydration	113
2.4.24. General Procedure for Trapping Partially Cyclized Species to Probe Directionality of Cyclization.....	114
2.4.25. Enzymatic Modification of Peptide 2.18 by ProcM-C971H.....	114
2.4.26. UV Mediated Deprotection of Cys14 in Peptide 2.33 and Enzymatic Cyclization by WT ProcM.....	115
2.4.27. Semi-Synthetically Generated Intermediates of ProcA3.3 with one Thioether Crosslink.....	115
2.4.28. Molecular Cloning of His ₆ -ProcA3.2 Leader-Intein-CBD.....	116
2.4.29. Mutagenesis of ProcA Genes	116
2.5. REFERENCES	117
CHAPTER 3: TOTAL SYNTHESIS OF LANTHIPEPTIDES - STUDIES WITH CYTOLYSIN	120
3.1. INTRODUCTION.....	120
3.2. RESULTS AND DISCUSSION	124
3.2.1. Choice of Cytolysin Variant to Study the Effect of the Unusual LL-Stereochemistry on Bioactivity	124
3.2.2. Bioactivity of CylL _S [”] -Dhb2Dha and WT-CylL _S [”] is Similar when Both have the Same Thioether Stereochemistry.....	127
3.2.3. Heterologous Expression of Cytolysin S with Cys at Position 2 to Assess the Elimination Chemistry.....	130
3.2.4. Total Synthesis of CylL _S [”] -Dhb2Dha with Non-Native DL-MeLan A-Ring and DL-Lan B-Ring	133
3.2.5. Total Synthesis of CylL _S [”] -Dhb2Dha with LL-MeLan A-Ring and DL-Lan B-Ring as a Control for Synthetic Fidelity.....	136
3.2.6. Evaluation of Antimicrobial Activities of Variants of Cytolysin S	136
3.2.7. Evaluation of Hemolytic Activities of Variants of Cytolysin S	137

3.3. CONCLUSION AND OUTLOOK	138
3.4. EXPERIMENTAL	140
3.4.1. Materials and General Methods.....	140
3.4.2. Synthesis of Fmoc-PheDhb-OH Building Block	141
3.4.3. Synthesis of LL-MeLan(Allyl/Alloc) Building Block	142
3.4.4. Synthesis of DL-MeLan(Allyl/Alloc) Building Block.....	147
3.4.5. General Procedure for Solid Phase Peptide Synthesis (SPPS).....	149
3.4.6. SPPS of CylL _S -Dhb2Cys with DL-MeLan (A-Ring) and DL-Lan (B-Ring).....	151
3.4.7. Cys to Dha Elimination Reaction on Synthesized CylL _S -T2C (DL-A Ring, DL-B Ring)	153
3.4.8. Mutagenesis of Cytolysin S Gene	154
3.4.9. General Procedure for Overexpression of Cytolysin Variants	155
3.5. REFERENCES	156
CHAPTER 4. SYNTHESIS OF MICROBISPORICIN ANALOGUES	159
4.1. INTRODUCTION.....	159
4.2. RESULTS AND DISCUSSION	163
4.2.1. Synthesis of the A and B Rings of Microbisporicin.....	163
4.2.2. Synthesis of Microbisporicin Tetrapeptide with Glutamylated Ser3 and its Analogue	166
4.3. CONCLUSION AND OUTLOOK	168
4.4. EXPERIMENTAL	169
4.4.1. Synthesis of Boc-ValDhb-OH Building Block	169
4.4.2. Synthesis of Fmoc-ValDhb-OH Building Block.....	171
4.4.3. SPPS of the Deschloro-Microbisporicin A and B Rings with Cys5	172
4.4.4. Synthesis of Peptide 4.1 by Cys to Dha Conversion in Peptide 4.6	174
4.4.5. SPPS of Microbisporicin Tetrapeptide with Ester-Linked Glutamylated Ser3.....	175
4.4.6. SPPS of Microbisporicin Tetrapeptide with Amide-linked Glutamylated 2,3-Diamino Propanoic Acid	176
4.5. REFERENCES	177
CHAPTER 5. SYNTHESIS TOWARDS UNDERSTANDING OF THE BIOSYNTHETIC PATHWAYS OF DEHYDROPHOS, FOSFAZINOMYCIN, AND RHIZOCTICIN	178
5.1. INTRODUCTION.....	178
5.1.1. Biosynthesis of Dehydrophos.....	180
5.2. RESULTS AND DISCUSSIONS.....	184
5.2.1. Dehydrophos.....	184
5.2.1.1. PLP-Dependent Activity of DhpD and DhpH.....	184
5.2.1.2. tRNA-Dependent Activity of DhpH	185
5.2.1.3. Fe(II)/ α -KG/O ₂ -Dependent Activity of DhpJ	188
5.2.1.4. Peptidyl-Transferase Activity of DhpK	189
5.2.2. Fosfazinomycin	191
5.2.3. Rhizocticin.....	193
5.3. CONCLUSION AND OUTLOOK	195
5.4. EXPERIMENTAL	196
5.4.1. General Procedure	196
5.4.2. Small Molecule Synthesis	197
5.5. REFERENCES	210

LIST OF FIGURES

FIGURE	PAGE
Figure 1.1. Distribution of FDA approved drugs of various therapeutic modalities-----	2
Figure 1.2. Structures of a few selected successful peptide drugs-----	5
Figure 1.3. Size distribution of approved peptide therapeutics-----	6
Figure 1.4. Structures of selected potent antibacterial peptides-----	10
Figure 1.5. Post Ribosomal Peptide Synthesis pathway-----	12
Figure 1.6. Structures of various RiPPs showing diverse modifications-----	13
Figure 1.7. Lanthipeptide biosynthesis and common post-translational modifications-----	15
Figure 1.8. Bubble-diagrams of various lanthipeptides-----	16
Figure 1.9. Different classes of lanthipeptide biosynthetic machinery-----	18
Figure 1.10. Different activation steps of Ser/Thr catalyzed by class I and II lanthipeptide synthetases-----	18
Figure 2.1. Sequences of 30 precursor peptides encoded by the genome of <i>Prochlorococcus</i> MIT 9313-----	31
Figure 2.2. Structures of several representative prochlorosins after maturation show the diverse ring topologies-----	32
Figure 2.3. Structures of prochlorosins 2.8 and 3.3-----	34
Figure 2.4. Strategy for determination of directionality of dehydration using [2,3,3- ² H]- Ser residue-----	34
Figure 2.5. MALDI-TOF MS of peptides 2.4 and 2.5 obtained after partial dehydration by ProcM, followed by digestion with endoprotease, GluC-----	36
Figure 2.6. CuAAC-generic reaction, and structures of peptides 2.10 and 2.11 -----	39
Figure 2.7. MALDI-TOF MS of peptides 2.10 and 2.11 obtained after partial dehydration by ProcM, followed by digestion with endoprotease, LysC-----	39
Figure 2.8. GC-MS analysis of a triazole linked peptide-----	40
Figure 2.9. Directionality of dehydration of ProcA3.3 analogues containing a triazole linker-----	42
Figure 2.10. Tandem MS of partially dehydrated WT-ProcA3.3 peptide to confirm C-to-N- terminal directionality-----	43
Figure 2.11. Directionality of cyclization of ProcA2.8 precursor peptide by ProcM-----	45
Figure 2.12. Directionality of cyclization of ProcA3.3 precursor peptide by ProcM-----	46
Figure 2.13. Probing non-enzymatic cyclization in ProcA2.8-----	48
Figure 2.14. Probing non-enzymatic cyclization in ProcA3.3-----	49
Figure 2.15. ESI-MS/MS analysis of intermediate 2.19 , after LysC cleavage-----	51
Figure 2.16. Tandem MS analysis on intermediate 2.20 , after LysC cleavage-----	51
Figure 2.17. Tandem MS on intermediate 2.21 , after LysC cleavage-----	53
Figure 2.18. Tandem MS on intermediates 2.22 and 2.26 , after LysC cleavage-----	54
Figure 2.19. Tandem MS analysis of a mixture of cyclized material derived from enzymatic cyclization of a mixtures of 2.22 and 2.26 after photolysis-----	55
Figure 2.20. Deuterium incorporation and exchange in ProcA2.8-----	57
Figure 2.21. Deuterium incorporation and exchange in ProcA3.3-----	58
Figure 2.22. D-H exchange in ProcA3.3 with duration and concentration of ProcM treatment-----	59

Figure 2.23.	Investigation of D-H exchange in ProcA2.8-S9T and ProcA2.8-S13T mutants	-60
Figure 2.24.	Investigation of D-H exchange in ProcA3.3-T11S	-62
Figure 2.25.	GC/MS analysis to identify the thioether residue in ProcA3.3-T11S mutant participating in DH exchange	-63
Figure 2.26.	GC/MS traces for the co-injection of hydrolyzed/derivatized Lan/MeLan residues from Figure 2.25 with synthetic standards	-63
Figure 2.27.	Sequence alignment of selected LanMs (cyclase domain) and LanCs	-64
Figure 2.28.	Comparison of the rate of dehydration and cyclization of ProcA2.8 by WT-ProcM and ProcM-C971H	-66
Figure 2.29.	The second cyclization in ProcA2.8 is catalyzed by ProcM-C971H	-67
Figure 2.30.	Comparison of the rate of dehydration and cyclization of ProcA3.3 by WT-ProcM and ProcM-C971H	-68
Figure 2.31.	Product distribution of ProcA3.3 treated with either WT-ProcM or ProcM-C971H	-69
Figure 2.32.	ESI-LC-MS of 3-fold dehydrated ProcA3.3 core peptides obtained by reaction with WT-ProcM, ProcM-C971A, and ProcM-C971H	-71
Figure 2.33.	Approach used to determine whether WT-ProcM can correct the non-native ring topology in an intermediate	-73
Figure 2.34.	Tandem ESI-MS evidence to establish that WT ProcM does not correct non-native ring topology	-74
Figure 2.35.	Evaluation of oligomerization states of ProcM under various conditions	-76
Figure 2.36.	Comparison of activity of monomer vs trimer of ProcM	-77
Figure 3.1.	Cytolysin biosynthetic gene cluster	121
Figure 3.2.	Structures of Cytolysin L and S peptides	122
Figure 3.3.	Michael-type addition of Cys thiol to a dehydrated residue to generate either DL or LL-configuration of thioether crosslinks	123
Figure 3.4.	Strategy to introduce thioether ring on solid phase	126
Figure 3.5.	Chiral GC/MS analysis of hydrolyzed and derivatized CylL _S -Dhb2Dha, obtained by in-vivo expression in <i>E.coli</i>	128
Figure 3.6.	Cytolysin S and its two mutants share similar antimicrobial activity against <i>L. lactis</i> HP, in synergy with cytolysin L	129
Figure 3.7.	Cytolysin S and its single mutant share similar hemolytic activity, in synergy with cytolysin L	129
Figure 3.8.	Chiral GC/MS analysis of hydrolyzed and derivatized CylL _S -Dhb1Dha/Dhb2Dha confirms the presence of both LL and DL-Lan	130
Figure 3.9.	Chiral GC/MS analysis of hydrolyzed and derivatized peptide 3.4 confirms the presence of a mixture of LL and DL-configurations of MeLan	132
Figure 3.10.	Analysis of pure synthetic CylL _S '-Dhb2Dha	135
Figure 3.11.	Comparison of antimicrobial activity of expressed and synthetic cytolysin S	136
Figure 3.12.	Comparison of antimicrobial activity of diastereomers of cytolysin S	137
Figure 3.13.	Comparison of hemolytic activity of diastereomers of cytolysin S	138
Figure 4.1.	Structures of microbisporicin A1 and A2	161
Figure 4.2.	Biosynthetic gene cluster for microbisporicin production	162
Figure 4.3.	Structure of the A and B ring of deschloro-microbisporicin	164
Figure 4.4.	Purification and analysis of A and B ring of deschloro-microbisporicin	166
Figure 4.5.	Microbisporicin tetrapeptide with glutamylated Ser3	166

Figure 4.6.	Microbisporicin tetrapeptide with glutamylated 2,3-diaminopropanoic acid----	167
Figure 5.1.	Structures of few notable phosphonate compounds-----	178
Figure 5.2.	Overview of the biosynthesis of a number of phosphonate and phosphinate natural products-----	180
Figure 5.3.	Structure of dehydrophos and its conversion into MAP-----	181
Figure 5.4.	Dehydrophos biosynthetic pathway proposed earlier to this work-----	183
Figure 5.5.	Biosynthetic gene cluster for dehydrophos production showing functional assignment of putative enzymes-----	183
Figure 5.6.	³¹ P-NMR studies on the activities of DhpD and DhpH-----	185
Figure 5.7.	Generation of L-Ala(P) from pSer(P) using DhpH and DhpD-----	185
Figure 5.8.	Radioactive TLC analysis of conversion of <i>rac</i> -pSer(P) to L-[¹⁴ C(U)]-Leu- Ala(P) by the activity of DhpH and DhpD in a one-pot reaction-----	187
Figure 5.9.	HPLC traces and ¹ H NMR comparing synthetically and enzymatically prepared L-Leu-L-Ala(P)-----	188
Figure 5.10.	HPLC traces of Gly-L-Leu-L-Ala(P)-----	190
Figure 5.11.	Revised biosynthesis of dehydrophos-----	191
Figure 5.12.	Identification of two novel phosphonates from <i>Streptomyces sp.</i> WM 6372----	192
Figure 5.13.	³¹ P NMR spiking experiments to confirm identity of phosphonates produced by <i>Streptomyces sp.</i> WM 6372-----	193
Figure 5.14.	Biosynthetic pathway of rhizotocins-----	194

LIST OF SCHEMES

SCHEME		PAGE
Scheme 1.1.	Labionin formation via double-Michael-type addition-----	19
Scheme 2.1.	Scheme showing enzymatic vs. non-enzymatic cyclization during prochlorosin maturation-----	32
Scheme 2.2.	Scheme showing the generation of ProcA2.8 analogues by NCL, used to determine the directionality of dehydration-----	35
Scheme 2.3.	Scheme for generation of ProcA leader peptide with a C-terminal alkyne-----	37
Scheme 2.4.	Scheme for the D–H exchange assay-----	57
Scheme 3.1.	Heterologous expression of CylL _S -T2C and CylL _S -T2C/T7A precursor peptides with CylM-----	131
Scheme 3.2.	Scheme showing Cys2 to Dha conversion in peptide 3.3 -----	132
Scheme 3.3.	Synthesis of cytolysin S-Dhb2Dha-----	134
Scheme 4.1.	Synthesis of peptide 4.1 -----	165
Scheme 4.2.	SPPS of microbisporicin tetrapeptide with ester-linked glutamylated Ser3-----	167
Scheme 4.3.	SPPS of microbisporicin tetrapeptide with amide-linked glutamylated 2,3- diamino propanoic acid-----	168
Scheme 5.1.	Synthesis of <i>rac</i> -pSer(P) starting from Cbz-L-Ser-OH-----	184
Scheme 5.2.	Scheme showing the synthesis of L-Leu-ΔAla(P)-----	186
Scheme 5.3.	Scheme showing the synthesis of L-Leu-Ala(P)-----	187
Scheme 5.4.	Representation of the activity of DhpJ where L-Leu-ΔAla(POMe) is the sole product arising from L-Leu-L-Ala(POMe)-----	189
Scheme 5.5.	Scheme showing the synthesis of (A) Gly-L-Leu-Ala(P) and (B) Gly-L-Leu- Ser(P)-----	190
Scheme 5.6.	Scheme showing the synthesis of compound 5.7 -----	192
Scheme 5.7.	Scheme for the synthesis of compound 5.9 -----	195

CHAPTER 1: PEPTIDE THERAPEUTICS AND LANTHIPEPTIDES

1.1. PEPTIDES AS THERAPEUTICS

The pharmaceutical industry's focus has been traditionally dominated by small molecules. A higher attrition of compounds in clinical trials, resulting in diminishing returns on investment in new compounds in recent times, has spurred interest in other modalities for treating diseases. Based on size and complexity of the molecule, biologics (including proteins such as antibodies and enzymes) occupy the other end of the size spectrum of chemical space compared to small molecules. Peptides fall in between, exhibiting properties of both small molecules and biologics (1). Currently, there are about 60 U.S. FDA-approved peptide therapeutics, 140 peptide-drugs in clinical trial, and 500 peptide-drugs in preclinical trials (2). The major therapeutic areas treated with peptide-drugs are oncology, infectious diseases, cardiovascular, and metabolic diseases (3).

1.1.1. Advantages of Peptide-Therapeutics

Traditionally, therapeutics span two major classes: small molecules (<500 Da) and biologics (>5000 Da) (4). Small molecules are designed to comply with Lipinski's "rule-of-five" (5, 6). Accordingly, to ensure oral bioavailability of the drug candidate, the molecular weight is kept lower than 500 Da, the compound should have less than 5 H-bond donors, 10 H-bond acceptors, and the calculated LogP (cLogP, measure of lipophilicity suggested by the ratio of compound's distribution between octanol and water) should be less than 5. Thus, Lipinsky's rules disfavor the use of peptides as drug candidates and they are less likely than small molecules to be absorbed in the gastrointestinal tract. However, small molecules often do not have high target specificity, which is associated with undesired off-target effects. Biologics, on the other hand, can have extremely high selectivity for their biological target along with high potency.

These molecules include proteins, antibodies, enzymes, and other macromolecules and account for a significant portion of FDA approved drugs (Figure 1.1). Biologics can be expensive to manufacture and can require special handling, storage, and analytical tools. Peptides bridge the gap between small molecule drugs and biologics (1, 4). Though peptides are less expensive to produce than biologics, they often share certain strengths with biologics that are absent in small molecules. Like biologics, peptides are associated with high selectivity towards targets and high potency. Peptides suffer less from instances of adverse immunogenic response, a problem often faced by biologics (7). Compared to biologics, peptides have greater stability, ease of handling and synthetic tractability. Compared to small molecules, peptides have better efficacy and high specificity towards their target (4). In targeting protein–protein interactions, which involve large surface areas, peptides are also better candidates than small molecules (8). Unlike many small molecules, the target-selectivity of peptides translates into better safety and tolerability (2), and peptides degrade to amino acids, and are therefore less toxic than small molecules (9). Furthermore, peptides have short half-lives and hence do not accumulate in the tissue.

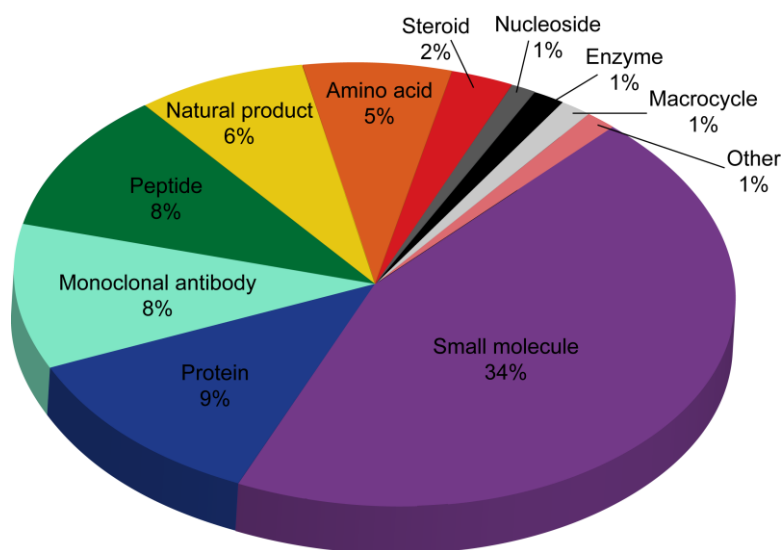


Figure 1.1. Distribution of FDA approved drugs of various therapeutic modalities. Adapted from Fernando *et al.* (10).

1.1.2. Overcoming Challenges of Peptide Therapeutics

Peptides have many advantageous properties, but they face several challenges as therapeutics, and such challenges have discouraged the pharmaceutical industry from investing in peptide research (11). Peptides tend to have short half-lives in the body and are rapidly degraded by proteases present in the digestive system and blood plasma. Generally, peptides suffer from poor oral bioavailability because of this proteolytic degradation. Furthermore, the liver and kidneys rapidly eliminate peptides from the blood stream, resulting in poor pharmacokinetics profiles. The hydrophilicity of the peptide chain can also make them unable to cross physiological barriers, including the plasma membrane. The production cost of peptides is less than that of biologics, but still higher than that of small molecules (11).

Several chemical modifications on peptide molecules allow their use as effective therapeutic agents (11). Substitution of proteinogenic amino acids with D-amino acids or unnatural amino acids to block potential protease cleavage sites improves plasma stability. Constraining the peptide with various macrocyclizations including head to tail, side chain to side chain, and side chain to backbone, lactam and lactone formation, disulfide formation, lanthionine formation, and many other less common forms of cyclization can also block protease degradation (12-14). Such macrocyclization also reduces the flexibility of peptides and improves target-binding. Isosteric or other replacement of amide bonds also improves the stability of peptides to endopeptidases. Often the N- and C-termini of peptide chains are blocked by N-acylation, N-pyrroglutamylation, C-amidation, etc. (Figure 1.2 shows some examples) to provide resistance towards exopeptidases. Peptides are sometimes bound to serum albumin protein or are PEG-ylated to improve pharmacokinetics by lowering the renal clearance.

1.1.3. Notable Peptide Therapeutics

Several ‘block-buster’ drugs treating a variety of diseases (see Figure 1.2 for examples), with sales in excess of a billion dollars are peptides. The majority of approved therapeutic peptides are short (less than 20 aa), representing around 70% of marketed peptide drugs (Figure 1.3) (4). It is to be noted that the mentioned therapeutic peptides (Figure 1.2) all bear structural modifications to improve their properties, as mentioned earlier. Leuprolide is a gonadotropin receptor agonist; octreotide inhibits secretion of growth hormone and treats acromegaly and cancer; goserelin treats breast and prostate cancer, endometriosis and fibroids; oxytocin is used to induce labor; and fuzeon is an anti-retroviral drug.

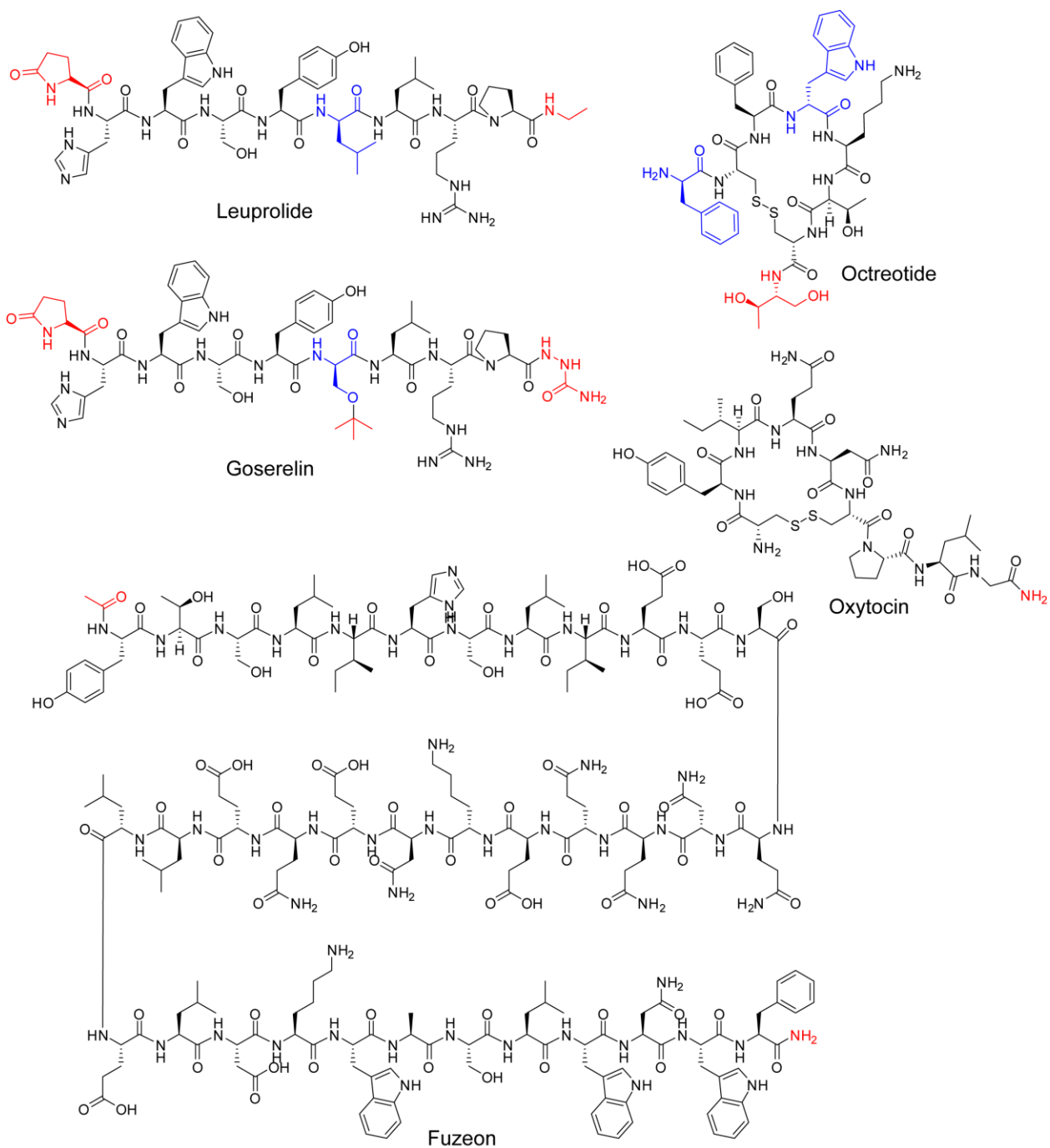


Figure 1.2. Structures of a few selected successful peptide drugs. D-amino acids are colored blue, non-native moieties are colored red.

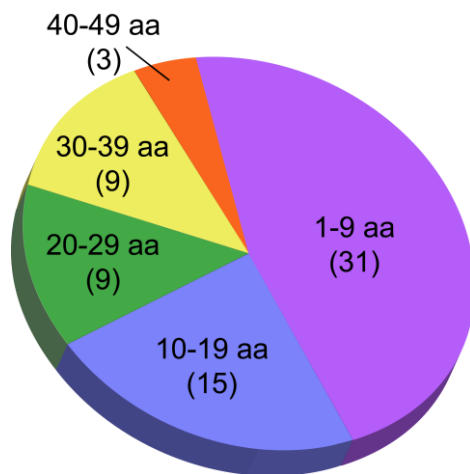


Figure 1.3. Size distribution of approved peptide therapeutics. The number of candidates is in parenthesis. The lengths were compiled from data on 67 reported peptide drugs (4, 11).

1.2. ANTIMICROBIAL DRUGS: NEED OF THE HOUR

Antimicrobial resistance is a growing problem in our society and is causing a great loss of life and resources (15). The U.S. centers for disease control and prevention (CDC) estimated in 2013 that over 2 million infections resistant to some classes of antibiotics result in 23,000 deaths in the U.S. each year, and require over 8 million days of hospital-stay. The illnesses and deaths cost over \$20 billion in healthcare costs, and an additional \$35 billion in lost productivity (16).

1.2.1. Mechanism of Antimicrobial Resistance

Bactericidal agents kill bacteria, while bacteriostatic agents result in cessation of bacterial growth. Antibiotics primarily target bacteria by inhibiting their cell wall biosynthesis (17), protein synthesis (18), or DNA replication and repair (19). The action of antibiotics pose survival stress on the bacteria and a combination of spontaneous mutations and horizontal gene transfer cause bacteria to acquire various mechanisms of resistance (Table 1.1). Three primary mechanisms of resistance are noted. First, the drug is effluxed out of the cytoplasm, lowering the

intracellular concentration of the drug below the therapeutic threshold, as is observed in the case of tetracycline resistance (20). Second, the drug may lose activity due to structural modifications, often catalyzed by enzymes produced by the resistant organism. A well-known example is the β -lactamase-catalyzed ring-opening of β -lactam antibiotics (21). Third, the target may be modified such that the drug can no longer bind to it, as is the case in vancomycin resistance (22).

Antibiotics (Target)	Specific Target	Mechanism	Resistance
β -lactams (Cell wall)	Transpeptidases/transglycosylases (PBPs)	Inhibits enzymes that generate crosslinks in peptidoglycan	β -lactamases, PBP mutants
Vancomycin (Cell wall)	D-Ala-D-Ala of peptidoglycan and lipid II	Blocks substrate to inhibit transpeptidation	Mutant D-Ala-D-Lac or D-Ala-D-Ser no longer blocked
Erythromycin class (Protein synthesis)	Peptidyl transferase, center of the ribosome	Blocks protein synthesis	rRNA methylation, drug efflux
Tetracyclines (Protein synthesis)	Peptidyl transferase	Blocks protein synthesis	Drug efflux
Aminoglycosides (Protein synthesis)	Peptidyl transferase	Blocks protein synthesis	Drug modified by enzymes
Oxazolidinones (Protein synthesis)	Peptidyl transferase	Blocks protein synthesis	Unknown
Fluoroquinolones (DNA replication)	DNA gyrase	Blocks DNA replication	Mutations of DNA gyrase

Table 1.1. The molecular targets, modes of action, and mechanism of resistance of major antibacterial drug classes are presented. Table adapted from Walsh (19).

1.2.2. *ESKAPE* Pathogens: Current Threats by Resistant Microbes

A group of antibiotic-resistant bacteria comprised of *Enterococcus faecium*, *Staphylococcus aureus*, *Klebsiella pneumoniae*, *Acinetobacter baumannii*, *Pseudomonas aeruginosa*, and *Enterobacter spp.* is referred to as ‘the *ESKAPE* pathogens’ (23). These pathogens are often resistant to most antibiotics (24). *E. faecium* is a Gram-positive, facultative anaerobic pathogen, which is usually resistant to β -lactam antibiotics. Vancomycin-resistant

enterococci (VRE) show high resistance to all glycopeptide antibiotics, and VRE also aids in biofilm formation. *S. aureus* is a Gram-positive bacterium commonly involved in biofilm formation. Methicillin resistant *S. aureus* (MRSA) shows resistance against all β -lactam antibiotics such as penicillin, cephalosporin, and carbapenem. MRSA is often treated with glycopeptide antibiotics like vancomycin, a treatment that is threatened by the occurrence of vancomycin-intermediate and vancomycin-resistant *S. aureus* (VISA and VRSA). *K. pneumonia* is a member of Gram-negative enterobacteriaceae, which readily accumulates and transfers genes responsible for multi-drug resistant infections. *K. pneumonia* is responsible for widespread resistance against β -lactam antibiotics including carbapenem, often used as a drug of last resort in Gram-negative infections. A recent report of emergence of New Delhi metallo- β -lactamase-1 among *K. pneumonia* causes great concern as it carries plasmid-encoded broad resistance genes against several antibiotics (25). *A. baumannii* is another Gram-negative pathogen, known for its persistence in the environment. Often found in intensive care units and surgical wards, some *A. baumannii* have acquired resistance against all known antibiotics. *P. aeruginosa* is a Gram-negative, facultatively anaerobic organism, often found in the mucous of cystic fibrosis patients. Resistant *P. aeruginosa* have efficient drug-efflux pumps that confer resistance towards fluoroquinolones and β -lactams, and can only be treated by colistin, a cyclic peptide antibiotic. *Enterobacter spp.* commonly cause urinary tract and bloodstream infections, and the resistant strains respond only to colistin and tigecyclin. Thus, ESKAPE pathogens represent a select group of pathogens which often exist as resistant strains immune to almost all known antibiotics (24).

1.2.3. Peptides as Antimicrobial Agents

Antibiotic resistance and the dwindling of novel antibiotics in the pharmaceutical industry pipeline urgently necessitate exploration of novel antibiotics. Antibiotics derived from

peptide scaffolds are proving to be potent agents for treating bacterial infections (26). Such peptide antibiotics often bear net positive charge and electrostatically bind to the negatively charged bacterial membranes (27). Besides membrane disruption by electrostatic interaction and other mechanisms such as binding to lipid II (28), peptides can also modulate the immunity of the host to kill pathogens (29). Interestingly, certain peptide-derived antibiotics have proven effective in penetrating biofilms and treating recalcitrant infections (30). The most recently reported novel antibiotic is teixobactin (reported in 2015), a depsipeptide that binds to lipid II and interferes with cell wall biosynthesis, and importantly is found to kill cells without detectable resistance (31). The last new class of antibiotic approved by FDA is daptomycin (reported in 1987 as LY146032 (32), approved in 2003), a cyclic lipopeptide that disrupts the bacterial cell membrane resulting in cell death (33, 34). It has been over 40 years since the discovery of fluoroquinolones, the last novel drugs for treating Gram-negative bacteria. Colistin is a cyclic peptide that is active against Gram negative bacilli and is used as a drug of last resort to treat infections caused by resistant pathogens (see Figure 1.4 for structures of some peptide-based antibiotics) (35). Colistin was previously rejected due to nephrotoxicity, but was revived to treat otherwise resistant microbes like carbapenem resistant enterococci (36). Given that it is difficult for bacteria to develop resistance against certain peptide-based antibiotics, such therapeutics are immensely promising in the fight against resistant infections.

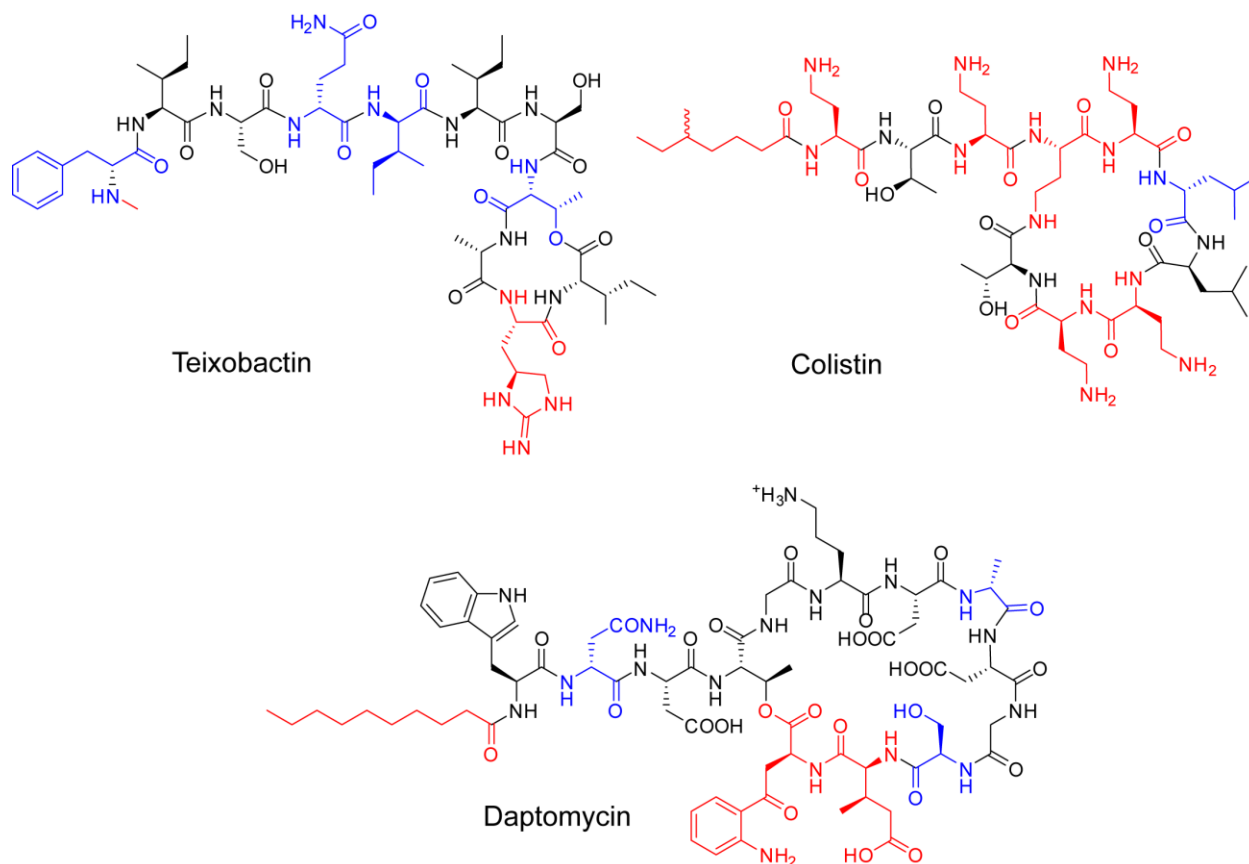


Figure 1.4. Structures of selected potent antibacterial peptides. D-amino acids are colored blue, non-proteinogenic moieties are colored red.

1.3. RIBOSOMALLY SYNTHESIZED AND POST-TRANSLATIONALLY MODIFIED NATURAL PRODUCTS

A major class of peptide natural products are generated by the ribosome and further modified post-translationally. Referred to by the acronym RiPPs (Ribosomally Synthesized and Post-Translationally Modified Peptides), they exhibit a tremendous structural diversity. Typically, only peptides below 10 kDa are considered part of RiPPs to distinguish them from post-translationally modified proteins. The biosynthesis of these compounds is termed as Post-Ribosomal Peptide Synthesis (PRPS) (37).

There are some common features of RiPPs biosynthesis. They are genetically encoded as a long precursor peptide, around 20-110 residues in length. The portion of the precursor peptide

that binds to enzymes responsible for installing the post-translational modifications is called the leader peptide (38). Leader peptides often span the N-terminal portion of the precursor peptides and are not post-translationally modified. In a few cases, such as in bottromycins, where such recognition peptides occupy the C-terminal portion, they are termed ‘follower’ peptides. The portion of precursor peptide that undergoes post-translational modification and gives rise to the final natural product is termed the core peptide. The precursor peptide is referred to as XaaA (eg. LanA for a lanthipeptide precursor), and the modified precursor peptide is designated mXaaA (Figure 1.5). The fact that the precursor peptides are genetically encoded allows genome-mining to identify novel members of the RiPPs family (39, 40).

Often the leader-peptide guided recognition of the precursor peptides by the modifying enzymes allows tolerance towards changes in the core region, leading to high structural diversity in the generated RiPPs (41). A winged helix-turn-helix (wHTH) motif within these enzymes has been found in various members of the RiPPs biosynthetic enzymes and is responsible for binding the precursor peptides (42, 43). This motif is described as the RiPP precursor peptide recognition element (RRE) (44). The observed substrate tolerance in the RiPPs system allows bio-engineering efforts to generate analogues of natural products (45). In many cases, the post-translational modifications ensure macrocyclization, which decreases the conformational flexibility and makes the mature peptides resistant to proteolysis. RiPPs exhibit a plethora of structural modifications giving rise to moieties such as lysinoalanine, hydroxyaspartate, lanthionine, and methyllanthionine in duramycin (46); pyroglutamate, 4-hydroxyproline, and disulfide linkages in conopeptide (XEN-2174) (47); thiazoles and oxazoles in plantazolicin (48, 49) and patellamides (50); dehydropiperidine, and a quinaldic acid core in thiostrepton A (51);

depsipeptide linkages in microviridin (52); and an amidine and methylations in bottromycins (53) (Figure 1.6).

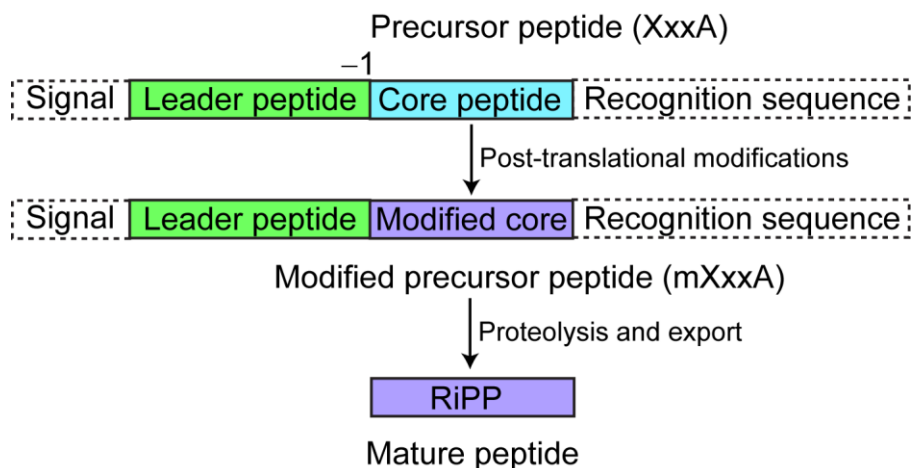


Figure 1.5. Post Ribosomal Peptide Synthesis pathway. The leader peptide is recognized by the post-translational modification machinery and the core peptide is post-translationally modified, followed by cleavage of the leader region to generate the mature product. In certain cases, an N-terminal signal sequence helps with the secretion of mature product. There are examples of the presence of a C-terminal recognition sequence that aids in peptide cyclization. Adapted from Arnison *et al.* (37).

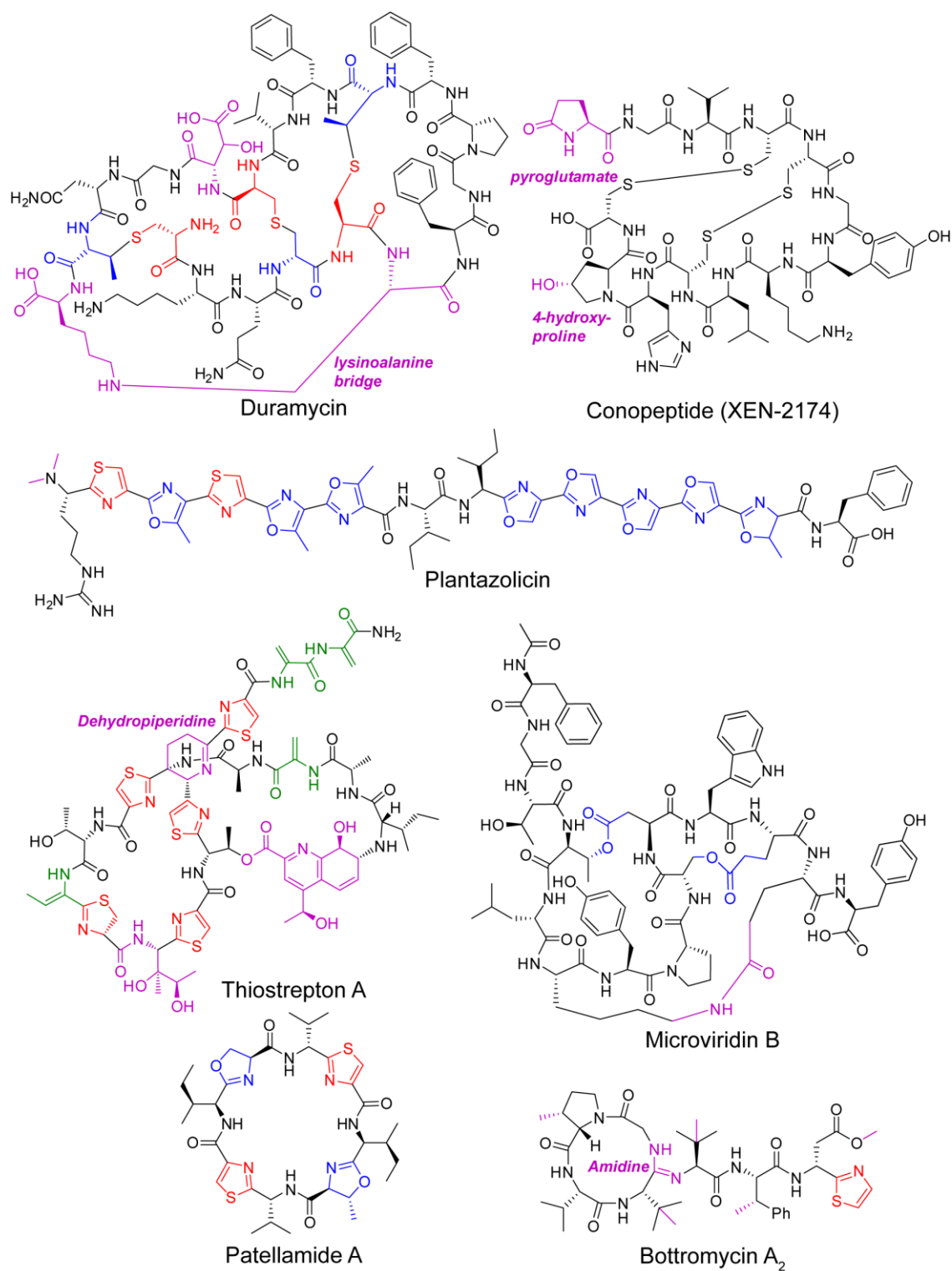


Figure 1.6. Structures of various RiPPs showing diverse modifications. Non-proteinogenic residues are in purple; thiazole, thiazoline, and Cys-derived portion of lanthionine/methylanthionine in red; oxazole/oxazoline, depsipeptide linkage, and Ser/Thr-derived portion of lanthionine/ methylanthionine in blue; dehydrated residues in green. Adapted from Arnison *et al.* (37).

1.4. LANTHIPEPTIDES*

Lanthipeptides are a class of RiPPs that contain the characteristic thioether residues lanthionine (Lan) and methyllanthionine (MeLan) (37, 45). A subclass of lanthipeptides with antibacterial activity are known as lantibiotics (55), which are effective against many Gram-positive bacteria including some drug-resistant species (56). For instance, nisin has been used for over 50 years as a preservative in the food industry to combat food-borne pathogens without significant bacterial resistance (57). Lanthipeptides that do not display antibacterial activity can exert antiviral (58), antiallodynic (59), antinociceptive (60), and morphogenetic (61) activities. Cyclic peptides such as lanthipeptides are also increasingly recognized as promising compounds for disrupting protein–protein interactions (62-67). Investigation of the synthetases that post-translationally generate lanthipeptides would aid in engineering efforts to produce molecules with desirable properties (68-70).

1.4.1. Lanthipeptide Biosynthesis

During lanthipeptide biosynthesis, the ribosomal machinery first synthesizes linear precursor peptides called LanAs (45). The LanA peptides are comprised of an N-terminal leader peptide that is believed to serve several possible roles, including recognition by the synthetase (38, 71), and a C-terminal core peptide that is post-translationally modified. Proteolytic cleavage then removes the leader peptide to produce the mature lanthipeptide. Lan and MeLan formation involves first the dehydration of Ser and Thr residues to generate dehydroalanine (Dha) and dehydrobutyrine (Dhb), respectively. The dehydrated residues then undergo stereoselective Michael-type addition by the side-chain thiol of cysteines to generate the thioethers Lan and

Introduction to Section 1.4. adapted in part from:

54. Mukherjee, S., and van der Donk, W. A. (2014) Mechanistic Studies on the Substrate-Tolerant Lanthipeptide Synthetase ProcM, *J. Am. Chem. Soc.* 136, 10450-10459.

MeLan, respectively (Figure 1.7) (72, 73). The Lan and MeLan crosslinks are mostly found to have the DL-configuration except in the case of cytolsins and haloduracin β (and putatively others bearing a certain pentapeptide motif), which also contain thioether crosslinks of LL-configuration (74). Certain lanthipeptides are characterized by additional post-translational modifications besides dehydration and cyclization. Such post-translational modifications include the introduction of labionin crosslinks (75), lysinoalanine (76), β -hydroxy-aspartate (76), 2-oxobutyrate (77, 78), pyruvate (79), lactate (80), *S*-aminovinyl-D-cysteine (81), and *S*-aminovinyl-D-methylcysteine (82) (see Figure 1.8 for structures of lanthipeptides exhibiting various post-translational modifications).

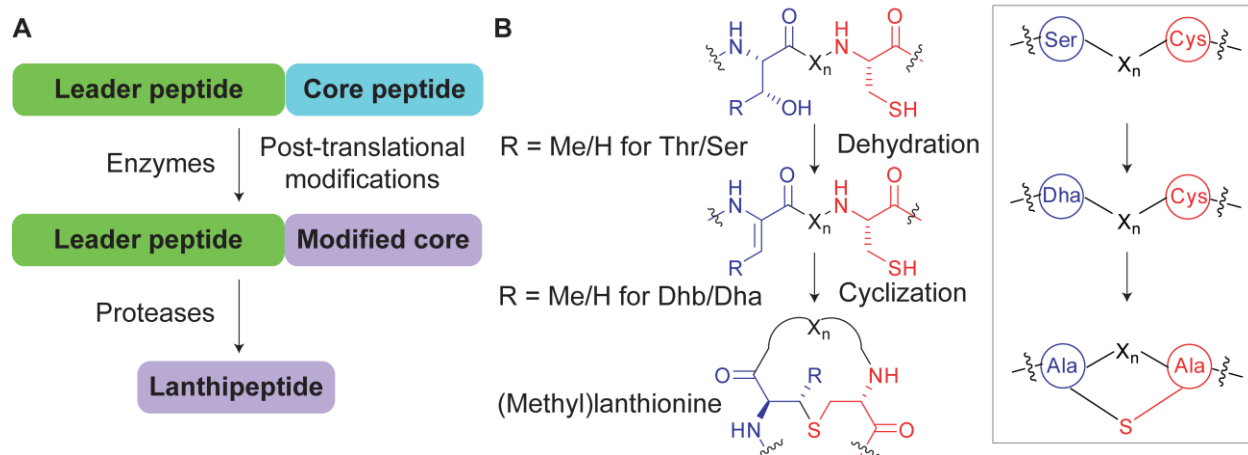


Figure 1.7. Lanthipeptide biosynthesis and common post-translational modifications. (A) Generic scheme for lanthipeptide biosynthesis. (B) Common post-translational modifications in lanthipeptides. The corresponding bubble-diagram is drawn in the box for Ser to Dha to Lan transformations.

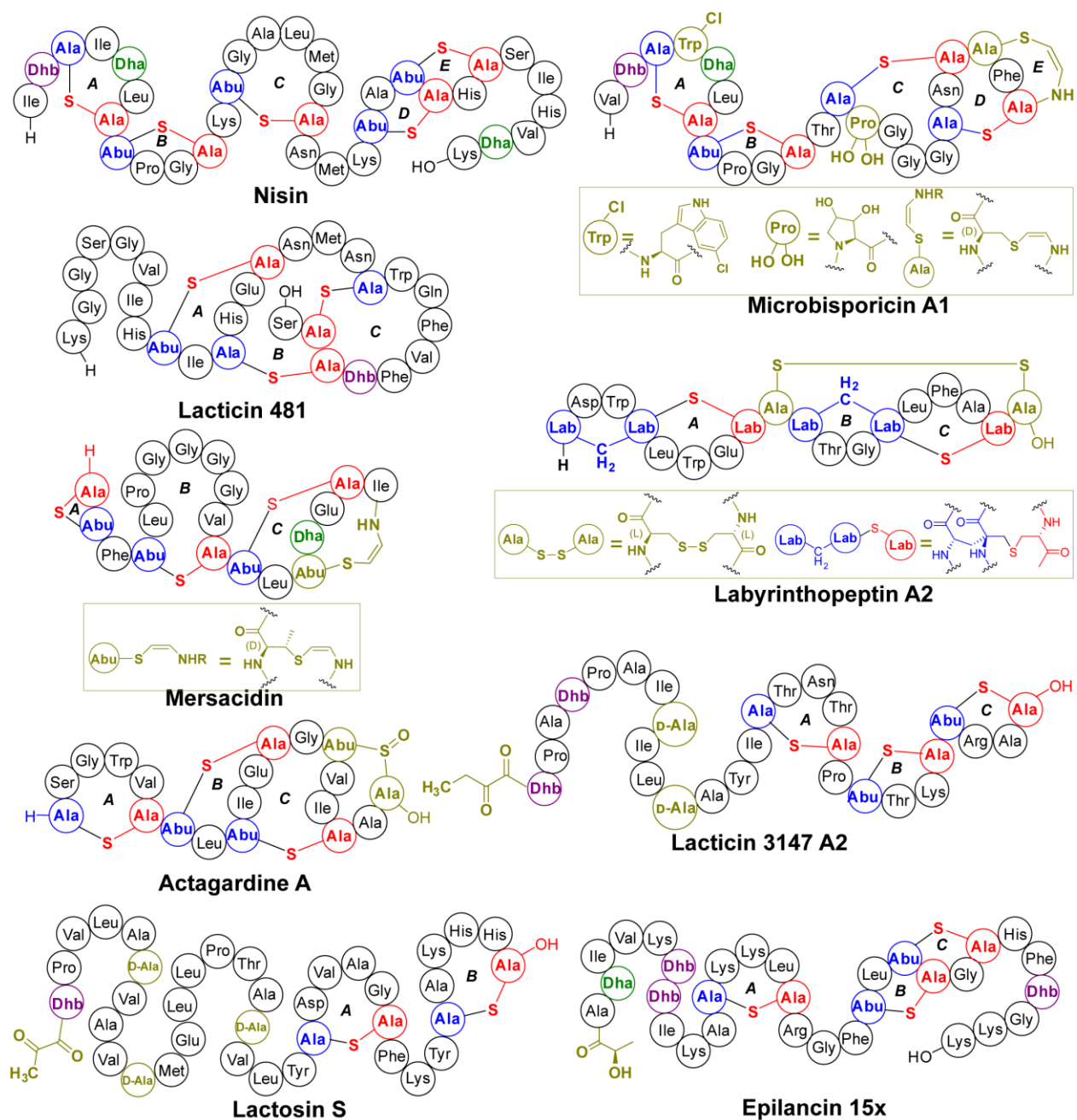


Figure 1.8. Bubble-diagrams of various lanthipeptides. Structures of some of the post-translational modifications are drawn inside the box. In Lan/MeLan crosslinks, residues arising from Cys are colored red, while those arising from Ser/Thr are in blue.

There are four classes of lanthipeptides based on their biosynthetic machinery (Figure 1.9). In class I lanthipeptides, two separate enzymes perform the dehydration and cyclization reactions. Members of this class include nisin and microbisporicin, among others. The

dehydratase is generically termed as LanB, which in the case of nisin (NisB), has been shown to glutamylate Ser/Thr residues followed by elimination (83). NisB has been crystallized bound to the precursor peptide NisA, and the hydrophobic β -sheet rich leader peptide binding site has been identified (42). The cyclization reaction leading to nisin is catalyzed by NisC (generically called LanC), the in vitro reconstitution and the crystal structure of which offered insights into its catalysis (84). NisC has a tetrahedral Zn(II) in the active site that has two Cys and one His residues in three of its vertices, with H₂O in the fourth vertex. Upon substrate binding to NisC, the reacting Cys-thiol is believed to displace the H₂O and bind to Zn(II), thus lowering the pK_a of the thiol. In a structurally similar protein, farnesyl transferase, the pK_a of Zn(II) coordinated Cys is lowered to around 6.4 (85). This results in generation of thiolate at physiological pH, which attacks the β -carbon of a dehydrated residue. The subsequent enolate is protonated to generate the cyclized product. In nisin, the modified peptide is exported from the cytoplasm by a transmembrane ATP-binding cassette (ABC) transporter, NisT (86). Often in class I systems, a dedicated subtilisin-like serine protease, LanP, removes the leader peptide.

In class II lanthipeptides, both the dehydration of Ser/Thr residues and the Michael-type cyclization reaction are catalyzed by a single bifunctional enzyme called LanM. LanMs contain an N-terminal dehydratase domain, which has no homology to the dehydratase LanB of class I systems. Unlike LanBs which glutamylate Ser/Thr residues, LanMs activate Ser/Thr residues via phosphorylation, followed by elimination to generate dehydrated residues (87) (Figure 1.10). The cyclase domain of LctM, the synthetase generating lactacin 481, shares homology with NisC and requires the Zn-ligand based active site to catalyze Michael-type addition (88). The mature precursor peptide (mLanA) is proteolyzed and transported outside the cytoplasm by a LanT,

which has a papain-like cysteine protease domain in the N-terminus, and an ABC transporter domain (73).

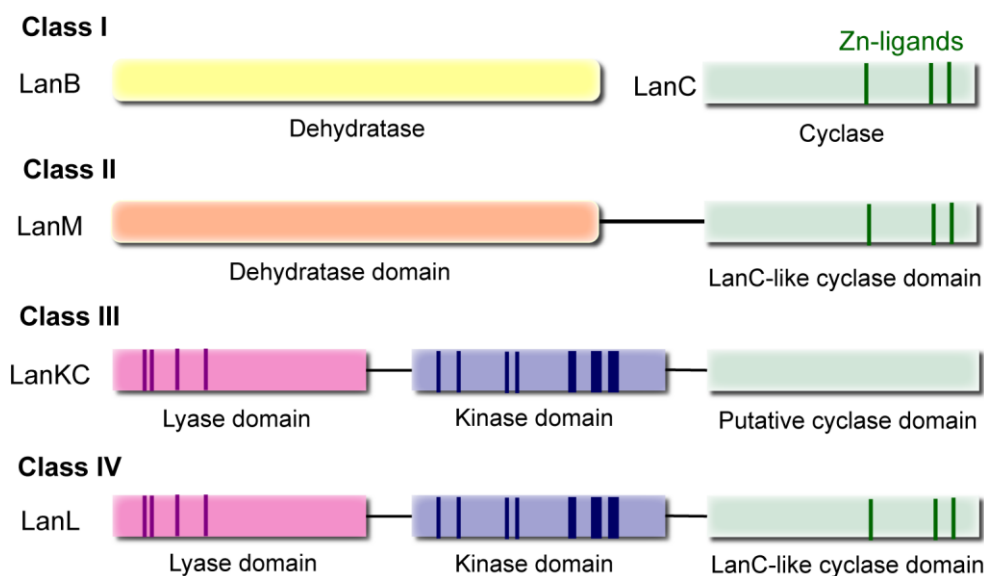


Figure 1.9. Different classes of lanthipeptide biosynthetic machinery. Conserved regions of the enzymes are denoted by the dark lines in the figure. The class III cyclase domain lacks the Zn ligands. Adapted from Knerr *et al.* (45)

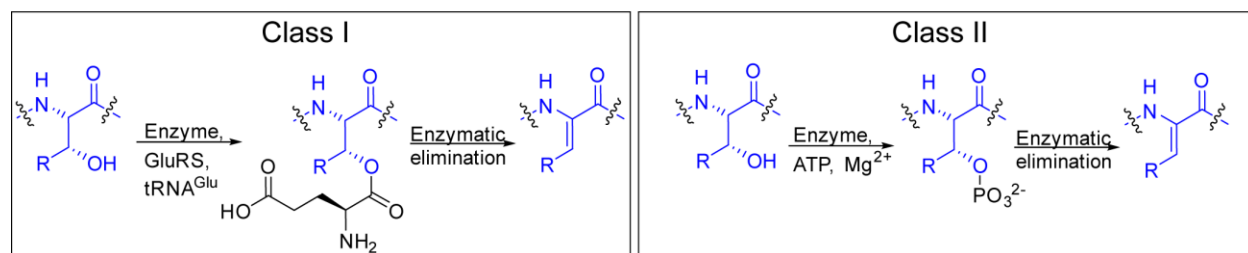
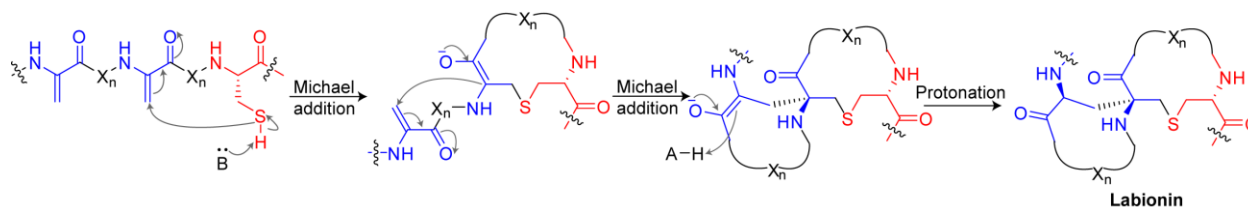


Figure 1.10. Different activation steps of Ser/Thr catalyzed by class I and II lanthipeptide synthetases. Class I synthetase, as established for nisin (42), glutamylates Ser/Thr in a glutamyl-tRNA^{Glu} dependent fashion. In class II synthetase, as established for many members including lacticin 481 (87), phosphorylation occurs in presence of ATP and Mg²⁺ ions.

Class III synthetases have separate kinase and lyase domains that generate dehydrated residues from Ser/Thr via phosphorylation (89). In LabKC, the synthetase generating labyrinthopeptin, the kinase activity requires GTP instead of ATP (75). In case of

labyrinthopeptin, the cyclase domain lacks the Zn(II) ligands and catalyzes a unique double Michael-type addition to form a carbacyclic labionin residue (Scheme 1.1) (59). Class IV synthetase, like VenL that catalyzes generation of venezuelin, have similar kinase and lyase domains as its class III counterpart, but the cyclase contains the Zn(II) active site similar to ones found in class I and II synthetases (90).



Scheme 1.1. Labionin formation via double-Michael-type addition.

1.4.2. Modes of Action of Lanthipeptides

Lantibiotics are a subset of lanthipeptides possessing antibiotic activity. Detailed modes of action are understood only for few lanthipeptides (91, 92). Nisin kills bacteria by inhibiting cell wall biosynthesis and forming pores in the membrane. Nisin is comprised of five thioether rings, with three N-terminal rings (known as A, B, and C) and two C-terminal rings (D and E) joined by a flexible hinge region (93). The amide backbone of the N-terminal A and B rings in nisin form a pyrophosphate-cage for binding lipid II (94, 95). The C-terminal rings of nisin penetrate the phospholipid bilayer in orientation that is perpendicular to the bilayer, and eventually form stable pores (2-2.5 nm diameter) (96, 97). The sequestering of the cell wall biosynthesis precursor lipid II by nisin and the pore formation activity is responsible for its potent antibacterial activity.

Amongst the class II lanthipeptides, mersacidin is active against MRSA in a murine-infection model (98). Mersacidin inhibits the transglycosylation step of peptidoglycan biosynthesis, however it does not form pores in the plasma membrane (99, 100). Like

mersacidin, lactacin 481 inhibits transglycosylation, and does not form pores in the membrane (101). The A-ring in lactacin 481 is similar to the C-ring in mersacidin, and is important for activity in both cases (See Figure 1.8) (101, 102). Among other members of class II lantibiotics are cinnamycin and duramycin, which bind to phosphatidylethanolamine (PE) with a 1:1 stoichiometry (103). The toxicity of cinnamycin is primarily caused by a transbilayer phospholipid movement that exposes PE present in the inner-leaflet of the eukaryotic membrane and causes morphological changes in the membrane (104).

Two component lanthipeptides either lack or exhibit poor individual bioactivity, but show synergistic bioactivity in combination (105). A model for lipid II binding by the two components of lactacin 3147 bears similarity to the nisin-lipid II binding (106). LtnA1, a component of lactacin 3147, is thought to interact with lipid II on the outer-leaflet of the bacterial cell membrane. LtnA2, the other component, then binds to the lipid II complexed with LtnA1 to form pores and inhibit cell wall biosynthesis. The residues in both components essential for inhibiting cell-wall biosynthesis were identified by complete Ala-scanning (107). Besides displaying antibacterial activity, cytolysin S and L make up a two component lanthipeptide that also exhibits cytolytic activity against erythrocytes and other eukaryotic cells (108), though the molecular level understanding of this phenomenon is yet to be reported.

Among class III lanthipeptides are SapB and SapT, which are morphogenetic peptides, and are involved in aerial hyphae formation in streptomyces (109). The peptides are amphiphilic, with the polar peptide backbone participating in hydrogen bonding with solvent water molecules, and the hydrophobic side chains sticking out of the water layer. This amphiphilicity allows the peptide to reside at the air-water interface, acting as a surfactant and facilitating the emergence of streptomycete aerial filaments (110).

1.5. CONCLUSION AND OUTLOOK

Peptides offer a promising prospect in the therapeutic landscape where traditionally small molecules have been the dominant player. Offering many of the advantages of biologics, combined with the synthetic tractability and better stability of small molecules, peptides occupy an attractive niche between the small molecules and biologics. Antimicrobial treatment is primed for peptide therapeutics as small molecules suffer from various forms of antimicrobial resistance. RiPPs have proven to be an important family of peptide natural products with various post-translational modifications improving the stability and efficacy of the peptide molecules. Our research focuses on lanthipeptides, characterized by the presence of lanthionine and methylanthionine thioether crosslinks, and often with other post-translational modifications. Several lanthipeptides have shown potent biological activity, and the significant clinical potential of the members of this class elicits a strong interest in this area. Understanding of the biosynthetic enzymes that install the post-translational modifications may eventually allow engineering of novel therapeutics. Chemical synthesis has also proven to be an important technology to generate non-native analogues of lanthipeptides in the hope of obtaining products with improved bioactivity, and answering fundamental biological questions.

This thesis describes my research on the mechanistic investigation of lanthipeptide biosynthesis and structure activity relationships using synthetic substrate analogues. The information offers fundamental insights into the biosynthetic machinery and bioactivity of selected lanthipeptides. In chapter 2, I focus on gaining a mechanistic understanding of the generation of a family of 30 lanthipeptides called prochlorosins by a single substrate-tolerant synthetase, ProcM. To investigate the substrate-tolerance of catalysis by ProcM, I adopted a hybrid ligation chemistry to generate a series of substrate analogues designed to address a

number of mechanistic questions. The dehydration by ProcM was established to occur from C-to-N-terminus. Cyclization also occurred with a specific order, which depended on the sequence of the substrate peptide. Furthermore, using photo-labile cysteine side-chain protection, I was able to rule out spontaneous non-enzymatic cyclization events to explain the very high substrate tolerance of ProcM. I also developed a deuterium-exchange assay to probe the reversibility of the Michael-type addition. The cyclization reaction by ProcM was established to be governed by kinetic control. Chapter 3 describes a strategy to obtain cytolysin S, a highly hydrophobic lanthipeptide, by total synthesis. An analogue of cytolysin S was generated to explore the importance of the thioether stereochemistry with respect to the bioactivity. I established that while the antibacterial activity was sensitive to the stereochemistry of the thioether crosslinks, the hemolytic activity was not. In chapter 4, I describe synthesis of another hydrophobic lanthipeptide analogue, the portion of microbisporicin containing the A and B rings, to address the minimum motif required for halogenation of a Trp within the A-ring by a flavin-dependent halogenase MibH. However, the C-terminus was found to be necessary for MibH activity, as the fragment containing the A and B rings was not modified by the enzyme. In chapter 5, I present my research on a different area of focus in our laboratory, the study of phosphonate natural products. I primarily synthesized the putative substrates and intermediates to elucidate the biosynthetic pathway of dehydrophos, fosfazinomycin, and rhizocticin. Further background and significance of the phosphonate project is described in chapter 5.

1.6. REFERENCES

1. Uhlig, T., Kyprianou, T., Martinelli, F. G., Oppici, C. A., Heiligers, D., Hills, D., Calvo, X. R., and Verhaert, P. (2014) The emergence of peptides in the pharmaceutical business: From exploration to exploitation, *EuPA Open Proteom.* 4, 58-69.
2. Fosgerau, K., and Hoffmann, T. (2015) Peptide therapeutics: current status and future directions, *Drug Discov. Today* 20, 122-128.

3. Kaspar, A. A., and Reichert, J. M. (2013) Future directions for peptide therapeutics development, *Drug Discov. Today* 18, 807-817.
4. Craik, D. J., Fairlie, D. P., Liras, S., and Price, D. (2013) The Future of Peptide-based Drugs, *Chem. Biol. Drug Des.* 81, 136-147.
5. Lipinski, C. A. (2000) Drug-like properties and the causes of poor solubility and poor permeability, *J. Pharmacol. Toxicol. Methods* 44, 235-249.
6. Lipinski, C. A., Lombardo, F., Dominy, B. W., and Feeney, P. J. (2001) Experimental and computational approaches to estimate solubility and permeability in drug discovery and development settings, *Adv. Drug Deliv. Rev.* 46, 3-26.
7. McGregor, D. P. (2008) Discovering and improving novel peptide therapeutics, *Curr. Opin. Pharmacol.* 8, 616-619.
8. Katz, C., Levy-Beladev, L., Rotem-Bamberger, S., Rito, T., Rudiger, S. G. D., and Friedler, A. (2011) Studying protein-protein interactions using peptide arrays, *Chem. Soc. Rev.* 40, 2131-2145.
9. Loffet, A. (2002) Peptides as Drugs: Is There a Market?, *J. Pep. Sci.* 8, 1-7.
10. Albericio, F., and Kruger, H. G. (2012) Therapeutic peptides, *Future Med. Chem.* 4, 1527-1531.
11. Vlieghe, P., Lisowski, V., Martinez, J., and Khrestchatisky, M. (2010) Synthetic therapeutic peptides: science and market, *Drug Discov. Today* 15, 40-56.
12. White, C. J., and Yudin, A. K. (2011) Contemporary strategies for peptide macrocyclization, *Nat. Chem.* 3, 509-524.
13. Fowler, S. A., Stacy, D. M., and Blackwell, H. E. (2008) Design and Synthesis of Macrocyclic Peptomers as Mimics of a Quorum Sensing Signal from *Staphylococcus aureus*, *Org. Lett.* 10, 2329-2332.
14. Tam, J. P., and Wong, C. T. T. (2012) Chemical Synthesis of Circular Proteins, *J. Biol. Chem.* 287, 27020-27025.
15. Nathan, C., and Cars, O. (2014) Antibiotic Resistance — Problems, Progress, and Prospects, *N. Engl. J. Med.* 371, 1761-1763.
16. Antibiotic Resistance Threats in the United States, 2013, *Center for Disease Control and Prevention*, <http://www.cdc.gov/drugresistance/threat-report-2013/> (accessed July 20, 2015).
17. Rogers, H. J., and Jeljaszewicz, J. (1961) Inhibition of the biosynthesis of cell-wall mucopeptides by the penicillins. A study of penicillin-sensitive and penicillin-resistant strains of *Staphylococcus aureus*, *Biochem. J.* 81, 576-584.
18. Wilson, D. N. (2014) Ribosome-targeting antibiotics and mechanisms of bacterial resistance, *Nat. Rev. Micro.* 12, 35-48.
19. Walsh, C. (2000) Molecular mechanisms that confer antibacterial drug resistance, *Nature* 406, 775-781.
20. Levy, S. B. (1992) Active efflux mechanisms for antimicrobial resistance, *Antimicrob. Agents Chemother.* 36, 695-703.
21. Paterson, D. L., and Bonomo, R. A. (2005) Extended-Spectrum β -Lactamases: a Clinical Update, *Clin. Microbiol. Rev.* 18, 657-686.
22. Walsh, C. T., Fisher, S. L., Park, I. S., Prahalad, M., and Wu, Z. (1996) Bacterial resistance to vancomycin: five genes and one missing hydrogen bond tell the story, *Chem. Biol.* 3, 21-28.

23. Rice, L. B. (2008) Federal Funding for the Study of Antimicrobial Resistance in Nosocomial Pathogens: No ESKAPE, *J. Infect. Dis.* 197, 1079-1081.
24. Pendleton, J. N., Gorman, S. P., and Gilmore, B. F. (2013) Clinical relevance of the ESKAPE pathogens, *Expert Rev. Anti Infect. Ther.* 11, 297-308.
25. Yong, D., Toleman, M. A., Giske, C. G., Cho, H. S., Sundman, K., Lee, K., and Walsh, T. R. (2009) Characterization of a New Metallo- β -Lactamase Gene, blaNDM-1, and a Novel Erythromycin Esterase Gene Carried on a Unique Genetic Structure in *Klebsiella pneumoniae* Sequence Type 14 from India, *Antimicrob. Agents Chemother.* 53, 5046-5054.
26. Steckbeck, J. D., Deslouches, B., and Montelaro, R. C. (2014) Antimicrobial peptides: new drugs for bad bugs?, *Expert Opin. Biol. Ther.* 14, 11-14.
27. Zasloff, M. (2002) Antimicrobial peptides of multicellular organisms, *Nature* 415, 389-395.
28. Brötz, H., and Sahl, H.-G. (2000) New insights into the mechanism of action of lantibiotics—diverse biological effects by binding to the same molecular target, *J. Antimicrob. Chemother.* 46, 1-6.
29. Hancock, R. E. W., Nijnik, A., and Philpott, D. J. (2012) Modulating immunity as a therapy for bacterial infections, *Nat. Rev. Microbiol.* 10, 243-254.
30. Park, S.-C., Park, Y., and Hahm, K.-S. (2011) The Role of Antimicrobial Peptides in Preventing Multidrug-Resistant Bacterial Infections and Biofilm Formation, *Int. J. Mol. Sci.* 12, 5971.
31. Ling, L. L., Schneider, T., Peoples, A. J., Spoering, A. L., Engels, I., Conlon, B. P., Mueller, A., Schaberle, T. F., Hughes, D. E., Epstein, S., Jones, M., Lazarides, L., Steadman, V. A., Cohen, D. R., Felix, C. R., Fetterman, K. A., Millett, W. P., Nitti, A. G., Zullo, A. M., Chen, C., and Lewis, K. (2015) A new antibiotic kills pathogens without detectable resistance, *Nature* 517, 455-459.
32. Jones, R. N., and Barry, A. L. (1987) Antimicrobial activity and spectrum of LY146032, a lipopeptide antibiotic, including susceptibility testing recommendations, *Antimicrob. Agents Chemother.* 31, 625-629.
33. Tedesco, K. L., and Rybak, M. J. (2004) Daptomycin, *Pharmacotherapy* 24, 41-57.
34. Carpenter, C. F., and Chambers, H. F. (2004) Daptomycin: Another Novel Agent for Treating Infections Due to Drug-Resistant Gram-Positive Pathogens, *Clin. Infect. Dis.* 38, 994-1000.
35. Michalopoulos, A. S., and Karatza, D. C. (2010) Multidrug-resistant Gram-negative infections: the use of colistin, *Expert Rev. Anti Infec. Ther.* 8, 1009-1017.
36. Yahav, D., Farbman, L., Leibovici, L., and Paul, M. (2012) Colistin: new lessons on an old antibiotic, *Clin. Microbiol. Infec.* 18, 18-29.
37. Arnison, P. G., Bibb, M. J., Bierbaum, G., Bowers, A. A., Bugni, T. S., Bulaj, G., Camarero, J. A., Campopiano, D. J., Challis, G. L., Clardy, J., Cotter, P. D., Craik, D. J., Dawson, M., Dittmann, E., Donadio, S., Dorrestein, P. C., Entian, K.-D., Fischbach, M. A., Garavelli, J. S., Goransson, U., Gruber, C. W., Haft, D. H., Hemscheidt, T. K., Hertweck, C., Hill, C., Horswill, A. R., Jaspars, M., Kelly, W. L., Klinman, J. P., Kuipers, O. P., Link, A. J., Liu, W., Marahiel, M. A., Mitchell, D. A., Moll, G. N., Moore, B. S., Muller, R., Nair, S. K., Nes, I. F., Norris, G. E., Olivera, B. M., Onaka, H., Patchett, M. L., Piel, J., Reaney, M. J. T., Rebuffat, S., Ross, R. P., Sahl, H.-G., Schmidt, E. W., Selsted, M. E., Severinov, K., Shen, B., Sivonen, K., Smith, L., Stein, T.,

- Süssmuth, R. D., Tagg, J. R., Tang, G.-L., Truman, A. W., Vederas, J. C., Walsh, C. T., Walton, J. D., Wenzel, S. C., Willey, J. M., and van der Donk, W. A. (2013) Ribosomally synthesized and post-translationally modified peptide natural products: overview and recommendations for a universal nomenclature, *Nat. Prod. Rep.* *30*, 108-160.
38. Oman, T. J., and van der Donk, W. A. (2010) Follow the leader: the use of leader peptides to guide natural product biosynthesis, *Nat. Chem. Biol.* *6*, 9-18.
39. Velásquez, J. E., and van der Donk, W. A. (2011) Genome mining for ribosomally synthesized natural products, *Curr. Opin. Chem. Biol.* *15*, 11-21.
40. Mohimani, H., Kersten, R. D., Liu, W.-T., Wang, M., Purvine, S. O., Wu, S., Brewer, H. M., Pasa-Tolic, L., Bandeira, N., Moore, B. S., Pevzner, P. A., and Dorrestein, P. C. (2014) Automated Genome Mining of Ribosomal Peptide Natural Products, *ACS Chem. Biol.* *9*, 1545-1551.
41. Zhang, Q., Yang, X., Wang, H., and van der Donk, W. A. (2014) High Divergence of the Precursor Peptides in Combinatorial Lanthipeptide Biosynthesis, *ACS Chem. Biol.* *9*, 2686-2694.
42. Ortega, M. A., Hao, Y., Zhang, Q., Walker, M. C., van der Donk, W. A., and Nair, S. K. (2015) Structure and mechanism of the tRNA-dependent lantibiotic dehydratase NisB, *Nature* *517*, 509-512.
43. Koehnke, J., Mann, G., Bent, A. F., Ludewig, H., Shirran, S., Botting, C., Lebl, T., Houssen, W. E., Jaspars, M., and Naismith, J. H. (2015) Structural analysis of leader peptide binding enables leader-free cyanobactin processing, *Nat. Chem. Biol.* *11*, 558-563.
44. Burkhart, B. J., Hudson, G. A., Dunbar, K. L., and Mitchell, D. A. (2015) A prevalent peptide-binding domain guides ribosomal natural product biosynthesis, *Nat. Chem. Biol.* *11*, 564-570.
45. Knerr, P. J., and van der Donk, W. A. (2012) Discovery, Biosynthesis, and Engineering of Lantipeptides, *Annu. Rev. Biochem.* *81*, 479-505.
46. Zhao, M. (2011) Lantibiotics as probes for phosphatidylethanolamine, *Amino Acids* *41*, 1071-1079.
47. Lewis, R. J. (2012) Discovery and development of the χ -conopeptide class of analgesic peptides, *Toxicon* *59*, 524-528.
48. Scholz, R., Molohon, K. J., Nachtigall, J., Vater, J., Markley, A. L., Süssmuth, R. D., Mitchell, D. A., and Borriss, R. (2011) Plantazolicin, a Novel Microcin B17/Streptolysin S-Like Natural Product from *Bacillus amyloliquefaciens* FZB42, *J. Bacteriol.* *193*, 215-224.
49. Kalyon, B., Helaly, S. E., Scholz, R., Nachtigall, J., Vater, J., Borriss, R., and Süssmuth, R. D. (2011) Plantazolicin A and B: Structure Elucidation of Ribosomally Synthesized Thiazole/Oxazole Peptides from *Bacillus amyloliquefaciens* FZB42, *Org. Lett.* *13*, 2996-2999.
50. García-Reynaga, P., and VanNieuwenhze, M. S. (2008) A New Total Synthesis of Patellamide A, *Org. Lett.* *10*, 4621-4623.
51. Walsh, C. T., Acker, M. G., and Bowers, A. A. (2010) Thiazolyl Peptide Antibiotic Biosynthesis: A Cascade of Post-translational Modifications on Ribosomal Nascent Proteins, *J. Biol. Chem.* *285*, 27525-27531.
52. Hemscheidt, T. K. (2012) Chapter Two - Microviridin Biosynthesis, In *Methods Enzymol.* (Hopwood, D. A., Ed.), pp 25-35, Academic Press.

53. Shimamura, H., Gouda, H., Nagai, K., Hirose, T., Ichioka, M., Furuya, Y., Kobayashi, Y., Hirono, S., Sunazuka, T., and Ōmura, S. (2009) Structure Determination and Total Synthesis of Bottromycin A2: A Potent Antibiotic against MRSA and VRE, *Angew. Chem. Int. Ed.* *48*, 914-917.
54. Mukherjee, S., and van der Donk, W. A. (2014) Mechanistic Studies on the Substrate-Tolerant Lanthipeptide Synthetase ProcM, *J. Am. Chem. Soc.* *136*, 10450-10459.
55. Schnell, N., Entian, K.-D., Schneider, U., Gotz, F., Zahner, H., Kellner, R., and Jung, G. (1988) Prepeptide sequence of epidermin, a ribosomally synthesized antibiotic with four sulphide-rings, *Nature* *333*, 276-278.
56. Cotter, P. D., Hill, C., and Ross, R. P. (2005) Bacterial lantibiotics: strategies to improve therapeutic potential, *Curr. Prot. Pept. Sci.* *6*, 61-75.
57. van Kraaij, C., M. de Vos, W., J. Siezen, R., and P. Kuipers, O. (1999) Lantibiotics: biosynthesis, mode of action and applications, *Nat. Prod. Rep.* *16*, 575-587.
58. Férir, G., Petrova, M. I., Andrei, G., Huskens, D., Hoorelbeke, B., Snoeck, R., Vanderleyden, J., Balzarini, J., Bartoschek, S., Brönstrup, M., Süßmuth, R. D., and Schols, D. (2013) The Lantibiotic Peptide Labyrinthopeptin A1 Demonstrates Broad Anti-HIV and Anti-HSV Activity with Potential for Microbicidal Applications, *PLoS ONE* *8*, e64010.
59. Meindl, K., Schmiederer, T., Schneider, K., Reicke, A., Butz, D., Keller, S., Gühring, H., Vértesy, L., Wink, J., Hoffmann, H., Brönstrup, M., Sheldrick, G. M., and Süßmuth, R. D. (2010) Labyrinthopeptins: A New Class of Carbacyclic Lantibiotics, *Angew. Chem. Int. Ed.* *49*, 1151-1154.
60. Iorio, M., Sasso, O., Maffioli, S. I., Bertorelli, R., Monciardini, P., Sosio, M., Bonezzi, F., Summa, M., Brunati, C., Bordoni, R., Corti, G., Tarozzo, G., Piomelli, D., Reggiani, A., and Donadio, S. (2014) A Glycosylated, Labionin-Containing Lanthipeptide with Marked Antinociceptive Activity, *ACS Chem. Biol.* *9*, 398-404.
61. Willey, J. M., and Gaskell, A. A. (2010) Morphogenetic Signaling Molecules of the Streptomycetes, *Chem. Rev.* *111*, 174-187.
62. Tavassoli, A., Lu, Q., Gam, J., Pan, H., Benkovic, S. J., and Cohen, S. N. (2008) Inhibition of HIV Budding by a Genetically Selected Cyclic Peptide Targeting the Gag-TSG101 Interaction, *ACS Chem. Biol.* *3*, 757-764.
63. Lian, W., Upadhyaya, P., Rhodes, C. A., Liu, Y., and Pei, D. (2013) Screening Bicyclic Peptide Libraries for Protein-Protein Interaction Inhibitors: Discovery of a Tumor Necrosis Factor- α Antagonist, *J. Am. Chem. Soc.* *135*, 11990-11995.
64. Verdine, G. L., and Hilinski, G. J. (2012) Chapter one - Stapled Peptides for Intracellular Drug Targets, In *Methods Enzymol.* (Wittrup, K. D., and Gregory, L. V., Eds.), pp 3-33, Academic Press.
65. Walensky, L. D., Kung, A. L., Escher, I., Malia, T. J., Barbuto, S., Wright, R. D., Wagner, G., Verdine, G. L., and Korsmeyer, S. J. (2004) Activation of Apoptosis in Vivo by a Hydrocarbon-Stapled BH3 Helix, *Science* *305*, 1466-1470.
66. Millward, S. W., Fiacco, S., Austin, R. J., and Roberts, R. W. (2007) Design of Cyclic Peptides That Bind Protein Surfaces with Antibody-Like Affinity, *ACS Chem. Biol.* *2*, 625-634.
67. Passioura, T., Katoh, T., Goto, Y., and Suga, H. (2014) Selection-Based Discovery of Druglike Macrocyclic Peptides, *Annu. Rev. Biochem.* *83*, 727-752.

68. Levensgood, M. R., Knerr, P. J., Oman, T. J., and van der Donk, W. A. (2009) In vitro mutasynthesis of lantibiotic analogues containing nonproteinogenic amino acids, *J. Am. Chem. Soc.* *131*, 12024-12025.
69. Molloy, Evelyn M., Ross, R. P., and Hill, C. (2012) 'Bac' to the future: bioengineering lantibiotics for designer purposes, *Biochem. Soc. Trans.* *40*, 1492-1497.
70. Field, D., Hill, C., Cotter, P. D., and Ross, R. P. (2010) The dawning of a 'Golden era' in lantibiotic bioengineering, *Mol. Microbiol.* *78*, 1077-1087.
71. Plat, A., Kuipers, A., Rink, R., and Moll, G. N. (2013) Mechanistic aspects of lanthipeptide leaders, *Curr. Protein Pept. Sci.* *14*, 85-96.
72. Willey, J. M., and van der Donk, W. A. (2007) Lantibiotics: Peptides of Diverse Structure and Function, *Annu. Rev. Microbiol.* *61*, 477-501.
73. Chatterjee, C., Paul, M., Xie, L., and van der Donk, W. A. (2005) Biosynthesis and mode of action of lantibiotics, *Chem. Rev.* *5*, 633-684.
74. Weixin, T., and van der Donk, W. A. (2013) The sequence of the enterococcal cytolysin imparts unusual lanthionine stereochemistry, *Nat. Chem. Biol.* *9*, 157-159.
75. Müller, W. M., Schmiederer, T., Enslé, P., and Süßmuth, R. D. (2010) In Vitro Biosynthesis of the Prepeptide of Type-III Lantibiotic Labyrinthopeptin A2 Including Formation of a C-C Bond as a Post-Translational Modification, *Angew. Chem. Int. Ed.* *49*, 2436-2440.
76. Ökesli, A., Cooper, L. E., Fogle, E. J., and van der Donk, W. A. (2011) Nine Post-translational Modifications during the Biosynthesis of Cinnamycin, *J. Am. Chem. Soc.* *133*, 13753-13760.
77. Ryan, M. P., Jack, R. W., Josten, M., Sahl, H.-G., Jung, G., Ross, R. P., and Hill, C. (1999) Extensive Post-translational Modification, Including Serine to d-Alanine Conversion, in the Two-component Lantibiotic, Lacticin 3147, *J. Biol. Chem.* *274*, 37544-37550.
78. Martin, N. I., Sprules, T., Carpenter, M. R., Cotter, P. D., Hill, C., Ross, R. P., and Vederas, J. C. (2004) Structural Characterization of Lacticin 3147, a Two-Peptide Lantibiotic with Synergistic Activity, *Biochemistry.* *43*, 3049-3056.
79. Skaugen, M., Nissen-Meyer, J., Jung, G., Stevanovic, S., Sletten, K., Inger, C., Abildgaard, M., and Nes, I. F. (1994) In vivo conversion of L-serine to D-alanine in a ribosomally synthesized polypeptide, *J. Biol. Chem.* *269*, 27183-27185.
80. Velásquez, Juan E., Zhang, X., and van der Donk, Wilfred A. (2011) Biosynthesis of the Antimicrobial Peptide Epilancin 15X and Its N-Terminal Lactate, *Chem. Biol.* *18*, 857-867.
81. Foulston, L. C., and Bibb, M. J. (2010) Microbisporicin gene cluster reveals unusual features of lantibiotic biosynthesis in actinomycetes, *Proc. Natl. Acad. Sci. U.S.A.* *107*, 13461-13466.
82. Majer, F., Schmid, D. G., Altena, K., Bierbaum, G., and Kupke, T. (2002) The Flavoprotein MrsD Catalyzes the Oxidative Decarboxylation Reaction Involved in Formation of the Peptidoglycan Biosynthesis Inhibitor Mersacidin, *J. Bacteriol.* *184*, 1234-1243.
83. Garg, N., Salazar-Ocampo, L. M. A., and van der Donk, W. A. (2013) In vitro activity of the nisin dehydratase NisB, *Proc. Natl. Acad. Sci. U.S.A.* *110*, 7258-7263.

84. Li, B., Yu, J. P. J., Brunzelle, J. S., Moll, G. N., van der Donk, W. A., and Nair, S. K. (2006) Structure and Mechanism of the Lantibiotic Cyclase Involved in Nisin Biosynthesis, *Science* 311, 1464-1467.
85. Hightower, K. E., and Fierke, C. A. (1999) Zinc-catalyzed sulfur alkylation: insights from protein farnesyltransferase, *Curr. Opin. Chem. Biol.* 3, 176-181.
86. Kuipers, A., de Boef, E., Rink, R., Fekken, S., Kluskens, L. D., Driessen, A. J. M., Leenhouts, K., Kuipers, O. P., and Moll, G. N. (2004) NisT, the Transporter of the Lantibiotic Nisin, Can Transport Fully Modified, Dehydrated, and Unmodified Prenisin and Fusions of the Leader Peptide with Non-lantibiotic Peptides, *J. Biol. Chem.* 279, 22176-22182.
87. Chatterjee, C., Miller, L. M., Leung, Y. L., Xie, L., Yi, M., Kelleher, N. L., and van der Donk, W. A. (2005) Lacticin 481 Synthetase Phosphorylates its Substrate during Lantibiotic Production, *J. Am. Chem. Soc.* 127, 15332-15333.
88. Paul, M., Patton, G. C., and van der Donk, W. A. (2007) Mutants of the Zinc Ligands of Lacticin 481 Synthetase Retain Dehydration Activity but Have Impaired Cyclization Activity, *Biochemistry.* 46, 6268-6276.
89. Goto, Y., Ökesli, A., and van der Donk, W. A. (2011) Mechanistic Studies of Ser/Thr Dehydration Catalyzed by a Member of the LanL Lanthionine Synthetase Family, *Biochemistry.* 50, 891-898.
90. Goto, Y., Li, B., Claesen, J., Shi, Y., Bibb, M. J., and van der Donk, W. A. (2010) Discovery of Unique Lanthionine Synthetases Reveals New Mechanistic and Evolutionary Insights, *PLoS Biol.* 8, e1000339.
91. Islam, Mohammad R., Nagao, J.-i., Zendo, T., and Sonomoto, K. (2012) Antimicrobial mechanism of lantibiotics, *Biochem. Soc. Trans.* 40, 1528-1533.
92. Bierbaum, G., and Sahl, H. G. (2009) Lantibiotics: Mode of Action, Biosynthesis and Bioengineering, *Current Pharm. Biotechnol.* 10, 2-18.
93. Van Den Hooven, H. W., Doeland, C. C. M., Van De Kamp, M., Konings, R. N. H., Hilbers, C. W., and Van De Ven, F. J. M. (1996) Three-Dimensional Structure of the Lantibiotic Nisin in the Presence of Membrane-Mimetic Micelles of Dodecylphosphocholine and of Sodium Dodecylsulphate, *Eur. J. Biochem.* 235, 382-393.
94. Hsu, S.-T. D., Breukink, E., Tischenko, E., Lutters, M. A. G., de Kruijff, B., Kaptein, R., Bonvin, A. M. J. J., and van Nuland, N. A. J. (2004) The nisin-lipid II complex reveals a pyrophosphate cage that provides a blueprint for novel antibiotics, *Nat. Struct. Mol. Biol.* 11, 963-967.
95. Wiedemann, I., Breukink, E., van Kraaij, C., Kuipers, O. P., Bierbaum, G., de Kruijff, B., and Sahl, H.-G. (2001) Specific Binding of Nisin to the Peptidoglycan Precursor Lipid II Combines Pore Formation and Inhibition of Cell Wall Biosynthesis for Potent Antibiotic Activity, *J. Biol. Chem.* 276, 1772-1779.
96. Hasper, H. E., Kruijff, B. d., and Breukink, E. (2004) Assembly and Stability of Nisin-Lipid II Pores, *Biochemistry.* 43, 11567-11575.
97. Hsu, S.-T., Breukink, E., de Kruijff, B., Kaptein, R., Bonvin, A. M. J. J., and van Nuland, N. A. J. (2002) Mapping the Targeted Membrane Pore Formation Mechanism by Solution NMR: The Nisin Z and Lipid II Interaction in SDS Micelles, *Biochemistry.* 41, 7670-7676.

98. Kruszewska, D., Sahl, H.-G., Bierbaum, G., Pag, U., Hynes, S. O., and Ljungh, Å. (2004) Mersacidin eradicates methicillin-resistant *Staphylococcus aureus* (MRSA) in a mouse rhinitis model, *J. Antimicrob. Chemother.* *54*, 648-653.
99. Brötz, H., Bierbaum, G., Reynolds, P. E., and Sahl, H.-G. (1997) The Lantibiotic Mersacidin Inhibits Peptidoglycan Biosynthesis at the Level of Transglycosylation, *Eur. J. Biochem.* *246*, 193-199.
100. Brötz, H., Bierbaum, G., Leopold, K., Reynolds, P. E., and Sahl, H.-G. (1998) The Lantibiotic Mersacidin Inhibits Peptidoglycan Synthesis by Targeting Lipid II, *Antimicrob. Agents Chemother.* *42*, 154-160.
101. Knerr, P. J., Oman, T. J., Garcia De Gonzalo, C. V., Lupoli, T. J., Walker, S., and van der Donk, W. A. (2012) Non-proteinogenic Amino Acids in Lactacin 481 Analogues Result in More Potent Inhibition of Peptidoglycan Transglycosylation, *ACS Chem. Biol.* *7*, 1791-1795.
102. Szekat, C., Jack, R. W., Skutlarek, D., Färber, H., and Bierbaum, G. (2003) Construction of an Expression System for Site-Directed Mutagenesis of the Lantibiotic Mersacidin, *Appl. Environ. Microbiol.* *69*, 3777-3783.
103. Wakamatsu, K., Choung, S. Y., Kobayashi, T., Inoue, K., Higashijima, T., and Miyazawa, T. (1990) Complex formation of peptide antibiotic Ro09-0198 with lysophosphatidylethanolamine: proton NMR analyses in dimethyl sulfoxide solution, *Biochemistry.* *29*, 113-118.
104. Makino, A., Baba, T., Fujimoto, K., Iwamoto, K., Yano, Y., Terada, N., Ohno, S., Sato, S. B., Ohta, A., Umeda, M., Matsuzaki, K., and Kobayashi, T. (2003) Cinnamycin (Ro 09-0198) Promotes Cell Binding and Toxicity by Inducing Transbilayer Lipid Movement, *J. Biol. Chem.* *278*, 3204-3209.
105. Breukink, E. (2006) A lesson in efficient killing from two-component lantibiotics, *Mol. Microbiol.* *61*, 271-273.
106. Wiedemann, I., Böttiger, T., Bonelli, R. R., Wiese, A., Hagge, S. O., Gutschmann, T., Seydel, U., Deegan, L., Hill, C., Ross, P., and Sahl, H.-G. (2006) The mode of action of the lantibiotic lactacin 3147 – a complex mechanism involving specific interaction of two peptides and the cell wall precursor lipid II, *Mol. Microbiol.* *61*, 285-296.
107. Cotter, P. D., Deegan, L. H., Lawton, E. M., Draper, L. A., O'Connor, P. M., Hill, C., and Ross, R. P. (2006) Complete alanine scanning of the two-component lantibiotic lactacin 3147: generating a blueprint for rational drug design, *Mol. Microbiol.* *62*, 735-747.
108. Cox, C. R., Coburn, P. S., and Gilmore, M. S. (2005) Enterococcal Cytolysin: A Novel Two Component Peptide System that Serves as a Bacterial Defense Against Eukaryotic and Prokaryotic Cells, *Curr. Protein Pept. Sci.* *6*, 77-84.
109. Kodani, S., Lodato, M. A., Durrant, M. C., Picart, F., and Willey, J. M. (2005) SapT, a lanthionine-containing peptide involved in aerial hyphae formation in the streptomycetes, *Mol. Microbiol.* *58*, 1368-1380.
110. Tillotson, R. D., Wösten, H. A. B., Richter, M., and Willey, J. M. (1998) A surface active protein involved in aerial hyphae formation in the filamentous fungus *Schizophillum commune* restores the capacity of a bald mutant of the filamentous bacterium *Streptomyces coelicolor* to erect aerial structures, *Mol. Microbiol.* *30*, 595-602.

CHAPTER 2: MECHANISTIC INVESTIGATION OF THE SUBSTRATE-TOLERANT LANTHIPEPTIDE SYNTHETASE PROC^M†

2.1. INTRODUCTION

Prochlorosins are a large group of lanthipeptides produced by marine cyanobacteria of the genus *Prochlorococcus*. In *Prochlorococcus* MIT9313, a single enzyme, ProcM, catalyzes the post-translational modification of 30 different substrates (ProcAs), thereby generating many distinct thioether ring topologies within the 30 prochlorosin products (Pcns, Figure 2.1) (2). As such, the Pcn biosynthetic system is intriguing with respect to the details of thioether ring formation that may explain the remarkable diversity of the products formed by ProcM. A previous study suggested that the enzyme might generate a subset of the thioether rings, which would then preorganize the substrate to facilitate non-enzymatic cyclization of the other rings (3), as illustrated schematically for a substrate with two thioether rings (Scheme 2.1). Investigation of the stereochemistry of the thioether rings in a subset of Pcns showed that they all had the DL stereochemistry (2*S*,6*R*-Lan and 2*S*,3*S*,6*R*-MeLan) (4), identical to what has been observed for the majority of lanthipeptides analyzed to date (5). Though this conserved stereochemistry of Michael-type addition suggested enzymatic cyclization, non-enzymatic cyclization of preorganized intermediates with high stereoselectivity could not be ruled out because in previous biomimetic studies of lanthipeptide biosynthesis, non-enzymatic cyclization also took place with high selectivity for the DL stereoisomers (6-8). In this study, I experimentally probed a potential role of non-enzymatic cyclization in prochlorosin maturation.

† Reproduced in part with permission from:

1. Mukherjee, S., and van der Donk, W. A. (2014) Mechanistic Studies on the Substrate-Tolerant Lanthipeptide Synthetase ProcM, *J. Am. Chem. Soc.* 136, 10450-10459. Copyright 2014 American Chemical Society.
2. Yu, Y., Mukherjee, S., and van der Donk, W. A. (2015) Product Formation by the Promiscuous Lanthipeptide Synthetase ProcM is under Kinetic Control, *ibid.* 137, 5140-5148. Copyright 2015 American Chemical Society.

The substrate-tolerant synthetase ProcM dehydrates core peptides containing a variety of sequences with different residues flanking Ser and Thr and also with different numbers of intervening residues (Figure 2.1). At the start of these studies, it was not known whether ProcM dehydrates its substrates in a directional fashion and whether any observed directionality is general for different substrates. In this work, I expanded upon a previously reported strategy (9) to assign the directionality of dehydration of substrates by ProcM. Additional experiments also revealed the order of ProcM-catalyzed cyclization of these substrates.

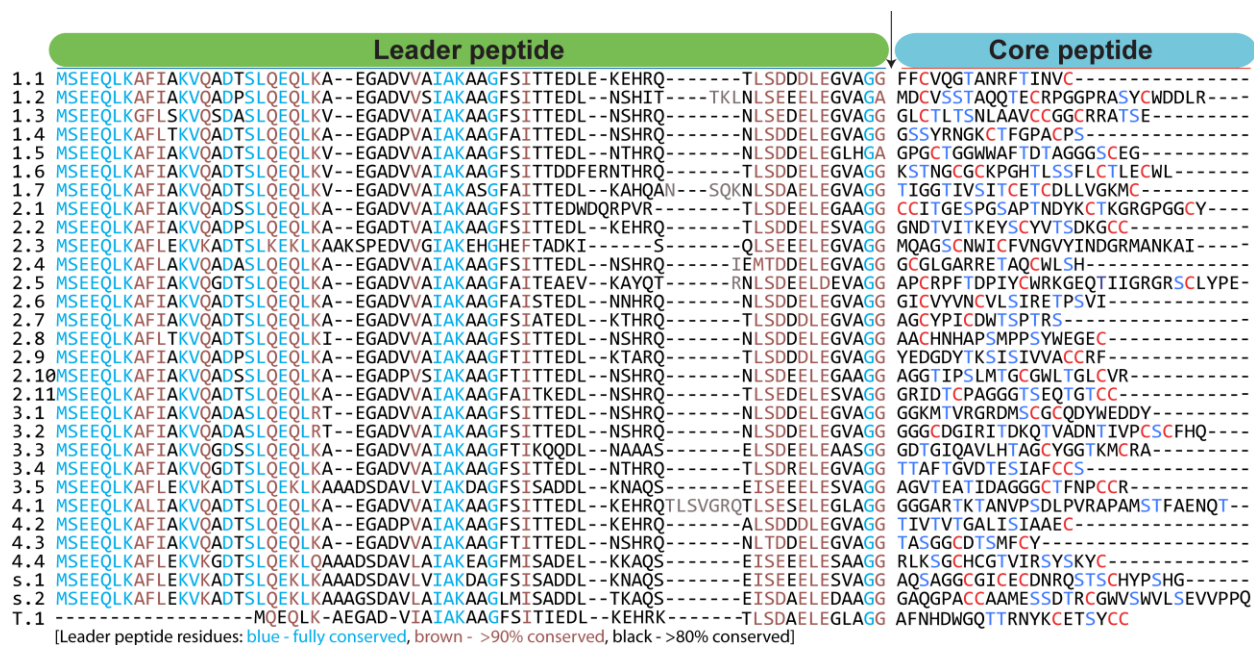
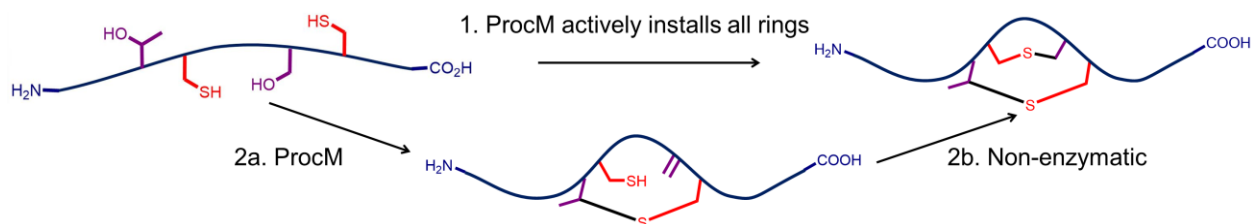


Figure 2.1. Sequences of 30 precursor peptides encoded by the genome of *Prochlorococcus* MIT 9313. Highly conserved leader peptide and diverse core peptides are presented. Of the 30 precursor peptides, the 18 investigated are all substrates of ProcM (3, 4, 10).

In the 30 prochlorosins with diverse ring topologies produced by ProcM, often a single ring structure out of several possible topologies is observed (Figure 2.2) (3, 4). The observed high site-selectivity in prochlorosin cyclization could be the result of either thermodynamic or kinetic control. Thermodynamic control would require the reversible installation of thioether rings, which ultimately results in the ring topology with the lowest free energy. On the other

hand, kinetic control would lead to thioether ring formation involving the lowest activation energy barrier. A previous study on the biomimetic cyclization of nisin's B-ring suggested that non-enzymatic thioether ring formation is governed by kinetic control and that the Michael-type addition is irreversible (11). We investigated the reversibility of cyclization in the presence of ProcM in the two studies that are summarized in this chapter (1, 2).



Scheme 2.1. Scheme showing enzymatic vs. non-enzymatic cyclization during prochlorosin maturation. Either all the thioether rings are installed by active participation of ProcM (1) or ProcM installs a subset of rings (2a) and pre-organizes the substrate for non-enzymatic cyclization (2b).

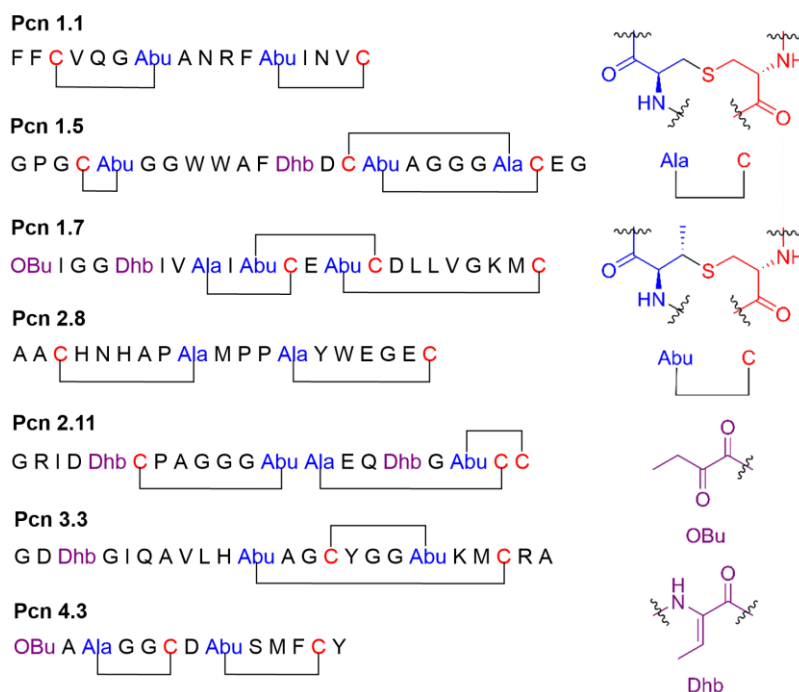


Figure 2.2. Structures of several representative prochlorosins after maturation show the diverse ring topologies. Portions of Lan/MeLan residues arising from Ser/Thr are shown in blue, and that derived from Cys is shown in red; dehydrated residues and residue after hydrolysis of N-terminal dehydrobutyrine in purple.

ProcM is highly selective for the formation of one product from each substrate peptide, despite their highly diverse sequences. The juxtaposition of high-substrate tolerance and product selectivity was investigated in a collaborative work with Dr. Yi Yu, a doctoral graduate student in biochemistry at UIUC (2). The cyclase domain of LanM shows homology to LanC of class I systems with an active site Zn(II) ligated by one His and two Cys. However, ProcM has three Cys as predicted ligands for Zn(II), and ProcM forms a distinct clade in the phylogenetic tree of class II LanM synthetases along with other ProcM homologues containing three Zn(II) binding Cys (12). Previous studies with other enzymes and model organometallic complexes have indicated that additional sulfur-based ligands increase the reactivity of Zn(II)-bound thiolates (13-17). The importance of the three Zn(II) bound Cys ligands towards the substrate-tolerance and the selectivity of product-formation of ProcM was explored in the current work.

2.2. RESULTS AND DISCUSSION

2.2.1. Choice of Substrates to Study ProcM

Two core peptides were chosen for investigation out of the repertoire of 30 possible substrates. The first choice was ProcA2.8, which is transformed into prochlorosin (Pcn) 2.8, a product with two non-overlapping lanthionine rings (Figure 2.3). In the majority of the lanthipeptides discovered to date, the thioether rings are installed by nucleophilic attack of cysteines onto dehydrated residues that are located toward the N-terminus. However, in prochlorosins, the thioether rings are formed by Cys residues located on either side of the dehydrated residues, as illustrated for Pcn2.8 generated from ProcA2.8. Thus, studies with Pcn2.8 could reveal whether perhaps enzymatic cyclization forms rings in one direction and nonenzymatic cyclization forms thioether rings in the opposite direction. In addition, we selected

Pcn3.3, a compound containing overlapping thioether rings, to probe the effect of substrate preorganization on non-enzymatic ring formation (Figure 2.3). As described below, for both substrates, we determined the order of dehydration and cyclization and investigated the possibility of non-enzymatic cyclization and reversibility as determinants of the ring topology.

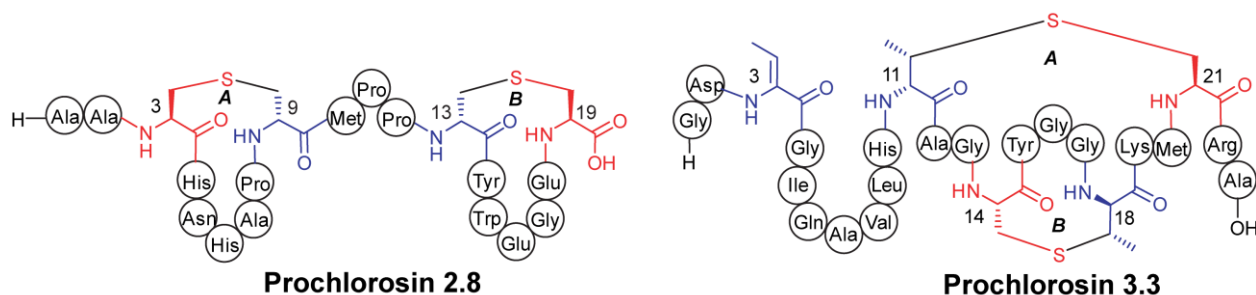


Figure 2.3. Structures of prochlorosins 2.8 and 3.3. The portion of the Lan/MeLan residues originating from Cys are in red, and those originating from Ser/Thr residues are in blue.

2.2.2. ProcM Dehydrates the ProcA2.8 Precursor Peptide in C-to-N-Terminal Fashion

Previous studies on LanM lanthipeptide synthetases showed that dehydration is directional, moving from the N-terminus to the C-terminus of the substrate (18). To investigate whether this would also be the case for the substrate-tolerant ProcM, we used the method developed by Süßmuth and co-workers (9), in which specific Ser residues are replaced by 2,3,3-deuterium-labeled serine. In such substrates, dehydration of unlabeled Ser involves loss of 18 Da ($-\text{H}_2\text{O}$) while dehydration of the labeled serine results in loss of 19 Da ($-\text{HDO}$; Figure 2.4).

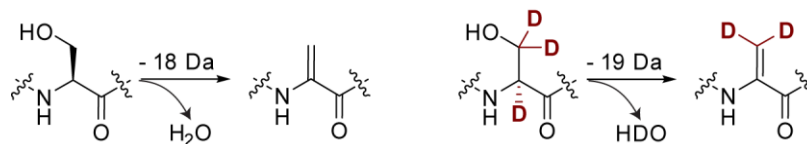
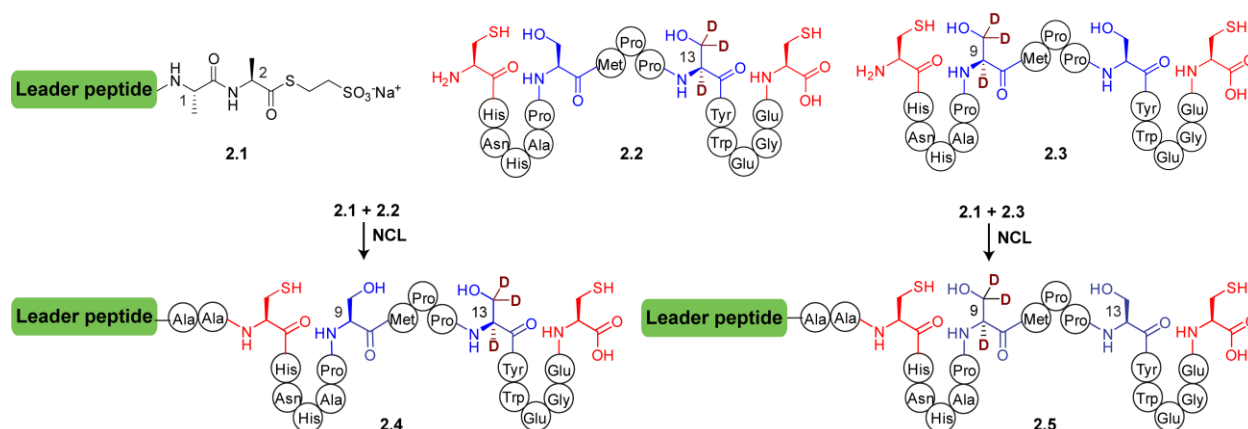


Figure 2.4. Strategy for determination of directionality of dehydration using [2,3,3- ^2H]-Ser residues. Dehydration of Ser incurs a loss of 18 Da, while dehydration of labeled Ser results in a loss of 19 Da (9).

The lanthipeptide synthetase ProcM requires an N-terminal leader peptide for maturation of the precursor peptide (3). The highly conserved leader peptide is ca. 65 amino acid residues

long, and the highly variable core peptides comprise between 13 and 32 amino acid residues (Figure 2.1), resulting in a precursor peptide that is too long to prepare conveniently by linear solid phase peptide synthesis (SPPS). Instead, we used expressed protein ligation (EPL) (19) to generate full-length precursor peptides containing deuterium labeled serine. The ProcA2.8 core peptide has a cysteine at position 3 that can be used for EPL. Peptide **2.1** corresponding to the ProcA2.8 leader peptide with two additional Ala residues from the N-terminus of the ProcA2.8 core peptide was generated with a peptide thioester at the C-terminus using intein chemistry[‡]. Two ProcA2.8 core peptides **2.2** and **2.3** spanning residues 3–19 were synthesized by SPPS with Ser13 or Ser9 replaced with 2,3,3-deuterium-labeled Ser. Native chemical ligation (NCL) of **2.2** and **2.3** with **2.1** afforded the substrates **2.4** and **2.5**, respectively (Scheme 2.2).



Scheme 2.2. Scheme showing the generation of ProcA2.8 analogues by NCL, used to determine the directionality of dehydration. Drawn are ProcA2.8 leader-AA-MESNa thioester (**2.1**), ProcA2.8 core peptide Δ 1-2 with Ser13 replaced with [2,3,3-²H]-Ser (**2.2**), and ProcA2.8 core peptide Δ 1-2 with Ser9 replaced with [2,3,3-²H]-Ser (**2.3**). Separate NCLs of peptide **2.1** with peptides **2.2** and **2.3** generated peptides **2.4** and **2.5**, respectively.

[‡] The plasmid pTXB1 encoding the ProcA2.8 leader-AlaAla fused to intein-CBD was provided by Dr. Christopher Thibodeaux, Institute of Genomic Biology, UIUC.

These substrates were treated with ProcM, and after various time points, ProcM was removed from a portion of the assay by ultrafiltration. The filtrate was incubated with endoproteinase GluC to remove most of the leader peptide, and the digest was analyzed by matrix-assisted laser desorption/ionization time-of-flight (MALDI-TOF) and electrospray ionization (ESI) mass spectrometry. With both substrates, the ESI and MALDI-TOF mass spectrometric analyses showed that Ser13 was dehydrated prior to Ser9 (Figure 2.5, MALDI-TOF MS data shown).

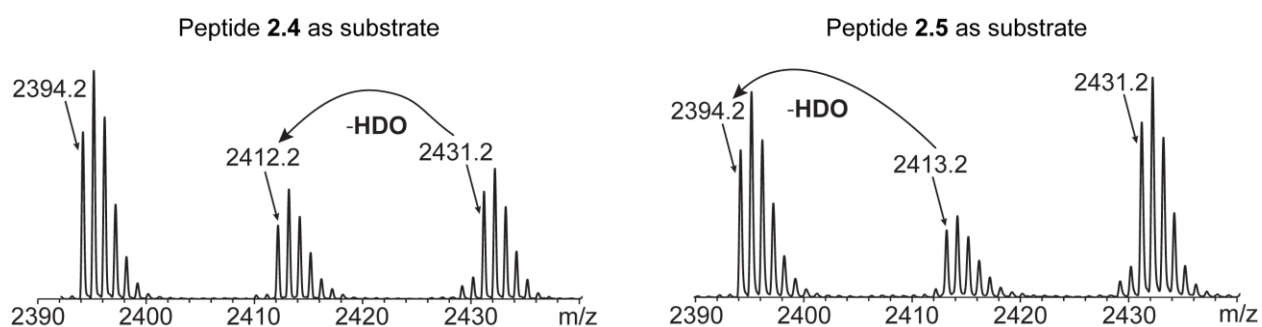
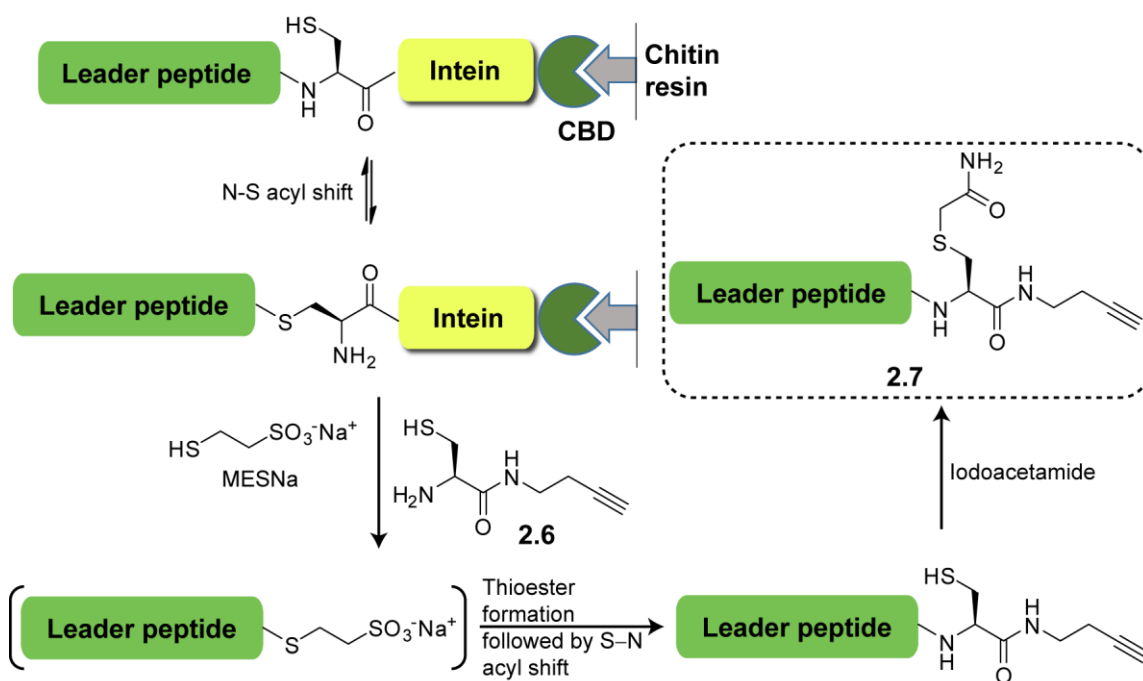


Figure 2.5. MALDI-TOF MS of peptides **2.4** and **2.5** obtained after partial dehydration by ProcM, followed by digestion with endoprotease, GluC.

Although EPL worked well to determine the directionality of dehydration of ProcA2.8, other substrates do not always have a conveniently located Cys. Hence, we evaluated another hybrid ligation strategy based on both EPL and copper-catalyzed alkyne–azide cycloaddition (CuAAC) (20, 21). In previous studies on lactacin 481 synthetase, an alkyne-containing leader peptide was generated by chemical synthesis (22, 23), but in this work, we elected to generate the much longer ProcA leader peptide by heterologous expression in *Escherichia coli* as a fusion protein to an intein and chitin-binding domain (24). Given the high-sequence similarity of the leader peptides of prochlorosin precursors (Figure 2.1), the ProcA3.2 leader peptide was arbitrarily chosen for the designed precursor peptides. The C-terminal Gly of the ProcA3.2 leader peptide was mutated to Lys to allow efficient cleavage of the peptide thioester linkage to

the chitin resin by 2-mercaptoethanesulfonate sodium salt (MESNa) (25), and to introduce a LysC endoproteinase cleavage site C-terminal to the leader peptide. EPL of the MES-thioester with (*R*)-2-amino-*N*-(but-3-yn-1-yl)-3-mercaptopropionamide (compound **2.6**, Scheme 2.3) generated the leader peptide with a C-terminal alkyne modification. The cysteine residue incorporated during EPL was protected with iodoacetamide to prevent any potential interference in the enzymatic cyclization reaction (peptide **2.7**, Scheme 2.3).



Scheme 2.3. Scheme for generation of ProcA leader peptide with a C-terminal alkyne. The leader peptide was expressed as a fusion protein with an intein and chitin binding domain at its C-terminus. Chitin resin was used to affinity purify the fusion protein, which was cleaved from the resin by transthioesterification with MESNa. The C-terminal MESNa thioester of the leader peptide formed in-situ reacted with compound **2.6** (expressed protein ligation) to generate the leader peptide with a C-terminal alkyne. The introduced cysteine was capped with iodoacetamide to generate peptide **2.7**.

The core peptides of ProcA2.8 were then synthesized by SPPS, again incorporating deuterium-labeled Ser at positions 9 and 13. In the last step prior to cleaving the peptides from the resin, the CuAAC ligation handles **2.8** or **2.9** (Figure 2.6) were coupled to their N-termini.

The building block **2.8** was expected to improve the efficiency of the ligation owing to the copper ligating ability of the pyridine ligand (26), whereas building block **2.9** would enable convenient removal of the leader peptide by photolysis (27). Two ProcA2.8 precursor peptides **2.10** and **2.11** were thus synthesized by CuAAC to probe directionality of dehydration (Figure 2.6). The substrates were treated with ProcM, and at several time points, ProcM was removed from a portion of the assay by ultrafiltration; the filtrate was incubated with protease LysC and the digest analyzed by MALDI-TOF MS. With both substrates **2.10** and **2.11**, the analysis showed that Ser13 was dehydrated prior to Ser9, indicating C-to-N-terminal dehydration (Figure 2.7). This observation demonstrated that the presence of a triazole linker in the designed substrate did not affect the directionality of dehydration. Furthermore, GC-MS analysis of the product revealed the presence of Lan rings of the same DL stereochemistry as in the wild-type (WT) product (Figure 2.8), thus suggesting that ProcM correctly recognizes the substrate with a triazole linker between leader and core peptides. The observation that the substrate analogue generated by CuAAC furnished the same product and with the same directionality as with native substrate enabled us to extend our investigation of directionality of dehydration to other substrates where the sequence of the core peptide does not allow EPL to assemble the native precursor peptide.

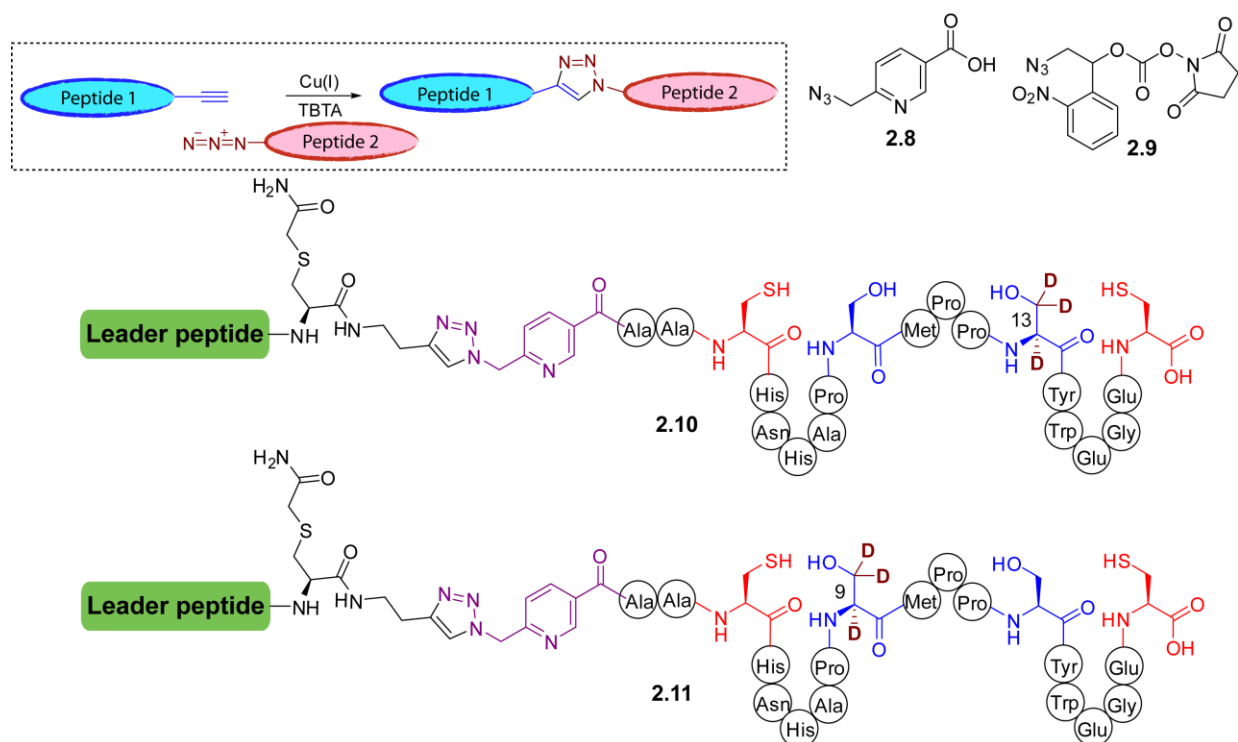


Figure 2.6. CuAAC-generic reaction, and synthesis of peptides **2.10** and **2.11**. Copper catalyzed azide–alkyne cycloaddition is generically drawn in the box. Building block **2.8** was used to facilitate the click reaction via a copper-chelating group, and compound **2.9** was used for installation of a photocleavable triazole linker between the leader and the core peptides. Also shown are the structures of ProcA2.8 precursor peptides obtained by CuAAC, **2.10** and **2.11**, with Ser13 or Ser9 replaced with [2,3,3-²H]-Ser, respectively.

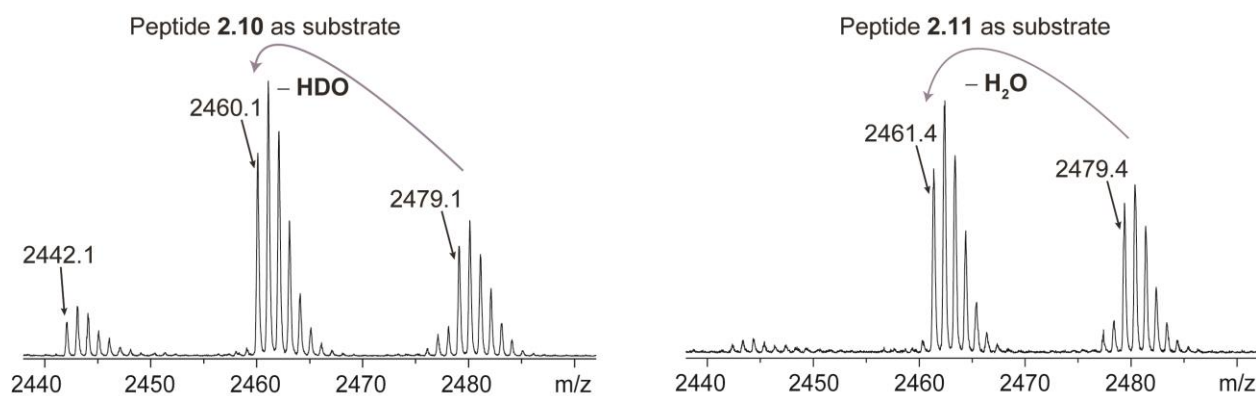


Figure 2.7. MALDI-TOF MS of peptides **2.10** and **2.11** obtained after partial dehydration by ProcM, followed by digestion with endoprotease, LysC.

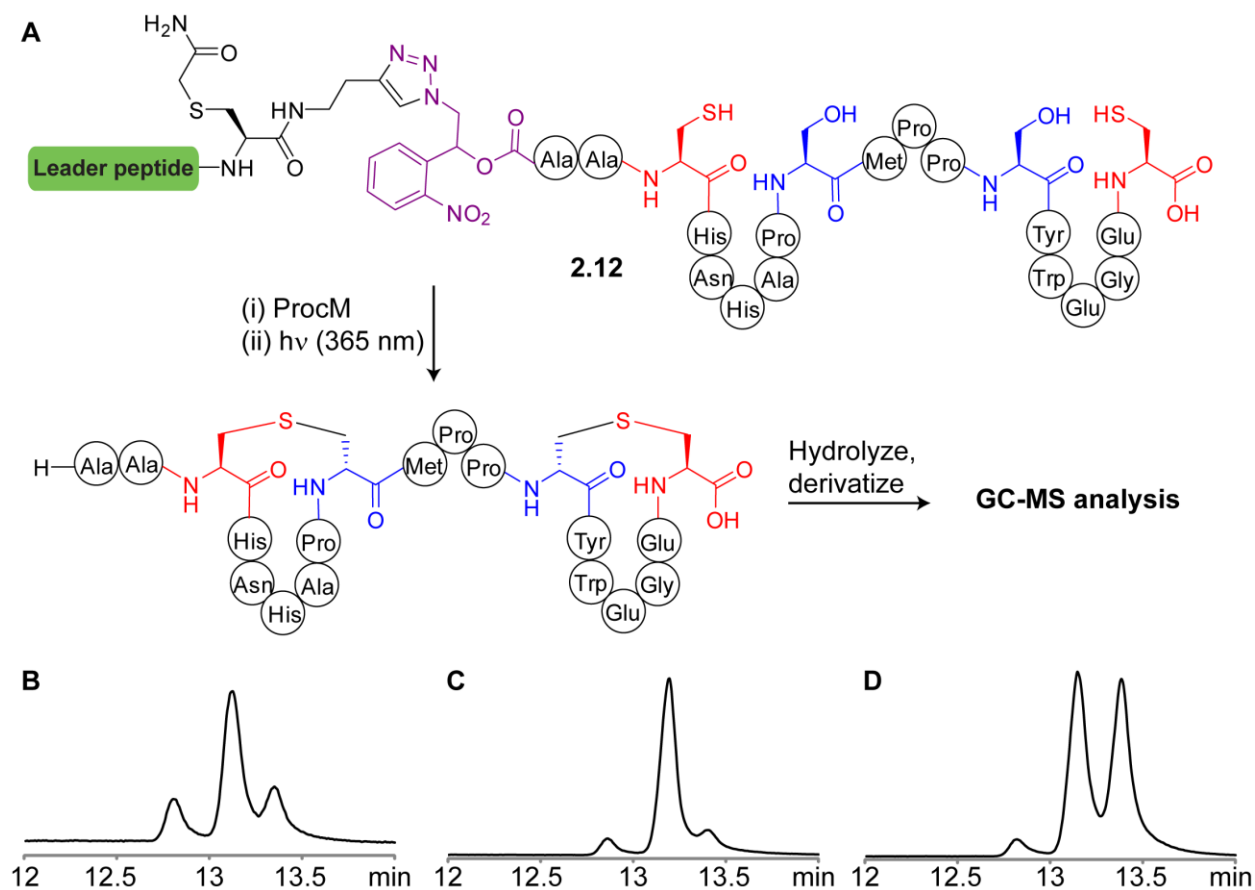


Figure 2.8. GC-MS analysis of a triazole linked peptide. (A) Peptide **2.12** was modified by ProcM, photocleaved, hydrolyzed in acid and the resulting amino acids were derivatized as reported previously (also as previously reported, this procedure leads to partial epimerization of Lan) (4). The derivatized material was analyzed by GC-MS using a chiral stationary phase as previously reported (4). Selected ion mode (SIM) trace for Lan ($m = 365$) of (B) ProcM-modified ProcA2.8 core (C) modified ProcA2.8 core spiked with synthetic DL-Lan standard, and (D) modified ProcA2.8 core spiked with synthetic DL-Lan and LL-Lan standards.

2.2.3. ProcM Dehydrates ProcA3.3 Precursor Peptide in C-to-N-Terminal Fashion

To probe directionality of dehydration in prochlorosins containing threonine residues and overlapping rings, we prepared the ProcA3.3 derivatives **2.13** and **2.14** with either Thr18 or Thr11 replaced with [2,3- ^2H]-Thr, respectively (Figure 2.9A). The peptides were treated with ProcM and after various time points, the enzyme was removed by ultrafiltration. The filtrate was incubated with endoproteinase GluC to remove most of the leader peptide, and the digest was

analyzed by MALDI-TOF MS. The data demonstrated that Thr18 was dehydrated first followed by Thr11 and Thr3 (Figure 2.9B), in agreement with the overall C-to-N-terminal dehydration observed with ProcA2.8. To confirm that the observed directionality of dehydration of WT-ProcA3.3 was the same as that of the analogues **2.13** and **2.14**, tandem MS was used to analyze partially dehydrated WT-ProcA3.3. The order of dehydration of Thr11 and Thr18 cannot be distinguished by this method because of the overlapping rings of Pcn3.3, but the timing of dehydration of Thr3 can be determined. Using ultraperformance liquid chromatography (UPLC) coupled with ESI-MS, peptide ions with predominantly two-fold dehydration were analyzed (Figure 2.10A). The ion was fragmented, and the observed fragment ions demonstrated that Thr3 escaped dehydration in the two-fold dehydrated ProcA3.3 (Figure 2.10B), in agreement with the conclusion that we reached from studies on the triazole-containing ProcA3.3 precursor peptide (i.e., Thr3 is dehydrated last).

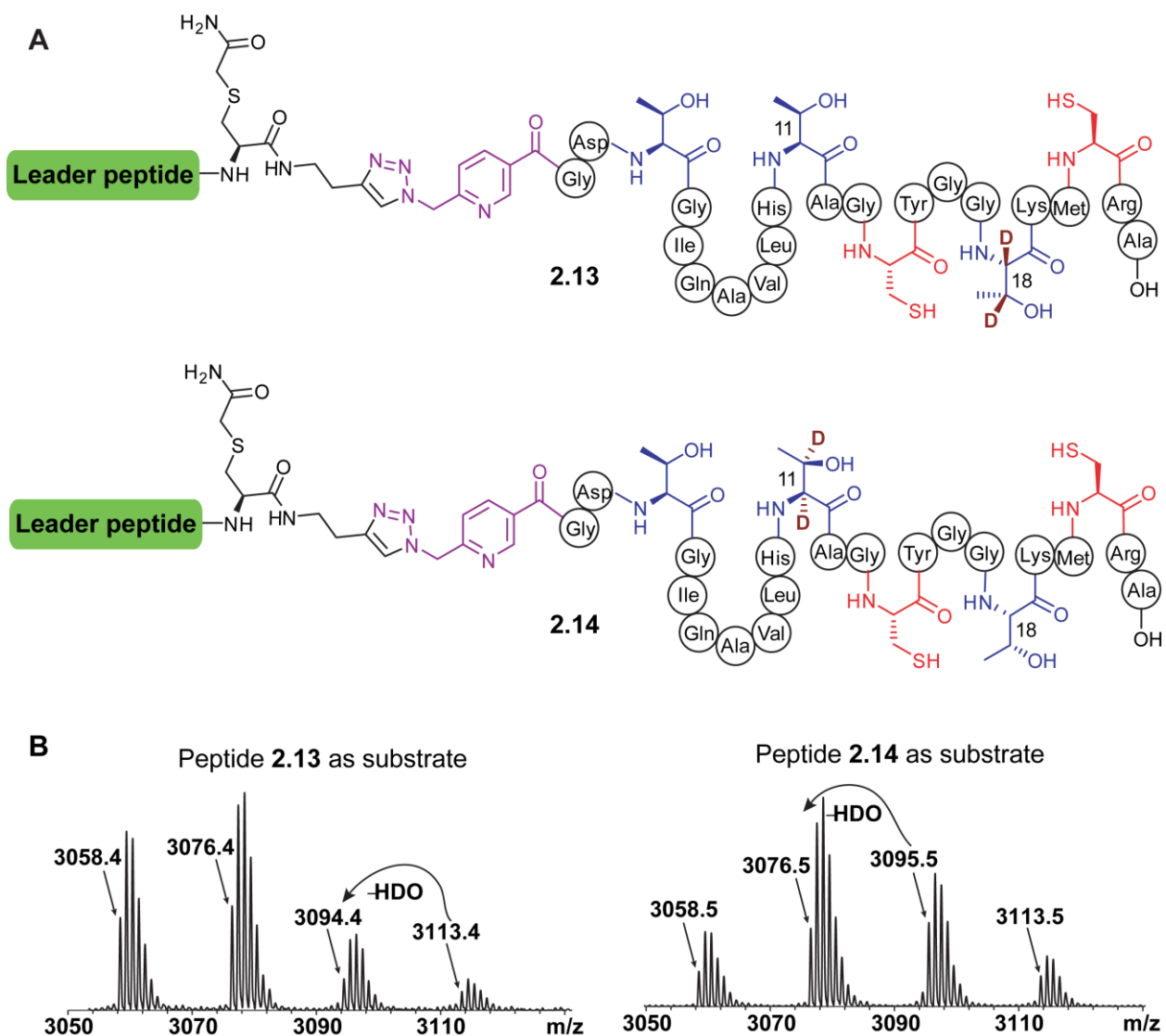


Figure 2.9. Directionality of dehydration of ProcA3.3 analogues containing a triazole linker. (A) Structures of ProcA3.3 analogues **2.13** and **2.14**, with either Thr18 or Thr11 replaced with [2,3- ^2H]-Thr, respectively. (B) MALDI-TOF MS spectra of peptides **2.13** and **2.14** partially dehydrated by ProcM and digested by GluC.

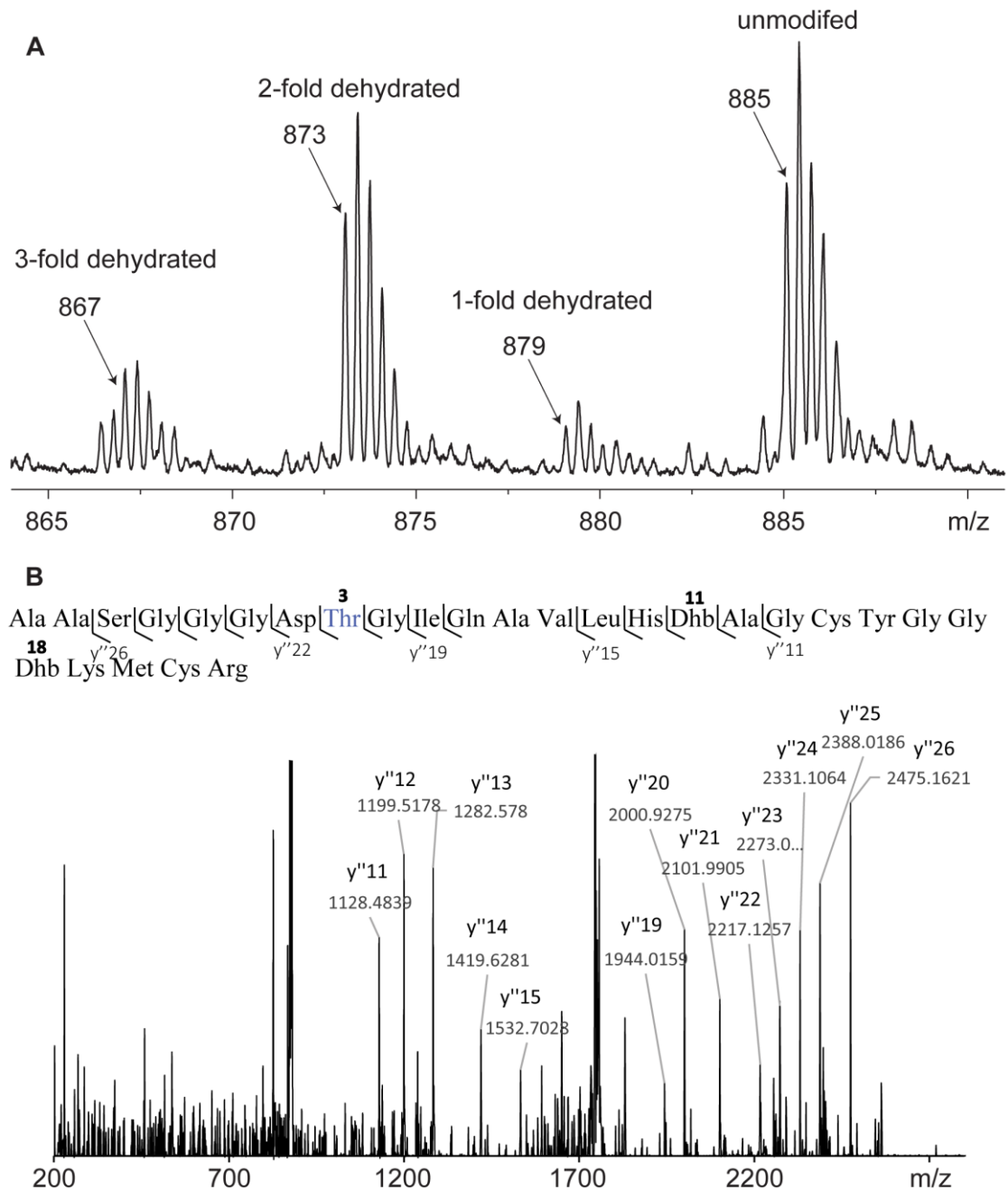


Figure 2.10. Tandem MS of partially dehydrated WT-ProcA3.3 peptide to confirm C-to-N-terminal directionality. (A) ESI-MS on WT-ProcA3.3 to trap partially dehydrated species generated by treating WT-ProcA3.3 precursor (100 μ M), and ProcM (2 μ M) using the standard ProcM assay conditions for 5 min at room temperature, after which ProcM was removed by ultrafiltration (14,000 \times g, 10 min) through Amicon Ultra 50 kDa MWCO filters. The assay contents were digested with GluC prior to MS analysis. The 3⁺ charged species are presented. (B) Tandem MS analysis on two-fold dehydrated species of m/z 873 (3⁺ charged). Thr3 that escapes dehydration is labeled in blue.

2.2.4. Directionality of Cyclization by ProcM

ProcM was incubated with expressed and purified His₆-ProcA2.8 obtained as reported previously (3), and the assay was quenched by removing ProcM at various time points. After incubation with endoproteinase LysC to remove most of the leader peptide, the digest was treated with iodoacetamide (IAA). Any noncyclized thiol would react with IAA, and the enzymatic assay conditions were optimized to allow buildup of an incompletely cyclized intermediate that resulted in one IAA adduct (Figure 2.11A). ESI-MS/MS was performed on this peptide, and Cys3 was found to be alkylated (Figure 2.11B). The fragmentation pattern suggested that the B-ring had formed in this intermediate. Hence, cyclization of Cys19 occurred prior to Cys3, suggesting C-to-N-terminal directionality of cyclization.

ProcM was also incubated with His₆-ProcA3.3, and the assay was quenched by removing ProcM at various time points. After endoproteinase LysC digestion, the peptides were treated with IAA. The ProcM assay conditions were again optimized to trap an intermediate that resulted in one IAA adduct (Figure 2.12A). The observed fragmentation pattern of this peptide by ESI-MS/MS showed that Cys21 was alkylated, suggesting that Cys14 had formed a thioether ring with Dhb18 (Figure 2.12B). The data suggest that cyclization of ProcA3.3 may not take place with C-to-N-terminal directionality, but that instead the MeLan ring between Cys14 and Dhb18 is formed in the monocyclic intermediate (see Figure 2.3 for the Pcn3.3 ring topology).

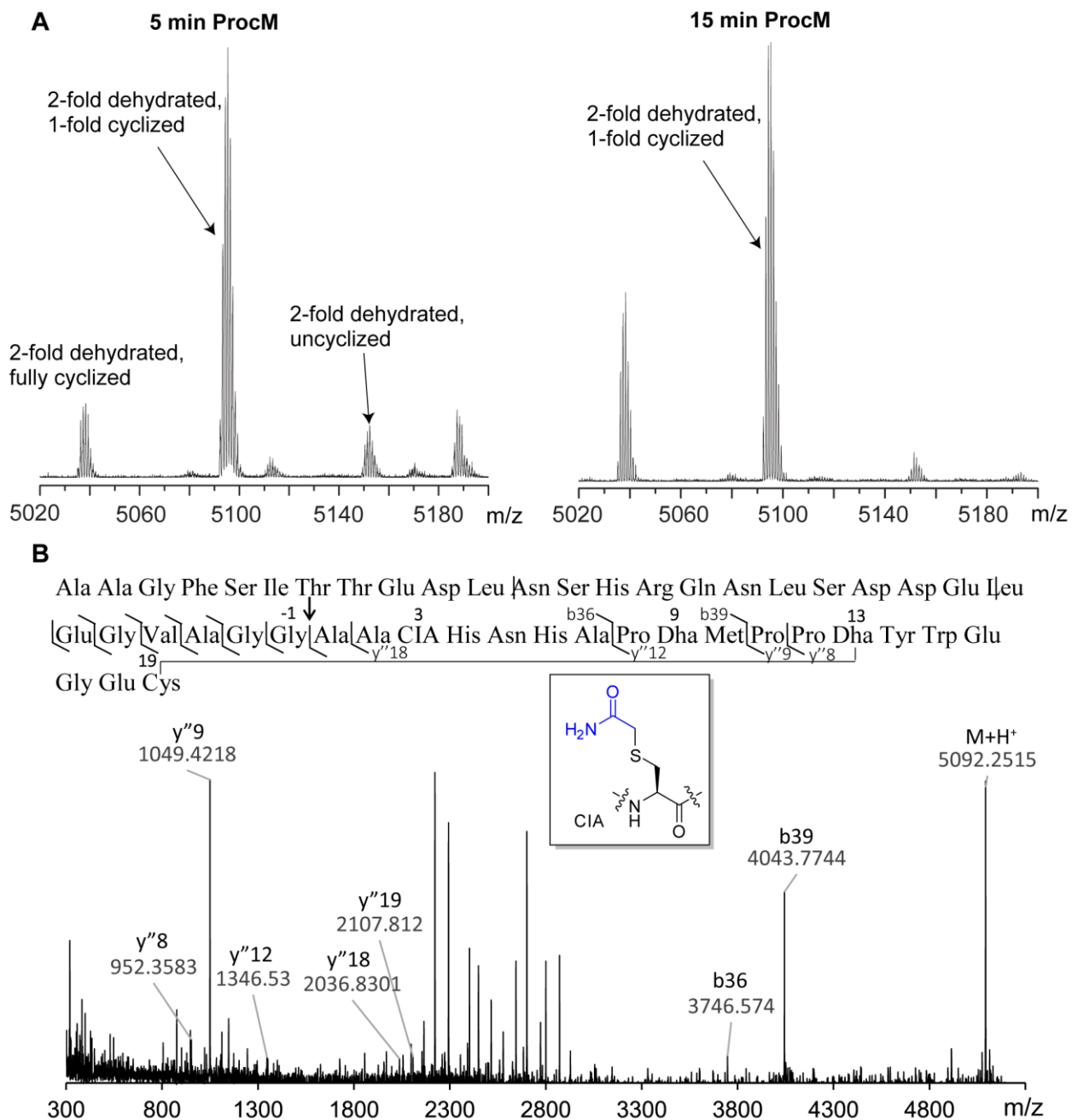


Figure 2.11. Directionality of cyclization of ProcA2.8 precursor peptide by ProcM. (A) Assay was performed for 15 min with His₆-tagged ProcA2.8 precursor peptide (100 μM), and ProcM (5 μM). Then ProcM was removed, the filtrate was digested with LysC, and the assay solution was treated with IAA prior to MALDI-TOF MS analysis. The two-fold dehydrated species with full cyclization has an m/z of 5035.3 (M+H⁺) and the two-fold dehydrated species with one IAA adduct has an m/z of 5092.3 (M+H⁺). (B) ESI-MS/MS was performed on fully dehydrated, one-fold cyclized species with one IAA adduct (m/z of 1019.2; 5⁺ charge state) present at the 15 min time point.

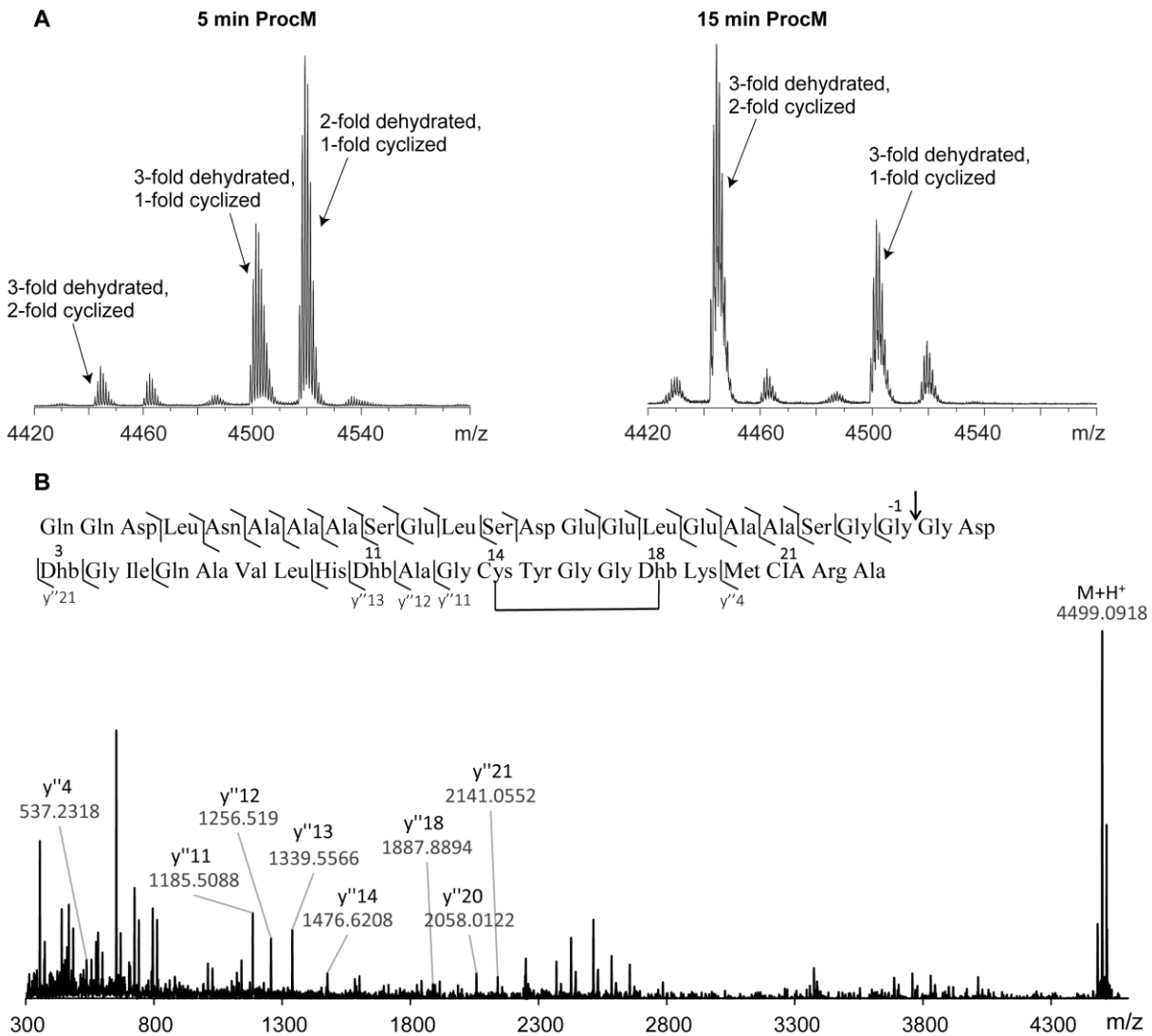


Figure 2.12. Directionality of cyclization of ProcA3.3 precursor peptide by ProcM. (A) Assay was performed with His-tagged ProcA3.3 precursor peptide (100 μ M), and ProcM (5 μ M). ProcM was removed after fixed time points by centrifugation through a 50 kDa cut-off filter. The filtrate was digested with LysC, and then the assay solution was treated with IAA. The three-fold dehydrated species with full cyclization has a m/z of 4442.4 ($M+H^+$) and the three-fold dehydrated species with one IAA adduct has a m/z of 4499.5 ($M+H^+$). Species were analyzed by MALDI-TOF MS. (B) ESI-MS/MS was performed on 3-fold dehydrated, one-fold cyclized species with one IAA adduct (m/z of 1125.5; 4^+ charge state) generated from the 15 min time point.

2.2.5. Substrate Design to Probe Non-Enzymatic Cyclization in Prochlorosin Maturation

To address whether non-enzymatic cyclization assists ProcM in the maturation of substrates with variable ring topologies, substrates were designed that restrict ProcM installation to selected thioether rings by orthogonal protection of a subset of cysteine thiols in the core peptide. Release of the protecting group would generate an intermediate that would allow investigation of non-enzymatic cyclization in the presence of other preinstalled thioether rings. A variety of orthogonal protecting groups for the cysteine thiols were tested. *tert*-Butyl disulfide protection proved not suitable because removal by reducing agents like tris(2-carboxyethyl)phosphine (TCEP) and tributylphosphine formed adducts with dehydrated residues. Conversely, acetamidomethyl protection was unsuccessful because its removal required oxidizing agents like iodine, which partially oxidized the thioether rings. However, the *o*-nitrobenzyl and 4,5-dimethoxy-*o*-nitrobenzyl groups were readily introduced into the peptide during SPPS (28) and were cleanly released by UV irradiation (365 nm). Hence, four precursor peptides were prepared using the previously described hybrid EPL/CuAAC ligation strategy (**2.15** and **2.16** in Figure 2.13 and **2.17** and **2.18** in Figure 2.14), which were treated with ProcM to produce the intermediates **2.19-2.22** and **2.26**. Photorelease of *o*-nitrobenzyl protecting groups then generated substrates to probe non-enzymatic cyclizations of each of the rings in ProcA2.8 and ProcA3.3 in the presence of other enzymatically installed rings.

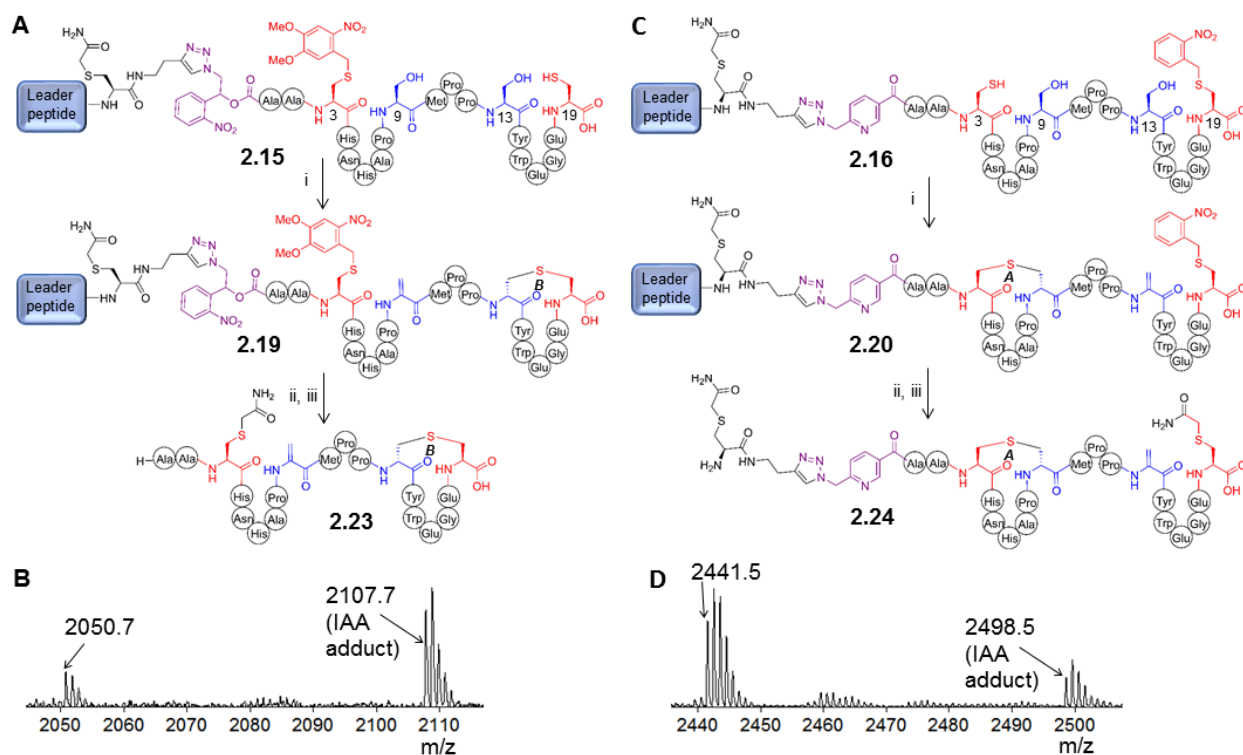


Figure 2.13. Probing non-enzymatic cyclization in ProcA2.8. (A) Non-enzymatic cyclization of the A-ring in the presence of the enzymatically preinstalled B-ring. Reagents and conditions: (i) HEPES, ATP, TCEP, MgCl₂, substrate **2.15** (50 μM), ProcM (30 μM); (ii) ProcM was removed, the intermediate **2.19** was desalted and lyophilized, dissolved in 0.1% TFA, and irradiated; (iii) the peptide was dissolved in HEPES buffer (pH 8.0) to allow non-enzymatic cyclization followed by treatment with IAA. (B) MALDI-TOF MS analysis showed that non-enzymatic cyclization was slow and incomplete, as indicated by the presence of IAA adduct **2.23**. (C) Non-enzymatic cyclization of the B-ring in ProcA2.8 in the presence of enzymatically preinstalled A-ring. Reagents and conditions: (i) HEPES, ATP, TCEP, MgCl₂, ProcM (30 μM), substrate **2.16** (50 μM); (ii) ProcM was removed, intermediate **2.20** was irradiated with UV light and lyophilized; (iii) the lyophilized peptide was dissolved in solution containing all components in (i) except ProcM, digested with LysC and treated with excess IAA. (D) MALDI-TOF MS analysis showed that nonenzymatic cyclization was incomplete, as indicated by the presence of IAA adduct **2.24**.

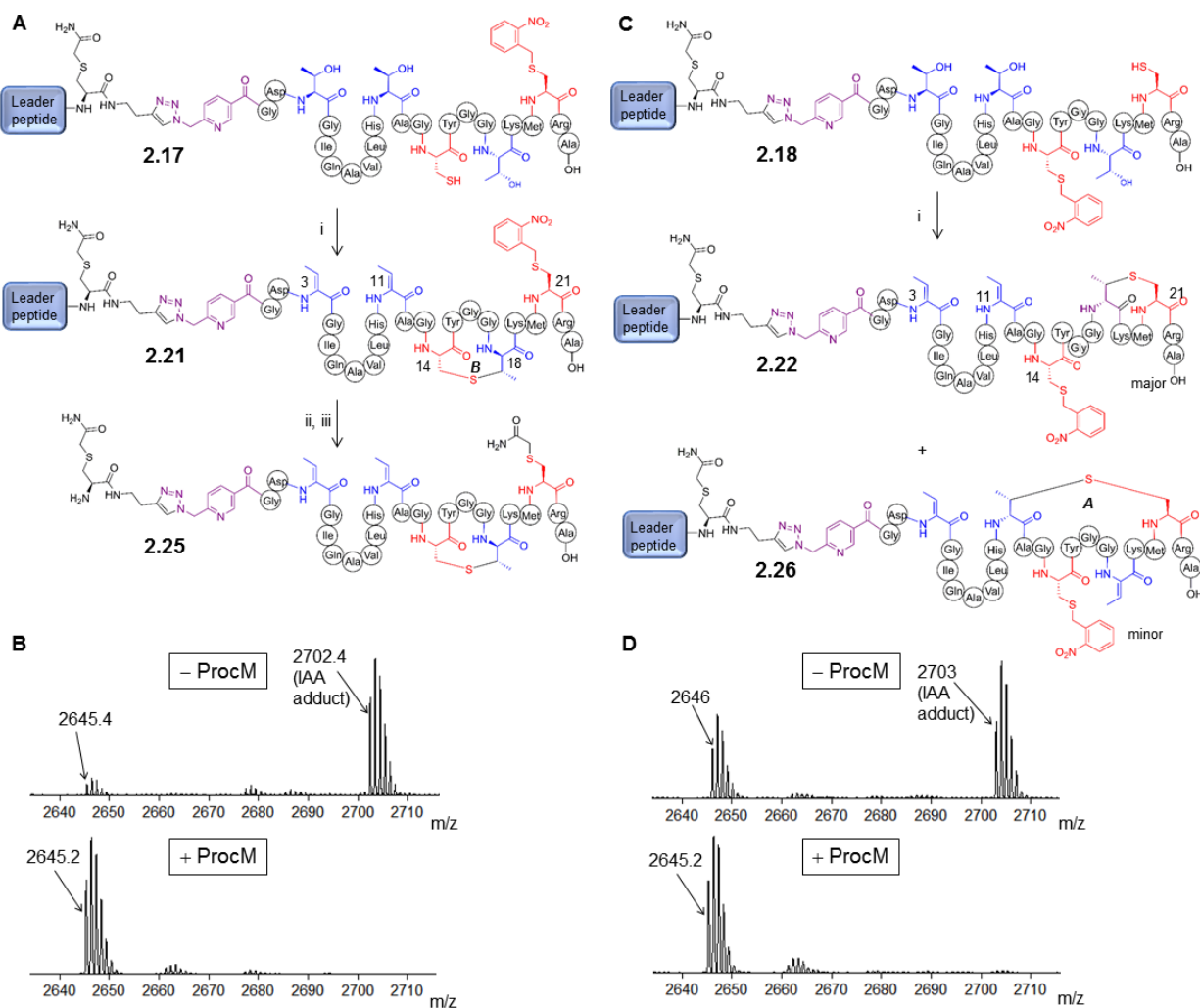


Figure 2.14. Probing non-enzymatic cyclization in ProcA3.3. (A) Non-enzymatic cyclization of the A-ring in the presence of enzymatically preinstalled B-ring. Reagents and conditions: (i) HEPES, ATP, TCEP, MgCl₂, substrate **2.17** (50 μM), ProcM (20 μM); (ii) ProcM was removed and the intermediate **2.21** was irradiated with UV light and lyophilized; (iii) the lyophilized peptide was dissolved in assay solution containing all components in (i) with or without ProcM, digested by LysC, and treated with IAA. (B) MALDI-TOF MS of solution obtained after treatment in (iii). (C) ProcM assay of substrate **2.18** generated a mixture of intermediates **2.22** and **2.26**. (D) ProcM was removed from the mixture of **2.22** and **2.26**, and the product mixture was irradiated with UV light and lyophilized. The peptide mixture was dissolved in solution containing all ProcM assay components with or without ProcM. The products were then treated with LysC and IAA. The MALDI-TOF MS spectra of the two assays are presented.

2.2.6. Efficient Cyclization of ProcA2.8 Requires ProcM

ProcM correctly processed the ProcA2.8 precursor peptide analogue **2.15** to generate the B-ring and a dehydroalanine at the ninth position of the core peptide (intermediate **2.19**) (Figure 2.13A) as demonstrated by tandem MS (Figure 2.15). The peptide **2.19** was irradiated at 365 nm to release the *o*-nitrobenzyl group on Cys3 along with the leader peptide that was attached via linker **2.9**. The resulting peptide was incubated in buffered solution at pH 8.0 to probe non-enzymatic cyclization under conditions where enzymatic cyclization is complete. The peptide was then treated with IAA to report on noncyclized Cys residues. MALDI-TOF MS analysis revealed the predominant presence of IAA adduct **2.23**, which indicated incomplete non-enzymatic cyclization of the A-ring of Pcn2.8 (Figure 2.13B). Thus, non-enzymatic cyclization of the A-ring in the presence of the B-ring is much slower than enzymatic cyclization. Non-enzymatic cyclization was also conducted at higher pH (pH 8.5) and for a longer time period (12 h), but non-enzymatic cyclization of the A-ring still did not proceed to completion. ProcM converted the ProcA2.8 analogue **2.16** (Figure 2.13C) to an intermediate **2.20** that contained the A-ring of prochlorosin 2.8 and a dehydroalanine at the 13th position as evidenced by tandem MS (Figure 2.16). The peptide **2.20** was irradiated to remove the *o*-nitrobenzyl group from Cys19 and was incubated with ProcM. The peptide was then treated with LysC to remove the leader peptide and with IAA to probe cyclization. Analysis by MALDI-TOF MS showed that, whereas the enzymatic cyclization under these conditions is complete in 1 h, the non-enzymatic cyclization still resulted in a mixture of cyclized product and IAA adduct **2.24** after 16 h (Figure 2.13D). Because the observed non-enzymatic cyclization of the B-ring was very slow compared to enzymatic cyclization, these experiments do not provide support for efficient non-enzymatic ring formation facilitated by preorganization upon formation of one of the rings.

Li1 Ala Ala MbC His Asn His Ala Pro Dha Met Pro Pro Dha Tyr Trp Glu Gly Glu Cys

b7 y''12 b11 y''8

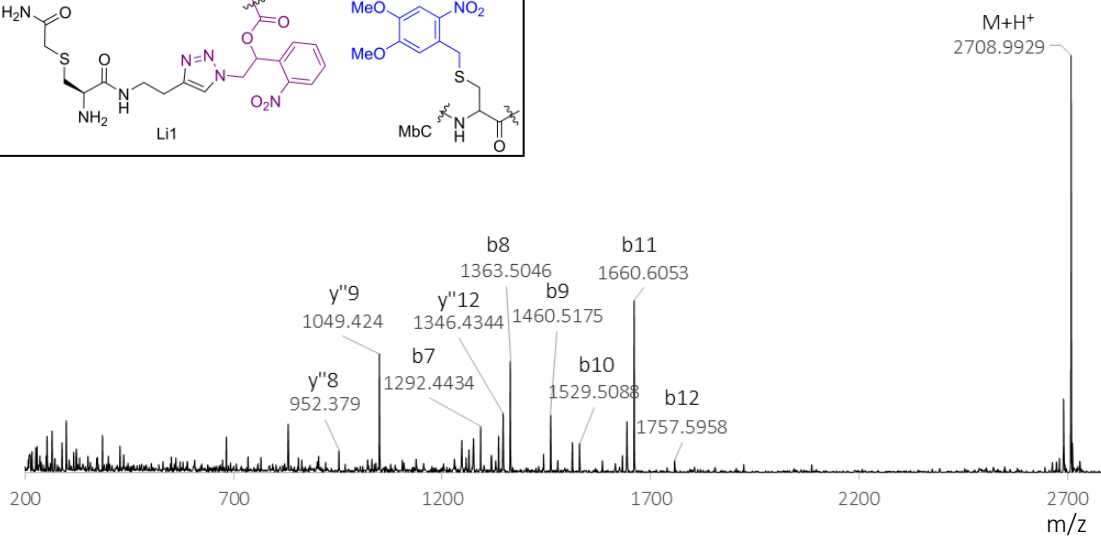
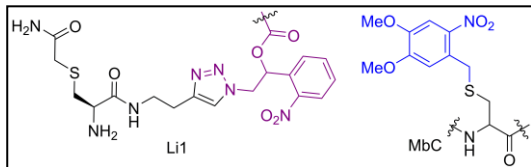


Figure 2.15. ESI-MS/MS analysis of intermediate **2.19** (Figure 2.13A) after LysC cleavage, which established that ring-B is formed between Cys19 and Dha13.

Li2 Ala Ala Cys His Asn His Ala Pro Dha Met Pro Pro Dha Tyr Trp Glu Gly Glu NbC

b11 y''9 b18 y''4 y''2

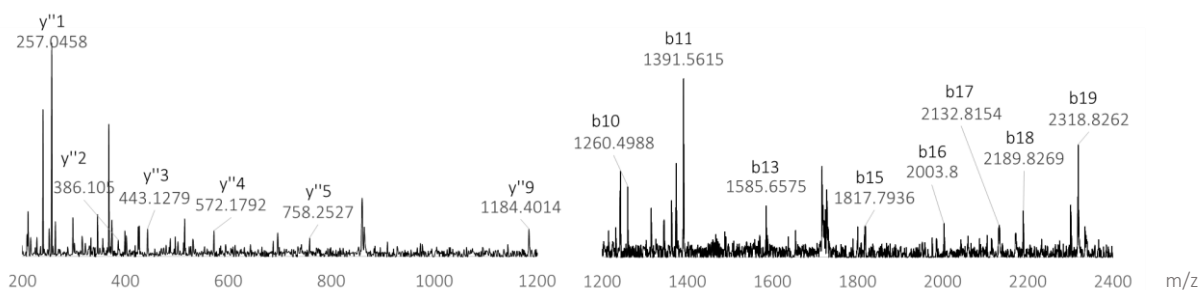
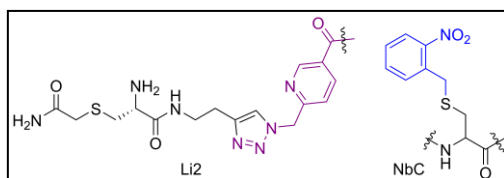


Figure 2.16. Tandem MS analysis on intermediate **2.20** (Figure 2.13C) after LysC cleavage, which established that ring-A is formed between Cys3 and Dha9.

2.2.7. Ring Formation in ProcA3.3 Requires ProcM

Treatment of the ProcA3.3 precursor analogue **2.17** with ProcM resulted in the formation of a product containing a dehydrobutyrine (Dhb) at positions 3 and 11 and a MeLan formed between Cys14 and Dhb18 (Figure 2.14A), as confirmed by tandem MS after LysC cleavage of **2.21** (Figure 2.17). The *o*-nitrobenzyl group was removed from Cys21 by UV irradiation, and the peptide was subjected to both enzymatic and nonenzymatic assay conditions. Following the cyclization assays, the peptides were digested with endoproteinase LysC and treated with IAA. The enzymatic assay did not show IAA adduct formation, whereas the non-enzymatic assay showed predominant formation of the IAA adduct **2.25** (Figure 2.14A) as demonstrated by MALDI-TOF MS (Figure 2.14B). Hence, non-enzymatic cyclization of the A-ring of Pcn3.3 in a peptide that already contained the B-ring is much slower than when this process is catalyzed by ProcM. Thus, the experiments with peptides **2.19-2.21** show that non-enzymatic cyclization is too slow to be kinetically competent to be a part of the overall process.

The product obtained after ProcM treatment of the ProcA3.3 precursor analogue **2.18** was not a single peptide but a mixture of peptides **2.22** and **2.26** with two different ring topologies (Figure 2.14C). The major product **2.22** had a MeLan formed between Cys21 and Dhb18 and the minor product **2.26** contained a MeLan formed between Cys21 and Dhb11 (as seen in native Pcn3.3, Figure 2.3), as evidenced by tandem ESI-MS on the individual products that were separated on analytical scale by UPLC (Figure 2.18). These findings can be explained based on the order of cyclization of ProcA3.3 discussed above. In WT-ProcA3.3, Cys14 forms a ring with Dhb18 in the observed monocyclic intermediate, and hence only Dhb11 is available to Cys21 for cyclization. However, in peptide **2.18**, Cys14 is protected, and therefore, both Dhb11 and Dhb18 are available for reaction with Cys21; apparently, the enzyme then prefers formation of the

smaller ring between Cys21 and Dhb18. Compounds **2.22** and **2.26** could not be separated on preparative scale, and therefore, the mixture was subjected to UV irradiation to release the *o*-nitrobenzyl group from Cys14. The mixture of deprotected peptides was subsequently subjected to both enzymatic and non-enzymatic cyclization assay conditions. The peptides were then digested with endoproteinase LysC followed by treatment with IAA. The non-enzymatic assay resulted in the formation of IAA adduct, thus indicating the absence of significant spontaneous non-enzymatic cyclization in the mixture of two peptides, whereas the enzymatic assay resulted in complete cyclization as evidenced by the lack of IAA adduct (Figure 2.14D). The cyclized product mixture was separated on analytical scale by UPLC and tandem MS analysis revealed the identity of the two products obtained from **2.22** and **2.26**. In addition to the overlapping ring topology as observed in Pcn3.3 (Figure 2.19A), an alternate non-overlapping ring topology was formed (Figure 2.19B). Hence, manipulation of the order of cyclization by using Cys protecting groups allows access to a ring topology not seen with the native substrate.

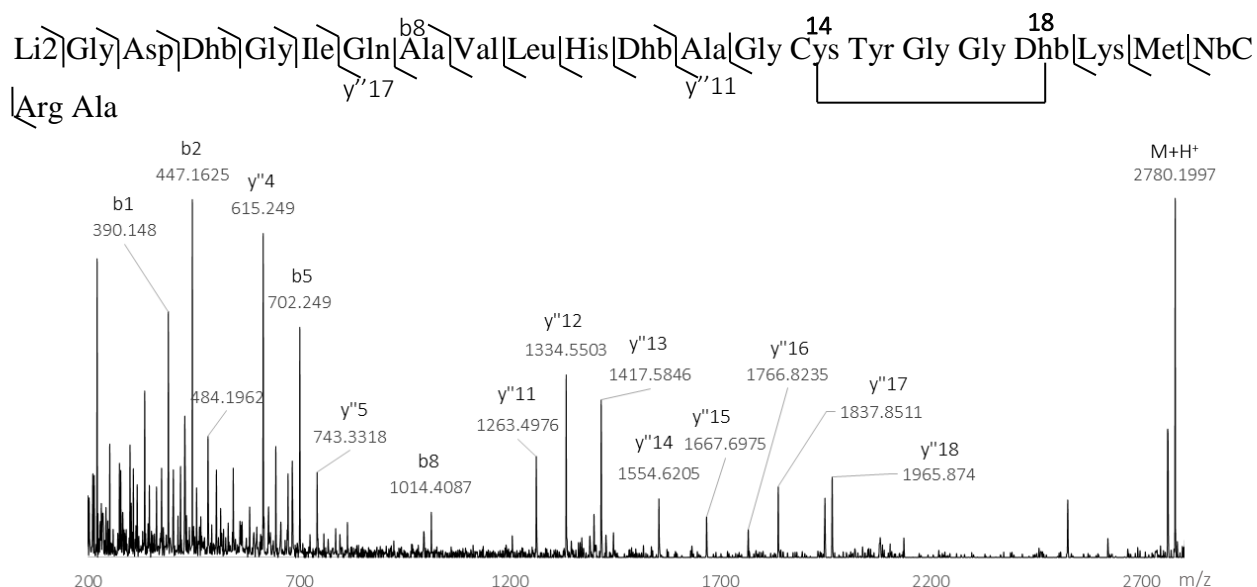


Figure 2.17. Tandem MS on intermediate **2.21** (Figure 2.14A) after LysC cleavage (parent ion m/z of 696, 4^+ charged state), showing the formation of a MeLan between Cys14 and Dhb18. For the structures of NbC and Li2, see Figure 2.16.

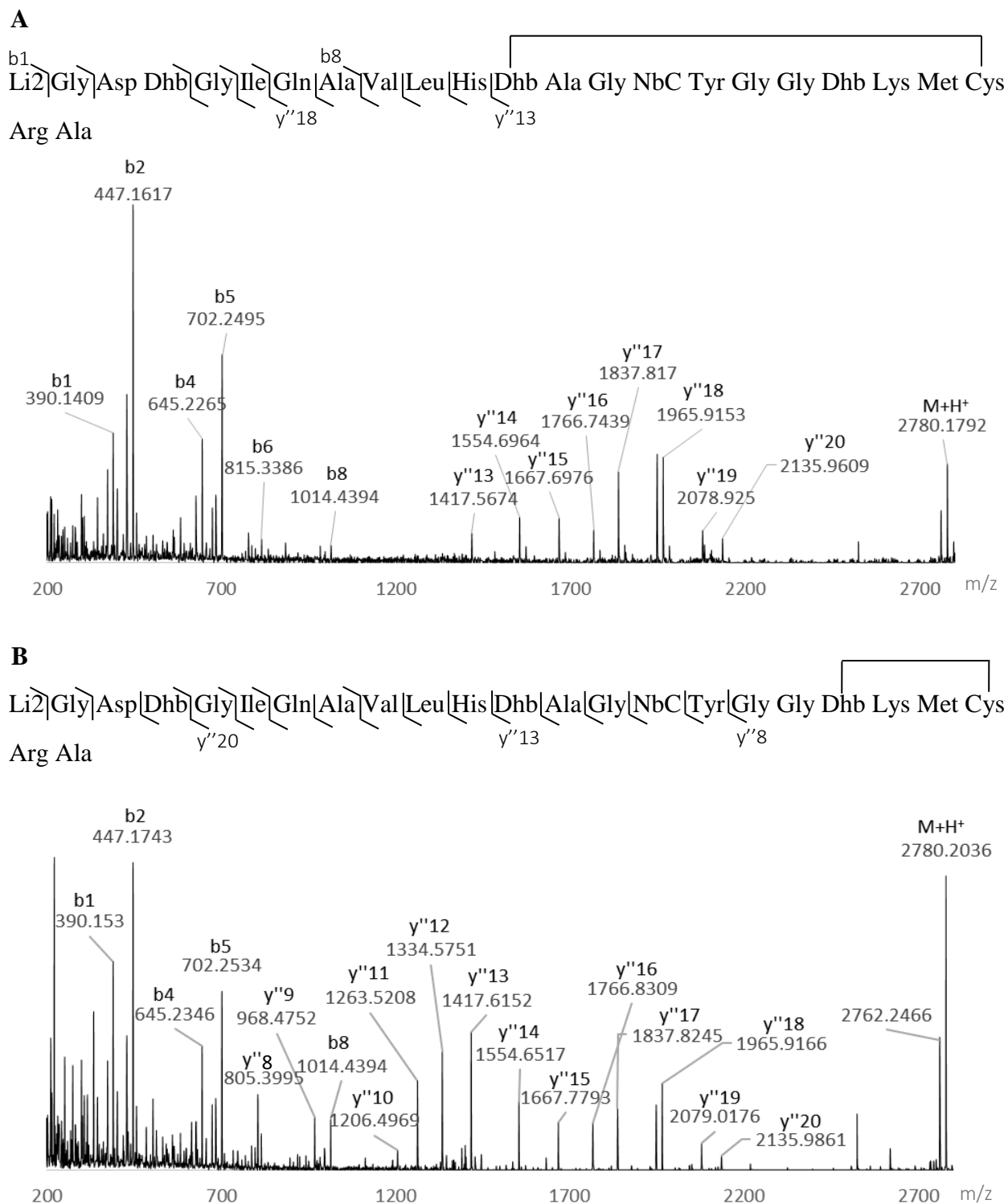


Figure 2.18. (A) Tandem-MS analysis of intermediate **2.26**, after LysC cleavage, and (B) tandem analysis of intermediate **2.22** after LysC cleavage. For the structures of NbC and Li2, see Fig. 2.16.

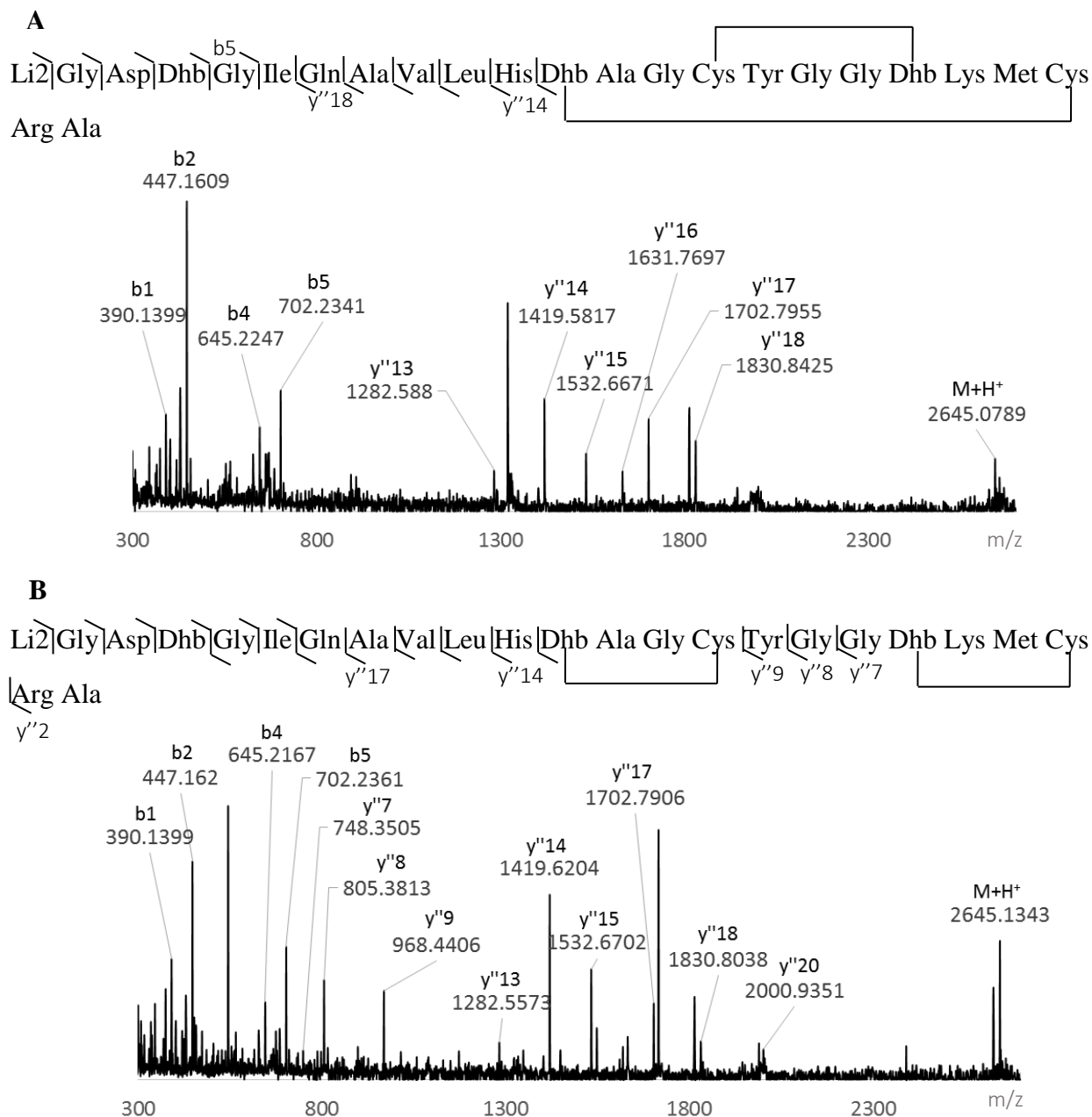
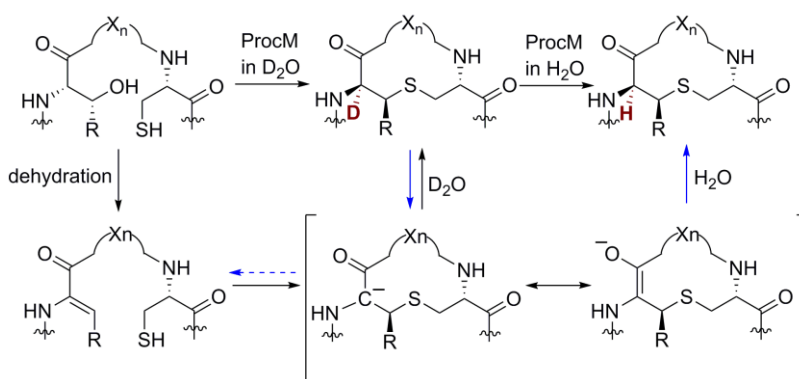


Figure 2.19. Tandem MS analysis of a mixture of cyclized material derived from enzymatic cyclization of a mixtures of **2.26** and **2.22** after photolysis. The cyclized mixture was separated on an analytical scale which confirmed (A) the native Pcn3.3 like overlapping ring-topology, and (B) the alternate nonoverlapping ring topology. For the structure of Li2, see Figure 2.16.

2.2.8. Reversibility of Thioether Ring Formation: Studies on D–H Exchange

To test whether thioether ring installation in prochlorosins is reversible, ProcA substrates were modified by ProcM in D₂O, resulting in incorporation of one deuterium at each newly formed α -stereocenter of Lan/MeLan. The modified precursor peptides were then purified and subjected to standard ProcM assay conditions in unlabeled aqueous buffer. If the Michael-type addition is reversible, then the incorporated deuterium would be expected to exchange with a protium in the assay in unlabeled buffer (Scheme 2.4). His-tagged ProcA2.8 was heterologously expressed in *E. coli* and purified and subjected to ProcM with all assay components dissolved in D₂O. ProcM was removed by ultrafiltration, and the peptide was desalted and lyophilized. A portion of the lyophilized peptide was digested with endoproteinase GluC to generate the modified core peptide with a five amino acid overhang at its N-terminus originating from the leader peptide (Figure 2.20A). As anticipated, both ESI and MALDI-TOF MS analysis demonstrated the incorporation of two deuterium atoms. The full-length peptide was then incubated in unlabeled buffer in the presence or absence of ProcM for 17 h. Exchange of deuterium with protium was not observed (Figure 2.20B, red). Hence, D–H exchange did not occur in ProcA2.8 containing two non-overlapping lanthionine rings, suggesting that such rings are not installed reversibly for this peptide.



Scheme 2.4. Scheme for the D–H exchange assay. Substrate is modified by ProcM in deuterium-labeled buffer to generate product with one deuterium per Lan/MeLan. Exchange of the installed deuterium was then investigated by treating the modified precursor peptide with ProcM in unlabeled buffer. Exchange can occur by abstraction of deuterium followed by protonation (solid blue arrows) or by retro-Michael-type addition (dashed blue arrow) and recyclozation.

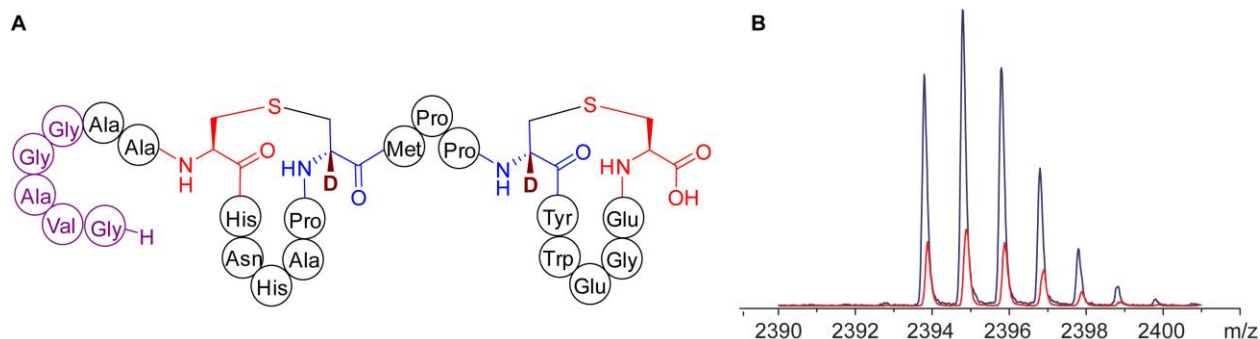


Figure 2.20. Deuterium incorporation and exchange in ProcA2.8. (A) Structure of GluC cleaved ProcA2.8 core peptide fragment incorporating two deuteriums. Residues in purple originate from the leader peptide. (B) MALDI-TOF MS of GluC cleaved fragment of deuterium-labeled ProcA2.8 (50 μ M) after assay without (blue trace) and with ProcM (20 μ M) treatment in aqueous buffer (red trace).

2.2.9. ProcM-Cyclized ProcA3.3 Undergoes Enzymatic D–H Exchange

To also explore a substrate containing overlapping rings, ProcA3.3 was heterologously expressed and purified. The peptide was modified by ProcM in D_2O , the enzyme was removed from the modified peptide by ultrafiltration, and the product peptide was desalted and lyophilized. Analysis by MALDI-TOF MS after endoproteinase GluC digestion demonstrated incorporation of two deuterium atoms as expected (Figure 2.21A). The full-length peptide was then incubated in unlabeled buffer with or without ProcM and digested with GluC before mass

spectrometric analysis. The modified ProcA3.3 treated in aqueous buffer without ProcM did not result in any exchange (Figure 2.21B, blue), but the modified substrate treated in aqueous buffer with ProcM showed exchange of both deuterium atoms with protium (Figure 2.21B, red). Analysis of the exchange over time at two different concentrations of ProcM revealed that the exchange was time-dependent and dependent on the concentration of ProcM (Figure 2.22). Also, exchange of one deuterium was significantly faster, with the second deuterium exchange requiring higher enzyme concentration and longer incubation time. Under the conditions of the assay (100 μ M modified ProcA3.3 and 5 μ M ProcM), the exchange of the first deuterium was already detected after short incubation times (15 min; Figure 2.22). The dehydration of ProcA3.3 catalyzed by ProcM under the same conditions is complete at this time point, but cyclization is still incomplete. Hence, the observed deuterium exchange could be kinetically competent with the cyclization process.

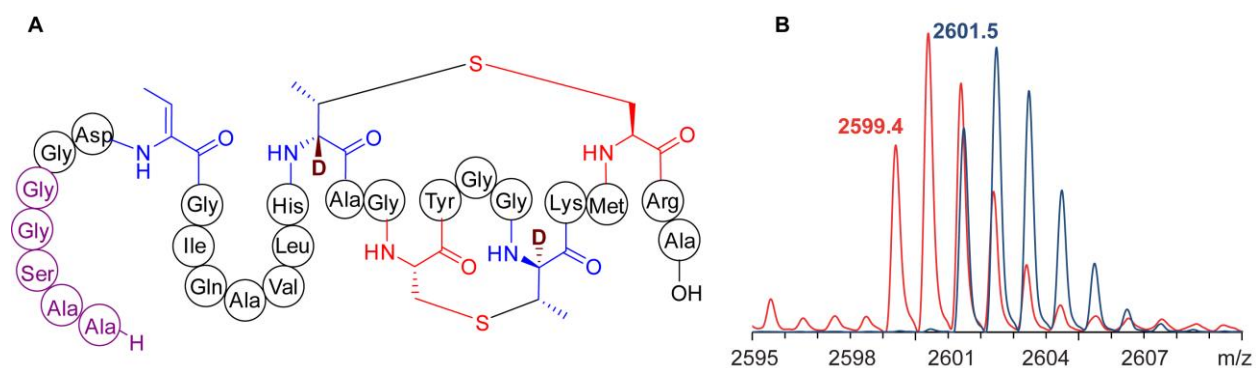


Figure 2.21. Deuterium incorporation and exchange in ProcA3.3. (A) GluC digested ProcA3.3 core peptide incorporating two deuteriums. Residues in purple originate from the leader peptide. (B) MALDI-TOF MS of GluC digested fragment of modified deuterium-labeled ProcA3.3 (100 μ M) without aqueous ProcM treatment (blue trace) and with aqueous ProcM (40 μ M) treatment (red trace).

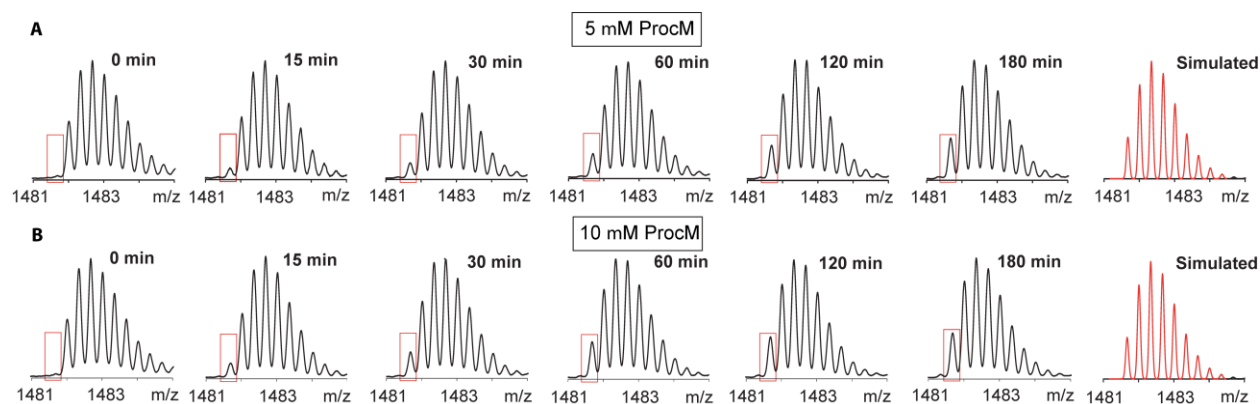


Figure 2.22. D–H exchange in ProcA3.3 with duration and concentration of ProcM treatment. Two sets of assays were performed: (A) with 5 μ M ProcM, and (B) with 10 μ M ProcM. In both cases, the assay solution contained HEPES (50 mM, pH 8.0), TCEP (0.5 mM), ATP (10 mM), MgCl₂ (10 mM), and ProcM-modified ProcA3.3 containing two deuterium atoms (100 μ M). Time points were taken at 15, 30, 60, 120, 180 min. The 0 min time point is taken as the substrate without ProcM. For each sample, ProcM was removed by filtration, and the filtrate was digested by LysC and analyzed by ESI-MS. The 3⁺ charged fragment ion is shown to show the extent of D–H exchange with time. The red box shows the appearance of the new peak in the isotopic pattern as the first D is exchanged by H. The spectra in red are the simulated 3⁺ charged spectra for species with one D exchanged with H (m/z: 1481.67).

2.2.10. D–H Exchange Is Not Observed in ProcA2.8 Substrates with Ser Mutated to Thr

Given the observation of D–H exchange in modified ProcA3.3 but not ProcA2.8, it is interesting to note the differences between the two substrates. Pcn3.3 contains overlapping rings whereas Pcn2.8 does not, and the rings in Pcn3.3 are formed by MeLan residues whereas both rings in Pcn2.8 are formed by Lan residues. To investigate if the lack of exchange in cyclized ProcA2.8 was because it contains Lan and not MeLan, two mutants of ProcA2.8 were generated by site-directed mutagenesis—one with Ser9 replaced with Thr (ProcA2.8-S9T) and another with Ser13 replaced with Thr (ProcA2.8-S13T). Both substrates were modified by ProcM in D₂O, incorporating two deuterium atoms in the process. The purified products were subjected to the D–H exchange assay conditions and were digested with GluC. Subsequent analysis by MALDI-TOF MS revealed that D–H exchange had not occurred (Figure 2.23A–D). Hence, in ProcA2.8 with two non-overlapping rings, even changing a Lan to a MeLan does not lead to D–H

exchange, suggesting that ring topology may instead dictate whether ProcM can exchange the α -proton of the cross-linked amino acids.

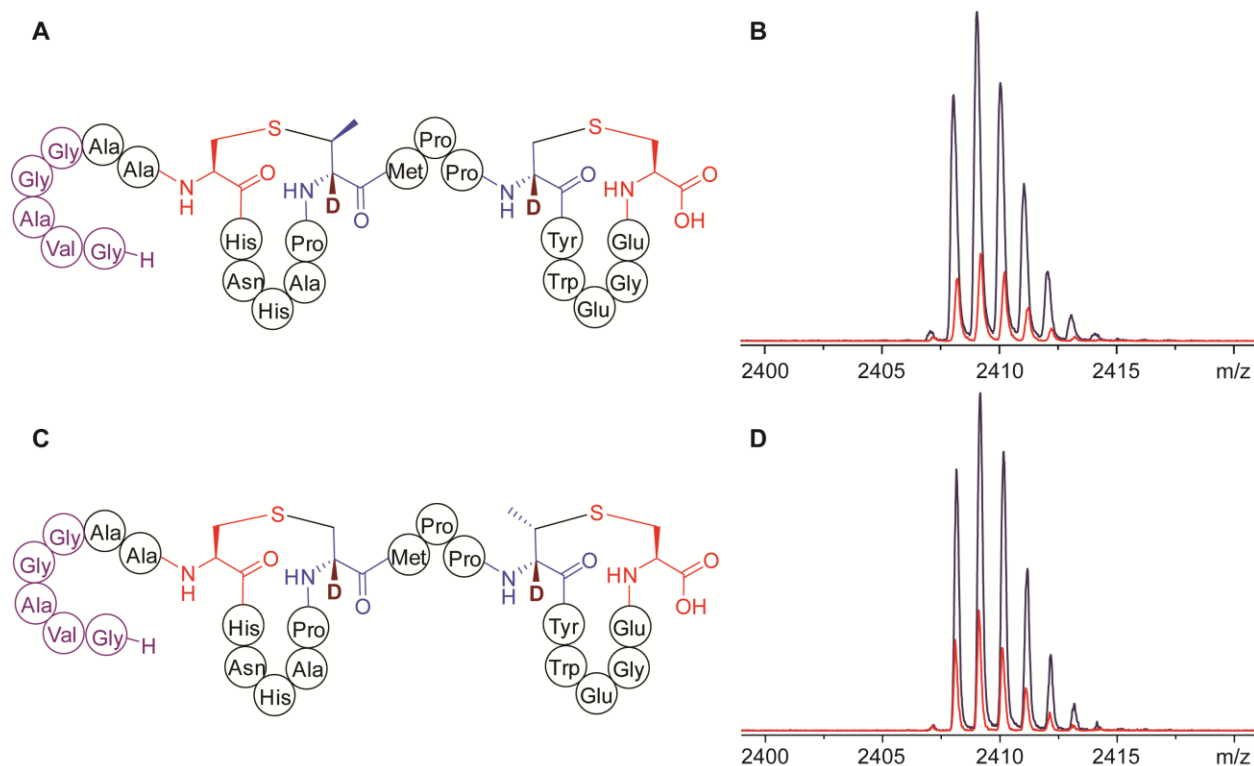


Figure 2.23. Investigation of D-H exchange in ProcA2.8-S9T and ProcA2.8-S13T mutants. (A) Structure of ProcM-modified ProcA2.8-S9T incorporating two deuteriums and after GluC digestion. (B) MALDI-TOF MS analysis on D-H exchange assay when modified precursor peptide ProcA2.8-S9T incorporating two D was treated with ProcM in standard assay conditions in aqueous buffer (red trace) and without ProcM in standard conditions in aqueous buffer (blue trace). (C) Structure of ProcM-modified ProcA2.8-S13T incorporating two deuteriums and after GluC digestion. (D) MALDI-TOF MS analysis of the D-H exchange assay when modified precursor peptide ProcA2.8-S13T incorporating two D was treated with ProcM in standard assay conditions in aqueous buffer (red trace) and without ProcM in standard conditions in aqueous buffer (blue trace).

2.2.11. Exchange in ProcA3.3 Involves the B-Ring

As noted above, the exchange process for cyclized ProcA3.3 involves one deuterium that was exchanged relatively rapidly with a proton from solvent, whereas the second deuterium exchange was much slower. Because cyclization of ProcA3.3 results in a ring within a ring,

tandem MS could not be used to determine which of the two MeLan residues is associated with the faster exchange. We therefore mutated Thr11 to Ser such that cyclization would result in one Lan and one MeLan, which in principle can be distinguished by GC–MS after acidic hydrolysis of the product. Thus, ProcA3.3-T11S was first incubated with ProcM under the standard conditions in D₂O. The resulting product was purified and shown to contain two deuterium atoms by mass spectrometry (Figure 2.24). The labeled peptide was then treated with ProcM in unlabeled buffer, resulting in relatively rapid exchange of one deuterium (Figure 2.24), similar to the observations with wild-type ProcA3.3. The resulting peptide containing one deuterium was then hydrolyzed, and the Lan and MeLan residues were derivatized as previously described (29, 30). Analysis by GC–MS resulted in detection of unlabeled derivatized MeLan and deuterium-labeled derivatized Lan (Figure 2.25). Hence, the relatively fast exchange occurs in the MeLan in ring B. Both Lan and MeLan residues had the correct DL stereochemistry as confirmed by co-injection with synthetic standards (Figure 2.26).

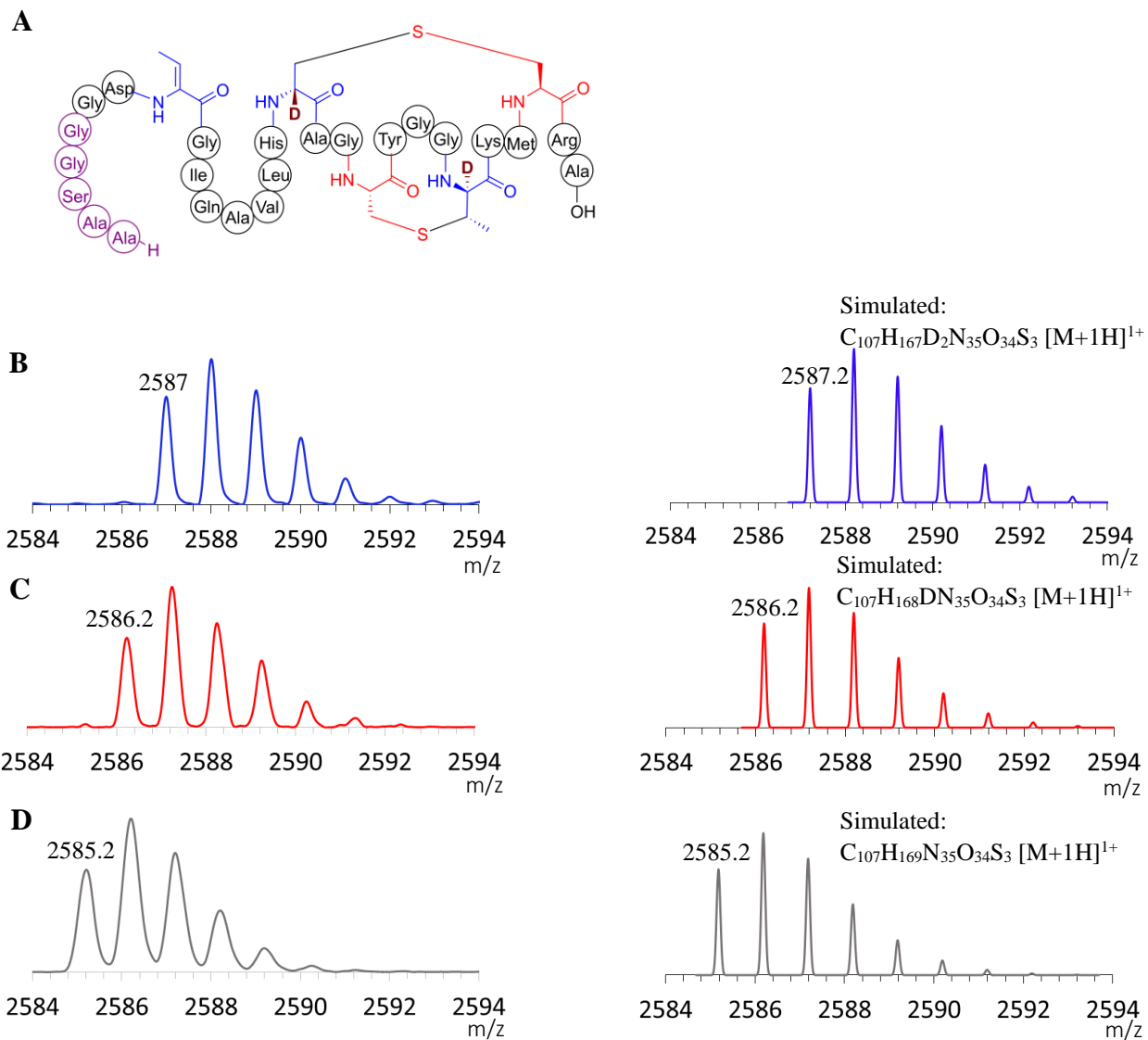


Figure 2.24. Investigation of D-H exchange in ProcA3.3-T11S. (A) Structure of the core region of ProcA3.3-T11S incorporating two deuterium atoms after GluC digestion. The amino acids remaining from the leader peptide are shown in magenta. (B) MALDI-TOF MS analysis after treatment of the modified ProcA3.3-T11S incorporating two deuterium atoms (100 μ M) with ProcM (10 μ M) in standard conditions in aqueous buffer (red trace), and in the absence of ProcM in standard ProcM assay conditions (blue trace). For comparison, also shown is the MALDI-TOF mass spectrum of unlabeled ProcA3.3-T11S modified by ProcM in aqueous buffer and then digested with GluC (gray trace). The corresponding simulated spectra are drawn to the right of the corresponding panels.

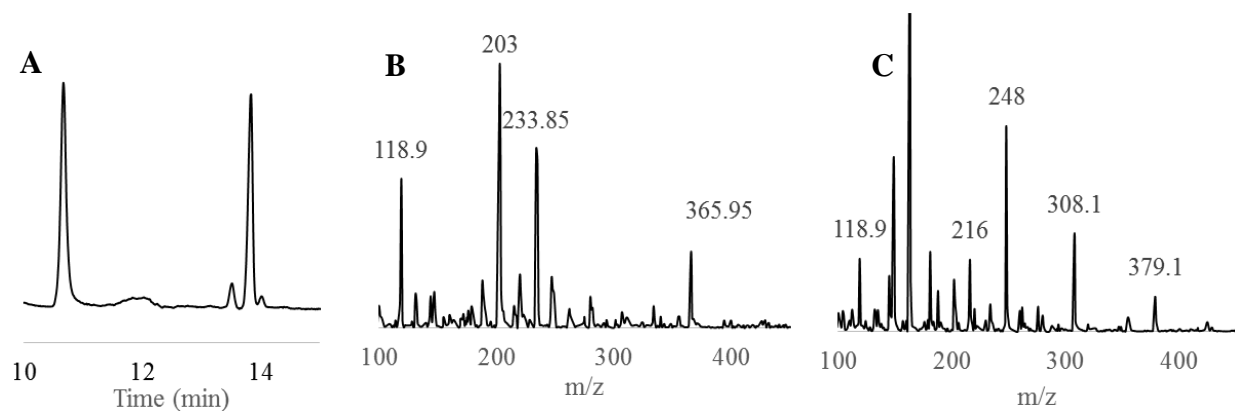


Figure 2.25. GC/MS analysis to identify the thioether residue in ProcA3.3-T11S mutant participating in DH exchange. (A) GC/MS traces for the hydrolyzed/derivatized Lan/MeLan residues obtained from ProcA3.3-T11S mutant with one α -deuterium exchanged with protium. (B) Mass spectrum of derivatized Lan showing fragments consistent with the Lan residue retaining the α -deuterium (m/z : 366, 203). (C) Mass spectrum of the derivatized MeLan showing fragments consistent with the MeLan residue not containing a deuterium atom (m/z : 379, 216) (29).

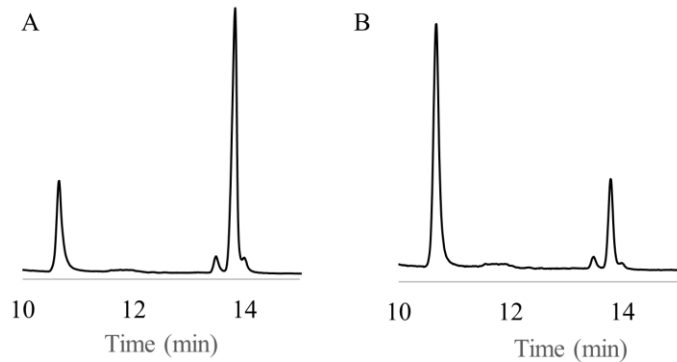


Figure 2.26. GC/MS traces for the co-injection of hydrolyzed/derivatized Lan/MeLan residues from Figure 2.25 with (A) synthetic, derivatized (2*S*,6*R*)-Lan standard, and (B) synthetic, derivatized (2*S*,3*S*,6*R*)-MeLan standard.

2.2.12. Mutations of Three Zn(II) Binding Cys Ligands in ProcM[§]

Most lanthipeptide cyclases (LanCs and the cyclase domains in LanMs) utilize two Cys and one His as the ligands binding the Zn(II) at the active site, whereas ProcM uses three Cys residues (Cys924, Cys970, and Cys971) (12). Cys971 is the unique residue present in ProcM, in place of His that is typically present in other LanMs and LanCs (Figure 2.27). To evaluate the importance of the Zn binding Cys residues, including Cys971, a series of mutants of ProcM (C924A, C970A, C971A, and C971H) were generated by site-directed mutagenesis. The Zn contents were very similar in WT-ProcM and ProcM-C971H, and this mutant was studied further to evaluate the importance of the Zn-binding Cys ligand.

	810	860	930	970
ProcM	LDLIGGCAGLI.....	GFS <u>HG</u> TAGY.....	AS---- <u>WC</u> <u>H</u> GAPGIALG.....	H-L <u>CC</u> GSLG
CinM	FDILHGAAGLI.....	GFS <u>HG</u> SGGI.....	NA---- <u>WC</u> <u>N</u> GAAIGLA.....	HTL <u>CH</u> GTSG
CylM	NDWIHGHSII.....	GFG <u>HG</u> IYSY.....	NS---- <u>WC</u> <u>K</u> GTVGELLA.....	-CL <u>CH</u> GNAG
GarM	PDLIAGLAGCA.....	GFS <u>HG</u> AAGI.....	AL---- <u>WC</u> <u>H</u> GAAGIGLS.....	HSL <u>CH</u> GDFG
HalM2	PDFVSGLSGVL.....	GLS <u>HG</u> AAGF.....	TF---- <u>WC</u> <u>H</u> GAPGIGIS.....	HSL <u>CH</u> GDFG
MrsM	NDILTGVAGTA.....	GFA <u>HG</u> ASGI.....	NDNFVA <u>WC</u> <u>N</u> GAAIGLS.....	HSL <u>CH</u> GDLG
LctM	DDVIAGEAGII.....	SYA <u>HG</u> NSGI.....	SQ---- <u>WC</u> <u>H</u> GASGQAIA.....	FCL <u>CH</u> GILG
NisC	YDVIEGLSGIL.....	GLA <u>HG</u> LAGV.....	SFIRDA <u>WC</u> <u>Y</u> GGPGISLL.....	YMI <u>CH</u> GYSG
PepC	FDIISGCAGTL.....	GYA <u>HG</u> IPGI.....	NDYRDA <u>WC</u> <u>Y</u> GLPSVAYT.....	PTL <u>CH</u> GFSG
EpiC	YDIIQGFSGIG.....	GLA <u>HG</u> ILGP.....	---RNG <u>WC</u> <u>Y</u> GDTGIMNT.....	PTF <u>CH</u> GLAS
MutC	YDVISGNAGVA.....	GLA <u>HG</u> LLGP.....	-ILRNG <u>WC</u> <u>Y</u> GDNGIYST.....	PTF <u>CH</u> GFAG
SpaC	YDVIEGVSGIA.....	GLA <u>HG</u> IPGP.....	NFSRDA <u>WC</u> <u>Y</u> GRPGVCLA.....	PTI <u>CH</u> GYSG
		**	** *	**

Figure 2.27. Sequence alignment of selected LanMs (cyclase domain) and LanCs. The conserved active-site residues are boldface underlined type. The unique Cys971 in ProcM is colored red. Figure courtesy, Dr. Yi Yu, biochemistry, UIUC (2).

[§] This experiment was performed by Dr. Yi Yu, biochemistry, UIUC. Adapted from:

2. Yu, Y., Mukherjee, S., and van der Donk, W. A. (2015) Product Formation by the Promiscuous Lanthipeptide Synthetase ProcM is under Kinetic Control, *J. Am. Chem. Soc.* 137, 5140-5148.

2.2.13. Differences in Enzymatic Activity between WT-ProcM and ProcM-C971H

ProcA2.8 was modified by either WT-ProcM or ProcM-C971H, and the rate of dehydration, cyclization, and the product distribution were studied. As the mutation of ProcM was in its cyclase domain, similar rate of dehydration was observed as expected, but the cyclization rate was found to be different. In case of WT-ProcM treated ProcA2.8, the first cyclization of Cys19 to Dha13 was completed in <15 min, and the second cyclization of Cys3 to Dha9 took about 1 h, under the employed conditions of the assay (Figure 2.28). In ProcM-C971H modified ProcA2.8, the same order of cyclization as in the case of cyclization by WT-ProcM was observed and the rate of the first cyclization was also found to be very similar in the two assays. The second cyclization rate decreased significantly for the mutant enzyme, with <30% fully cyclized ProcA2.8 observed after 90 min (Figure 2.28). ProcA2.8 was subjected to increasing concentrations of ProcM-C971H for 60 min, and the extent of fully cyclized material was found to increase with the increasing enzyme concentration, suggesting that the second cyclization is catalyzed by ProcM-C971H, albeit at a slower rate (Figure 2.29).

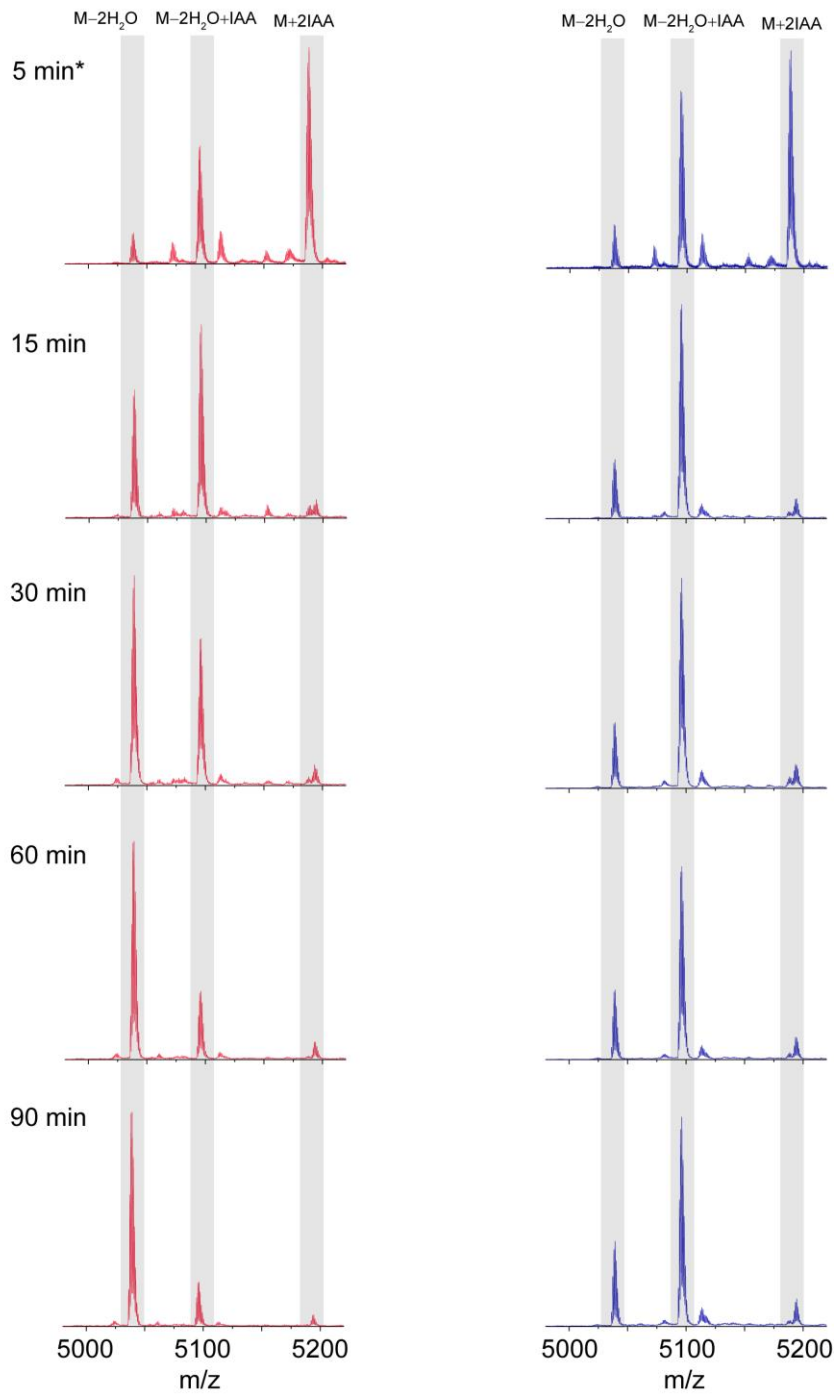


Figure 2.28. Comparison of the rate of dehydration and cyclization of ProcA2.8 by WT-ProcM and ProcM-C971H. MALDI-TOF mass spectra are displayed of 100 μ M ProcA2.8 modified by 2 μ M (5 min*) or by 10 μ M WT ProcM (red) and ProcM-C971H (blue) for 15, 60, and 90 min, and subsequently digested by LysC and treated with IAA.

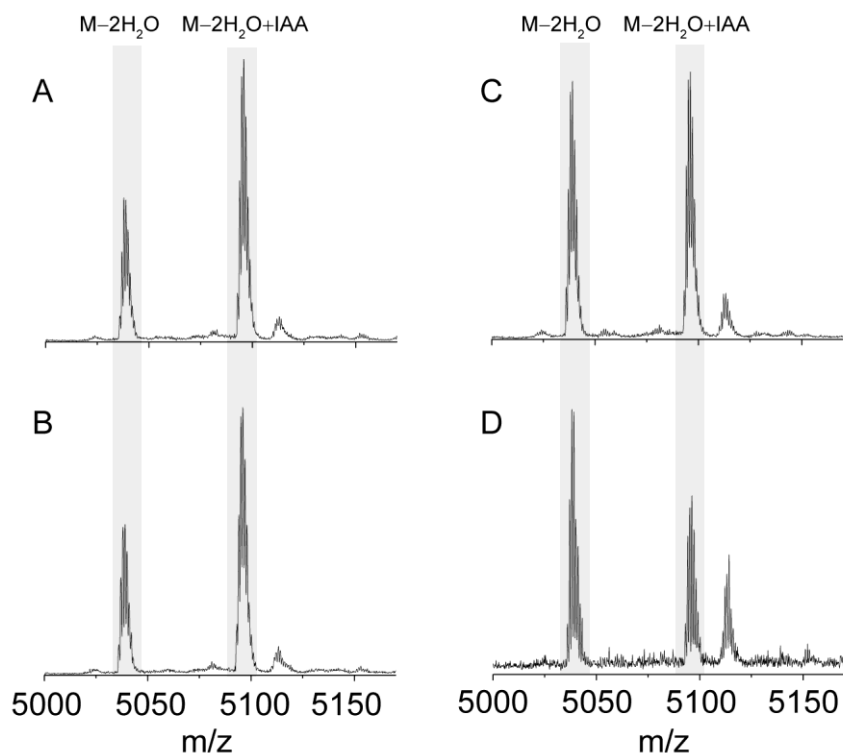


Figure 2.29. The second cyclization in ProcA2.8 is catalyzed by ProcM-C971H. MALDI-TOF mass spectra are depicted of 50 μM of ProcA2.8 modified by (A) 5 μM , (B) 10 μM , (C) 20 μM , and (D) 30 μM of ProcM-C971H for 60 min prior to digestion by endoproteinase LysC and alkylation by IAA. The peak not assigned in the figure arises from a digested fragment of the ProcM enzyme.

Similar comparison of rates of dehydration and cyclization was carried out for ProcA3.3. WT-ProcM led to the formation of the first ring in ProcA3.3 in 15 min, while the second cyclization took ca. 90 min to complete (Figure 2.30). In comparison, when ProcA3.3 was treated by ProcM-C971H, the first cyclization was nearly completed in 90 min, but <10% of the second cyclization was observed in ca. 90 min (Figure 2.30).

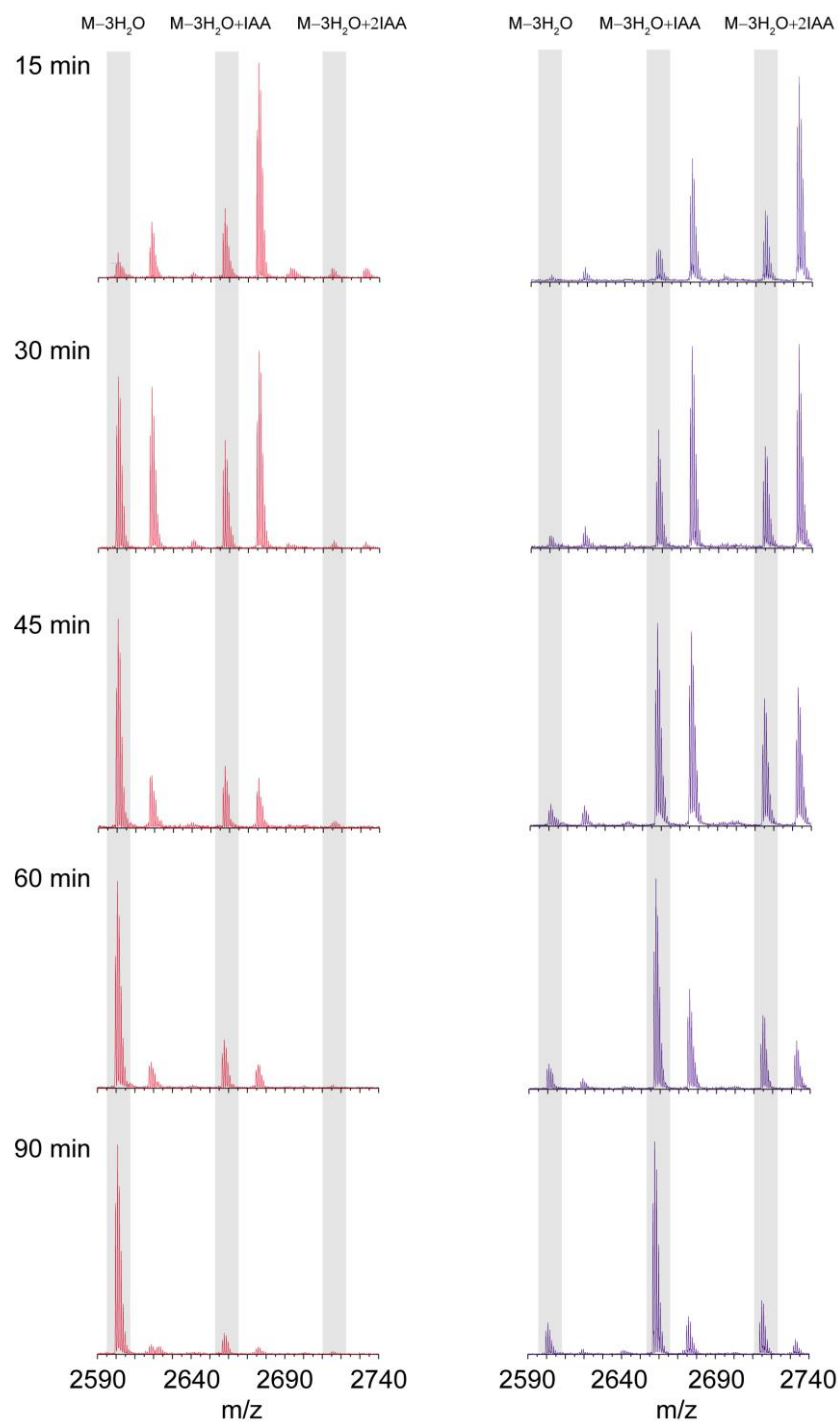


Figure 2.30. Comparison of the rate of dehydration and cyclization of ProcA3.3 by WT-ProcM and ProcM-C971H. MALDI-TOF mass spectra are shown of ProcA3.3 (100 μ M) peptide modified by either 5 μ M WT ProcM (red) or ProcM-C971H (blue) for 15, 30, 45, 60, and 90 min, and subsequently digested by LysC and treated with IAA.

2.2.14. Product Distribution in ProcA3.3 Modified by WT-ProcM or ProcM-C971H**

When ProcA3.3 was treated with ProcM-C971H, two products were observed, while WT-ProcM modified ProcA3.3 to generate one product. The products obtained from the separate treatments of ProcA3.3 with the two enzymes were digested with endoproteinase AspN and then subjected to tandem-MS analyses. As known previously, WT-ProcM treated ProcA3.3 generated a product with an overlapping ring-topology (see Figure 2.3 for structure of mature Pcn3.3), which upon AspN digestion, generated the modified Δ 1-ProcA3.3 core (peptide **2.27**, Figure 2.31). The major product obtained from the treatment of ProcA3.3 with ProcM-C971H contained a non-overlapping ring topology (peptide **2.28**, Figure 2.31).

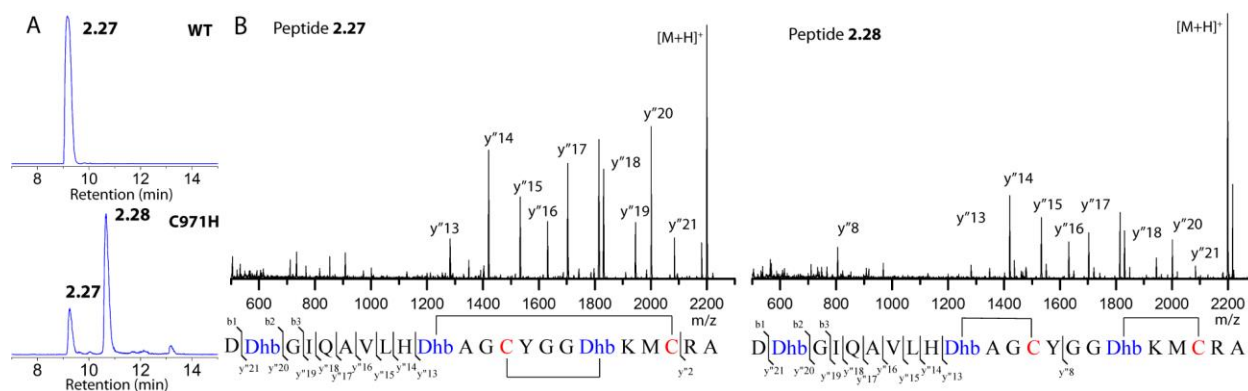


Figure 2.31. Product distribution of ProcA3.3 treated with either WT-ProcM or ProcM-C971H. (A) ESI-LC-MS experiment showing the chromatogram obtained by selected ion monitoring for fully dehydrated and fully cyclized Δ 1 ProcA3.3 core (obtained after AspN treatment). (B) Tandem ESI-MS indicates the topology of thioether crosslinks in peptides **2.27** and **2.28**. Figure courtesy of Dr. Yi Yu, biochemistry, UIUC.

ProcA3.3 was incubated with WT-ProcM and its various mutants and the reactions were quenched before complete cyclizations could occur. The ring patterns of each intermediate were

** I have generated the semi-synthetic peptide intermediates (peptides **2.29**, **2.30**, and **2.31**). All other experiments in this section were performed by Dr. Yi Yu, biochemistry, UIUC.

determined by tandem-MS and by comparison with semi-synthetic standards (Figure 2.32). For modifications by all the mutant enzymes, peptide **2.31** was the major intermediate forming the peptide **2.28** as the major product. The inherent regioselectivity of ring formation was determined by effecting non-enzymatic cyclization on the dehydrated substrate. The two Cys in ProcA3.3 were protected by a disulfide bridge using oxidized glutathione, and the oxidized ProcA3.3 was successfully dehydrated by WT-ProcM. Upon disulfide reduction, and incubation of the dehydrated peptide in buffer of pH 8.0, very little cyclization occurred at 3 h, suggesting that the mutant enzymes indeed catalyzed the cyclization process. However, non-enzymatic cyclization was enforced upon extended incubation of the dehydrated peptide at pH 8.0 for 72 h, upon which similar product distribution was observed as that obtained from the reaction with the mutant enzyme, with peptide **2.28** as the major product (Figure 2.32). The different regiochemistry of cyclized product obtained from the reaction of ProcA3.3 with WT-ProcM from that observed during non-enzymatic cyclization suggests that the enzyme plays a role in the site-selectivity of the Michael-type addition, besides accelerating it.

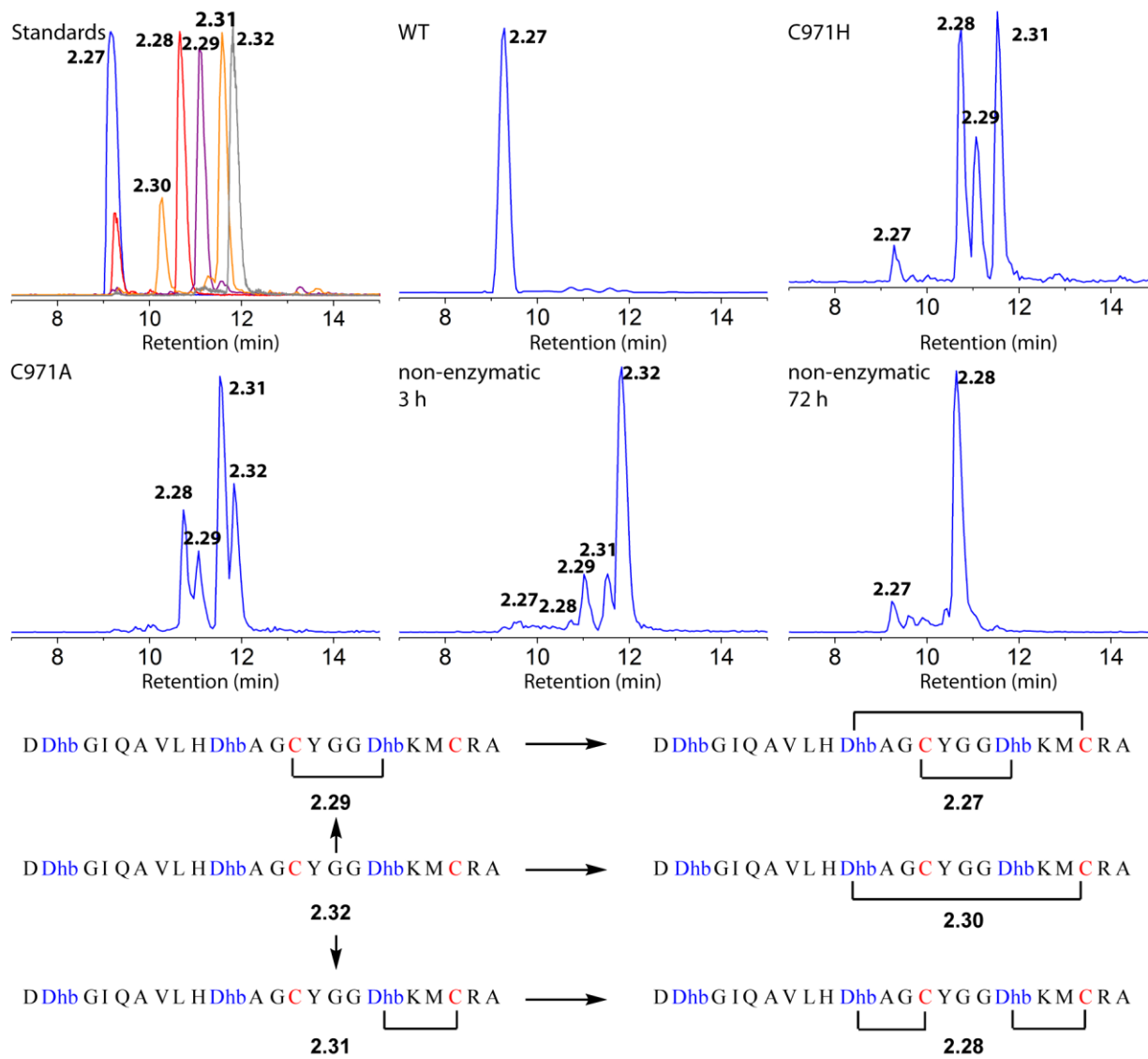


Figure 2.32. ESI-LC-MS (selected ion monitoring) showing 3-fold dehydrated $\Delta 1$ ProcA3.3 core peptides obtained by treating ProcA3.3 precursor peptide (25 μM) with 2 μM of WT-ProcM, ProcM-C971A, and ProcM-C971H for 3 h. Standard peptides: **2.27** (blue), ProcA3.3 co-expressed with WT-ProcM; **2.27** and **2.28** (red), ProcA3.3 co-expressed with ProcM-C971H; **2.29** (purple), semisynthetic ProcA3.3 containing a ring between Cys14 and Dhb18 (described in section 2.4.27); **2.30** and **2.31** (orange), semisynthetic ProcA3.3 with Cys14 protected that was modified by WT-ProcM and subsequently deprotected (described in section 2.4.27); and **2.32** (gray), 3-fold dehydrated and non-cyclized ProcA3.3. Non-cyclization was performed by incubation in buffer of pH 8.0. All peptides except the semisynthetic ones were digested by AspN to remove the leader peptides. Figure courtesy, Dr. Yi Yu, biochemistry, UIUC.

2.2.15. Thioether Formation in ProcA3.3 Is Not Reversible

One possible explanation of the catalytic selectivity of ProcM is that the thioether formation is reversible with product formation guided by thermodynamic control. D–H exchange assays performed on ProcA3.3 showed that the protonation of enolate obtained from Michael-type addition is reversible for ProcA3.3 (Scheme 2.4 and Figure 2.21). However, the α -deuterium exchange does not indicate the occurrence of a retro-Michael-type addition. Such reversibility has been observed for haloduracin synthetase HalM2 and the nisin cyclase NisC (31). Thermodynamic control would involve the ring-opening of both the final product and that of the intermediates with incorrectly formed rings. A ProcA3.3 derived intermediate **2.33** with a thioether ring between Cys21 and Dhb18 was generated by treating peptide **2.18** with ProcM-C971H. The *o*-nitrobenzyl group was removed from Cys14 of intermediate **2.33**, to yield an intermediate peptide with an “incorrect” thioether ring. This intermediate peptide was incubated with WT-ProcM (Figure 2.33) and the product was analyzed by ESI-LC-MS/MS (Figure 2.34). Once the “incorrect” intermediate with Cys21-Dhb18 ring was present, the only product observed was that containing the non-overlapping topology (peptide **2.34**). Thus, no retro-Michael-type ring-opening followed by WT-ProcM catalyzed formation of the overlapping ring topology, as found in the native Pcn3.3, was observed. This result suggests that the thioether formation is kinetically driven and the final ring topology is guided by the topology of the initially installed ring.

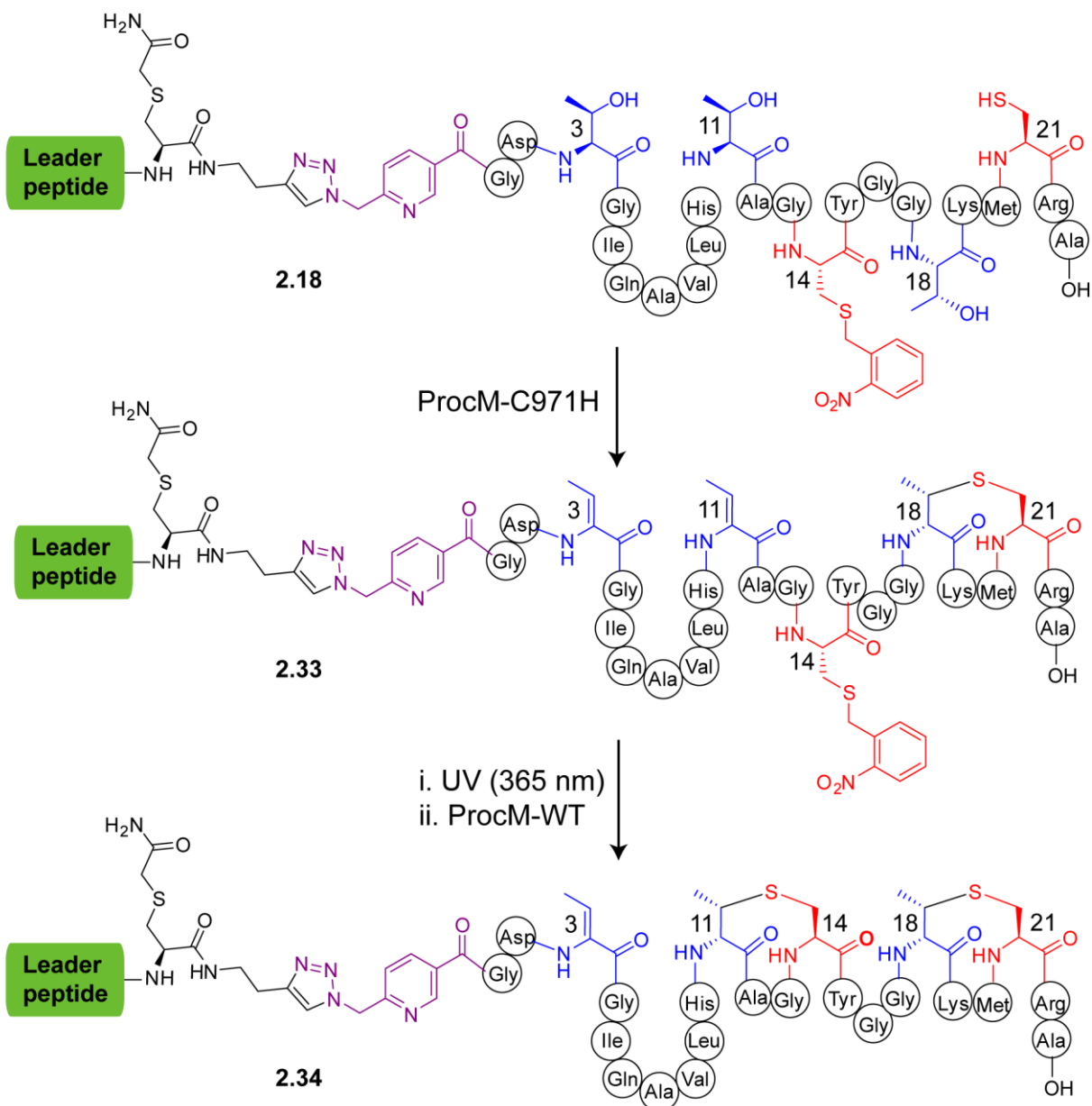


Figure 2.33. Approach used to determine whether WT-ProcM can correct the non-native ring topology in an intermediate. A ProcA3.3 semisynthetic analog with Cys14 protected with a photolabile protecting group was modified by ProcM-C971H to generate the non-native MeLan cross-link between Cys21 and Dhb18. After UV-mediated deprotection of Cys14, treatment with WT-ProcM generated a thioether cross-link between Cys14 and Dhb11, thus showing no evidence of correction of the initially formed ring to generate the native overlapping ring topology.

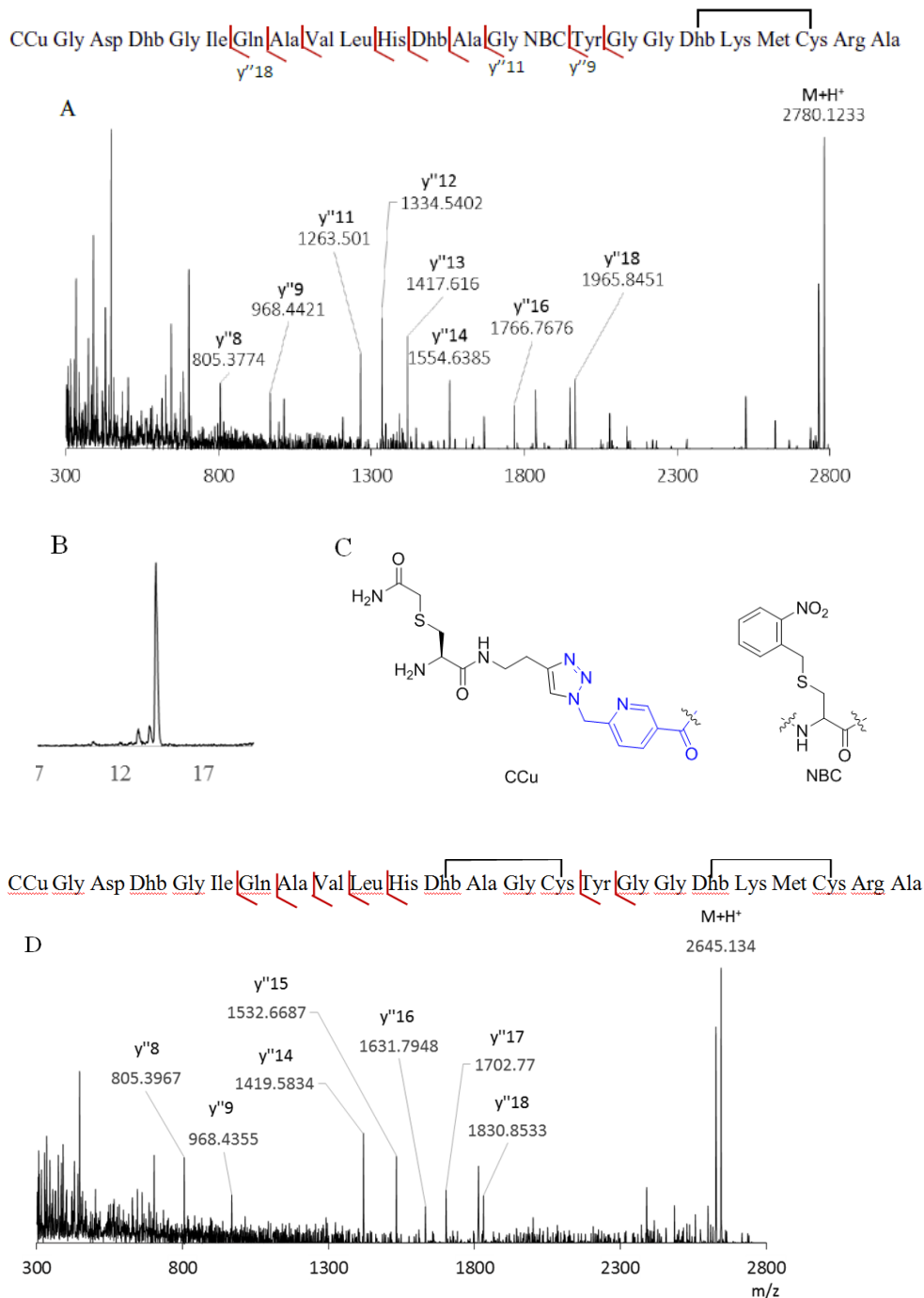


Figure 2.34. Tandem ESI-MS evidence to establish that WT ProcM does not correct non-native ring topology. (A) Tandem ESI-MS of peptide **2.33** after treatment with endoproteinase LysC to remove the leader peptide. (B) EIC for peptide **2.33** after LysC treatment; a C₁₈-Phenomenex column was used at 0.2 mL/min. (C) Structures of CCu and NBC, two acronyms used in the sequence shown above panel A. (D) ESI-MS/MS analysis of peptide **2.34** after removal of the leader peptide by endoproteinase LysC.

2.2.16. Oligomerization State of ProcM

ProcM was found to exist primarily as a monomer, as deduced from a calibration curve (Figure 2.35A). When ProcM was analyzed by size exclusion chromatography (SEC), besides observing the monomer, we found trimer, hexamer, and other higher oligomeric species (Figure 2.35B and C). We were intrigued by the possibility that the C-to-N-terminal directionality of the dehydration could be explained by invoking the interaction of a trimer species of ProcM with its substrate. Upon increasing the pH of the mobile phase from 7.2 to 7.5, the ratio of the monomer increased over that of the other higher oligomers, suggesting that ProcM is more prone to aggregation at lower pH. ProcM readily aggregated upon concentration. When the concentrated monomer was reinjected, only a small amount of monomer, and primarily aggregates were formed (Figure 2.35D). Similarly, upon reinjecting the concentrated trimer, mainly aggregates and a smaller portion of trimer were obtained (Figure 2.35E). When, ProcM was injected along with ATP and Mg^{2+} , as present during typical assay conditions, primarily monomer and aggregates, with little trimer species were formed (Figure 2.35F). This last observation indirectly indicated that the monomers are the active species involved in catalysis.

To evaluate if the trimer is also an active form of ProcM besides the monomer, equimolar amounts of the monomer and trimer species were separately reacted with ProcA2.8. Interestingly, the trimer was found to be able to catalyze the dehydration of ProcA2.8. However, in presence of the substrate, slow dissociation of the trimer to monomer was observed, and the proportion of monomer increased with time, as seen in the trace obtained after injecting the trimer species after incubating it with the substrate for 3 h vs 1 h (Figure 2.36). This observation suggested that the monomer could be the sole active species. However, it is difficult to completely rule out the activity of the trimer species of ProcM. Nonetheless, as the monomer is

definitely an active form of ProcM, the directionality has to be a result of the binding-mode of substrate to ProcM.

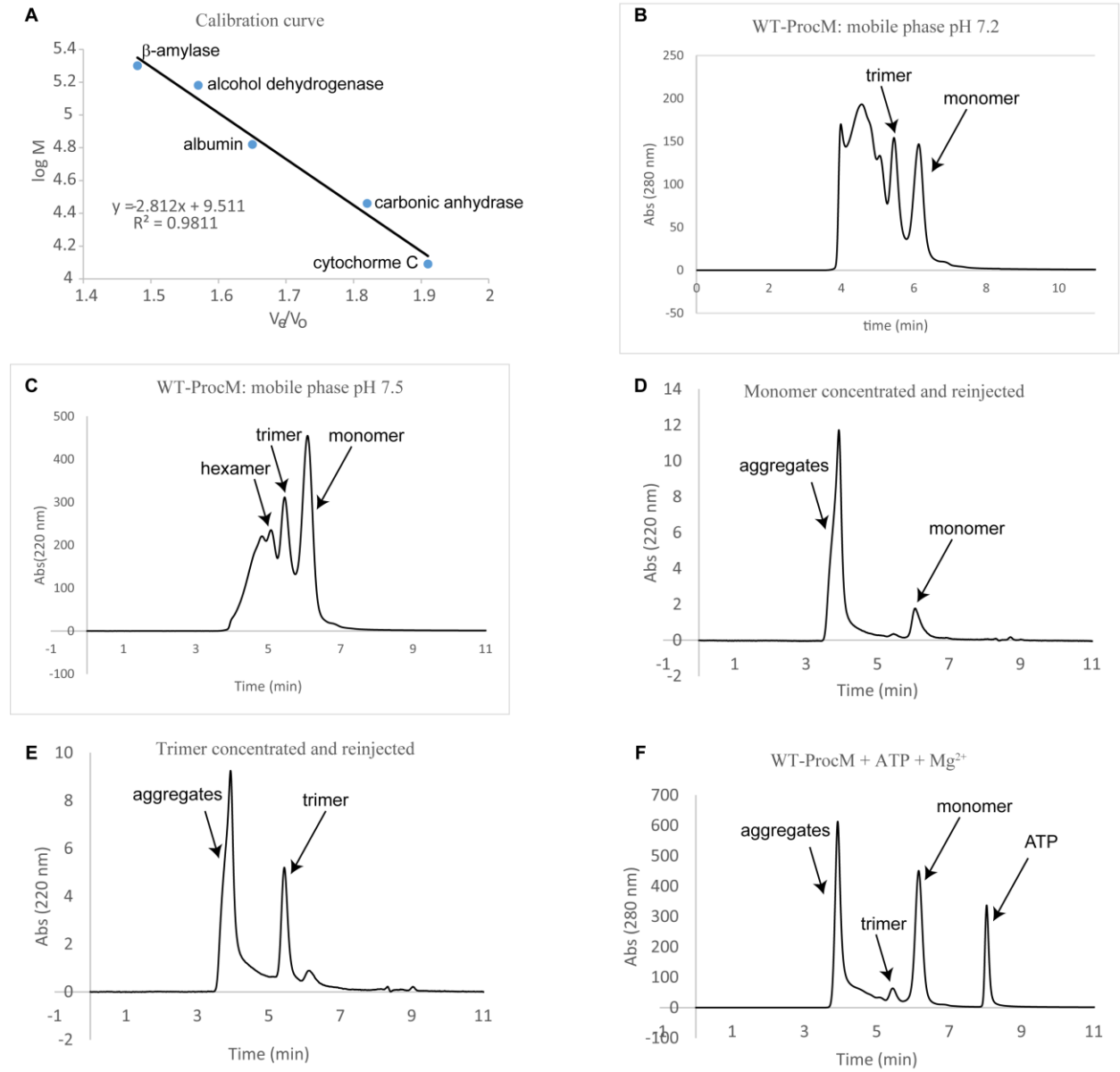
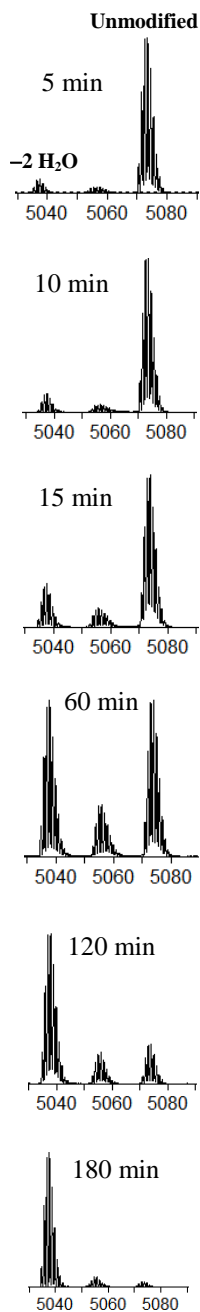
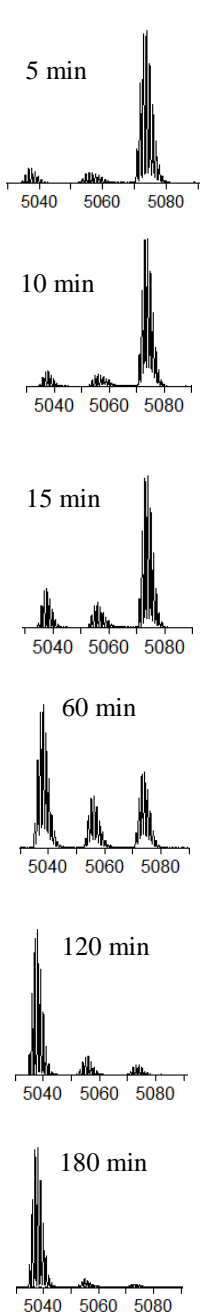


Figure 2.35. Evaluation of oligomerization states of ProcM under various conditions.

Monomer assay



Trimer assay



SEC analytical chromatograms

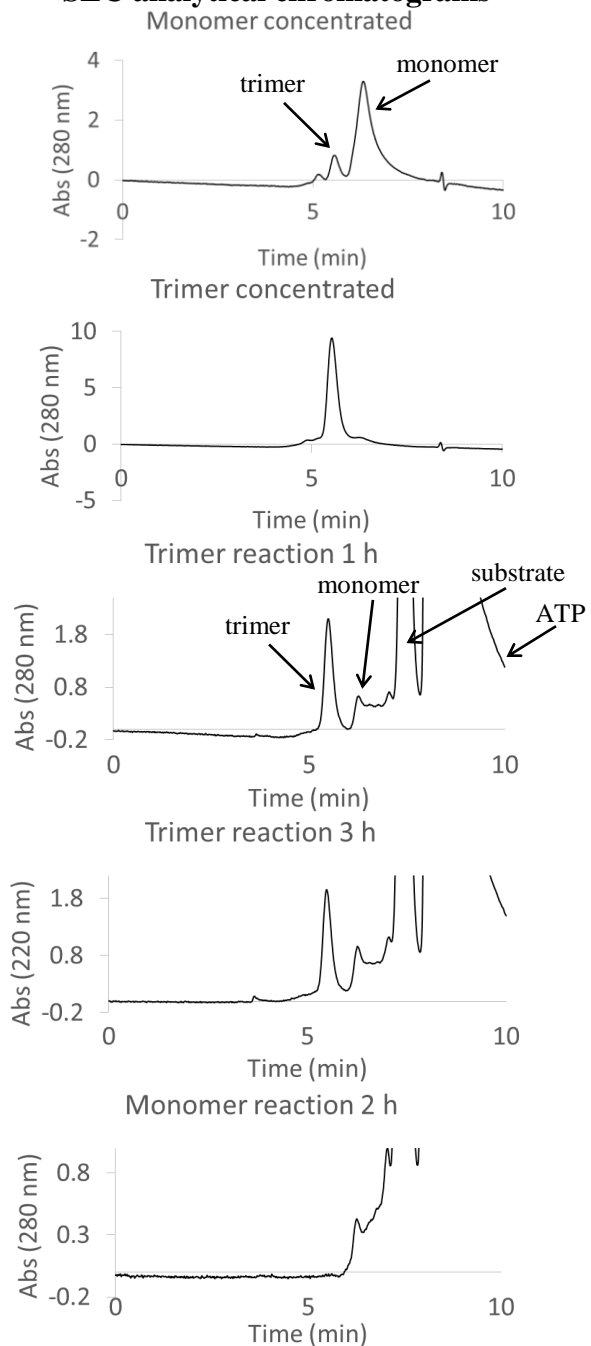


Figure 2.36. Comparison of activity of monomer vs trimer of ProcM, as evaluated for the dehydration reaction of ProcA2.8 (100 μM) by equimolar enzyme (0.52 μM , mass of trimer 3 times over monomer species). From left to right panels: MALDI-TOF MS of dehydration assay of ProcA2.8 by ProcM-monomers with time, MALDI-TOF MS of dehydration assay of ProcA2.8 by ProcM-trimer with time, and SEC showing that when trimer along with its substrate is injected, evidence of monomer formation is found.

2.3. CONCLUSIONS AND OUTLOOK

In an effort to understand the remarkable substrate tolerance of ProcM, several aspects of the lanthionine synthetase were investigated. Aided by a hybrid ligation protocol that allowed us to install synthetic core peptides onto a heterologously expressed leader peptide, we investigated the directionality of both dehydration and cyclization, the possibility that a nonenzymatic cyclization step might account for the high diversity of ring topologies of the products, and the possibility of reversibility of ring formation. Use of labeled ProcA substrate unequivocally demonstrated that ProcM dehydrates two very different substrate peptides in a C-to-N-terminal fashion. Although we cannot completely rule out that the directionality of dehydration by ProcM is simply reflecting the reactivity of each individual site as a result of different flanking residues or secondary structure, the lack of any sequence similarity in the two peptides that are both shown to be dehydrated in C-to-N-terminal direction in this study leads us to favor an explanation that involves a specific juxtaposition of the leader and core peptide binding sites that favors dehydration of C-terminal residues. Structural studies will be required to provide further information.

Interestingly, the cyclization of the two peptides also occurred with a specific order, but this order was not necessarily directional. Whereas for ProcA2.8 the Cys that is located closer to the C-terminus reacted first, in ProcA3.3, it was the Cys that was closer to the N-terminus that appeared to react first. In the latter substrate, this results in the smaller B ring being formed in the observed intermediate.

The remarkable substrate tolerance of ProcM suggested the possibility that perhaps only a subset of the rings are generated enzymatically and that these enzymatically formed macrocycles

preorganize the peptide for subsequent non-enzymatic cyclization. However, my current data show that, for two different substrates, non-enzymatic cyclization of intermediates that contain one ring is too slow to be kinetically competent for the enzymatic process. Another question that had not been previously addressed in lanthipeptide biosynthesis is whether thioether ring formation is reversible or not. The experiments presented here suggest that enzymatic deprotonation at the α -position of MeLan residues does occur in some rings. It is important to note that the D–H exchange assay reports on the reversibility of the protonation of the enolate during MeLan formation; it does not necessarily indicate that the cyclization is reversible (i.e., a reversible Michael-type reaction).

Indeed, in a collaborative work with Dr. Yi Yu, we ruled out reversible Michael-type reaction. All attempts to trap free Cys or dehydrated residues that would arise in case of a retro-Michael-type reaction (31) were unsuccessful. We also established that the unique three Cys-ligated Zn(II) in the active site of ProcM, as opposed to two Cys and one His in other LanMs and LanCs, is important for the high reactivity of ProcM towards its substrates. We demonstrated that the kinetic control over the site-selectivity of formation of the first ring determines the final ring topology in the products formed by ProcM. How the enzyme ensures site-selectivity for the kinetically driven formation of the first ring in the diverse set of 30 substrates is currently not understood. Structural information on ProcM will likely provide molecular details of the interaction of ProcM with its substrates.

2.4. EXPERIMENTAL

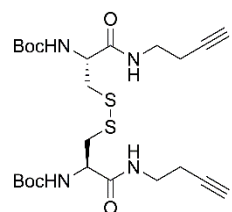
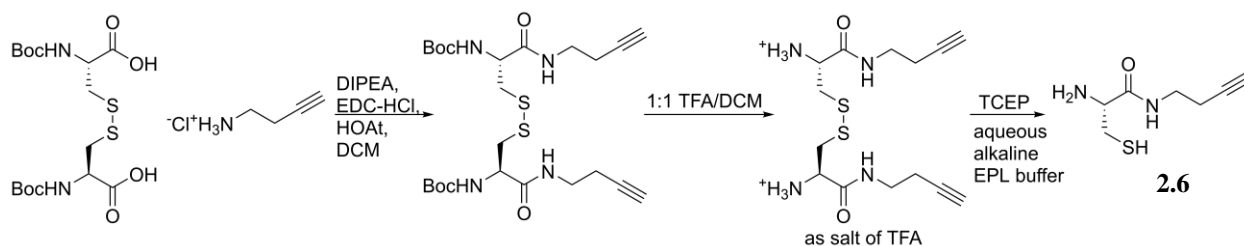
2.4.1. Characterization of Small Molecules and Peptides

Nuclear magnetic resonance (NMR) spectra were recorded on Varian Unity 400, Unity Inova 500, or Varian VXR 500 spectrometers. Small molecules (MW < 1000 Da) were analyzed by electrospray ionization/time-of-flight (ESI-TOF) mass spectrometry on a Waters Quattro II quadrupole spectrometer. Peptides (MW > 800 Da) were analyzed by matrix-assisted laser desorption ionization/time-of-flight (MALDI-TOF) mass spectrometry on a Bruker UltrafleXtreme spectrometer using a matrix solution consisting of saturated α -cyano-4-hydroxycinnamic acid in 1:1 H₂O/MeCN with 0.1% TFA. For larger peptides (MW>5000, or for endoproteinase digested mixtures), 3-(4-hydroxy-3,5-dimethoxyphenyl)prop-2-enoic acid (sinapic acid) dissolved in 1:1 H₂O/MeCN with 0.1% TFA was used as matrix. For smaller peptide fragments (500-1000 Da), MALDI-TOF analysis was performed with 2,5-dihydroxybenzoic acid (DHB) dissolved in 1:1 H₂O/MeCN with 0.1% TFA. ESI-MS on peptides and their tandem MS analysis was carried out with a Synapt Waters G1 system. Samples were separated by liquid chromatography using a Phenomenex Jupiter C₁₈ 300a column using an elution gradient of 3% solvent A, 97% solvent B to 40% solvent A, 60% solvent B over 20 min at a flow-rate of 0.2 mL/min (solvent A: 99.9% acetonitrile, 0.1% formic acid, solvent B: 0.1% formic acid in 99.9% water). For analysis of larger fragments (MW>4000), an elution gradient of 3% solvent A, 97% solvent B to 70% solvent A, 30% solvent B over 20 min was used. The LC-system was directly connected to the MS chamber, where ESI was used to analyze samples, using Glu-1-Fibrinopeptide B (Glu-Fib) as external calibrant.

2.4.2. Small Molecule Synthesis: Materials and Methods

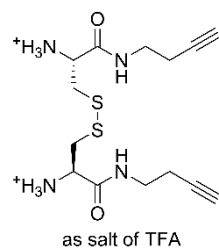
Standard Fmoc-amino acids and resins, Boc-protected Cys and peptide coupling reagents- 1-[bis(dimethylamino)methylene]-1*H*-1,2,3-triazolo[4,5-*b*]pyridinium 3-oxid hexafluorophosphate (HATU), 2-(6-chloro-1*H*-benzotriazole-1-yl)-1,1,3,3-tetramethyluronium hexafluorophosphate (HCTU), (7-azabenzotriazol-1-yloxy)tripyrrolidinophosphonium hexafluorophosphate (PyAOP), *N,N'*-diisopropylcarbodiimide (DIC), 1-ethyl-3-(3-dimethylaminopropyl)carbodiimide hydrochloride (EDC), 1-hydroxy-7-azabenzotriazole (HOAt) and 1-hydroxybenzotriazole (HOBt) were purchased from Chem-Impex. [2,3,3-²H]-L-Ser was purchased from Cambridge Isotope Laboratories, and [2,3-²H]-L-Thr was purchased from CDN-isotopes. Chitin resin was purchased from New England Biolabs. Dimethylformamide (DMF), dichloromethane (DCM), tetrahydrofuran (THF), methanol, and 1,4-dioxane were purchased at reaction grade from Fisher Scientific and dried via a solvent dispensing system prior to use. Other chemical reagents and reaction-grade solvents were purchased from Sigma Aldrich or Alfa Aesar and used without further purification. All reactions and chromatography fractions were monitored by thin layer chromatography (TLC) on silica-gel-coated glass plates with a F254 fluorescent indicator. Visualization was achieved by UV absorption by fluorescence quenching or permanganate stain (1.5 g KMnO₄, 10 g K₂CO₃, 1.25 mL 10% NaOH in 200 mL of H₂O), or ninhydrin stain (0.2% ninhydrin in EtOH) for visualizing compounds with free amines. For visualizing compounds with free carboxylic acids, bromocresol green (0.04% in EtOH) was used. Flash chromatography was performed using Silicycle SiliaFlash® P60, 230-400 mesh silica gel.

2.4.3. Synthesis of Compound 2.6 to Introduce C-Terminal Alkyne



Compound **2.35**. In a round bottom flask, 3-butyn-1-amine hydrochloride (0.21g, 1.99 mmol) was dissolved in 30 mL of DCM and neutralized with DIPEA (0.38 mL, 2.2 mmol). To the reaction mixture, Boc-L-cystine was

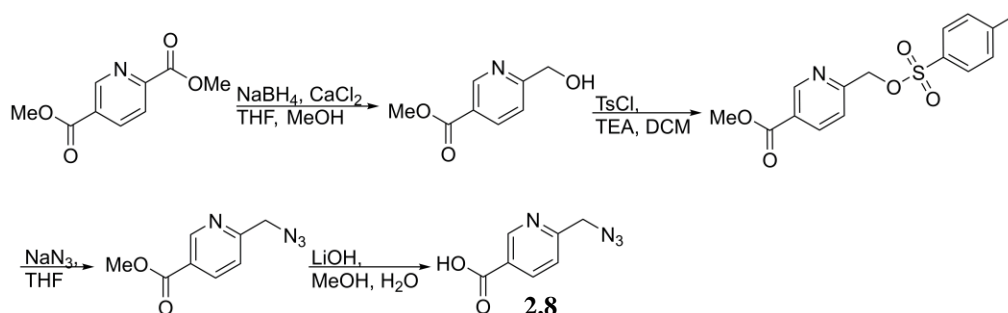
added (0.44 g, 1 mmol), followed by EDC-HCl (0.39 g, 2.01 mmol) and HOAt (0.27 g, 2.02 mmol) and the reaction mixture was stirred at room temperature for 30 h. The reaction mixture was washed with sodium bicarbonate (1 x 15 mL), 10% citric acid (1 x 15 mL), and brine (1 x 15 mL), respectively. All aqueous layers were back-extracted with DCM (1 x 10 mL). The organic layers were collected, dried over sodium sulfate and concentrated to yield **2.35** (0.42 g, 77%). ^1H NMR (500 MHz, CDCl_3) δ 7.93 (t, $J = 6.2$ Hz, 2H), 5.57 (d, $J = 9.4$ Hz, 2H), 4.82 (ddd, $J = 14.1$, 7.2, 4.0 Hz, 2H), 3.46 (app dq, $J = 13.3$, 6.7 Hz, 2H), 3.34 (app dq, $J = 13.3$, 6.7 Hz, 2H), 3.01-2.97 (m, 2H), 2.92-2.87 (m, 2H), 2.48 (dtd, $J = 16.5$, 6.9, 2.7 Hz, 2H), 2.39 (dtd, $J = 16.5$, 6.9, 2.7 Hz, 2H), 1.96 (t, $J = 2.5$ Hz, 2H), 1.47 (s, 18 H). ^{13}C NMR (125 MHz, CDCl_3) δ /ppm = 170.6, 156, 81.4, 80.4, 70, 54.8, 47.4, 38.6, 28.6, 19.5. HRMS (ESI) m/z calc. for $\text{C}_{24}\text{H}_{39}\text{N}_4\text{O}_6\text{S}_2$ ($\text{M}+\text{H}^+$) 543.2311, found 543.2310. (*Notebook II, page 88*)



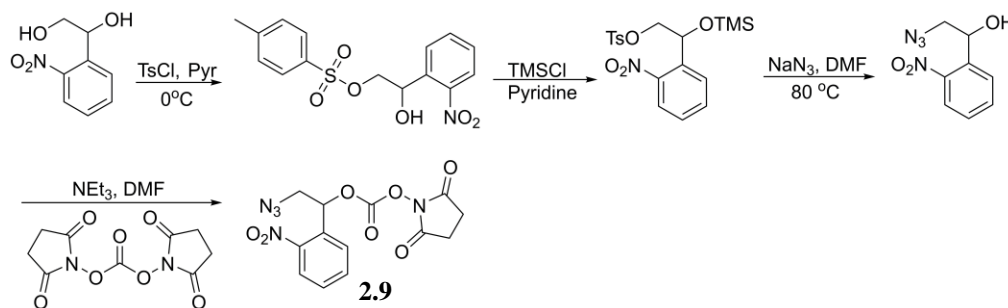
Compound **2.36**. Compound **2.35** (0.42 g, 0.79 mmol) was suspended in 6 mL of dry DCM to form a milky suspension. To this suspension, 6 mL of trifluoroacetic acid (TFA) was added when a clear yellowish solution formed,

which was stirred at room temperature for 1 h. TFA was then evaporated using a stream of N₂. The residue was dissolved in water and lyophilized to yield **2.36** as white fluffy solid (0.34 g, 95%). ¹H NMR (500 MHz, D₂O) δ 4.31 (t, *J* = 6.5 Hz, 2H), 3.49-3.43 (m, 2H), 3.37-3.33 (m, 2H), 3.33-3.28 (m, 2H), 3.23-3.18 (m, 2H), 2.47-2.42 (m, 2H), 2.36-2.35 (t, *J* = 2.5 Hz, 2H). ¹³C NMR (125 MHz, CDCl₃) δ/ppm = 168, 82.4, 70.8, 52.1, 38.5, 37.7, 18.4. HRMS (ESI) *m/z* calc. for C₁₄H₂₃N₄O₂S₂ 343.1262, found 343.1256. During EPL, compound **2.36** was reduced in situ to **2.6**. (Notebook II, page 90)

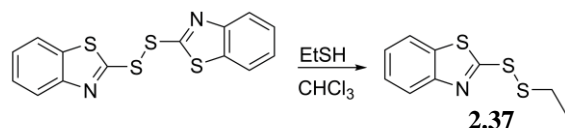
2.4.4. Scheme for the Synthesis of Azide Building Block **2.8** (26) (Notebook V, pages 22-24)



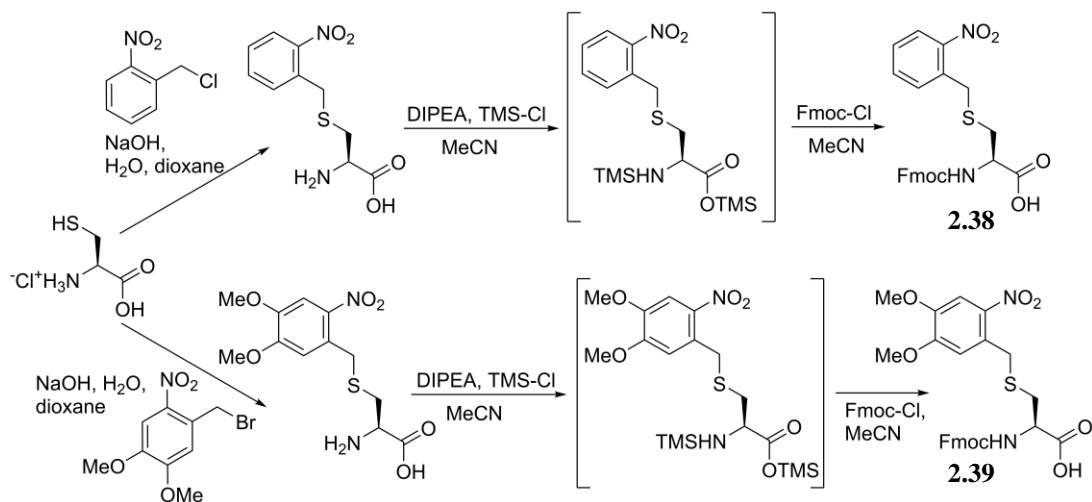
2.4.5. Scheme for the Synthesis of Azide Building Block **2.9** (27) (Notebook V, pages 50, 51, 53, 54)



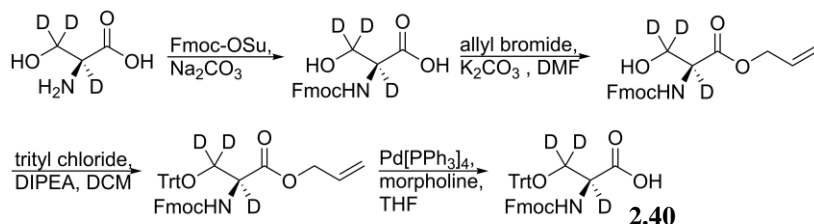
2.4.6. Synthesis of Benzothiazolyl-Ethyl Disulfide **2.37** (22, 32) (Notebook III, pages 27, 87)



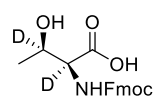
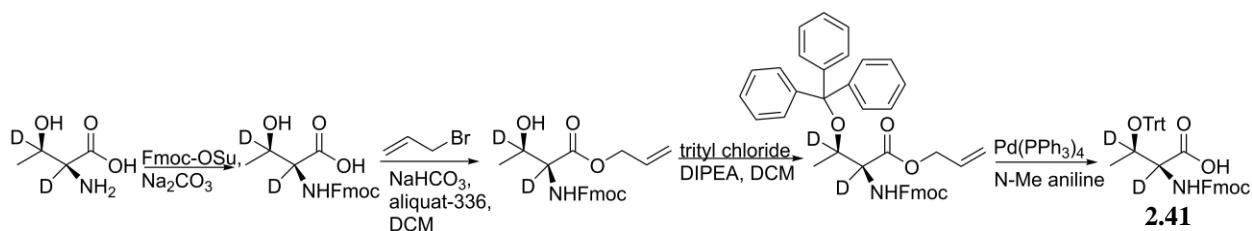
2.4.7. Scheme for Synthesis of Cys(*o*-NO₂Bn) Building Blocks **2.38 (33),(28) and **2.39** (34) for SPPS** (Compound **2.38** - Notebook VI, pages 5, 9; compound **2.39** - Notebook V, pages 31-32)



2.4.8. Scheme for Synthesis of [2,3,3-²H]-Ser Building Block **2.40 for SPPS** (9) (Notebook VI, pages 47, 50, 51, 60)



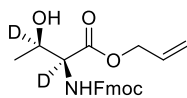
2.4.9. Scheme for Synthesis of Protected [2,3-²H]-Thr Building Block **2.41 for SPPS**



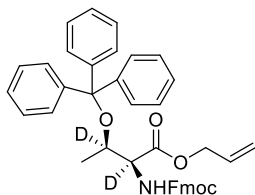
Compound **2.42**. L-[2,3-²H]-Thr-OH (0.25 g, 2.06 mmol) and Na₂CO₃ (0.25 g, 2.36 mmol) was dissolved in 3 mL of H₂O. Fmoc-OSu (0.75 g, 2.22 mmol) dissolved in

4 mL of dry dioxane was stirred in an ice-bath, and the amino acid solution was added slowly to the dioxane solution. The ice-bath was removed and the reaction was stirred for 20 h to form a

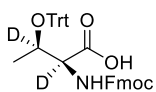
milky suspension. The solvent was then removed on a rotary evaporator, and the residue was dissolved in H₂O (20 mL) to generate a colorless solution. 10% citric acid was used to acidify the solution to pH 4.0, when a thick white solution formed. The aqueous layer was extracted with EtOAc (10 x 25 mL) and the organic layer was washed with brine (1 x 50 mL) and concentrated on a rotary evaporator followed by drying using a vacuum pump to generate a white solid, which was carried over to the next step without purification. Yield (crude): 0.97 g (calculated 0.71 g) (*Notebook VII, page 42*)



Compound **2.43**. Compound **2.42** (0.97 g) was suspended in a solution of NaHCO₃ (0.18 g, 2.1 mmol) in 6 mL of H₂O. The suspension was stirred under N₂ and to it, 13 mL of dry DCM was added, while stirring vigorously. Aliquat-336 (0.96 mL, 2.1 mmol) was added followed by allyl bromide (1.3 mL, 15 mmol) and then the reaction was continued to be stirred vigorously for 22 h. The reaction mixture was then diluted with 15 mL of H₂O and extracted with DCM (4 x 20 mL). The organic layers were collected, washed with brine (1 x 20 mL), dried over Na₂SO₄ and concentrated on a rotary evaporator to generate a pale-yellow oil. The crude mass was purified by flash chromatography (SiO₂, 30% EtOAc in hexanes) to generate **2.43** as a white solid upon concentrating on a rotary evaporator. R_f 0.21 (30% EtOAc in hexanes). Yield: 0.59 g (75%). ¹H NMR (500 MHz, CDCl₃) δ 7.7 (d, *J* = 7.5 Hz, 2H), 7.61 (t, *J* = 7.5 Hz, 2H), 7.40 (t, *J* = 7.5 Hz, 2H), 7.31 (t, *J* = 7.5 Hz, 2H), 6.10-5.89 (m, 1H), 5.60 (s, 1H), 5.39-5.33 (m, 1H), 5.26 (d, *J* = 10.5 Hz, 1H), 4.68 (d, *J* = 5.5 Hz, 2H), 4.46-4.39 (m, 2H), 4.25 (t, *J* = 7.0 Hz, 1H), 2.70 (s, 1H), 1.26 (s, 3H). ¹³C NMR (125 MHz, CDCl₃) δ 171.5, 156.9, 143.9, 143.7, 141.3, 131.5, 131, 127.8, 127.1, 125.2, 122.7, 120, 119, 67.3, 66.3, 47.2, 25.5, 19.9. HRMS (ESI) calculated for C₂₂H₂₂D₂NO₅ (M+H⁺) 384.1777, observed 384.1780. (*Notebook VII, page 43*)



Compound **2.44**. Compound **2.43** (0.59 g, 1.54 mmol) was dissolved in 13 mL of dry DCM and DIPEA (0.83 mL, 4.8 mmol) was added to the solution. Trityl chloride (1.09 g, 3.9 mmol) dissolved in 5 mL of dry DCM was added dropwise and the reaction was stirred for 21 h. The reaction turned from colorless to light pink to dark pink over time. The reaction was concentrated on a rotary evaporator and the product purified twice by SiO₂ gel flash chromatography. Elution was performed by a stepwise gradient from 10% EtOAc in Hex to 20% to 30% EtOAc in Hex. Product **2.44** eluted with an R_f of 0.57 (3:1 Hex:EtOAc). Yield: 0.38 g (39%). Unreacted starting material **2.43** (0.27 g, 45%) was also recovered (R_f 0.15, 3:1 Hex:EtOAc). ¹H NMR (500 MHz, CDCl₃) δ 7.82 (dd, *J* = 7.6, 2.9 Hz, 2H), 7.70 (dd, *J* = 19.5, 7.5 Hz, 2H), 7.43-7.41 (m, 4H), 7.32-7.27 (m, 15H), 5.77-5.69 (m, 1H), 5.23-5.17 (m, 2H), 4.54-4.53 (dd, *J* = 13.0, 6.1 Hz, 1H), 4.32-4.27 (m, 2H), 0.91 (s, 3H). ¹³C NMR (125 MHz, CDCl₃) δ 156.8, 147.0, 144.6, 144.2, 144.0, 141.5, 131.7, 129.0, 128.0, 127.9, 127.8, 127.4, 127.2, 125.3, 120.1, 119.0, 82.2, 67.4, 66.4, 47.4, 18.8. HRMS (ESI) calculated for C₄₁H₃₅D₂NO₅Na (M+Na⁺) 648.2695, observed 648.2695. (*Notebook VII, pages 44-45*)



Compound **2.41**. Compound **2.44** (0.38 g, 0.61 mmol) was dissolved in 4 mL of dry THF and the round bottom flask was covered in Al-foil. Pd[PPh₃]₄ (0.05 g, 0.04 mmol) was added followed by *N*-methyl aniline (0.07 mL, 0.65 mmol) as a solution in 3 mL of dry THF and the reaction was stirred for 2.5 h. The reaction mixture was diluted with 100 mL of EtOAc and washed with brine (2 x 30 mL). The aqueous layer was extracted with EtOAc (5 x 25 mL) and concentrated on a rotary evaporator and dried using a vacuum pump. The product was used without further purification. HRMS (ESI) calculated for C₃₈H₃₁D₂NO₅Na (M+Na⁺) 608.2380, observed 608.2378. (*Notebook VII, page 46*)

2.4.10. Solid Phase Peptide Synthesis (SPPS)

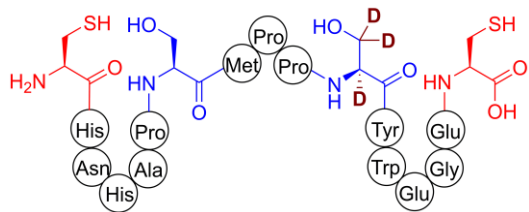
The automated peptide coupling was performed on a CEM Liberty microwave peptide synthesizer using standard Fmoc protected amino acids, 2-(6-chloro-1*H*-benzotriazole-1-yl)-1,1,3,3-tetramethyluronium hexafluorophosphate (HCTU) as activator, 2 M *N,N*-diisopropylethylamine (DIPEA) in *N*-methyl-2-pyrrolidone (NMP) as the activator base, 20% piperidine in dimethylformamide (DMF) as the deprotection agent and 90/8/2 DMF/acetic anhydride/DIPEA as the capping agent. Coupling of each amino acid in the microwave synthesizer occurred at 75 °C except for Cys and His residues for which coupling was performed at 50 °C to prevent racemization. Typically each residue was double coupled followed by a capping step, unless otherwise noted. Coupling of any synthesized non-proteinogenic amino acid residues and the azide linker at the *N*-terminus was performed manually using either diisopropyl carbodiimide (DIC) as the coupling agent with 1-hydroxy-7-azabenzotriazole (HOAt) as the racemization suppressant, or HCTU as activator. Unless otherwise stated, manual couplings were performed as follows. Fmoc deprotection was performed using 20% piperidine in DMF while sparging the resin with N₂ for agitation (2 x 5 min). After draining the reaction vessel, the resin was washed with DMF (6 x 30 s). The appropriate moiety to be coupled (4 equiv.) was dissolved in DMF (5-10 mL) and pre-activated with DIC/HOAt (4 equiv.) for 5 min, then added to the resin and the reaction was agitated by sparging with N₂ for 1 h. After draining the reaction vessel, the resin was washed as before. Kaiser test was performed to monitor the completion of coupling and double coupling was performed as needed. The coupling of [2,3,3-²H]-L-Ser and [2,3-²H]-L-Thr building blocks were performed under optimized conditions using (7-azabenzotriazol-1-yloxy)tripyrrolidinophosphonium hexafluorophosphate (PyAOP) as activator and HOAt as racemization suppressant using 2,4,6-collidine as base to prevent partial loss of the

α -deuterium during coupling. After the completion of SPPS, the resin was washed with ca. 5 mL of DMF (3 x 30 s) and then ca. 5 mL of DCM (3 x 30 s) and drained under vacuum to dry the resin. The cleavage of the synthesized peptide from the resin was performed in a cleavage cocktail of 95/2.5/2.5 TFA/triisopropyl silane/H₂O for 1 h and then the solution was filtered through a fritted funnel and the filtrate was evaporated under a stream of N₂ to remove most of the TFA. Peptide was precipitated by adding 10-15 mL of cold diethyl ether to the solution. The mixture was centrifuged and the supernatant was discarded. The precipitate was dissolved in 50% MeCN, 0.05% TFA in H₂O, flash frozen in liquid N₂ and lyophilized to generate white to pale yellow amorphous powder, which was stored at -20 °C.

Often, the free thiols were protected as ethylthio disulfide to increase the yield of CuAAC. Such protection was carried out in solution phase. HPLC purified peptide was dissolved in H₂O and about 10 equiv. of compound **2.37** (2-(ethylidisulfanyl)benzo[*d*]thiazole) dissolved in 20-50 μ L of EtOH was added and the reaction was stirred at room temperature for 7 h. The reaction mixture was centrifuged and the supernatant was further purified by HPLC using methods described later.

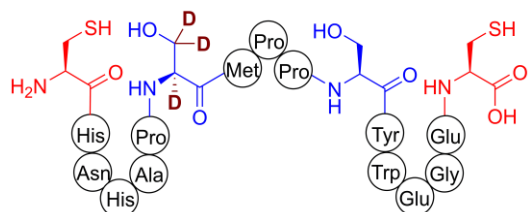
Analytical reversed-phase high-performance liquid chromatography (RP-HPLC) was performed on an Agilent 1260 Infinity system with a Phenomenex Luna C₁₈, a Waters Vydac C₁₈, or a Waters Vydac C₄ column with a flow rate of 1 mL/min and a solvent gradient of 2-100% solvent A over 45 min. Preparatory RP-HPLC was performed on a Waters 600 system with a Phenomenex Luna C₁₈ or C₅ semi-preparative column using a gradient of 2% solvent A to 67% solvent A in 30 min. Any change from these standard HPLC conditions is noted in the procedures. All HPLC solvents were filtered with a Millipore filtration system equipped with a

0.22 μm nylon membrane filter prior to use. HPLC solvent compositions: solvent A was 80% acetonitrile in water with 0.086% trifluoroacetic acid (TFA), solvent B was 0.1% TFA in water.



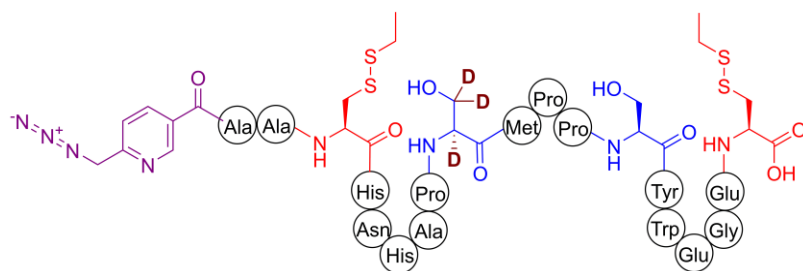
Peptide 2.2. H-Cys(Trt)-2-chlorotrityl resin (0.05 mmol) was used. All amino acids (0.25 mmol) were manually coupled using HCTU (0.25 mmol) as activator and DIPEA (0.5 mmol) as base, except for

the deuterated Ser residues. All residues were double coupled (2 x 1 h coupling time) followed by capping procedure. Coupling of [2,3,3- ^2H]-L-Ser was performed using PyBOP (0.25 mmol) as activator, HOAt (0.25 mmol) as racemization suppressant, and 2,4,6-collidine as base, with a 3 h coupling time. Post cleavage from the resin, 54 mg of crude peptide was obtained. Of the crude peptide, 25 mg was purified in 7 injections by preparative RP-HPLC using the standard gradient to elute **2.2** with a retention time (R_t) of 15.0 – 15.7 min (34% to 36% solvent A). Yield: 7.5 mg. MALDI-TOF (LR-MS) m/z calculated for $\text{C}_{83}\text{H}_{111}\text{D}_3\text{N}_{23}\text{O}_{26}\text{S}_3$ 1947.76 ($\text{M}+\text{H}^+$), observed 1947.69. (*Notebook VII, page 28*)



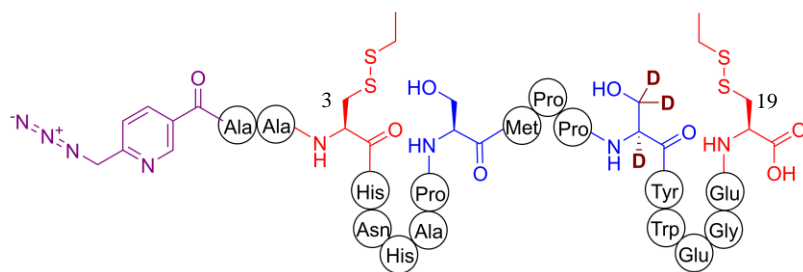
Peptide 2.3. Using similar chemistry as for peptide **2.2**, 53 mg of crude peptide was synthesized on a 0.05 mmol scale. Of the crude peptide, 22 mg was purified

in 8 injections by RP-HPLC using the standard gradient to elute **2.3** with an R_t of 15.2 – 16.1 min (35% to 37% solvent A). Yield: 8 mg. MALDI-TOF (LR-MS) m/z calculated for $\text{C}_{83}\text{H}_{111}\text{D}_3\text{N}_{23}\text{O}_{26}\text{S}_3$ 1947.76 ($\text{M}+\text{H}^+$), observed 1947.69. (*Notebook VII, pages 26-27*)



Peptide 2.45. H-Cys(Trt)-2-chlorotrityl resin (0.05 mmol) was used. Each residue was double coupled followed by

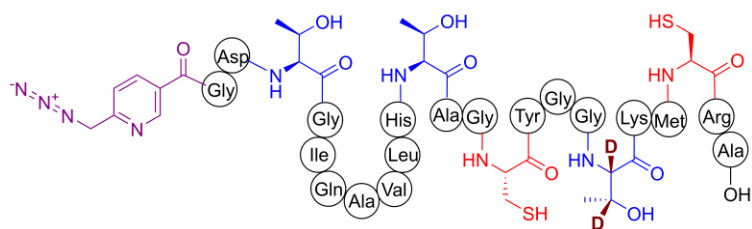
capping on a CEM microwave synthesizer except for the following. Compound **2.40** (0.2 mmol) was coupled with PyAOP (0.2 mmol) as activator, HOAt (0.2 mmol) as racemization suppressant, and 2,4,6-collidine (0.4 mmol) as base in 5 mL of DMF with 3 h coupling time. Final coupling of **2.8** (0.15 mmol) was performed manually using HCTU (0.15 mmol) and DIPEA (0.3 mmol) for 3 h. Post cleavage from the resin, 3.2 mg of crude peptide was obtained. RP-HPLC using the standard gradient was used to purify the crude peptide, with the precursor to **2.45** with free thiols eluting with a R_t of 17.4 min (40% solvent A). Yield: 0.7 mg. This peptide (0.7 mg, 0.31 μ mol) was dissolved in 0.4 mL of H₂O and stirred. Compound **2.37** (0.92 mg, 4.05 μ mol) dissolved in 20 μ L of EtOH was added to the peptide solution and the reaction mixture was stirred for 4 h. The reaction mixture was diluted with 3 mL of starting eluent for RP-HPLC (2% solvent A, 98% D) and then centrifuged (15000 x g, 5 min) and the supernatant was purified by HPLC in two injections using the standard conditions to elute **2.45** with a R_t of 21.1 min. Yield: 0.18 mg. MALDI-TOF MS calculated for C₁₀₀H₁₃₃D₃N₂₉O₂₉S₅ (M+H)⁺ 2369.9, observed 2370.1. (*Notebook VI, pages 87, 92*)



Peptide 2.46. Using similar chemistry as described for peptide **2.45**, this peptide was synthesized from 0.05 mmol

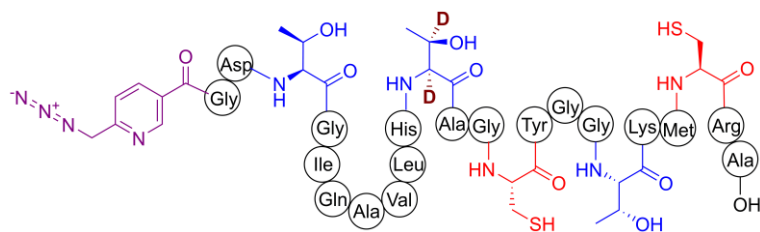
resin to yield 9.8 mg of crude peptide, which was purified using the standard conditions to yield

1.4 mg of pure peptide with unprotected Cys3 and Cys19 (R_t 17.5 min, 40% solvent A). Compound **2.37** (2.22 mg, 9.8 μmol) dissolved in 40 μL of EtOH was added to the 5 mL of peptide solution (1.37 mg) and the reaction mixture was stirred for 12 h at room temperature. The reaction mixture was diluted with 3 mL of starting eluent for RP-HPLC (2% solvent A, 98% solvent D) and then centrifuged (15000 x g, 5 min) and the supernatant was purified by HPLC in two injections using the standard conditions to elute **2.46** with a R_t of 21.1 min. Yield: 0.17 mg. MALDI-TOF MS calculated for $\text{C}_{100}\text{H}_{133}\text{D}_3\text{N}_{29}\text{O}_{29}\text{S}_5$ ($\text{M}+\text{H}$)⁺ 2369.9, observed 2370.2. (*Notebook VI, pages 88, 93*)



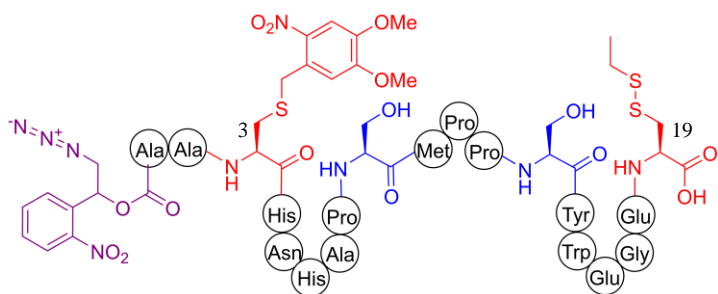
Peptide 2.47. Each residue was triple coupled followed by capping on a microwave synthesizer except for coupling [2,3-²H]-L-Thr.

Coupling of **2.41** was performed manually using PyBOP as activator, HOAt as racemization suppressant and 2,4,6-collidine as base. Final coupling of **2.8** was performed using HCTU/DIPEA chemistry. Post cleavage from the resin, 41 mg of crude peptide was obtained, which was purified using a C₁₈ Phenomenex column using the standard conditions to elute target peptide with a R_t of 19.4 min (44% solvent A). Yield: 1.7 mg. MALDI-TOF (LR-MS), m/z calculated for $\text{C}_{102}\text{H}_{159}\text{D}_2\text{N}_{34}\text{O}_{32}\text{S}_3$ 2472.12, observed 2471.97. (*Notebook VII, pages 70, 71*)



Peptide 2.58. Using similar chemistry as for the synthesis of peptide **2.47**, peptide **2.48** was prepared. Post cleavage from the

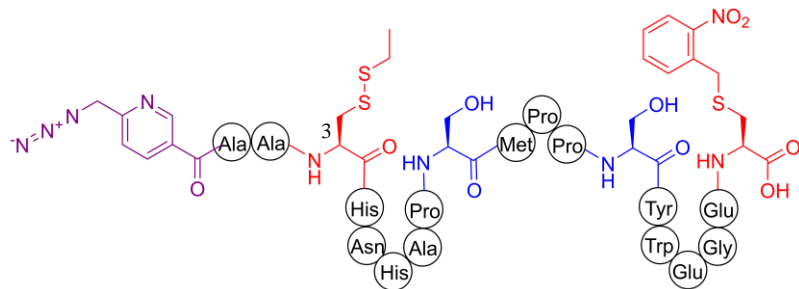
resin, 37.7 mg of crude peptide was obtained, which was purified using a C₁₈ Phenomenex column using the standard conditions in four injections, with **2.48** eluting at a R_t of 19.4 min (44% solvent A). Yield: 0.61 mg. MALDI-TOF (LR-MS), m/z calculated for C₁₀₂H₁₅₉D₂N₃₄O₃₂S₃ (M+H⁺) 2472.12, observed 2472.06. (*Notebook VII, page 80*)



Peptide 2.49. The first residue Glu was coupled manually to H-Cys(Trt)-2-chlorotrityl resin using DIC/HOAt chemistry in the absence of base. Compound **2.39** was used to manually

install Cys3 with 4,5-dimethoxy-2-nitrobenzyl protection using DIC/HOAt chemistry. All other residues were coupled using a CEM microwave synthesizer. The final coupling of the *N*-terminal azide-containing moiety was performed as follows. The peptide-bearing 2-chlorotrityl resin (0.05 mmol) was placed in a 5 mL round bottom flask. To the resin, a solution of compound **2.9** (45 mg, 0.13 mmol, 2.6 equiv.) in 2 mL of dry DMF was added, followed by 50 μ L of DIPEA (0.22 mmol, 4.5 equiv) and the reaction was stirred overnight for 15 h. The solution was drained over a fritted funnel and the resin was washed with DMF (3 x 30 s) and DCM (3 x 30 s). Standard cleavage conditions yielded 5.5 mg of crude product, which was purified using a Phenomenex Luna C₁₈ column using the standard gradient and flow-rate conditions as previously described to yield pure precursor peptide to **2.49** (1.1 mg) with a free Cys19. R_t 22.7 min, eluting at 52% of solvent A. The peptide was reacted with **2.37** and further purified by RP-HPLC using the standard conditions to generate **2.49** eluting with a R_t of 23.5

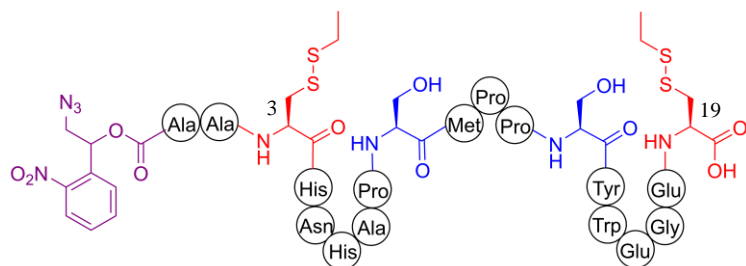
min to 25 min (53% solvent A). Yield: 0.25 mg. LR-MS (MALDI-TOF) calculated for $C_{109}H_{143}N_{30}O_{36}S_4$ 2575.9 ($M+H^+$), observed 2576.3. (*Notebook V, pages 57, 58*)



Peptide 2.50. Compound **2.38**

(0.16 g, 0.33 mmol) was dissolved in 5 mL of dry DCM and 1 mL of dry DMF and this solution was added to 500 mg

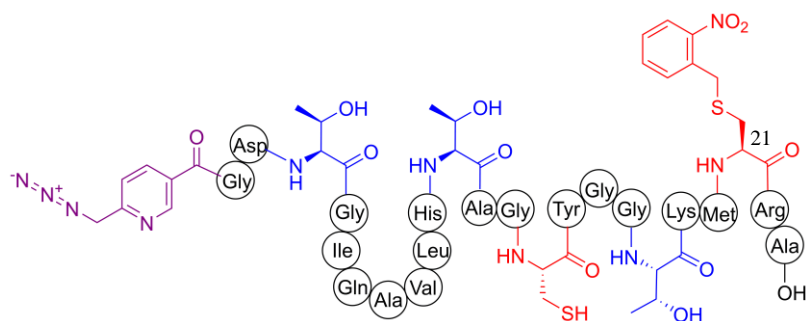
of 2-chlorotrityl choride resin (0.65 meq g^{-1}) pre-swelled in DMF. To this mixture, DIPEA (0.23 mL, 1.3 mmol) was added and the reaction was stirred for 14 h under N_2 . The solution was drained through a fritted funnel and the resin was washed successively with 5 mL of DCM, MeOH and again DCM. Subsequent iterative Fmoc deprotection and amino acid coupling (DIC/HOBt chemistry) was carried out on 0.1 mmol of resin. Standard cleavage generated the precursor to **2.50** with a free thiol at Cys3. About 11 mg of crude peptide was purified by RP-HPLC using the standard conditions to generate pure precursor to **2.50** (3.6 mg), R_t : 20.2 min, eluted at 46% solvent A. The free thiol at the Cys3 was protected by reaction with **2.37** and the obtained peptide was purified by HPLC using a Phenomenex Luna C_{18} column using the standard conditions to obtain pure **2.50** (1.9 mg), R_t : 20.6 min, eluting at 47% solvent A. LR-MS (MALDI-TOF) calculated for $C_{105}H_{137}N_{30}O_{31}S_4$ 2441.88, ($M+H^+$), observed 2441.94. (*Notebook VI, pages 13, 14, 16*)



Peptide 2.51. H-Cys(Trt)-2-

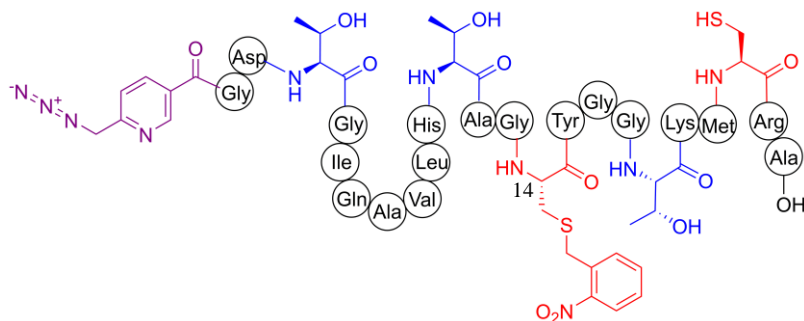
chlorotrityl resin was used. The first residue Glu was coupled manually to H-Cys(Trt)-2-chlorotrityl resin using

DIC/HOAt chemistry in the absence of base. All residues except Cys3 were coupled on the microwave synthesizer using the standard conditions. Cys3 was coupled manually using diisopropylcarbodiimide (DIC) as activator and HOAt as racemization suppressant. Standard cleavage generated the precursor to **2.51** with a free thiol at Cys3 and Cys19. Crude peptide (30.6 mg) was purified by RP-HPLC using the standard conditions to elute precursor to **2.51** (7.4 mg, R_t 20.2 min, 46% solvent A). The precursor to **2.51** (4.2 mg) was reacted with **2.37** and the product was purified by RP-HPLC using the standard conditions to yield pure **2.51** (2.2 mg), R_t 23.8 min (54% solvent A). LR-MS (MALDI-TOF) calculated for $C_{102}H_{138}N_{29}O_{32}S_5$ 2440.88, ($M+H^+$), observed 2441.11. (*Notebook V, pages 82, 85, 87*)



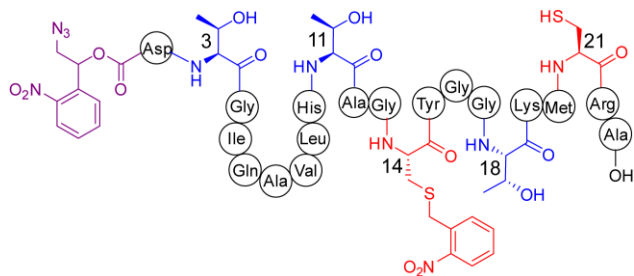
Peptide 2.52. Fmoc-Ala-Wang resin (0.1 mmol) was used. Each residue was triple coupled followed by capping on a microwave synthesizer except

for the following. Cys21 with an *o*-nitrobenzyl protected thiol was installed by coupling **2.38** manually using HCTU as activator and DIPEA as base. Final coupling of 6-azidomethyl nicotinic acid (compound **2.8**) was performed manually using the same chemistry. After cleavage of the peptide from the resin, the yield of crude peptide was 103 mg. Of the crude peptide, 59 mg was loaded onto a Phenomenex C_{18} column in 5 injections and purified using the standard gradient to elude **2.52** with a R_t of 21.1 min (48% solvent A). Yield: 2.2 mg. MALDI-TOF (LR-MS) for $C_{109}H_{166}N_{35}O_{34}S_3$ calculated 2605.1 ($M+H^+$), observed 2605.1. (*Notebook VII, page 79*)



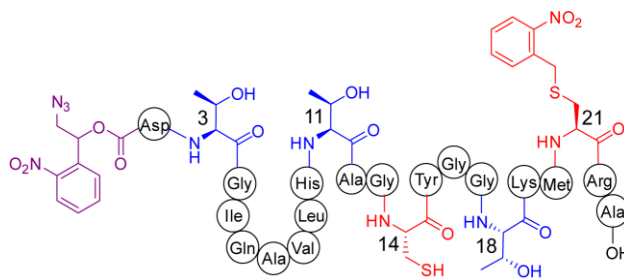
Peptide 2.53. Fmoc-Ala-Wang resin (0.05 mmol) was used. Each residue was triple coupled followed by capping on a microwave synthesizer except

for the following. Coupling of **2.38** (0.2 mmol) was performed manually on 0.05 mmol of resin using 1-[bis(dimethylamino)methylene]-1*H*-1,2,3-triazolo[4,5-*b*]pyridinium 3-oxid hexafluorophosphate (HATU, 0.2 mmol) as activator and DIPEA (0.4 mmol) as base, with 5 h coupling time. Final coupling of **2.8** (0.15 mmol) was performed manually using HATU (0.15 mmol) and DIPEA (0.3 mmol) for 4 h. After cleavage from the resin, 43 mg of crude peptide was obtained. The standard gradient was used to purify the crude peptide, with **2.53** eluting with a R_t of 21.5 min. Yield: 0.9 mg. MALDI-TOF MS for $C_{109}H_{166}N_{35}O_{34}S_3$ calculated 2605.1 ($M+H^+$), observed 2604.7. (*Notebook VIII, page 9*)



Peptide 2.54. All residues other than 2-nitrobenzyl cysteine and the N-terminal azide moiety were coupled on the automated microwave peptide synthesizer. The two

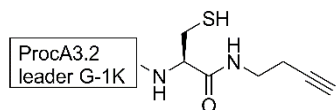
residues mentioned were coupled manually using HCTU/DIPEA chemistry. After cleavage of the peptide from the resin, 47 mg of crude peptide was obtained from a 0.1 mmol reaction which was purified by RP-HPLC purification to generate 1.1 mg of purified peptide (R_t 24 min). (*Notebook VIII, page 68*)



Peptide **2.55**. In a similar fashion as peptide **2.54**, 58 mg of crude peptide was obtained which was purified by RP-HPLC to generate 1.4 mg of pure peptide. (*Notebook VIII, page*

67)

2.4.11. Generation of the Alkyne Modified ProcA3.2 Leader Peptide



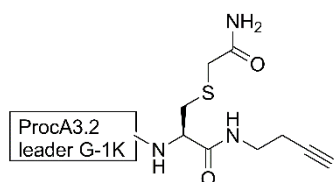
Peptide **2.56**. An aliquot of BL21 (DE3) *E. coli* cells was transformed with pET15b plasmid encoding His₆-ProcA3.2-leader-

intein-CBD (CBD: chitin binding domain) and then the transformed cells were spread on a LB + ampicillin (100 µg/mL) agar plate and incubated overnight at 37 °C. Cells from a single colony were used to inoculate two 25 mL LB + Amp (100 µg/mL) cultures, which were incubated overnight. The starter cultures were used to inoculate 2 x 1.5 L cultures in LB + Amp (100 µg/mL) and the cells were grown until the OD_{600 nm} for each set was ca. 0.6 when IPTG (final concentration 0.5 mM) was added and the cultures were incubated in a 18 °C shaker overnight (final OD_{600 nm} 2.5-3.0). The cells were harvested by centrifugation (10,500 x g, 30 min). The cell pellets were suspended in 40 mL of lysis buffer (50 mM HEPES, 500 mM NaCl, 1 mM EDTA, 0.1 % Triton-X, PMSF (dissolved in 20 mL of isopropanol, final concentration ca. 1 mM), TCEP-HCl (1 mM, pH- 7.5) and the cells were lysed by sonication (4.4 s pulse, 9.9 s interval, 35% amplitude). The cell lysate was centrifuged (22800 x g, 30 min) and the supernatant was filtered through 0.45 µm amicon filters. The chitin resin (NEB) was loaded into a column and equilibrated with column buffer (50 mM HEPES, 500 mM NaCl, 1 mM EDTA). To the resin, the cell lysate was applied and the column was shaken in the cold room (4 °C) on a rocker for 4 h to allow proper mixing. The cell lysate was allowed to drain from the resin at 2 mL/min. The resin

was washed further with column buffer (ca. 400 mL at 2 mL/min). Cleavage buffer (40 mL) consisted of column buffer containing MESNa (50 mM), TCEP-HCl (5 mM), compound **2.36** (60 mg, ca. 2 mM), and the pH was adjusted to 7.5. The cleavage buffer was added to the resin and the column was rocked for 16 h, after which the buffer was eluted. The resin was washed with 20 mL of column buffer and the washing along with the eluted cleavage buffer was concentrated on 3000 Da MWCO Amicon filter (4000 x g, 45 min) and the concentrated peptide was desalted on a C₄ SPE column and lyophilized. Yield: 45 mg. LR-MS (MALDI-TOF) calculated for C₃₈₄H₆₁₀N₁₂₁O₁₂₈S₂ 9028.4 (M+H⁺), observed 9031. His-tag-ProcA3.2 G-1K sequence:

GSSHHHHHSSGLVPRGSHMSEELKAFIAKVQADASLQELRTEGADVVAIAKAAGF
SITTEDLNSHRQNLSDDLEGVAGK (*Notebook VI, pages 32, 48*)

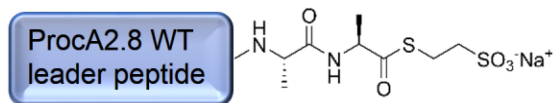
2.4.12. Iodoacetamide Capping of the Free Cys Generated During EPL



Peptide 2.7. Peptide **2.56** (41.8 mg, 4.6 μmol) was dissolved in 2 mL of 100 mM NH₄HCO₃ buffer, pH 8.1. TCEP-HCl (7.2 mg, 25.3 μmol, 5.4 equiv.) was dissolved in 1 mL of 100 mM NH₄HCO₃

buffer and was added to the peptide solution. Iodoacetamide (7.5 mg, 40.5 μmol, 8.7 equiv.) dissolved in 1 mL of H₂O was added to the reaction mixture and the solution was stirred at room temperature for 16 h. The 4 mL of reaction mixture was diluted in 14 mL of 2% solvent A (80% MeCN in 0.086% TFA) and 98% solvent D (0.1% aqueous TFA) and purified using a Phenomenex Luna C₅ column in Waters Delta 600 HPLC purification system using a flow rate of 7 mL/min. A gradient of 2% A to 67% solvent A in 30 min was employed and **2.7** eluted with a R_t between 21.4 min – 23.6 min. Yield: 28 mg. LR-MS (MALDI-TOF) calculated for C₃₈₆H₆₁₃N₁₂₂O₁₂₉S₂ 9085.45 (M+H⁺), observed 9089. (*Notebook VI, page 49*)

2.4.13. Generation of ProcA2.8 Leader-AlaAla-MESNa Thioester



Peptide 2.1. *E.coli* BL21(DE3) cells were transformed with pTXB1 plasmid encoding His₆-

tag-ProcA2.8 leader-AlaAla-intein-chitin binding domain^{††}, and the cells were spread on a LB + Ampicillin (100 µg/mL) agar plate and incubated overnight at 37 °C. Cells from a single colony were used to inoculate two 25 mL LB + Amp (100 µg/mL) starter cultures, which were incubated overnight. The starter culture was used to inoculate 5 L (2 x 1.5 L, and 2 x 1 L) LB + Amp (100 µg/mL) medium. The cultures were shaken at 37 °C to an OD_{600nm} of ca. 0.6. After cooling the cultures to room temperature, IPTG (final concentration: 0.5 mM) was added to induce the cells and the cells were shaken at 18 °C for 17 h. The cells were harvested by centrifugation (10,500 x g, 20 min) and frozen at – 80 °C until further use. The cell pellet (from 2.5 L culture) was thawed on ice and 30 mL of lysis buffer [NaP_i (50 mM, pH 7.0), NaCl (500 mM), and TCEP (1 mM)] was added and the cells were homogenized. Cells were then lysed by sonication (4.4 sec pulse, 9.9 sec interval, 35% amplitude) on ice. The cells were centrifuged (22,800 x g, 30 min) and the supernatant was filtered through a 0.45 µm filter. The filtered supernatant was loaded onto a column packed with chitin resin (25 mL) equilibrated with column buffer [NaP_i (50 mM, pH 7.0), NaCl (500 mM)]. The column was shaken on a rocker in a cold room (4 °C) for 2 h. The slurry was drained (1 mL/min) and the column was then washed with 250 mL (~10 CV) of column buffer. To the resin, 30 mL of cleavage buffer (column buffer + 50 mM MESNa) was applied and the column was shaken overnight on a rocker at 4 °C. The eluent was collected (~35 mL) and acidified to 0.1 % TFA to lower the pH (~4), desalted on a C₄ SPE column and eluted with 80% MeCN, 0.1% TFA in H₂O and lyophilized. The lyophilized peptide

^{††} Provided by Dr. Christopher Thibodeaux, Institute of Genomic Biology, UIUC.

was dissolved in 15 mL of starting eluent: 2% solvent A (80% MeCN, 0.086% TFA in H₂O), 98% solvent D (0.1% TFA in H₂O) and then purified in 5 injections using a C₅-Phenomenex semi-prep column using a flow-rate of 7 mL/min. Elution gradient: 2% A to 67% solvent A over 30 min. Product eluted with a R_t of 21.9 min - 22.9 min (50% - 52% solvent A). Yield: 9 mg (from 2.5 L culture). MALDI-TOF MS calculated 9117 (M+H⁺), observed 9119.

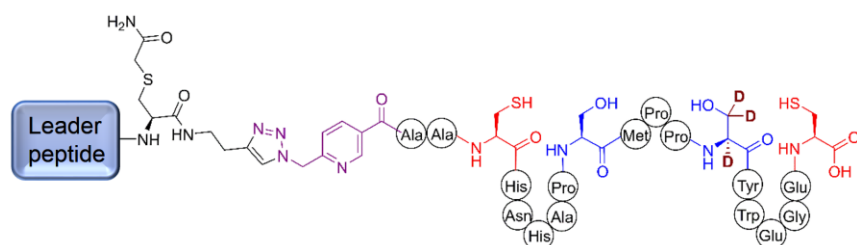
Peptide sequence of His-tag-ProcA2.8-AlaAla:

GSSHHHHHHSSGLVPRGSHMSEELKAFLLTKVQADTSLQEQLKIEGADVVAIAKAAGFS
ITTEDLNHRQNLSDDELEGVAGGAA (*Notebook VII, pages 23, 24*)

2.4.14. Copper Catalyzed Azide–Alkyne Cycloaddition (CuAAC) - ‘Click Chemistry’

Equivalent amounts of the two reacting peptide partners were dissolved in H₂O or 50% aqueous MeCN (if not completely soluble in H₂O), frozen with liquid N₂ and lyophilized. The lyophilized mixture of two peptides was dissolved in 30 mM aqueous degassed phosphate buffer, pH 7.8 to a concentration of about 1 to 2 mM for each peptide. Activated catalyst solution was prepared by mixing 5 μL of 100 mM CuSO₄ in degassed H₂O, 25 μL of 20 mM TBTA in MeOH, 10 μL of 200 mM sodium ascorbate in degassed H₂O and stirred under N₂ for 5 min. The activated catalyst solution (40 μL) was added to the peptide solution (60 μL) and the reaction was stirred for 1 h. The final concentrations in the reaction mixture were 5 mM CuSO₄, 5 mM TBTA, and 20 mM sodium ascorbate. Generally completion of the reaction was achieved in 1 h, as observed by MS (MALDI-TOF). If after 1 h, a significant fraction of starting peptide remained, further addition of activated catalyst followed by stirring at room temperature under N₂ was performed. The crude reaction mixture was desalted using a C₄ solid phase extraction (SPE) column and lyophilized.

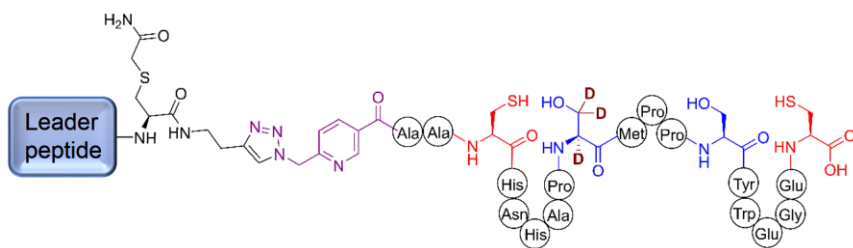
The thioethyl protection group was removed from Cys by dissolving the semi-synthetic precursor in 3 mM TCEP-HCl in 2 mM Tris buffer, pH 7.5, and stirring at room temperature for 3 to 5 h, unless otherwise noted. The reaction mixture was purified using a Phenomenex Luna C₅ column using a gradient of 2% to 67% solvent A in 30 min with a flow rate of 7 mL/min using a Waters HPLC instrument to generate the precursor peptide with one free Cys.



Peptide 2.10.

Peptide **2.7** (0.63 mg, 0.07 μ mol) and peptide **2.46** (0.17 mg, 0.07 μ mol) were

mixed and to the reaction was added four batches of 40 μ L of freshly prepared catalyst solution with an interval of one hour between each addition. The crude reaction mixture was desalted using a C4 SPE column to yield peptide precursor to **2.10** with thioethyl protected Cys residues. The peptide was reduced with TCEP and purified by RP-HPLC using the standard conditions to generate peptide **2.10** (0.2 mg, 26%). MALDI-TOF MS calculated 11336 ($M+H^+$), observed 11339. (*Notebook VI, page 99; Notebook VII, page 6*)

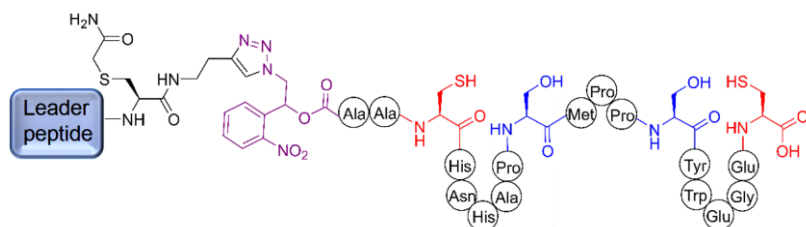


Peptide 2.11.

Peptide **2.7** (0.46 mg, 0.05 μ mol) and peptide **2.45** (0.13 mg, 0.05 μ mol) were

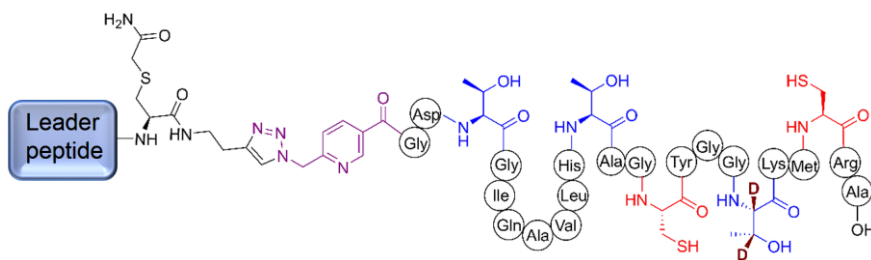
mixed and to the reaction was added three batches of 40 μ L of freshly prepared catalyst solution with an interval of 1 h between additions. The product was reduced with TCEP as described in the section on General Methodology and further purified by RP-HPLC using a C₅ Phenomenex

column. The gradient was 2% to 100% solvent A over 45 min with a flow rate of 8 mL/min. Yield: 0.15 mg (27%). MALDI-TOF MS calculated 11336 (M+H⁺), observed 11338. (*Notebook VI, pages 94, 95*)



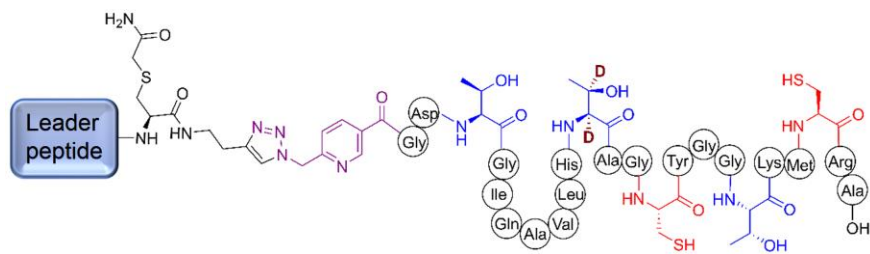
Peptide 2.12. Peptide **2.7** (0.95 mg, 0.1 μmol) and peptide **2.51** (0.37 mg, 0.15 μmol) were mixed and to the reaction was

added two batches of 40 μL of freshly prepared catalyst solution with an interval of one hour. The reaction was stirred for 2 h after the second addition of catalyst solution. The reaction mixture was desalted using a C₄ SPE column to yield peptide precursor with thioethyl protected Cys residues, which was reduced with TCEP and purified by RP-HPLC using a C₅ Phenomenex column, the standard gradient, and an 8 mL/min flow rate. The product **2.12** eluted with an R_t of 21.4 min. MALDI-TOF MS calculated 11410, observed 11396. Yield: 0.6 mg (50 %). (*Notebook V, pages 90, 92*)



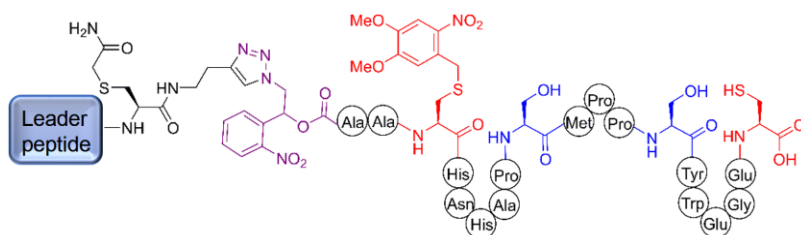
Peptide **2.13.** Peptide **2.7** (0.73 mg, 0.08 μmol) and peptide **2.47** (0.24 mg, 0.1 μmol) were mixed and to

the reaction was added three batches of 40 μL of freshly prepared catalyst solution with an interval of 1 h after each addition. The reaction mixture was desalted, reduced with TCEP and purified by RP-HPLC using a C₅ Phenomenex column using a gradient of 2% to 100% solvent A over 45 min with a flow rate of 8 mL/min. The product eluted with an R_t of 21 min, 48% solvent A. Yield: 0.42 mg (45%) (*Notebook VII, page 75*)



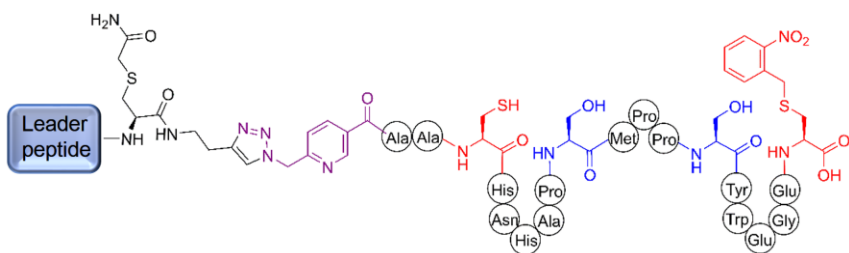
Peptide 2.14. Peptide **2.7** (0.81 mg, 0.09 μmol) and peptide **2.48** (0.25 mg, 0.1 μmol) were mixed and to

the reaction was added three batches of 40 μL of freshly prepared catalyst solution with an interval of one hour between additions. The reaction was stirred for another 2 h after the third addition of catalyst solution. The reaction mixture was desalted, reduced with TCEP and purified by RP-HPLC using a C₅ Phenomenex column using a gradient of 2% to 100% solvent A over 45 min with a flow rate of 8 mL/min. The product **2.14** eluted with a R_t of 21.1 min (48% solvent A). Yield: 0.56 mg (54%). (*Notebook VII, page 83*)



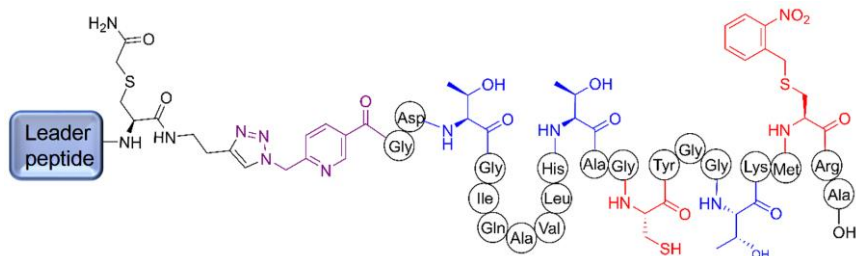
Peptide 2.15. Peptides **2.7** (440 μg , 0.05 μmol) and **2.49** (130 μg , 0.05 μmol) were mixed together and two batches of 40

μL of catalyst solution were added. The reaction mixture was desalted using a C₄ SPE column and lyophilized to generate precursor to **2.15** with thioethyl protected Cys19 (550 μg). The product was reduced with TCEP as described in General Methodology and further purified by RP-HPLC using the standard gradient to yield pure **2.15** (430 μg , 76%). (*Notebook V, page 59*)



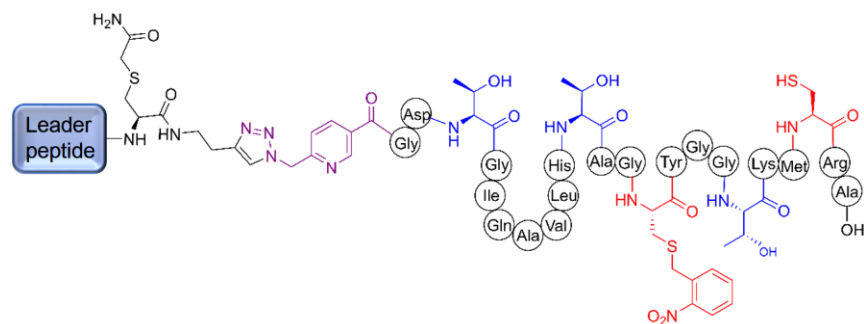
Peptide 2.16. Peptide **2.7** (925 μg , 0.1 μmol) was mixed with **2.50** (320 μg , 0.13 μmol) and the two

batches of 40 μL of catalyst solution were added. The reaction mixture was desalted using a C_4 SPE column and lyophilized to yield crude precursor to **2.16** with thioethyl protected Cys3 (1.1 mg). MS (MALDI-TOF) indicated complete conversion to product. The crude precursor to **2.16** was reduced with TCEP followed by RP-HPLC purification with a C_5 Phenomenex Luna column using the standard conditions to yield pure **2.16** (0.64 mg, 55%). R_t 20.8 min, eluting at 47% solvent A. LR-MS (MALDI-TOF) calculated 11466 ($\text{M}+\text{H}^+$), observed 11472. (*Notebook VI, pages 17, 18*)



Peptide 2.17. Peptide **2.7** (0.79 mg, 0.09 μmol) and peptide **2.52** (0.3 mg, 0.11 μmol) were mixed and three

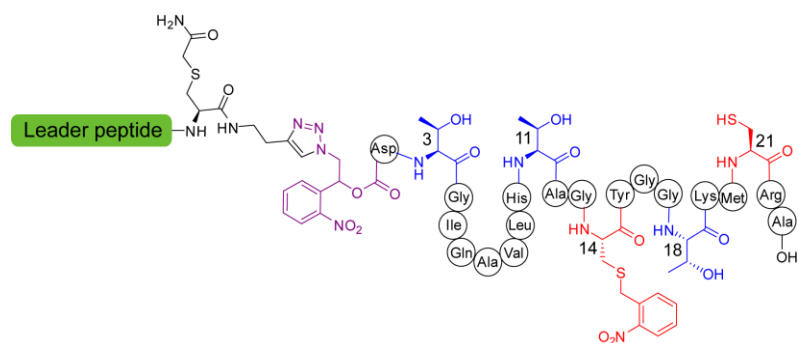
batches of 40 μL of freshly prepared catalyst solution were added with an interval of one hour between additions. The reaction mixture was desalted using a C_4 SPE column and lyophilized, reduced with TCEP and purified by RP-HPLC. The gradient was 2% to 100% solvent A over 45 min with a flow rate of 8 mL/min. The product **2.17** eluted with an R_t of 21.5 min. MALDI-TOF MS calculated 11694, observed 11693. Yield: 0.33 mg (33%). (*Notebook VII, page 82*)



Peptide 2.18. Peptide **2.7** (0.84 mg, 0.09 μmol) and peptide **2.53** (0.36 mg, 0.14 μmol) were mixed and three batches of 40 μL of freshly

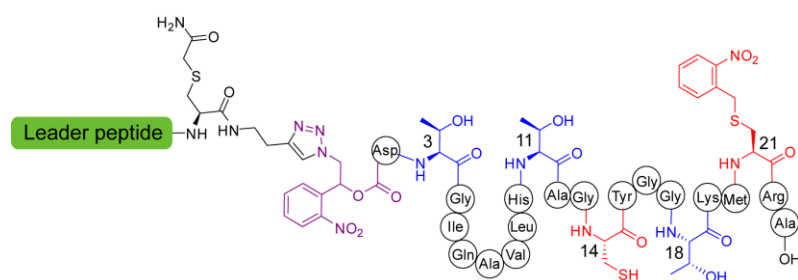
prepared catalyst solution were added with an interval of one hour between additions. The

reaction was stirred for 2.5 h after the third addition of catalyst solution. The reaction mixture was desalted using a C₄ SPE column to yield peptide precursor with thioethyl protected Cys, which was reduced with TCEP and purified by RP-HPLC using a C₅ Phenomenex column using the standard gradient and a 8 mL/min flow rate. The product **2.18** eluted with an R_t of 21.4 min. MALDI-TOF MS calculated 11694, observed 11694. Yield: 0.52 mg (49%). (*Notebook VIII, page 11*)



Peptide **2.57**. Peptide **2.7** (0.73 mg, 0.08 μ mol) and peptide **2.54** (0.28 mg, 0.11 μ mol) were reacted under conditions of Copper Catalyzed Azide-Alkyne

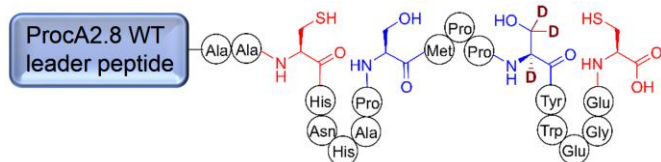
Cycloaddition (CuAAC) to generate product, which after RP-HPLC purification yielded 390 μ g of material. (*Notebook VIII, page 76*)



Peptide **2.58**. Peptide **2.7** (0.78 mg, 0.086 μ mol) and peptide **2.55** (0.28 mg, 0.11 μ mol) were reacted under conditions of

CuAAC to generate product, which after RP-HPLC purification yielded 510 μ g of material. (*Notebook VIII, page 75*)

2.4.15. Peptides Generated by Native Chemical Ligation

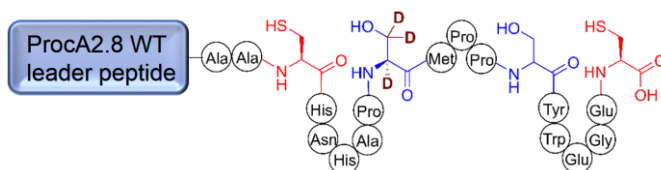


Peptide 2.4. Native chemical reaction was

performed in a reaction volume of 500 μL .

The final concentration of components are

given in parenthesis. In an eppendorf tube, 250 μL of a 1 mM solution of peptide **2.2** (0.5 mM) was mixed with 25 μL of 20 mM TCEP (1 mM), 125 μL of 1 M NaP_i , pH 7.2 (250 mM), 50 μL of 1 M MESNa (100 mM), 25 μL of 10 mM EDTA (0.5 mM), and finally 25 μL of a 1 mM solution of peptide **2.1** (0.05 mM). The reaction was stirred at room temperature for 20 h when MALDI-TOF MS of crude product indicated the consumption of peptide **2.1**. The reaction mixture was acidified with TFA to pH \sim 6.8 and purified using an analytical HPLC column (C₄ Vydac) using a gradient of 2% solvent A (80% MeCN, 0.086% TFA in H₂O), 98% solvent D (0.1% TFA in H₂O) to 80% solvent A over 45 min using a flow rate of 1 mL/min. The product **2.4** eluted with a R_t of 28.2 min (50% solvent A), while starting synthetic peptide **2.2** eluted earlier (R_t of 18 min, 32% solvent A). Yield: 0.13 mg (48%). MALDI-TOF MS calculated 10918 ($\text{M}+\text{H}^+$), observed 10921 ($\text{M}+\text{H}^+$), 11099 (phosphogluconylation of His-tag). (*Notebook VII, page 31*)



Peptide 2.5. Native chemical reaction was

performed in a total reaction volume of

500 μL . The final concentrations of

components are given in parenthesis. In an eppendorf tube, 250 μL of 1 mM solution of peptide **2.3** (0.5 mM) was mixed with 25 μL of 20 mM TCEP (1 mM), 125 μL of 1 M NaP_i , pH 7.2 (250 mM), 50 μL of 1 M MESNa (100 mM), 25 μL of 10 mM EDTA (0.5 mM), and finally 25 μL of

1 mM solution of peptide **2.1** (0.05 mM). The reaction was stirred at room temperature for 20 h when MALDI-TOF MS analysis indicated consumption of peptide **2.1**. The reaction mixture was acidified with TFA to pH ~ 6.8 and purified using an analytical HPLC column (C₄ Vydac) using a gradient of 2% solvent A (80% MeCN, 0.086% TFA in H₂O), 98% solvent D (0.1% TFA in H₂O) to 80% solvent A in 45 min using a flow-rate of 1 mL/min. The product **2.5** eluted with a R_t of 28.2 min (50% solvent A), while starting synthetic peptide **2.3** eluted earlier (R_t of 18 min, 32% solvent A). Yield: 0.1 mg (37%). MALDI-TOF MS calculated 10918 (M+H⁺), observed 10925 (M+H⁺), 11104 (phosphogluconylation of His-tag). (*Notebook VII, page 30*)

2.4.16. Purification of ProcM

The enzyme was overexpressed as reported earlier, with the exception that ProcM gene was cloned in a pRSFDuet vector instead of pET28b vector as originally reported (3). After IMAC purification, ProcM was further purified by size-exclusion chromatography (Superdex 200 resin, 120 mL column volume) using an FPLC (Akta P-920) and was obtained as a mixture of monomer and dimer/trimer; when separated, both were active. A brief procedure for ProcM purification is as follows. All steps were carried out in the cold room (4 °C) or on an ice-bath. Crude cell lysate (from 3 L culture) was suspended in 50 mL of ProcM start buffer (1 M NaCl, 20 mM Tris, pH 8.0), along with protease inhibitor (Roche cOmplete), and lysed by passing through a French-press and centrifuged (14,000 x g, 30 min). The supernatant was filtered through 0.45 µm syringe filters and loaded onto a Ni-HiTrap column equilibrated with 4 column volumes (CV) of ProcM start buffer. The column was washed by 6 CV of ProcM wash buffer (1 M NaCl, 20 mM Tris, pH 8.0, 30 mM imidazole) and then the column was attached to the FPLC and the protein was eluted using wash buffer and elute buffer (EB: 1 M NaCl, 20 mM Tris, pH-8.0, 200 mM imidazole). The following gradient was applied: 6 CV of 5% EB, then 6 to 10 CV

of 5% to 40% EB, 10 to 12 CV: 40% to 100% EB, 12 to 18 CV: 100% EB. The fractions containing the protein were 8 CV to 14 CV, as monitored by absorbance at 280 nm. The purified protein was concentrated using an Amicon ultrafilter (50 kDa cut-off) and desalted/purified by gel-filtration on FPLC (using ProcM start buffer (1 M NaCl, 20 mM Tris, pH-8.0) at a flow rate of 1 mL/min. The aggregated protein (40 mL to 55 mL elution volume) was discarded and the monomer and oligomer fractions (60 mL to 85 mL elution volume) were collected and concentrated using 30 kDa cut-off Amicon centrifugation filters to a concentration of ca. 60 μ M to 250 μ M, depending on the batch. (*Notebook IV, pages 61, 63*)

2.4.17. Purification of ProcM in D₂O Containing Buffer

The monomer-oligomer mixture obtained from size-exclusion chromatography (15 mL), as mentioned in the previous section, was concentrated to 1 mL by ultrafiltration (2,300 x g), and then 10 mL of 1 M NaCl, 50 mM HEPES, pH 8.0 in D₂O was added and the protein was again concentrated to 1 mL by centrifugation. Further addition of 10 mL of 1 M NaCl, 50 mM HEPES, pH 8.0 in D₂O to the concentrated protein solution followed by ultrafiltration to generated a stock of 84 μ M ProcM (10 mg/mL, D₂O:H₂O over 99:1). The solution was aliquoted in fractions of 25 μ L. (*Notebook VI, pages 82, 83*)

2.4.18. General Procedure for Heterologous Expression of Precursor Peptides

ProcA2.8, ProcA3.3, ProcA2.8-S9T, ProcA2.8-S13T, and ProcA3.3-T11S were generated by the following general methodology.

E. coli BL21 cells were transformed with pET-15b plasmid encoding the desired gene and the transformed cells were spread on an LB + Amp (100 μ g/ mL) agar plate and the plate was incubated overnight at 37 °C. Cells from single colonies were used to inoculate starter cultures (2

x 25 mL) in LB + Amp (100 µg/mL) and incubated at 37 °C in a shaker for 16 h. The starter cultures were centrifuged (4,300 x g, 10 min) and the LB media was replaced with fresh LB and was used to inoculate a large scale culture (2 x 1.5 L) of LB + Amp (100 µg/mL). The flasks were incubated at 37 °C with shaking until an OD_{600 nm} of 0.6 was reached (typically 3-4 h). The culture was induced with IPTG (0.5 mM final concentration) and further incubated at 37 °C in a shaker for 3 h when a final OD_{600 nm} in the range of 1.0 - 2.5 was reached. The cells were harvested by centrifugation (10,500 x g, 15 min), flash frozen and stored at -80 °C for future use. The cells were thawed on ice and suspended in 30 mL of LanA start buffer (20 mM NaH₂PO₄, pH 7.5 at 25 °C, 500 mM NaCl, 0.5 mM imidazole, 20% glycerol) and lysed by sonication (4.4 s pulse, 9.9 s off, 35% amplitude, pulse time 6 min). The cell lysate was centrifuged (22,800 x g, 30 min) and the supernatant, referred as 'soluble fraction' was filtered through a 0.45 µm filter. The cell residue was resuspended in 25 mL of Lan buffer 1 (6 M guanidine hydrochloride, 20 mM NaH₂PO₄, pH 7.5 at 25 °C, 500 mM NaCl, 0.5 mM imidazole), sonicated, and centrifuged as described above. The supernatant referred to as 'insoluble fraction' was filtered through a 0.45 µm filter. A 5 mL Ni-His trap column charged with NiSO₄ was equilibrated with two column volumes (CV) of LanA start buffer after which the 'soluble fraction' was loaded at flow rate of 2 mL/min. The column was then equilibrated with two CV of Lan buffer 1 and loaded with the 'insoluble fraction' at 2 mL/min. The column was washed with two CV of Lan buffer 1 and two CV of Lan buffer 2 (4 M guanidine hydrochloride, 20 mM NaH₂PO₄, pH 7.5 at 25 °C, 300 mM NaCl, 30 mM imidazole) and eluted with LanA elution buffer (4 M guanidine hydrochloride, 20 mM Tris, pH 7.5 at 25 °C, 100 mM NaCl, 1 M imidazole) where 10 mL of the elution fraction was collected as fraction 1 and 5 mL was collected as fraction 2. Both fractions were desalted using C₄ SPE columns and lyophilized.

ProcA2.8 precursor peptide: The desalted peptide was injected onto a Phenomenex Luna C₅ column and eluted with a gradient of 2% to 67% solvent A in 30 min, and a flow rate of 7 mL/min. R_t 22 - 24.5 min. 13.3 mg of crude peptide yielded 10.8 mg of purified peptide.

MALDI-TOF MS calculated 10,915 (M+H⁺), observed 10,917. Peptide sequence:

GSSHHHHHHSSGLVPRGSHMSEEQLKAFLTKVQADTSLQEQLKIEGADVVAIAKAAGFS
ITTEDLNHRQNLSDDELEGVAGGAACHNHAPSMPPSYWEGEC (*Notebook VI, pages 33, 35, 69*)

ProcA3.3 precursor peptide: The desalted peptide was purified using a Phenomenex Luna C₅ column with a gradient of 2% to 65% solvent A over 65 min with a flow rate of 7 mL/min. The fraction eluting with a R_t of 44.8 min (46% solvent A) was pure product. MALDI-TOF MS calculated 10,934 (M+H⁺), observed 10,927.

Peptide sequence:

GSSHHHHHHSSGLVPRGSHMSEEQLKAFIAKVQGDSSLQEQLKAEGADVVAIAKAAGF
TIKQQDLNAAASELSDEELEAASGGGDTGIQAVLHTAGCYGGTKMCRA (*Notebook VI, pages 33, 52*)

ProcA2.8-S13T precursor peptide: Desalted peptide was used without further purification. MALDI-TOF MS calculated 10,936 (M+H⁺), observed 10,934. Yield: 50 mg from 2 L of culture.

Peptide sequence (mutation underlined):

GSSHHHHHHSSGLVPRGSHMSEEQLKAFLTKVQADTSLQEQLKIEGADVVAIAKAAGFS
ITTEDLNHRQNLSDDELEGVAGGAACHNHAPSMPPTYWEGEC (*Notebook VII, pages 51, 54*)

ProcA2.8-S9T precursor peptide: Desalted peptide was used without further purification. MALDI-TOF MS calculated 10,936 (M+H⁺), observed 10,932. Yield: 49 mg from 1.5 L of culture.

Peptide sequence (mutation underlined):

GSSHHHHHHSSGLVPRGSHMSEEQLKAFLTKVQADTSLQEQLKIEGADVVAIAKAAGFS
ITTEDLNHRQNLSDDELEGVAGGAACHNHAPTMPPSYWEGEC (*Notebook VII, pages 52, 54*)

ProcA3.3-T11S precursor peptide: Desalted peptide was used without further purification. MALDI-TOF MS calculated 10,920 (M+H⁺), observed 10,920. Yield: 57 mg from 1.5 L of culture.

Peptide sequence (mutation underlined):

GSSHHHHHHSSGLVPRGSHMSEEQLKAFAIAKVQGDSSLQEQLKAEGADVVAIAKAAGF
TIKQQDLNAAASELSDEELEAASGGGDTGIQAVLHSAGCYGGTKMCRA (*Notebook VII, pages 51, 55*)

2.4.19. General Procedure for Selective Thioether Formation by ProcM

Substrates with one Cys protected with an *o*-nitrobenzyl group was treated with ProcM under the following typical conditions (any changes from these standard conditions are noted in the individual procedures). The assays were carried out in 200 μ L scale containing HEPES (50 mM, pH 8.0), TCEP (0.2 mM), ATP (10 mM), $MgCl_2$ (10 mM), ProcM (20 μ M), substrate (50 μ M), and allowed to react at room temperature for 16-20 h. ProcM was removed from the assay mixtures by ultrafiltration through 50 kDa molecular weight cut-off filters (Amicon) by centrifugation (14,000 x g, 10 min). To improve recovery of processed peptide, water (50 μ L) was added to the retentate, and the solution was filtered by centrifugation (14,000 x g, 10 min). This process was repeated twice. The combined filtrates were collected and desalted on a C₄ solid phase extraction column (Vydac BioSelect). The SPE column was first wetted with 2 column volumes (CV) of 80% MeCN in H₂O. The column was washed with 0.1% trifluoroacetic acid (TFA) in H₂O (3 CV) and then the assay product was diluted with 0.1 % TFA in H₂O (1:1) and passed through the column. The column was further washed with 0.1 % TFA in H₂O (3 CV) and finally the product was eluted with 80% MeCN in H₂O (2 x 1 mL). The eluents were lyophilized to yield the processed peptide with selectively formed thioether rings and one *o*-nitrobenzyl protected cysteine.

The lyophilized peptide obtained from the previous step was dissolved in 0.1% formic acid in H₂O and subjected to UV (365 nm) irradiation for 4 h, using a portable UV lamp source (Spectroline ENF-240C). After irradiation, the solution was lyophilized.

2.4.20. General Procedure for Probing Enzymatic vs. Non-Enzymatic Cyclization

Non-enzymatic cyclization: The peptide obtained from the previous step was incubated at room temperature in solution containing all components used in standard ProcM assay except the enzyme. A typical non-enzymatic assay solution comprised HEPES (50 mM), ATP (10 mM), TCEP (0.2 mM), MgCl₂ (10 mM), and substrate (ca. 50 μM) with a final pH of 8.0. A second assay was conducted at higher pH 8.5, and assays were kept at room temperature for 16 h.

Enzymatic cyclization: Control assays of the substrate generated in the previous step in the presence of ProcM (20 μM) were also set up under identical conditions and incubated at room temperature for 16 h. The enzymatic and the non-enzymatic cyclization assays were carried out and analyzed in parallel.

To probe the extent of cyclization of the second thioether ring, iodoacetamide (IAA) assays were performed on the products of the non-enzymatic and the enzymatic assays. The pH of the assay solution was raised to 8.5 by the addition of NH₄HCO₃ buffer (100 mM), TCEP (0.5 mM) and excess IAA (ca. 20 mM) was added, and the assay was incubated at room temperature for 3 h, before analysis by MALDI-TOF MS.

2.4.21. General Procedure for the Incorporation of Deuterium in the ProcM Product

ProcM assays were conducted at room temperature for 20 h with the following compositions in D₂O: HEPES (50 mM, pH 8.0), TCEP (0.5 mM), ATP (10 mM), MgCl₂ (10 mM), ProcM (10 μM), and (50 μM) substrate. ProcM was removed by centrifugation through Amicon 50 kDa MWCO filters (14,000 x g, 20 min), and the flow through was desalted using C₄ SPE column and lyophilized. MALDI-TOF analysis demonstrated the incorporation of one deuterium per Lan/MeLan.

2.4.22. General Procedure for D–H Exchange Assays

Each lyophilized deuterium labeled peptide was dissolved in H₂O and ProcM assays were conducted at room temperature for 20 h in aqueous solution with the following composition: HEPES (50 mM, pH 8.0), TCEP (0.5 mM), ATP (10 mM), MgCl₂ (10 mM), ProcM (10 μM), and substrate (50 μM). Control assays in which the substrates were treated with all components except ProcM were also performed. MALDI-TOF MS analysis was carried out after digesting the peptide with GluC by adding 1 μL of GluC (20 μg/μL) or 1 μL of LysC (30 U/mL) to 20 μL of assay mixture. Simulation of extent of exchange was carried out using mmass software (35).

2.4.23. General Procedure for Trapping Partially Dehydrated Peptides Containing Deuterium Labeled Ser/Thr to Probe Directionality of Dehydration

Substrates assembled by CuAAC with deuterium labeled Ser/Thr were treated with ProcM under the following conditions unless otherwise noted. A typical assay volume of 20 μL contained HEPES (50 mM, pH 8.0), ATP (10 mM), TCEP (0.5 mM), MgCl₂ (10 mM), ProcM (2 μM), and substrate (50 μM). The assays were kept at room temperature and after each time-point, one assay sample was filtered through 50 kDa cut-off filters by centrifugation to remove ProcM (14,000 x g, 10 min). The chosen time-points were 10 min, 30 min, and 1 h. An assay with higher ProcM concentration (10 μM), and longer incubation (9 h) was also performed.

Substrates assembled by expressed protein ligation (EPL) with deuterium labeled Ser/Thr were treated with ProcM under the following conditions unless otherwise noted. A typical assay volume of 20 μL contained HEPES (50 mM, pH 8.0), ATP (10 mM), TCEP (0.5 mM), MgCl₂ (10 mM), ProcM (2 μM), and substrate (100 μM). The assays were kept at room temperature and

after each time-point, one assay sample was filtered through a 50 kDa cut-off filter by centrifugation (14,000 x g, 10 min). The chosen time-points were 5 min, 10 min, and 30 min.

The filtered peptides were digested with endo-proteinase GluC (1 $\mu\text{g}/\mu\text{L}$) or LysC (0.3 U/ μL), as noted, and then analyzed by MALDI-TOF MS and ESI-MS.

2.4.24. General Procedure for Trapping Partially Cyclized Species to Probe Directionality of Cyclization

ProcA precursor peptides were modified by ProcM at room temperature in solutions containing HEPES (50 mM, pH 8.0), ATP (10 mM), TCEP (1.0 mM), MgCl_2 (10 mM), ProcM (5 μM), and substrate (100 μM). After each time point (15 min, 30 min, 1 h), 100 μL aliquots were taken and filtered through 50 kDa cut-off filters by centrifugation (14,000 x g, 10 min). The filtrates were digested with GluC (1 $\mu\text{g}/\mu\text{L}$) for 1 h. The endoproteinase digested filtrate (16 μL) was then diluted with 24 μL of 200 mM NH_4HCO_3 (pH 8.8), 1 μL of TCEP (10 mM), and 10 μL of iodoacetamide (10 mg/mL) was added. The solution was incubated at room temperature for 2 h. The samples were frozen and stored at $-80\text{ }^\circ\text{C}$, until analyzed by ESI LC-MS and tandem MS. Prior to loading the samples onto the LC system, 0.1% formic acid was added (1:1) to lower the pH to ca. 6.5.

2.4.25. Enzymatic Modification of Peptide 2.18 by ProcM-C971H

Peptide **2.18** (64 μM) was treated with ProcM-C971H (20 μM) in HEPES (50 mM, pH 8.0) containing TCEP (1 mM), ATP (10 mM), and MgCl_2 (10 mM). The assay was incubated at room temperature for 16 h. Following enzymatic reaction, the assay mixture was filtered by an amicon filter (50 kDa MWCO) by centrifugation (14000 x g) to remove ProcM-C971H. The filtrate was free from the enzyme. The retentate was diluted with 100 μL of H_2O and filtered, and this process was repeated once. The filtrates were collected and desalted using C₄ SPE column

and lyophilized. A portion of the peptide was digested with endoproteinase LysC and analyzed by tandem ESI-MS (Figure 2.33) which indicated the formation of a MeLan between Cys21 and Dhb18. (*Notebook IX, page 4*)

2.4.26. UV Mediated Deprotection of Cys14 in Peptide 2.33 and Enzymatic Cyclization by WT ProcM

Solution of peptide **2.33** (200 μ L, ca. 50 μ M) was irradiated with a Blak-Ray UV lamp ($\lambda = 365$ nm) for 45 min. To evaluate the extent of photodeprotection, a 5 μ L aliquot of the solution was diluted with 14 μ L of HEPES (50 mM, pH 7.5) and digested with endoproteinase LysC (1.5 U/mL) for 30 min before analysis by MALDI-TOF MS, which suggested completion of photodeprotection. The remaining deprotected peptide was lyophilized and subsequently subjected to WT ProcM assay with following compositions in a 50 μ L reaction volume: HEPES (50 mM, pH 8.0), TCEP (1 mM), ATP (10 mM), MgCl₂ (10 mM), WT ProcM (20 μ M). The assay was incubated at room temperature for 14 h. The assay mixture (25 μ L) was digested with LysC (1.5 U/mL) for 1 h before analysis by tandem ESI-MS. (*Notebook IX, page 6*)

2.4.27. Semi-Synthetically Generated Intermediates of ProcA3.3 with one Thioether Crosslink

Peptide **2.57** (0.39 mg) was modified by WT ProcM under following conditions: HEPES (50 mM, pH 8.0), TCEP (0.5 mM), ATP (10 mM), MgCl₂ (10 mM), substrate (100 μ M), WT ProcM (30 μ M) and incubated at room temperature for 22 h. The assay mixture was filtered to remove enzyme, and desalted using a C₄ SPE column, and lyophilized. The peptide content was dissolved in 0.1% formic acid solution (ca. 50 μ M) and irradiated with UV light (365 nm) to render a mixture of two peptides **2.30** and **2.31** (Figure 2.32). The peptide **2.58** (0.51 mg) was

treated as above and led to the intermediate **2.29** (Figure 2.32). (*For 2.30 and 2.31, see Notebook VIII, pages 79, 81; for 2.29, see Notebook VIII, pages 78, 80*)

2.4.28. Molecular Cloning of His₆-ProcA3.2 Leader-Intein-CBD

The DNA sequence encoding the ProcA3.2 leader peptide was cloned between NdeI and SapI restriction sites of a pTXB1 vector to position the ProcA3.2 leader gene before the gene encoding intein and chitin binding domain (CBD). pET28b encoding the ProcA3.2 precursor peptide gene was used as template (3). The primers were 5'-GGT GGT CAT ATG ATG TCA GAA GAA CAA CTC AAG GCA TTT ATT G-3' (ProcA3.2-leader_NdeI_FP), and 5'-GGT GGT TGC TCT TCC GCA TCC CCC AGC CAC ACC TTC 3' (ProcA3.2-leader_SapI_RP). The generated pTXB1 plasmid encoding 'ProcA3.2-leader_intein_CBD' was used as template to insert 'ProcA3.2-leader_intein_CBD' between the NdeI and BamHI restriction sites of a pET15b plasmid after the DNA sequence encoding the His-tag. The primers used were 5'-GGT GGT CAT ATG TCA GAA GAA CAA CTC AAG GCA TTT ATT G-3' (His-tag_ProcA3.2-leader_intein_CBD_NdeI_FP) and 5'-GGT GGT GGA TCC TCA TTG AAG CTG CCA CAA GG-3' (His-tag_ProcA3.2-leader_intein_CBD_BamHI_RP) to generate the final pET15b construct of 'His-tag_ProcA3.2-leader_intein_CBD'. (*Notebook I, pages 10, 12, 13, 41; Notebook II, pages 22, 25, 26, 28, 63*)

2.4.29. Mutagenesis of ProcA Genes

The first residue of the core peptide is designated as 1 and the last residue of the leader peptide is designated as -1. Mutation of the C-terminal Gly of ProcA3.2 leader to Lys in 'His-tag_ProcA3.2-leader_intein_CBD' was performed by QuikChange site directed mutagenesis. The primers were 5'-GAA GGT GTG GCT GGG AAA TGC ATC ACG GGA GAT G-3' (His-

tag_ProcA3.2-leader-G-1K_intein_CBD_FP) and 5'-CCC AGC CAC ACC TTC CAG CTC ATC ATC-3' (His-tag_ProcA3.2-leader-G-1K_intein_CBD_RP), which were used to generate pET15b construct encoding 'His-tag_ProcA3.2-leader-G-1K_intein_CBD'.

The ProcA2.8 and ProcA3.3 Ser/Thr mutants were generated using the following primers by QuikChange site directed mutagenesis based on a modified protocol (36). (*Notebook VII, pages 47-49*)

Primer Name	Primer Sequences (5'-3')
ProcA2.8_S9T_FP	GTC ATA ACC ATG CTC CAA CCA TGC CTC CAT CCT ATT G
ProcA2.8_S9T_RP	CAA TAG GAT GGA GGC ATG GTT GGA GCA TGG TTA TGA C
ProcA2.8_S13T_FP	CCA TCT ATG CCT CCA ACC TAT TGG GAG GGT G
ProcA2.8_S13T_RP	CAC CCT CCC AAT AGG TTG GAG GCA TAG ATG G
ProcA3.3_T11S_FP	GGT GCT GCA CAG CGC TGG ATG TTA C
ProcA3.3_T11S_RP	GTA ACA TCC AGC GCT GTG CAG CAC C

2.5. REFERENCES

1. Mukherjee, S., and van der Donk, W. A. (2014) Mechanistic Studies on the Substrate-Tolerant Lanthipeptide Synthetase ProcM, *J. Am. Chem. Soc.* *136*, 10450-10459.
2. Yu, Y., Mukherjee, S., and van der Donk, W. A. (2015) Product Formation by the Promiscuous Lanthipeptide Synthetase ProcM is under Kinetic Control, *J. Am. Chem. Soc.* *137*, 5140-5148.
3. Li, B., Sher, D., Kelly, L., Shi, Y., Huang, K., Knerr, P. J., Joewonod, I., Rusche, D., Chisholm, S. W., and van der Donk, W. A. (2010) Catalytic promiscuity in the biosynthesis of cyclic peptide secondary metabolites in planktonic marine cyanobacteria, *Proc. Nat. Acad. Sci. U.S.A.* *107*, 10430-10435.
4. Tang, W., and van der Donk, W. A. (2012) Structural Characterization of Four Prochlorosins: A Novel Class of Lantipeptides Produced by Planktonic Marine Cyanobacteria, *Biochemistry.* *51*, 4271-4279.
5. Chatterjee, C., Paul, M., Xie, L., and van der Donk, W. A. (2005) Biosynthesis and mode of action of lantibiotics, *Chem. Rev.* *5*, 633-684.

6. Burrage, S., Raynham, T., Williams, G., Essex, J. W., Allen, C., Cardno, M., Swali, V., and Bradley, M. (2000) Biomimetic Synthesis of Lantibiotics, *Chem. Eur. J.* **6**, 1455-1466.
7. Okeley, N. M., Zhu, Y., and van der Donk, W. A. (2000) Facile Chemoselective Synthesis of Dehydroalanine-Containing Peptides, *Org. Lett.* **2**, 3603-3606.
8. Zhou, H., and van der Donk, W. A. (2002) Biomimetic Stereoselective Formation of Methyllanthionine, *Org. Lett.* **4**, 1335-1338.
9. Krawczyk, B., Enslé, P., Müller, W. M., and Süßmuth, R. D. (2012) Deuterium Labeled Peptides Give Insights into the Directionality of Class III Lantibiotic Synthetase LabKC, *J. Am. Chem. Soc.* **134**, 9922-9925.
10. Zhang, Q., Yang, X., Wang, H., and van der Donk, W. A. (2014) High Divergence of the Precursor Peptides in Combinatorial Lanthipeptide Biosynthesis, *ACS Chem. Biol.* **9**, 2686-2694.
11. Zhu, Y., Gieselmann, M. D., Zhou, H., Averin, O., and van der Donk, W. A. (2003) Biomimetic studies on the mechanism of stereoselective lanthionine formation, *Org. Biomol. Chem.* **1**, 3304-3315.
12. Zhang, Q., Yu, Y., Vélasquez, J. E., and van der Donk, W. A. (2012) Evolution of lanthipeptide synthetases, *Proc. Natl. Acad. Sci. U.S.A.* **109**, 18361-18366.
13. Wilker, J. J., and Lippard, S. J. (1997) Alkyl Transfer to Metal Thiolates: Kinetics, Active Species Identification, and Relevance to the DNA Methyl Phosphotriester Repair Center of Escherichia coli Ada, *Inorg. Chem.* **36**, 969-978.
14. Hightower, K. E., and Fierke, C. A. (1999) Zinc-catalyzed sulfur alkylation: insights from protein farnesyltransferase, *Curr. Opin. Chem. Biol.* **3**, 176-181.
15. Harris, C. M., Derdowski, A. M., and Poulter, C. D. (2002) Modulation of the Zinc(II) Center in Protein Farnesyltransferase by Mutagenesis of the Zinc(II) Ligands, *Biochemistry.* **41**, 10554-10562.
16. Penner-Hahn, J. (2007) Zinc-promoted alkyl transfer: a new role for zinc, *Curr. Opin. Chem. Biol.* **11**, 166-171.
17. Morlok, M. M., Janak, K. E., Zhu, G., Quarless, D. A., and Parkin, G. (2005) Intramolecular NH \cdots S Hydrogen Bonding in the Zinc Thiolate Complex [TmPh]ZnSCH₂C(O)NHPH: A Mechanistic Investigation of Thiolate Alkylation as Probed by Kinetics Studies and by Kinetic Isotope Effects, *J. Am. Chem. Soc.* **127**, 14039-14050.
18. Lee, M. V., Ihnken, L. A. F., You, Y. O., McClerren, A. L., van der Donk, W. A., and Kelleher, N. L. (2009) Distributive and Directional Behavior of Lantibiotic Synthetases Revealed by High-Resolution Tandem Mass Spectrometry, *J. Am. Chem. Soc.* **131**, 12258-12264.
19. Muir, T. W. (2003) Semisynthesis of Proteins by Expressed Protein Ligation, *Annu. Rev. Biochem.* **72**, 249-289.
20. Rostovtsev, V. V., Green, L. G., Fokin, V. V., and Sharpless, K. B. (2002) A Stepwise Huisgen Cycloaddition Process: Copper(I)-Catalyzed Regioselective "Ligation" of Azides and Terminal Alkynes, *Angew. Chem. Int. Ed.* **41**, 2596-2599.
21. Tornøe, C. W., Christensen, C., and Meldal, M. (2002) Peptidotriazoles on Solid Phase: [1,2,3]-Triazoles by Regiospecific Copper(I)-Catalyzed 1,3-Dipolar Cycloadditions of Terminal Alkynes to Azides, *J. Org. Chem.* **67**, 3057-3064.

22. Levensgood, M. R., and van der Donk, W. A. (2008) Use of lantibiotic synthetases for the preparation of bioactive constrained peptides, *Bioorg. Med. Chem. Lett.* *18*, 3025-3028.
23. Levensgood, M. R., Kerwood, C. C., Chatterjee, C., and van der Donk, W. A. (2009) Investigation of the Substrate Specificity of Lacticin 481 Synthetase by Using Nonproteinogenic Amino Acids, *ChemBioChem* *10*, 911-919.
24. Evans, T. C., and Xu, M.-Q. (1999) Intein-mediated protein ligation: Harnessing nature's escape artists, *Pept. Sci.* *51*, 333-342.
25. (Accessed June 5, 2014) IMPACT kit instruction manual, New England Biolabs.
26. Uttamapinant, C., Tangpeerachaikul, A., Grecian, S., Clarke, S., Singh, U., Slade, P., Gee, K. R., and Ting, A. Y. (2012) Fast, Cell-Compatible Click Chemistry with Copper-Chelating Azides for Biomolecular Labeling, *Angew. Chem. Int. Ed.* *51*, 5852-5856.
27. Bindman, N., Merckx, R., Koehler, R., Herrman, N., and van der Donk, W. A. (2010) Photochemical cleavage of leader peptides, *Chem. Comm.* *46*, 8935.
28. Smith, A. B., Savinov, S. N., Manjappara, U. V., and Chaiken, I. M. (2002) Peptide–Small Molecule Hybrids via Orthogonal Deprotection–Chemoselective Conjugation to Cysteine-Anchored Scaffolds. A Model Study, *Org. Lett.* *4*, 4041-4044.
29. Küsters, E., Allgaier, H., Jung, G., and Bayer, E. (1984) Resolution of sulphur-containing amino acids by chiral phase gas chromatography, *Chromatographia* *18*, 287-293.
30. Liu, W., Chan, A. S. H., Liu, H., Cochrane, S. A., and Vederas, J. C. (2011) Solid Supported Chemical Syntheses of Both Components of the Lantibiotic Lacticin 3147, *J. Am. Chem. Soc.* *133*, 14216-14219.
31. Yang, X., and van der Donk, W. A. (2015) Michael-Type Cyclizations in Lantibiotic Biosynthesis Are Reversible, *ACS Chem. Biol.* *10*, 1234-1238.
32. Brzezinska, E., and Ternay, A. L. (1994) Disulfides. 1. Syntheses Using 2,2'-Dithiobis(benzothiazole), *J. Org. Chem.* *59*, 8239-8244.
33. Wang, S.-S., Gisin, B. F., Winter, D. P., Makofske, R., Kulesha, I. D., Tzougraki, C., and Meienhofer, J. (1977) Facile synthesis of amino acid and peptide esters under mild conditions via cesium salts, *J. Org. Chem.* *42*, 1286-1290.
34. Pedersen, H., Hölder, S., Sutherlin, D. P., Schwitter, U., King, D. S., and Schultz, P. G. (1998) A method for directed evolution and functional cloning of enzymes, *Proc. Natl. Acad. Sci. U.S.A.* *95*, 10523-10528.
35. Strohm, M., Hassman, M., Košata, B., and Kudiček, M. (2008) mMass data miner: an open source alternative for mass spectrometric data analysis, *Rapid Commun. Mass Spectrom.* *22*, 905-908.
36. Edelheit, O., Hanukoglu, A., and Hanukoglu, I. (2009) Simple and efficient site-directed mutagenesis using two single-primer reactions in parallel to generate mutants for protein structure-function studies, *BMC Biotechnol.* *9*, 61.

CHAPTER 3: TOTAL SYNTHESIS OF LANTHIPEPTIDES - STUDIES WITH CYTOLYSIN

3.1. INTRODUCTION

Enterococci are responsible for the majority of nosocomial surgical site, bloodstream, and urinary tract infections (1, 2). Certain *Enterococcus faecalis* and *Enterococcus faecium* strains have lytic activity against erythrocytes (i.e. red blood cells), as first reported in 1934 (3). Enterococci isolated from the site of infection more commonly exhibited hemolytic activity than those isolated from healthy volunteers. These *E. faecalis* strain show acute hemolytic toxicity and this activity is thought to contribute to bacterial virulence (4). The virulence factor was attributed to a cytolysin produced by enterococci. In addition to the hemolytic activity, the *E. faecalis* cytolysin uniquely exhibits antibacterial activity versus a broad range of gram-positive bacteria (5). It was later found that such hemolytic activity was restricted to erythrocytes from certain animals such as rabbit, cow, horse, and human, but was not observed in sheep and goat (6). A higher amount of phosphatidylcholine on the outer leaflet of the erythrocytes of human, horse, rabbit and mouse was found to correlate with the higher susceptibility of these erythrocytes to cell-lysis (1, 7).

E. faecalis cytolysin is encoded by operons analogous to those responsible for producing antibiotics in other gram-positive bacteria. Cytolysin is the first member of this class of antimicrobial agents with hemolytic activity (8). Nucleotide sequence determination, mutagenesis, and complementation analysis enabled identification of genes responsible for producing cytolysin, and demonstrated that the gene cluster encodes two putative lanthipeptide natural products. These lanthipeptides, known as Cyl_L” and Cyl_S”, are both required for the cytolytic activity (8). The genes encoding the precursor peptides, Cyl_L and Cyl_S, as well as

the gene products of *cylM*, *cylB*, and *cylA*, are critical to the cytolytic activity. CylA is a subtilisin-like serine protease and can generate the mature cytolytins extracellularly via proteolysis (9). CylB is structurally similar to the members of the *Escherichia coli* α -hemolysin determinant which includes HlyB, and is believed to be involved with cytolytin externalization (10). An immunity protein encoded by the gene *cylI* renders the producing organism immune to cytolytin (11). The products of two genes *cylR1* and *cylR2* regulate cytolytin production (12). The genes *cylL_L*, *cylL_S*, *cylM*, *cylB*, *cylA*, and *cylI* are collinear while *cylR1* and *cylR2* are immediately upstream of the cytolytin promoter and oriented in the opposite direction of the cytolytin operon (Figure 3.1). Both the proteins CylR1 and CylR2 are required for the repression of the promoter responsible for cytolytin production. CylL_S” was found to induce transcription of cytolytin by derepression of the promoter. The control of cytolytin production by the presence of a threshold amount of CylL_S” is part of a quorum sensing mechanism (12). When *E. faecalis* senses target cells, it produces cytolytin in response (13).

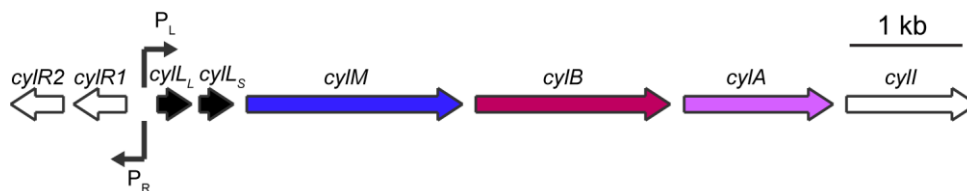
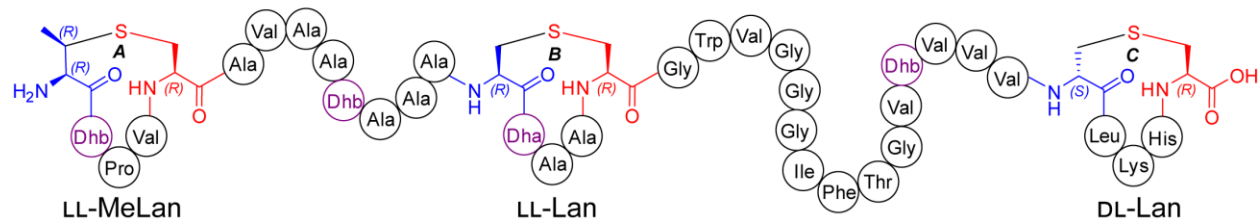


Figure 3.1. Cytolytin biosynthetic gene cluster. Adapted from Gilmore and co-workers (1).

Preliminary structures of the cytolytin components were proposed based on Edman degradation and amino acid analysis of hydrolyzed and *o*-phthaldialdehyde (OPA) derivatized peptides (14). The detailed structural elucidation of the two cytolytin peptides was achieved upon their successful heterologous production in *E. coli* (15). The number of dehydrations in cytolytin observed with heterologous expression matched with that in cytolytin obtained from

the producing organism. Tandem mass spectrometry (MS/MS) revealed the thioether-ring topology of the seven-fold dehydrated Cyl_L and four-fold dehydrated Cyl_S (Figure 3.2).

Cytolysin L



Cytolysin S

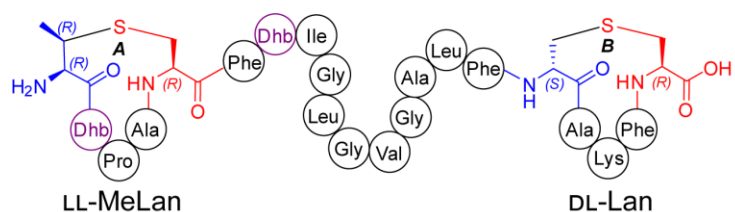
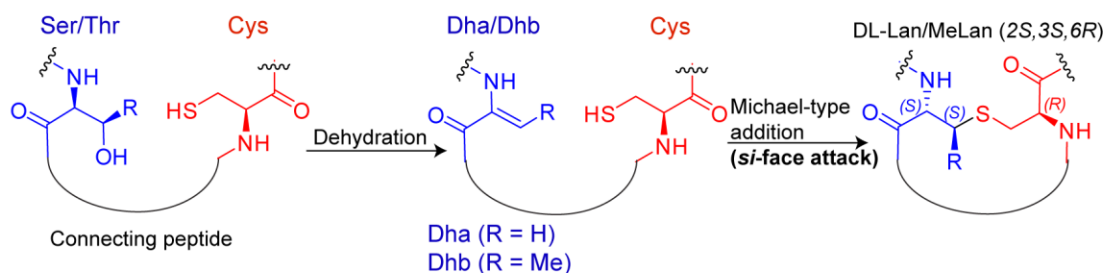


Figure 3.2. Structures of Cytolysin L and S peptides.

Previously characterized lanthipeptides possess Lan and MeLan thioether crosslinks with DL-configuration (16), which denotes an L-configuration of the Cys residue and a D-configuration of the residue that was formerly Ser/Thr, resulting in (2*S*,6*R*)-Lan and (2*S*,3*S*,6*R*)-MeLan. Intriguingly, GC/MS of the hydrolyzed and derivatized peptides suggested that certain thioether crosslinks in the cytolysin peptides bear an LL-configuration ((2*R*,6*R*)-Lan and (2*R*,3*R*,6*R*)-MeLan) (15). This unusual stereochemistry results from a Michael-type addition of a Cys thiol to the dehydrated residue from the opposite face compared to that resulting in DL-stereochemistry (Figure 3.3). In both cases, the overall addition is anti-selective. Notably, the unusual LL-configuration has only been observed for a “Dhx-Dhx-Xaa-Xaa-Cys” pentapeptide-motif, where Dhx stands for either Dha or Dhb and Xaa stands for any residue other than Ser, Thr, or Cys. Computational evidence from quantum mechanical (QM) simulations of dehydrated

peptides substantiated substrate-control by this pentapeptide-motif in formation of the LL-configuration. Molecular dynamics (MD) simulations of cyclization within the pentapeptide motif suggested that the experimentally observed *re*-face attack of Cys thiol onto Dhb is stabilized by favorable hydrogen bonding that is not accessible in the *si*-face attack (17).

Standard stereochemistry



Unusual stereochemistry

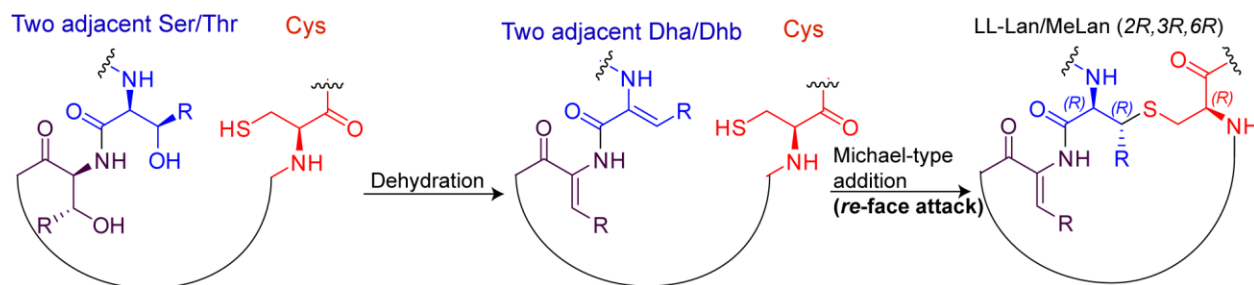


Figure 3.3. Michael-type addition of Cys thiol to a dehydrated residue to generate either DL or LL-configuration of thioether crosslinks.

Additional support for substrate-controlled stereoselectivity in cytolysin was obtained from the study of chimeric peptides (17). The N-terminus of the cytolysin S core peptide was tethered to the C-terminus of leader peptides of other lanthipeptides including HalA2, LtnA2, and ProcA3.2. For each chimeric peptide, modification was carried out by the synthetases corresponding to the leader peptide used (HalM2 for HalA2-CylL_S, LtnM2 for LtnA2-CylL_S, and ProcM for ProcA3.2-CylL_S). In all cases, an LL-configuration of the MeLan A-ring was observed. Hence, the LL-configuration is independent of the employed synthetase, thus providing strong evidence that the observed stereochemistry is guided by the substrate. Furthermore, when

the second Dhb of the “DhxDhxXaaXaaCys” motif was mutated to Ala by using HalA2-T2A as the substrate, HalM2 modification resulted in a DL-configuration of the thioether crosslink. In the WT-version of HalA2, the crosslink obtained from the “DhxDhxXaaXaaCys” motif resulted in the LL-configuration. Upon testing cyclization of the dehydrated CylL_S peptide, it was also found that the A-ring in CylL_S was installed non-enzymatically (Dr. Weixin Tang, manuscript in preparation). However, in the mutant CylL_S-T2A, non-enzymatic cyclization of the A-ring was no longer viable. Surprisingly, cyclization of CylL_S-T2A catalyzed by CylM afforded the LL-stereochemistry of the A-ring, despite the absence of the pentapeptide motif with two consecutive dehydrated residues. This observation suggests that unlike other synthetases, CylM has evolved to enforce the LL-stereochemistry at the A-ring of CylL_S (Dr. Weixin Tang, manuscript in preparation).

The biological importance of the unusual LL-stereochemistry in the cytolysin peptides is investigated herein. We aimed to understand if the observed antimicrobial and hemolytic activities of cytolysin require the LL-configuration of the thioether crosslink. I embarked on the synthesis of cytolysin analogues with the stereochemistry of the thioether crosslink switched to the DL-configuration. Our ultimate goal is to compare the bioactivities of the synthetic analogues with the WT-cytolysin peptides.

3.2. RESULTS AND DISCUSSION

3.2.1. Choice of Cytolysin Variant to Study the Effect of the Unusual LL-Stereochemistry on Bioactivity

Cytolysin peptides belong to the class of two-component lanthipeptides, with the longer peptide named CylL_L” and the shorter one named CylL_S” (Figure 3.2). In order to evaluate the effects of the thioethers with uncommon LL-stereochemistry on the bioactivity of cytolysin, we

initiated studies toward the generation of variants with the more prevalent DL-thioether crosslinks. Though both peptides are characterized by highly hydrophobic sequences, CylL_S'' is relatively short and less hydrophobic than CylL_L''; thus, CylL_S'' is more amenable to synthetic and biochemical manipulations. CylL_S'' comprises two non-overlapping thioether crosslinks, an N-terminal LL-MeLan (A-ring) and a C-terminal DL-Lan (B-ring).

A variant of CylL_S'' with the MeLan A-ring bearing DL-stereochemistry was desired to enable comparison of its bioactivity with WT-CylL_S''. In both cases, synergistic bioactivity would be analyzed in the presence of WT-CylL_L''. Total chemical synthesis could generate such a diastereomer of CylL_S''. This synthesis has to overcome two major hurdles. First, the synthesis and down-stream purification strategy must be compatible with the high hydrophobicity of the target peptide. Hydrophobic peptides are prone to forming β -sheet structures and this conformational transition from a random coil results in incomplete coupling during solid phase peptide synthesis due to inaccessibility of the reagents to the N-terminus of the elongating peptide chain (18, 19). Second, the presence of a dehydrobutyrine as the second residue from the N-terminus of the cytolyisin core peptide poses a challenge to the traditional route to generating such macrocycles. The enamine liberated upon Fmoc deprotection would tautomerize to the imine followed by hydrolysis to the ketone, which is unreactive to further peptide coupling conditions (Figure 3.4).

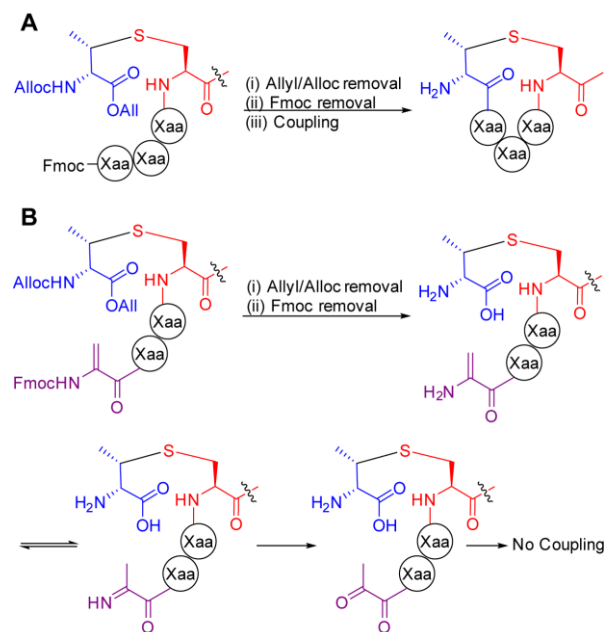


Figure 3.4. Strategy to introduce thioether ring on solid phase. Orthogonal protecting groups on the (methyl)lanthionine building block (DL-MeLan drawn here) allow elongation of a peptide. (A) Sequential deprotection of the allyl/alloc and the Fmoc groups followed by coupling to effect cyclization. (B) If the amine coupling partner is a dehydrated residue (dehydroalanine shown here), Fmoc deprotection affords an enamine that tautomerizes to an imine, followed by hydrolysis to a ketone with adventitious H₂O. The low reactivity of the amine group in an enamine for coupling further promotes this hydrolysis. Conversion to the ketone terminates further coupling.

A route involving access to the dehydrated residue at a late-stage after incorporating the macrocycle would avoid undesired hydrolysis. A facile approach to obtain dehydroalanine from cysteine has been reported by Davis and co-workers (20). Specifically, conversion of a Cys thiol to a cyclic sulfonium cation in-situ followed by base-mediated elimination yields dehydroalanine. With this in mind, we planned to generate a CylLs'' variant with dehydroalanine as the second residue from the N-terminus in place of dehydrobutyrine, henceforth named CylLs''-Dhb2Dha.

3.2.2. Bioactivity of CylL_S''-Dhb2Dha and WT-CylL_S'' is Similar when Both have the Same Thioether Stereochemistry

To rule out any effect on bioactivity because of the switch from dehydrobutyrine to dehydroalanine, we compared the bioactivities of CylL_S''-Dhb2Dha and WT-CylL_S'', with both peptides bearing the native LL-MeLan A-ring and DL-Lan B-ring. WT-CylL_S'' was obtained by heterologous expression in *E. coli* followed by removal of the leader peptide as previously reported (15). To obtain CylL_S''-Dhb2Dha, site-directed mutagenesis was employed to mutate the Thr at position 2 of CylL_S to Ser. Gratifyingly, co-expression of the mutant precursor peptide with CylM in *E. coli* followed by leader peptide removal afforded CylL_S''-Dhb2Dha with an LL-MeLan A-ring and a DL-Lan B-ring, as evidenced by gas chromatography coupled with electrospray ionization mass spectrometry (GC/MS) analysis (Figure 3.5). Synergistic antimicrobial as well as hemolytic activity was tested for both expressed CylL_S''-Dhb2Dha and WT-CylL_S'' in the presence of WT-CylL_L''. Antimicrobial activity against *Lactococcus lactis* HP strain was identical for WT-CylL_S'' and CylL_S''-Dhb2Dha (Figure 3.6). Similar hemolytic activity was also evidenced for the two molecules (Figure 3.7). Based on the similar bioactivity profiles of the two molecules when the stereochemistry of the thioether crosslinks was held constant, we chose to pursue the synthetically tractable CylL_S''-Dhb2Dha as the target in lieu of WT-CylL_S''. It should be noted that a double mutant of CylL_S''-Dhb1Dha/Dhb2Dha exhibits LL-Lan instead of LL-MeLan as the A-ring (Figure 3.8). This variant was initially considered owing to the synthetic ease in accessing a Lan over a MeLan building block. Synergistically with CylL_L''-WT, this molecule exhibits similar antimicrobial activity but lower hemolytic activity as compared to CylL_S''-WT (Figures 3.6 and 3.7). Hence, this molecule was not considered for synthesis.

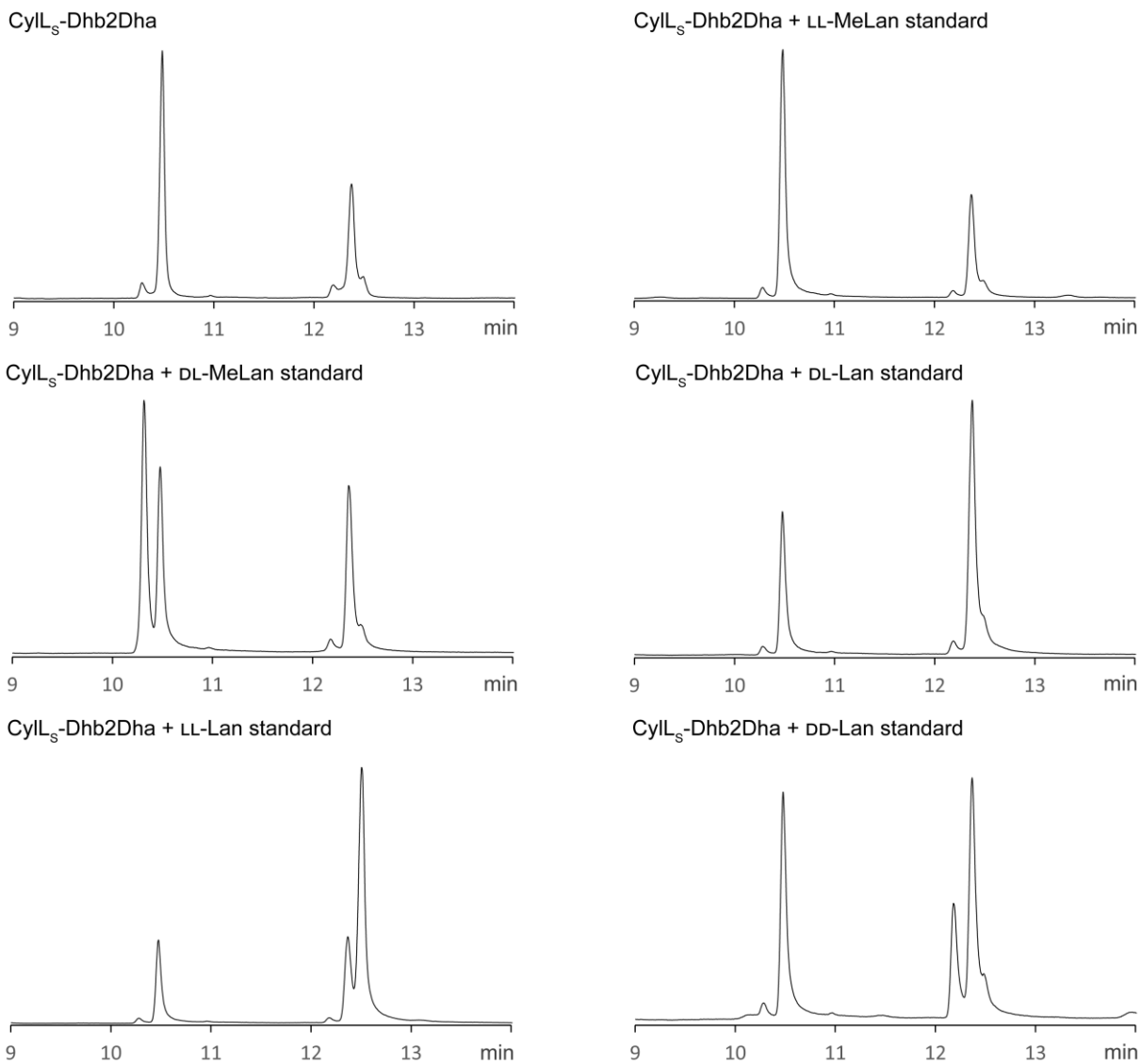
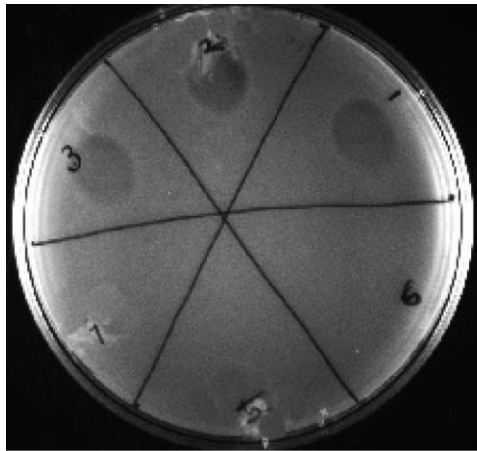


Figure 3.5. Chiral GC/MS analysis of hydrolyzed and derivatized CyLL₅-Dhb2Dha, obtained by in-vivo expression in *E.coli*, confirms the LL-configuration of the MeLan A-ring and DL-configuration of the Lan B-ring. Sample was either injected alone or co-injected with synthetic MeLan and Lan standards. Selected ion monitoring (SIM) was set at 365 Da for Lan and 379 Da for MeLan. Data were recorded at the Metabolomics Center (UIUC).



- Lane (1) Cyl_L^{WT} + Cyl_S^{WT}
- Lane (2) Cyl_L^{WT} + Cyl_S^{WT}-Dhb1Dha/Dhb2Dha
- Lane (3) Cyl_L^{WT} + Cyl_S^{WT}-Dhb2Dha
- Lane (4) Cyl_S^{WT}-Dhb2Dha
- Lane (5) Cyl_S^{WT}-Dhb1Dha/Dhb2Dha
- Lane (6) Buffer

Figure 3.6. Cytolysin S and its two mutants share similar antimicrobial activity against *L. lactis* HP, in synergy with cytolysin L. None of the peptides show independent antimicrobial activity. In all cases, 100 pmol of each peptide was added.

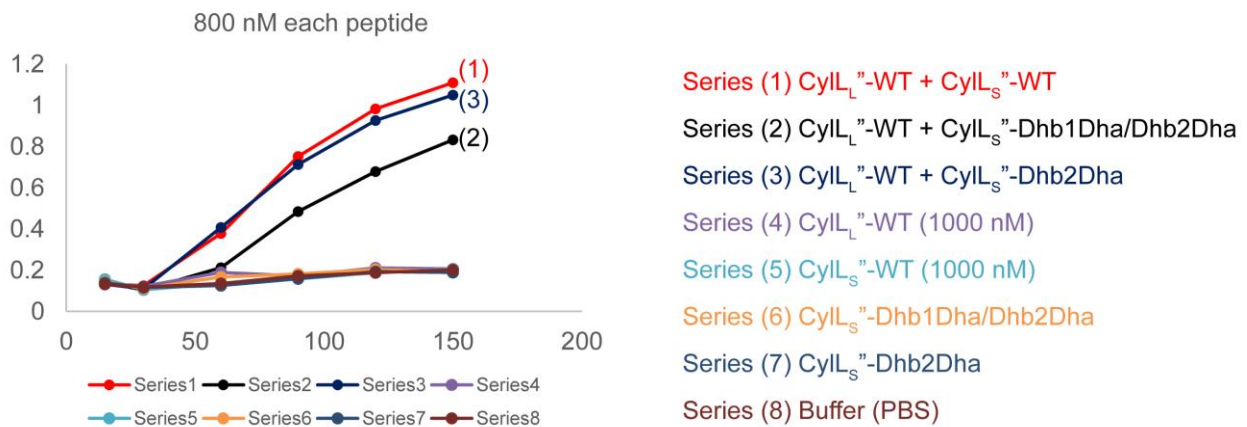


Figure 3.7. Cytolysin S and its single mutant share similar hemolytic activity, in synergy with cytolysin L. However, for the double mutant where the A-ring is Lan instead of MeLan, hemolytic activity was reduced.

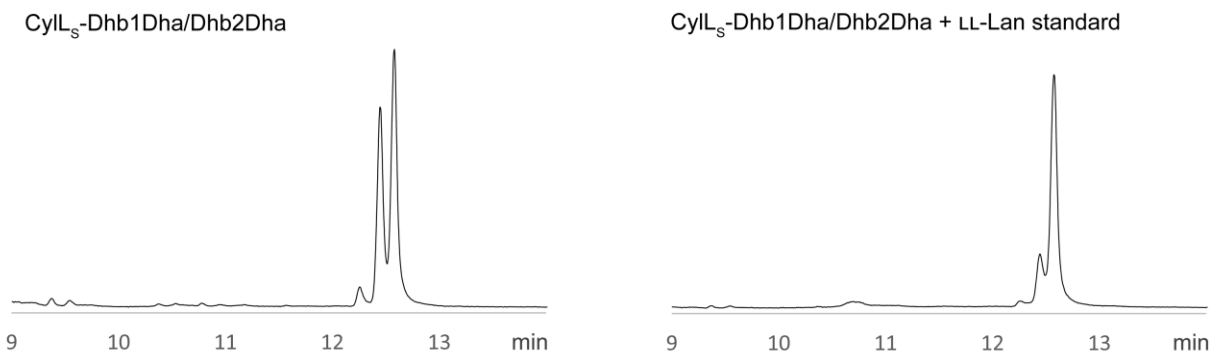
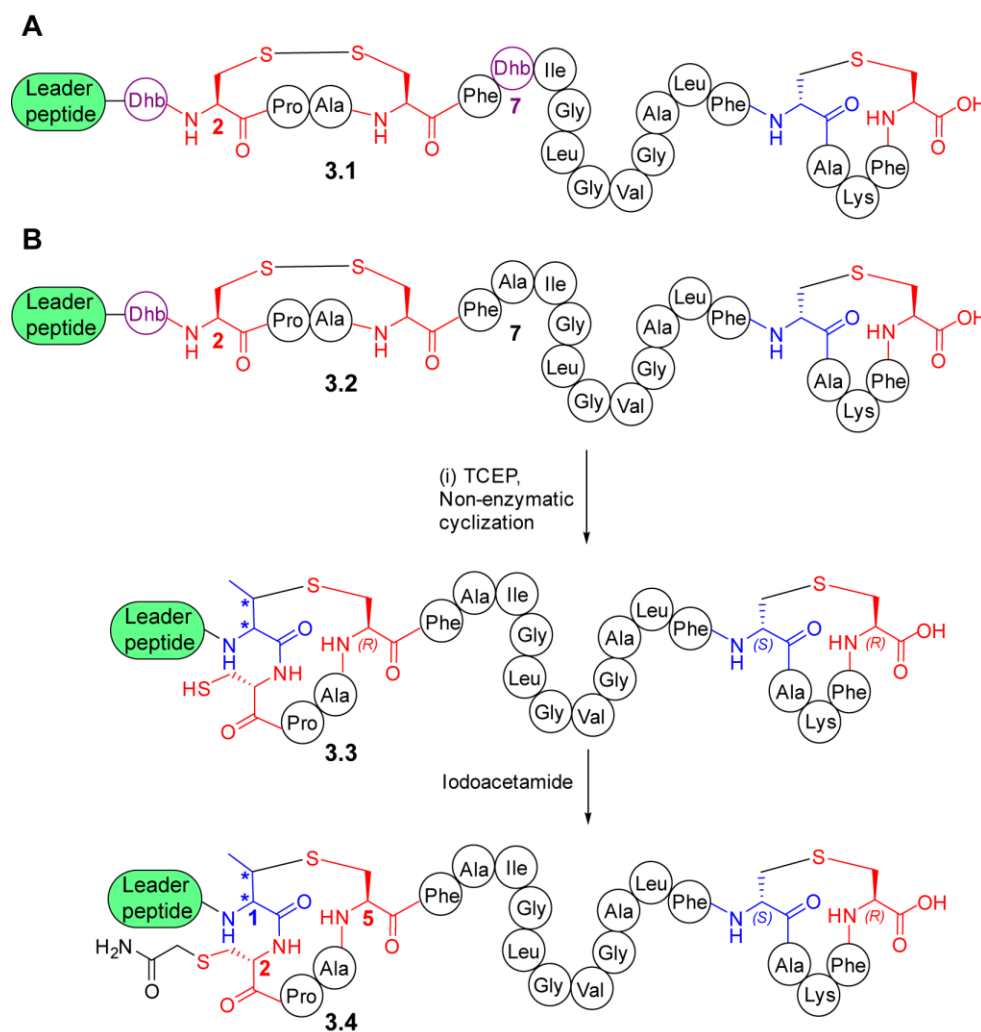


Figure 3.8. Chiral GC/MS analysis of hydrolyzed and derivatized CylL_S-Dhb1Dha/Dhb2Dha confirms the presence of both LL and DL-configurations of Lan. Sample was either injected alone or co-injected with synthetic LL-Lan standard. Selected ion monitoring (SIM) was set at 365 Da for Lan and 379 Da for MeLan. Data were recorded at the Metabolomics Center (UIUC).

3.2.3. Heterologous Expression of Cytolysin S with Cys at Position 2 to Assess the Elimination Chemistry

Our strategy for synthesizing CylL_S-Dhb2Dha involves solution-phase elimination of Cys to Dha after solid phase peptide synthesis. To ensure compatibility of the elimination chemistry with the thioether crosslinks, we wanted to first heterologously express a CylL_S'' variant with Cys at position 2, henceforth referred to as CylL_S''-Dhb2Cys. However, in vivo maturation of the precursor peptide with Cys at position 2 instead of Thr generated the disulfide containing species **3.1** and lacked the A-ring (Scheme 3.1). We were pleased to find that after reduction, non-enzymatic cyclization at pH 9.0 afforded the desired peptide with a Cys in position 2 within the A-ring. To prevent any undesired non-enzymatic cyclization with Dhb7, we accessed another disulfide containing species **3.2** from the heterologous co-expression of precursor peptide CylL_S-T2C/T7A. The disulfide in **3.2** was reduced and the peptide was subjected to non-enzymatic cyclization, which rendered **3.3** with correct ring topologies. The Cys at position 2 was then capped with iodoacetamide to generate **3.4** (Scheme 3.1). Analysis of the stereochemistry of the thioether crosslinks in **3.4** indicated a mixture of LL and DL-MeLan A-ring, and DL-Lan B-ring (Figure 3.9). The LL-stereochemistry of the A-ring is thought to be dependent on the

“DhxDhxXaaXaaCys” pentapeptide motif of the substrate (17), and hence, predominant formation of the LL-MeLan when Dhb at the position 2 is replaced with Cys is surprising. This suggested that cytolysin S peptide has other factors favoring the formation of LL-stereochemistry of ring A. Peptide **3.3** was subjected to elimination chemistry and gratifyingly generated the desired product (Scheme 3.2). This result illustrated the compatibility of the elimination reaction with the presence of the thioether crosslinks.



Scheme 3.1. Heterologous expression of Cyl_LS-T2C and Cyl_LS-T2C/T7A precursor peptides with CylM led to the formation of disulfide-linked peptides **3.1** and **3.2**. Reduction of peptide **3.2**, followed by non-enzymatic cyclization led to thioether formation between Cys5 and Dhb1 resulting in peptide **3.3**. Iodoacetamide treatment of peptide **3.3** yielded Cys-capped peptide **3.4**.

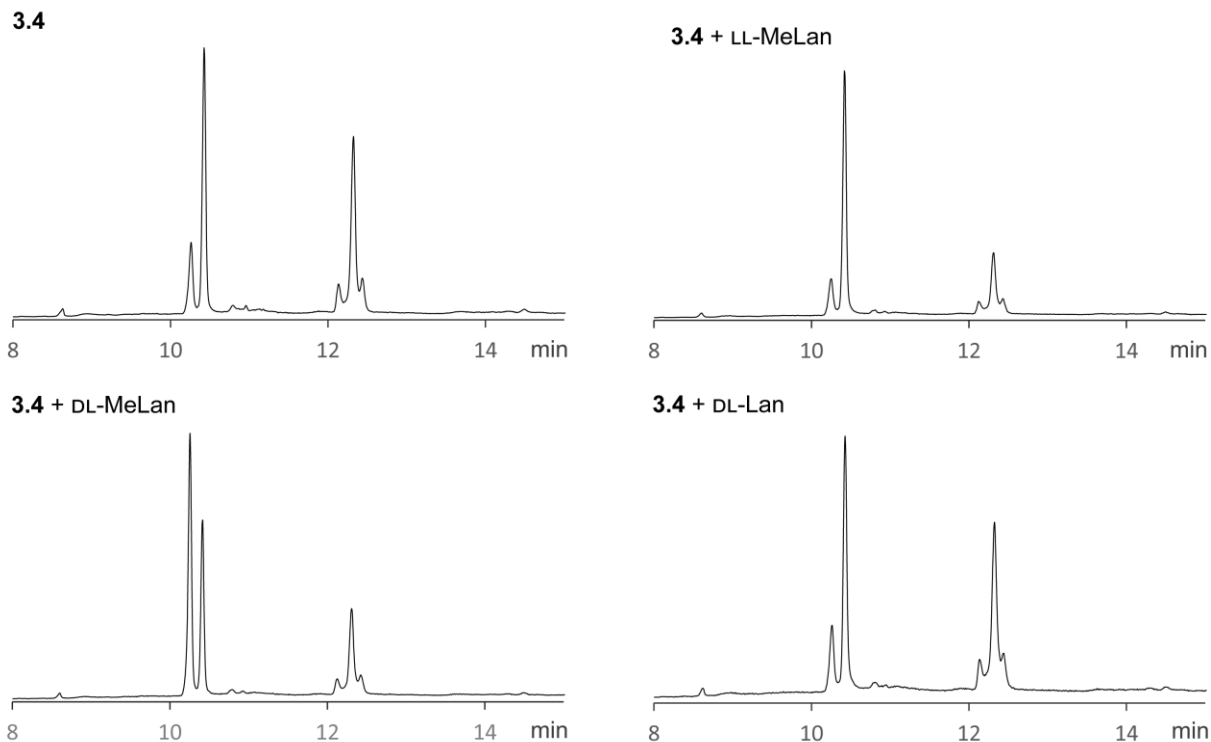
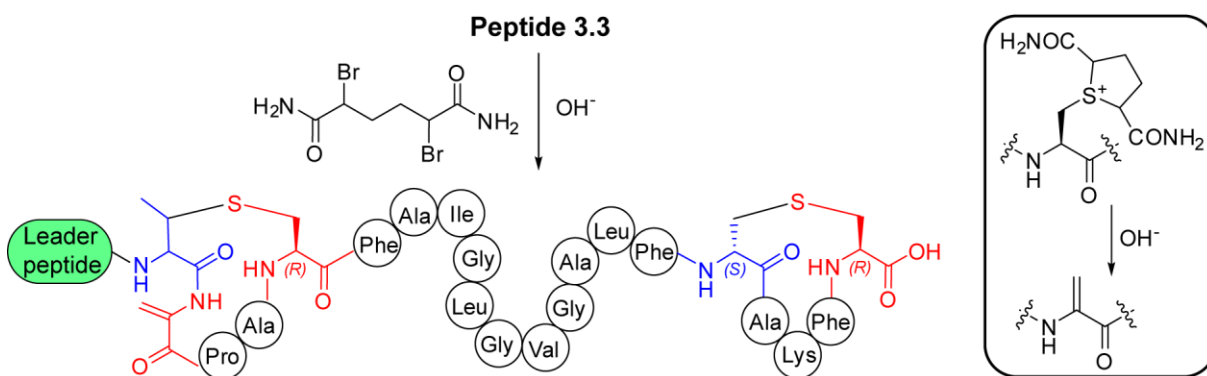


Figure 3.9. Chiral GC/MS analysis of hydrolyzed and derivatized peptide **3.4** confirms the presence of a mixture of LL and DL-configurations of MeLan, while only DL-Lan was observed. Sample was either injected alone or co-injected with synthetic standards. SIM was set at 365 Da for Lan and 379 Da for MeLan. Data were recorded at the Metabolomics Center (UIUC).

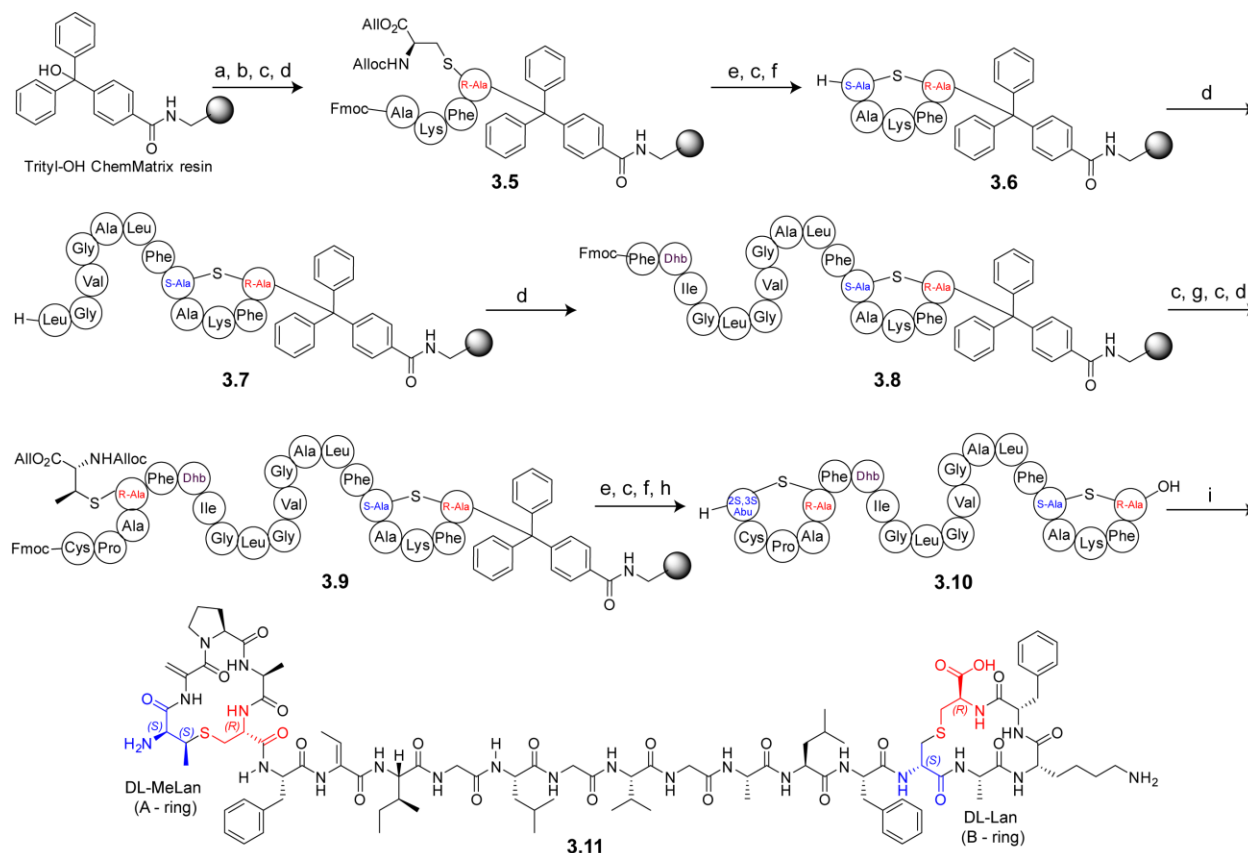


Scheme 3.2. Scheme showing Cys2 to Dha conversion in peptide **3.3**. Cys2 of peptide **3.3** was converted to Dha by reaction with 2,5-dibromohexanediamide followed by elimination (20). In the box, the cyclic sulfonium intermediate obtained from reaction of cysteine thiol with 2,5-dibromohexanediamide is drawn. Under alkaline condition, elimination occurs to generate dehydroalanine.

3.2.4. Total Synthesis of CylL_S''-Dhb2Dha with Non-Native DL-MeLan A-Ring and DL-Lan B-Ring

The high hydrophobicity of our target peptide demands the usage of modern innovations in SPPS. Aggregation of growing hydrophobic peptide chains is a common issue with polystyrene based resin (18). Polyethylene glycol-polystyrene based resins are better for hydrophobic peptides but those resins suffer from low resin loading, and in some cases poor chemical stability (21-25). ChemMatrix resins have recently been introduced that combine improved chemical stability with the beneficial properties of the traditional polyethylene glycol resins (26); owing to its polar nature, this resin does not interact with the side-chain protected peptides (27). This resin also shows excellent mechanical stability due to its extensive cross-linked structure. Additionally, ChemMatrix resin has enhanced swelling properties in a wide range of solvents, which physically minimizes the peptide self-association on the resin (26).

Cytolysin S has a C-terminal Lan residue. Prior experience with incorporating C-terminal protected Cys residues in the prochlorosin system (Section 2.4.10) suggested a bulky trityl-group as linker connecting the peptide with the ChemMatrix resin would be appropriate. This is because the protected C-terminal Cys thiol is prone to base catalyzed elimination resulting in dehydroalanine formation, followed by nucleophilic addition of subsequently added piperidine to result in β -piperidyl-alanine (28, 29). I successfully synthesized the CylL_S''-Dhb2Cys by manual SPPS using uronium and phosphonium based reagents depending on which residues were coupled (Scheme 3.3). Employing appropriately protected DL-MeLan and DL-Lan building blocks ensured the DL-configuration of the A and B-rings (30). The elimination reaction cleanly converted Cys at position 2 to Dha, to yield the desired CylL_S''-Dhb2Dha after HPLC purification (Figure 3.10).



Scheme 3.3. Synthesis of cytolysin S-Dhb2Dha. Reagents and conditions: (a) SOCl₂; (b) DL-Lan building block coupling; (c) piperidine, DMF; (d) SPPS; (e) Pd(PPh₃)₄, PhSiH₃, DMF, CH₂Cl₂; (f) PyAOP, HOAt, 2,4,6-collidine, DMF; (g) DL-MeLan building block coupling; (h) cleavage from resin using 95:2.5:2.5 of TFA:H₂O:triisopropylsilane; (i) 2,5-dibromohexanediamide, elimination carried at pH 8.4. Prior to cleavage from resin, all residues contained appropriate side-chain protecting groups for Fmoc SPPS.

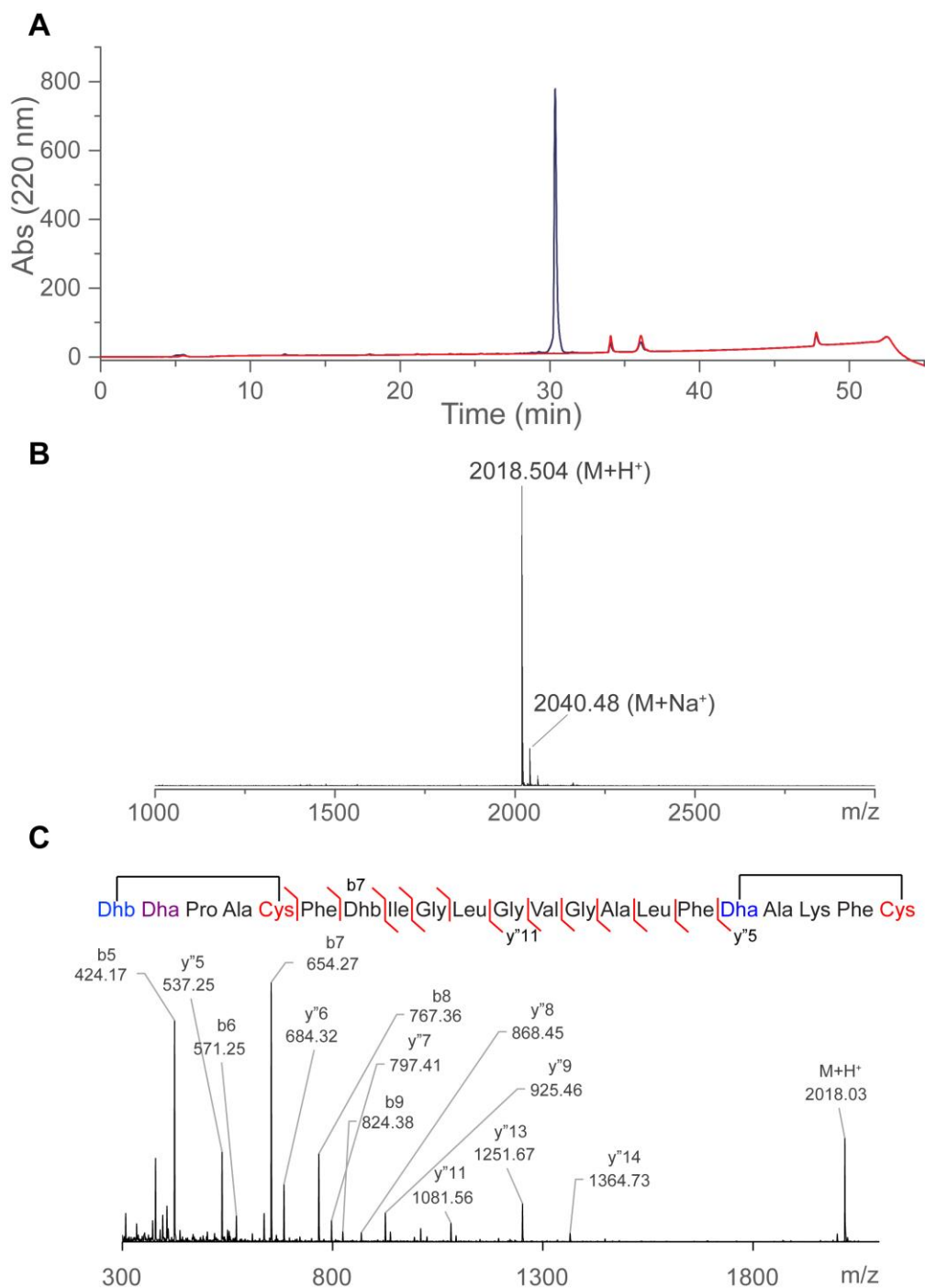
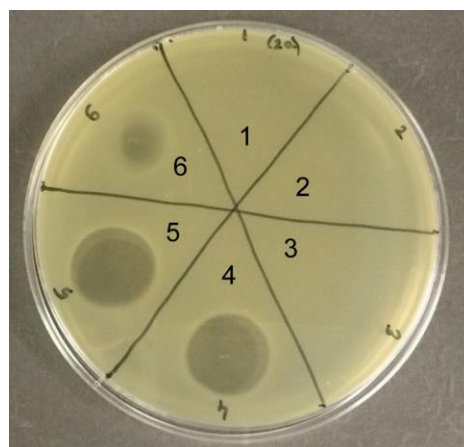


Figure 3.10. Analysis of pure synthetic CylLs''-Dhb2Dha. (A) HPLC trace of sample (blue trace) overlaid on the blank (red trace). (B) MALDI-TOF MS of the sample. (C) ESI-MS/MS of the sample.

exhibited significantly weaker synergistic bioactivity with WT-CylL_L" (lane 3 of Figure 3.11 and lane 6 of Figure 3.12).



- (1) PBS buffer (negative control)
- (2) CylL_L"-wt
- (3) CylL_S"-Dhb2Dha (synthesized, DL-A ring)
- (4) CylL_L"-wt + CylL_S"-wt (expressed, LL-A ring)
- (5) CylL_L"-wt + CylL_S"-Dhb2Dha (expressed, LL-A ring)
- (6) CylL_L"-wt + CylL_S"-Dhb2Dha (synthesized, DL-A ring)

Figure 3.12. Comparison of antimicrobial activity of diastereomers of cytolysin S. The synthesized CylL_S"-Dhb2Dha, with a DL-ring A, showed attenuated antimicrobial activity against *L. lactis* HP, in synergy with cytolysin L. In each lane, 100 pmol of each peptide component was added.

3.2.7. Evaluation of Hemolytic Activities of Variants of Cytolysin S

Various cytolysin S peptides were tested with WT-CylL_L" for synergistic hemolytic activity against rabbit blood cells. Both the WT-CylL_S" and expressed CylL_S"-Dhb2Dha, containing an LL-MeLan A-ring and DL-Lan B-ring, exhibited very similar hemolytic activity. Surprisingly, the synthesized CylL_S"-Dhb2Dha with a DL-MeLan A-ring and DL-Lan B-ring, exhibited no loss of hemolytic activity (Figure 3.13).

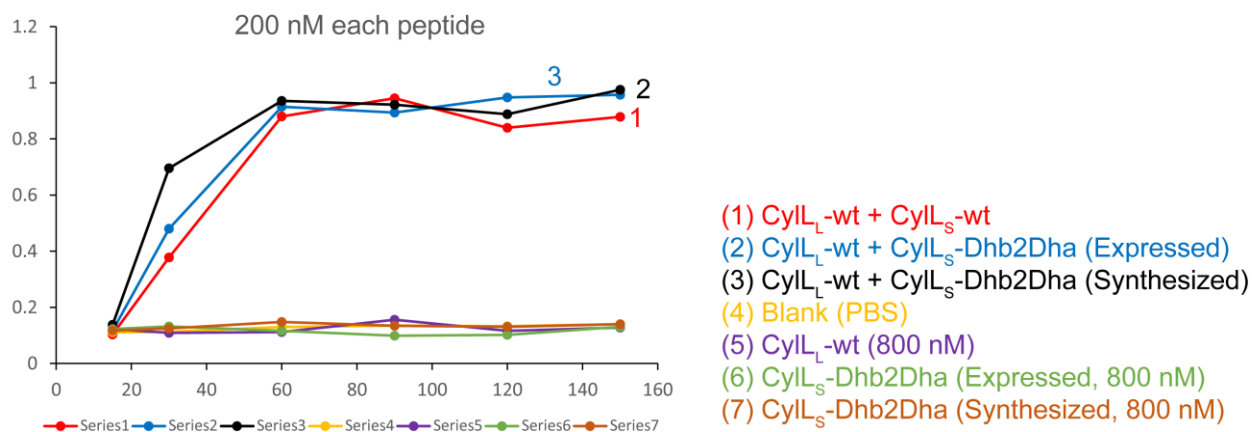


Figure 3.13. Comparison of hemolytic activity of diastereomers of cytolysin S. The synthesized CyLL_S-Dhb2Dha, with DL- ring A, showed modest increase in hemolytic activity compared to WT- CyLL_S, in synergy with cytolysin L.

3.3. CONCLUSION AND OUTLOOK

Total syntheses of lanthipeptides offer a flexible platform to study structure-activity relationships (SAR) by allowing introduction of unnatural amino acid residues and non-native stereochemistry of thioether crosslinks (31, 32). Synthesis of only five lanthipeptides – nisin (33), lactosin S (30), both components of lacticin 3147 (34), epilancin 15x (35), and lacticin 481 (32) have been reported so far. The synthesis of one of the two cytolysin components, CyLL_S is described here. We wanted to investigate the importance of the unusual LL-stereochemistry of the A-ring formed from the “DhxDhxXaaXaaCys” motif to cytolysin’s hemolytic and antibacterial activity. SPPS was chosen as a robust platform to generate a CyLL_S mutant bearing a DL-A-ring. We selected polyethylene glycol based ChemMatrix resin to efficiently synthesize the hydrophobic sequence of CyLL_S. A bulky trityl-linker was adopted to connect the peptide chain to the resin to prevent side-reactions of the C-terminal Lan residue. Realizing the problems associated with synthesizing the A-ring with a dehydrobutyryne as the second residue within the MeLan crosslink, the peptide was synthesized with a Cys mutation at this position. A late-stage

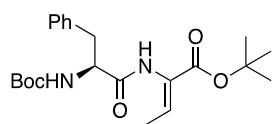
elimination generated Cyl_S” with Dhb at position 2 substituted with Dha. Hence, we successfully synthesized Cyl_S”-Dhb2Dha (DL-ring A), and compared its bioactivity with WT-Cyl_S”. Essentially identical bioactivities were observed for WT-Cyl_S” and Cyl_S”-Dhb2Dha (LL-ring A), both bearing only native stereochemistry. However, the diastereomer with a DL-crosslink of the “DhxDhxXaaXaaCys” motif exhibited reduced antimicrobial activity while maintaining similar hemolytic activity. The results lead us to hypothesize that Cyl_S” with the LL-stereochemistry of the A-ring has evolved to be complementary with native Cyl_L” in which two of the three thioether crosslinks exhibit the unusual LL-stereochemistry. This complementarity results in strong antimicrobial activity while in Cyl_S” with DL-stereochemistry of the A-ring, the synergy with native Cyl_L” is attenuated. Regarding the hemolytic activity, it is possible that the thioether stereochemistry of the A-ring of Cyl_S” is not important and that a non-specific interaction between the two hydrophobic peptides Cyl_S” and Cyl_L” leads to lysis of red blood cells. Another possibility is that the stereochemistry of the crosslinks in Cyl_L” is more critical than in Cyl_S”. Further insight would require synthesis of diastereomers of Cyl_L”. Such an endeavor would have to overcome the challenges of synthesizing a fairly long (with 38 amino acids, Cyl_L” is the longest lanthipeptide reported so far) peptide with a very hydrophobic sequence. Future efforts will involve synthesizing diastereomers of Cyl_L” or that of a synthetically tractable mutant. As another route to accessing diastereomers of Cyl_L”, mutation of “DhxDhxXaaXaaCys” motif to “DhxCysXaaXaaCys” can be attempted on rings A and B of Cyl_L” (similar to studies with Cyl_S”). If these mutants non-enzymatically cyclize to generate rings with DL-stereochemistry, then we can potentially study the effect of stereochemistry of thioether crosslinks in Cyl_L” on the synergistic bioactivity.

3.4. EXPERIMENTAL

3.4.1. Materials and General Methods

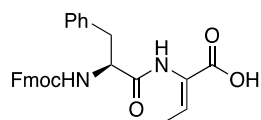
General characterization remains same as in sections 2.4.1 and 2.4.2. Additional purifications and analyses of cytolysin peptides are mentioned in this section. Cytolysin peptides required special method to ensure dissolution. Neat acetonitrile was added to the peptide, and vortexed to generate a milky suspension. To the suspension, equal volume of 0.1% aqueous TFA was added to generate a clear solution, which was diluted with 0.1% TFA to obtain peptide solution with a final acetonitrile concentration of 4%. Analytical reversed-phase high-performance liquid chromatography (RP-HPLC) was performed on an Agilent 1260 Infinity system with a Hypersil-Gold C₄ column with a flow rate of 1 mL/min and a solvent gradient of 2-100% solvent A over 45 min. Preparatory RP-HPLC was performed on a Waters 600 system with a Phenomenex Jupiter C₁₂, 4 μm Proteo 90 Å column with a flow rate of 4 mL/min and a solvent gradient of 2% solvent A, 98% solvent B to 100% solvent A in 45 min. All HPLC solvents were filtered with a Millipore filtration system equipped with a 0.22 μm nylon membrane filter prior to use. HPLC solvent compositions: solvent A was 80% acetonitrile in water with 0.086% trifluoroacetic acid (TFA), solvent B was 0.1% TFA in water.

3.4.2. Synthesis of Fmoc-PheDhb-OH Building Block



Compound **3.12**. Boc-PheThr-OtBu* (**prepared by Dr. Patrick Knerr*)

(0.8 g, 1.89 mmol) was dissolved in DCM (21 mL). The solution was cooled in an ice-bath following which trimethylamine (0.66 mL, 4.74 mmol) was added. Methanesulfonyl chloride (0.3 mL, 3.8 mmol) was added dropwise and the reaction was stirred for 1 h, gradually warming to room temperature. The reaction was concentrated under reduced pressure, re-dissolved in 1,2-DCE (21 mL) and DBU (1.14 mL, 7.6 mmol), and then heated to reflux in an oil-bath for 4 h, and concentrated under reduced pressure. The residue was dissolved in EtOAc, washed with 10% citric acid, saturated aqueous NaHCO₃, and brine, dried over Na₂SO₄, filtered, and concentrated. The residue was purified by flash chromatography (SiO₂, 7:1 hexanes/EtOAc, and then 4:1 hexanes/EtOAc). Yield: 0.61 g (80%). Spectral data matched those previously reported (35). (*Notebook IX, Page 77*)

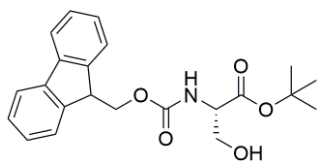


Compound **3.13**. Compound **3.12** (0.6 g, 1.48 mmol) was dissolved in 5

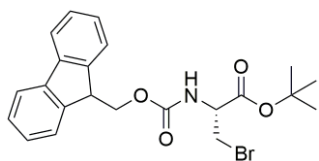
mL of DCM, 5 mL of TFA, and the reaction was stirred for 1.5 h. The reaction was concentrated under reduced pressure, repeatedly dissolved in DCM, and re-concentrated to finally generate a white residue. To the residue was added Na₂CO₃ (0.32 g, 2.97 mmol), water (14 mL), 1,4-dioxane (14 mL) and the mixture was chilled in an ice-bath. Fmoc-OSu (0.5 g, 1.48 mmol) was added as a solid. The reaction was stirred for 20 h, and gradually warmed to room temperature. The volatile components were removed under reduced pressure, and the residue diluted with water and acidified to pH 2 with 2 M HCl. The aqueous suspension was extracted with EtOAc (3x), the combined organic layer was dried over Na₂SO₄, filtered, and concentrated to 10 mL. To the residue, hexanes was added (100 mL) to generate a white

precipitate which was filtered over Buchner funnel to generate white powder. Yield: 0.7 g (quantitative). Spectral data matched those previously reported (35). (*Notebook IX, Page 78*)

3.4.3. Synthesis of LL-MeLan(Allyl/Alloc) Building Block

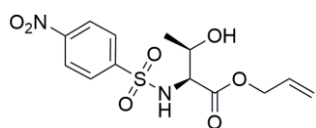


Compound **3.14**. Fmoc-L-Ser-OH (8.22 g, 25.1 mmol) was suspended in EtOAc (125 mL). To the suspension, *tert*-butyl 2,2,2-trichloroacetimidate (11.03 g, 50.48 mmol) dissolved in 50 mL of cyclohexane was added by addition funnel over 15 min. The reaction was stirred at room temperature for 20 h. The reaction was washed with saturated aqueous NaHCO₃ (1 x 100 mL), H₂O (1 x 100 mL), and brine (1 x 70 mL). The yellow clear solution was dried over Na₂SO₄, and evaporated on a rotary evaporator. The crude material was purified by flash chromatography (SiO₂, 3:1 hexanes/EtOAc) to yield the product as a white solid. R_f 0.5 (1:1 hexanes/EtOAc). Yield: 5.83 g (60%). Spectral data matched those previously reported (35). (*Notebook IX, Page 61*)

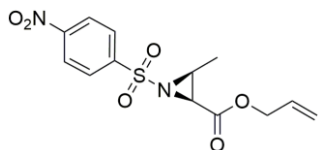


Compound **3.15**. Compound **3.14** (2.0 g, 5.22 mmol) and carbon tetrabromide (2.08 g, 6.26 mmol) were dissolved in DCM (10 mL) and the solution was chilled in an ice-bath. To the chilled solution, triphenylphosphine (1.64 g, 6.26 mmol) dissolved in DCM (10 mL) was added dropwise, and the reaction was stirred for 3.5 h while allowing to come to room temperature. The reaction mixture was washed with H₂O and brine, dried over Na₂SO₄, filtered, and concentrated under reduced pressure to generate yellow oil. Excess 5:1 hexanes/EtOAc was added to precipitate phosphine oxide and the washings were filtered over celite. The filtrate was concentrated, purified by flash chromatography (SiO₂, 15% EtOAc in hexanes) to yield product. R_f in 3:1 hexanes/EtOAc 0.58.

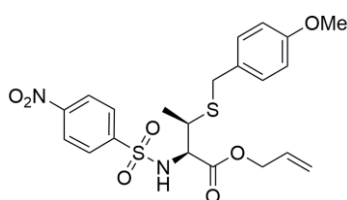
Yield: 1.43 g (62%). Spectral data matched those previously reported (35). (*Notebook IX, Page 81*)



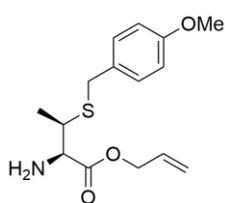
Compound **3.16**. L-Threonine (4.17 g, 35 mmol) and p-toluenesulfonic acid monohydrate (8 g, 42 mmol) were mixed in toluene (90 mL). To the suspension, allyl alcohol (24 mL) was added and the reaction was refluxed on an oil bath (110 °C) connected to a Dean-Stark apparatus for 18 h. The pale yellow solution was evaporated on a rotary evaporator azeotropically with benzene (4 x 50 mL). The brown oil was diluted in DCM (175 mL) and chilled in an ice bath. Triethylamine (14.6 mL, 105 mmol) was added and the reaction was stirred for 10 min. To the reaction, 4-nitrobenzenesulfonyl chloride (8.53 g, 38.5 mmol) was added portion wise and the reaction was stirred for 4 h at 0 °C. The reaction mixture was washed with 1 M NaH₂PO₄ (1 x 100 mL), saturated aqueous NaHCO₃ (1 x 100 mL), and brine (1 x 100 mL), dried over Na₂SO₄, filtered and concentrated on a rotary evaporator to yield a brown solid. The solid residue was dissolved in DCM (80 mL) and SiO₂ was added and the solvent evaporated on the rotary evaporator. The solid was transferred to a column and purified by flash chromatography (SiO₂, 7:3 hexanes: EtOAc to 3:2 hexanes: EtOAc). The fractions containing product (R_f 0.45 in 1:1 hexanes: EtOAc) was concentrated on a rotary evaporator to generate brown oil which was immediately transferred to two 20 mL scintillation vials, when solid crashed out and the residue was dried overnight in a vacuum pump to generate yellow solid. Yield: 9.8 g (81% over two steps). Spectral data matched that of the reported enantiomer (35). (*Notebook IX, Page 62*)



Compound **3.17**. Compound **3.16** (3 g, 8.71 mmol) and triphenylphosphine (2.97 g, 11.3 mmol) were dissolved in THF (33 mL) and the reaction was chilled in an ice-bath. To the chilled solution, diisopropyl azodicarboxylate (1.9 mL, 9.6 mmol) was added and the reaction was stirred for 2.5 h at 0 °C. The solution was concentrated under reduced pressure, the residue dissolved in EtOAc, washed with saturated aqueous NaHCO₃, and brine, dried over Na₂SO₄, and concentrated under reduced pressure. The residue was purified by flash chromatography (SiO₂, 5:1 hexanes/EtOAc) to yield product (R_f 0.55 in 2:1 hexanes/EtOAc). Yield: 1.76 g (62%). Spectral data matched that of the reported enantiomer (35). (*Notebook IX, Page 69*)

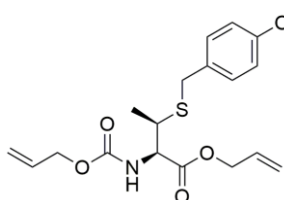


Compound **3.18**. Compound **3.17** (1.75 g, 5.4 mmol) was dissolved in DCM (54 mL), and to the solution was added 4-methoxybenzyl mercaptan (3.1 mL, 22 mmol). The solution was chilled in an ice-bath, following which boron trifluoride diethyl ether (2.4 mL, 16.2 mmol) was added dropwise to the stirring solution. The reaction was stirred at 4 °C for 26 h. The reaction was diluted with DCM and washed with saturated aqueous NaHCO₃, and brine, dried over Na₂SO₄, filtered, and concentrated under reduced pressure. The residue was purified by flash chromatography (SiO₂, 4:1 hexanes/ EtOAc) to yield product as yellow solid. Yield: 2.06 g, 80%. Spectral data matched that of the reported enantiomer (35). (*Notebook IX, Page 70*)

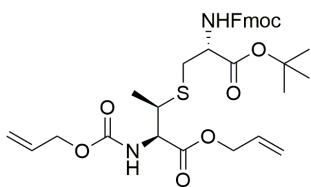


Compound **3.19**. Compound **3.18** (1.64 g, 3.41 mmol) was dissolved in 25 mL of 49:1 MeCN/DMSO and stirred. To the stirring solution, 4-methoxybenzyl mercaptan (1.26 mL, 10.3 mmol) and potassium carbonate (1.89 g, 13.7 mmol) were added. The heterogeneous reaction mixture was stirred for 3 h and concentrated under reduced pressure. The concentrated residue was taken up in EtOAc, washed

with H₂O, and brine, dried over Na₂SO₄, filtered, and concentrated. The crude product was purified by flash chromatography (SiO₂, 3:2 then 2:3 hexanes/EtOAc) to yield product as pale yellow oil. R_f = 0.25 (1:1 hexanes/EtOAc). Yield: 0.93 g (93%). Spectral data matched that of the reported enantiomer (35). (*Notebook IX, Page 71*)



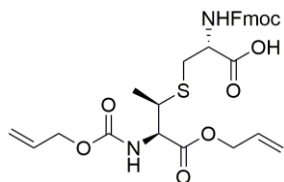
Compound **3.20**. Compound **3.19** (0.93 g, 3.14 mmol) was dissolved in DCM (18 mL). Diisopropylethylamine (0.66 mL, 3.8 mmol) and allyloxycarbonyloxysuccinimide (AlocOSu, 0.68 g, 3.36 mmol) were added to the stirring solution, and the reaction was stirred for 12 h. The reaction was diluted with DCM, washed with H₂O, 10% citric acid, and brine, dried over Na₂SO₄, filtered, and concentrated under reduced pressure. The crude material was purified by flash chromatography (SiO₂, 4:1 hexanes/EtOAc) to yield product as colorless oil. R_f = 0.58 in 2:1 hexanes/EtOAc. Yield: 1.06 g (89%). Spectral data matched that of the reported enantiomer (35). (*Notebook IX, Page 72*)



Compound **3.21**. Compound **3.20** (0.36 g, 0.95 mmol) was dissolved in TFA (5.3 mL) and anisole (413 μL, 3.81 mmol). Hg(OAc)₂ (0.61 g, 1.9 mmol) was added as solid and then the yellow solution turned brown, and then purple. The solution was stirred for 4 h. Dithiothreitol (DTT, 0.3 g, 1.93 mmol) was added, forming a grey precipitate, and the suspension was stirred for 18 h. The suspension was diluted with DCM, and centrifuged (4600 x g, 10 min) to remove the residue, while the supernatant was retained. The residue was re-suspended in DCM and further centrifuged. The combined supernatants were concentrated on a rotary evaporator. The crude residue was dissolved in DCM (50 mL), to which water (10 mL) was added and the pH adjusted to 5.0 by addition of solid NaHCO₃. The organic layer was collected, concentrated on a rotary evaporator

and then the crude residue was purified on a flash chromatography (SiO₂, 15% EtOAc in hexanes) to yield compound **3.20** without the thiol protecting group (R_f 0.52 in 3:1 hexanes/EtOAc, as visualized by KMnO₄ stain). The product was immediately moved to the next reaction without prolonged drying on vacuum pump and spectroscopic characterization.

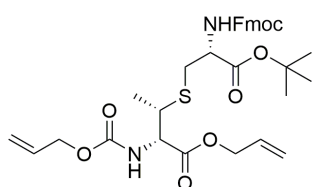
To the concentrated product from the above reaction was added compound **3.15** (0.25 g, 0.56 mmol), and N₂-sparged EtOAc (3.5 mL). Tetrabutylammonium bromide (1.02 g, 3.17 mmol) dissolved in 3.5 mL degassed aqueous NaHCO₃, pH 8.5, was added and the biphasic solution was stirred for 5 h. Tributylphosphine (80 μL, 0.32 mmol) was added and the reaction was stirred overnight. The organic layer was separated and washed with water and brine, dried over Na₂SO₄, filtered, and concentrated and the crude was purified over flash chromatography (4:1 hexanes/EtOAc) to obtain product (R_f 0.25 in 3:1 hexanes/EtOAc). Yield: 0.25 g (71%, considering Fmoc-bromoalanine as the limiting reagent). ¹H NMR (500 MHz, CDCl₃) δ 7.77 (d, *J* = 7.5 Hz, 2H), 7.62 (t, *J* = 7.5 Hz, 2H), 7.41 (t, *J* = 7.5 Hz, 2H), 7.32 (t, *J* = 7.5 Hz, 2H), 5.96-5.84 (m, 2H), 5.72-5.66 (d, *J* = 7.5 Hz, 2H), 5.69 (d, *J* = 7.5 Hz, 2H), 5.59 (d, *J* = 7.5 Hz, 2H), 5.39-5.17 (m, 4H), 4.66 (d, *J* = 6.0 Hz, 2H), 4.62-4.48 (m, 4H), 4.42-4.37 (d, *J* = 7.5 Hz, 2H), 4.26-4.22 (t, *J* = 7.0 Hz, 1H), 3.52-3.45 (m, 1H), 3.04-2.94 (m, 2H), 1.49 (s, 9H), 1.34 (d, *J* = 7.0 Hz, 1H). ¹³C NMR (125 MHz, CDCl₃) δ 170.3, 169.4, 156.4, 155.9, 144, 143.9, 141.4, 132.6, 131.4, 127.8, 127.2, 125.26, 125.23, 120.1, 119.6, 118, 83.1, 67.3, 66.6, 66.2, 58.7, 54.7, 47.2, 43.8, 33.9, 28.1, 19.5. HRMS (ESI) calculated for C₃₃H₄₁N₂O₈S 625.2584 (M+H⁺), observed 625.2573. (*Notebook IX, Page 80*)



Compound **3.22**. Compound **3.21** (0.2 g) was dissolved in 2.5 mL of dry DCM, and to the solution was added phenylsilane (80 μL), followed by

TFA (2.5 mL). The reaction was stirred for 2 h, the solution was concentrated, and the residue was dissolved in DCM and concentrated further. This step was repeated twice more to remove the residual TFA. The concentrated residue was purified by flash chromatography (SiO₂, 1-2 % MeOH in DCM) to generate product. The product was concentrated, dissolved in 1:1 (MeCN/benzene), and lyophilized. Yield: 0.14 g (77%). ¹H NMR (400 MHz, CD₃OD) δ 7.78 (d, *J* = 7.5 Hz, 2H), 7.67 (t, *J* = 7.5 Hz, 2H), 7.34 (t, *J* = 7.5 Hz, 2H), 7.30 (t, *J* = 7.5 Hz, 2H), 5.98-5.83 (m, 2H), 5.38-5.28 (m, 2H), 5.26-5.11 (m, 2H), 4.62 (m, 2H), 4.57-4.49 (m, 2H), 4.44 (d, *J* = 5.2 Hz, 1H), 4.41-4.32 (m, 3H), 4.22 (t, *J* = 7.0 Hz, 1H), 3.46-3.37 (m, 1H), 3.07 (dd, *J* = 14 Hz, 4.4 Hz, 1H), 2.93 (dd, *J* = 14 Hz, 8.8 Hz, 1H), 1.32 (d, *J* = 6.8 Hz, 3H). ¹³C NMR (100 MHz, CDCl₃) δ 173.7, 171.6, 158.5, 145.3, 145.1, 142.53, 142.51, 134.1, 133.1, 129.3, 128.8, 128.2, 126.3, 126.26, 120.9, 119.25, 117.75, 68.2, 67.2, 66.8, 60.3, 55.5, 48.3, 44.3, 34.3, 19.7. HRMS (ESI) calculated for C₂₉H₃₃N₂O₈S 569.1958, observed 569.1965. (*Notebook IX, Page 74*)

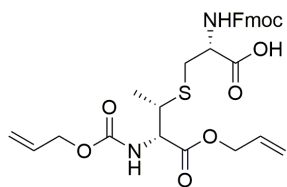
3.4.4. Synthesis of DL-MeLan(Allyl/Alloc) Building Block



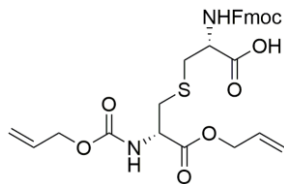
Compound **3.23**. Diastereomer of compound **3.20** with 2*S*,3*S* stereochemistry* (**prepared by Dr. Patrick Knerr*) (0.6 g, 1.64 mmol) was dissolved in TFA (9 mL) and anisole (710 μL, 3.81 mmol).

Hg(OAc)₂ (1.04 g, 3.23 mmol) was added as solid and then the yellow solution turned brown, and then purple. The solution was stirred for 4 h. Dithiothreitol (DTT, 0.48 g, 3.1 mmol) was added, forming a grey precipitate, and the suspension was stirred for 16 h. The suspension was diluted with DCM, and centrifuged (4600 x g, 10 min) to remove the solid, while retaining the supernatant. The solid was re-suspended in DCM and further centrifuged. The combined supernatants were concentrated on a rotary evaporator. The crude residue was dissolved in DCM (50 mL), water (10 mL) was added, and the solution adjusted to pH 5.0 by addition of solid

NaHCO₃. The organic layer was collected, concentrated on a rotary evaporator and then the crude residue was purified by flash chromatography (SiO₂, 15% EtOAc in hexanes) to yield product (R_f 0.52 in 3:1 hexanes/EtOAc, as visualized by KMnO₄ stain), which was immediately moved to the next reaction without prolonged drying on vacuum pump and spectroscopic characterization. To the concentrated product from the above reaction was added compound **3.15** (0.43 g, 0.94 mmol), and N₂-sparged EtOAc (5.3 mL). Tetrabutylammonium bromide (1.2 g, 3.73 mmol) dissolved in 5.3 mL aqueous NaHCO₃, pH 8.5, and the biphasic solution was stirred for 5 h. Then, tributylphosphine (133 μL, 0.53 mmol) was added and the reaction was stirred overnight. The organic layer was separated and washed with water and brine, dried over Na₂SO₄, filtered, concentrated and the crude was purified over flash chromatography (4:1 hexanes/EtOAc) to obtain product (R_f 0.28 in 3:1 hexanes/EtOAc). Yield: 0.22 g (37%, considering Fmoc-bromoalanine as the limiting reagent). Spectral data matched those previously reported (35). (*Notebook IX, Page 82*)



Compound **3.24**. Compound **3.23** (0.22 g) was dissolved in 2.6 mL of dry DCM, and to the solution was added phenylsilane (85 μL), followed by TFA (2.6 mL). The reaction was stirred for 2 h, concentrated, dissolved in DCM and concentrated further. This step was repeated twice more to remove the residual TFA. The concentrated residue was purified by flash chromatography (SiO₂, 1-2 % MeOH in DCM) to generate product. The product was concentrated, dissolved in 1:1 (MeCN/benzene), and lyophilized. Yield: 0.17 g (86%). Spectral data matched those previously reported (35). (*Notebook IX, Page 83*)



Compound **3.25**. Prepared by Dr. Patrick Knerr and Mr. Evert Peterse using a previously reported procedure (35).

3.4.5. General Procedure for Solid Phase Peptide Synthesis (SPPS)

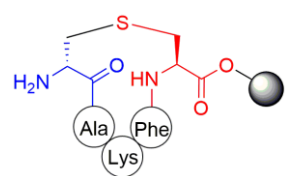
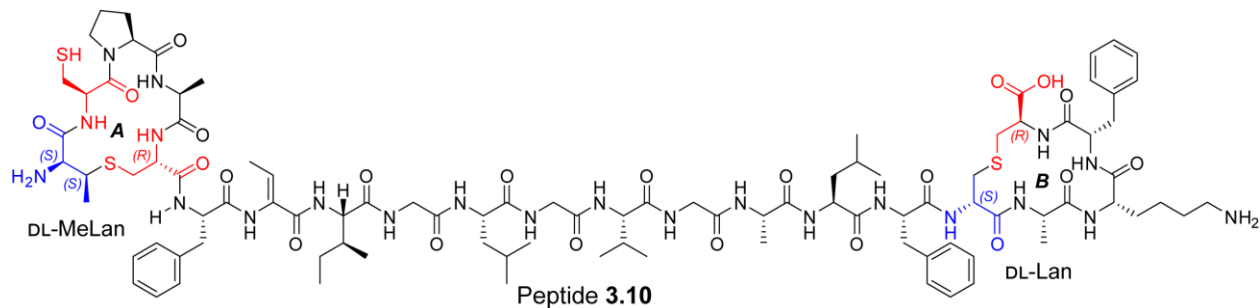
Unless otherwise noted, the general synthetic strategy involved the use of *N*-[(dimethylamino)-1*H*-1,2,3-triazolo-[4,5-*b*]pyridin-1-ylmethylene]-*N*-methylmethanaminium hexafluorophosphate *N*-oxide (HATU) as coupling agent. Additionally, 1-hydroxy-7-azabenzotriazole (HOAt) was used as a racemization suppressant. Diisopropylethylamine (DIPEA) was used as a base. Tritel-OH ChemMatrix resin was used as the solid support. The resin was swelled and loaded with the first amino acid residue as follows. The resin (1 g) was swelled in 15 mL of DCM, and to the suspension, 0.4 mL of thionyl chloride was added and the resin was agitated under N₂ for 4 h. Then, the resin was washed with DCM (5x) and 2% DIPEA in DCM (3x). Next, protected amino acid building block was loaded to the resin to result in amino acid loaded resin with lower resin substitution. Protected amino acid building block (0.15 mmol), and DIPEA (0.75 mmol, 0.13 mL) in DCM was reacted for 3 h. The resin was washed with DCM and the remaining chloride substitutions on the resin were capped by treating with acetic acid (0.5 mmol, 0.03 mL), and DIPEA (2 mmol, 0.35 mL) in DCM for 2 h. The resin was washed with DCM and dried overnight.

The amino acid substitution of the resin was calculated as follows. Fmoc protected resin (~ 10 mg) was suspended in 1 mL of 20% piperidine in DMF for 15 min. From the solution, 20 μ L of aliquot was diluted in 1980 μ L of DMF. The absorbance (λ 301 nm) was measured with

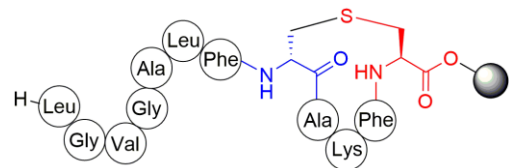
DMF as blank. The substitution was calculated (substitution = $101 \cdot \text{abs} / 7.8 \cdot \text{resin weight}$) (36, 37). The absorbance was measured in duplicate and averaged.

The resin was swelled in 1:1 DMF/DCM for 30 min. Fmoc was removed by agitating the resin with 20% piperidine in DMF (2 x 10 min). The resin was subjected to a wash cycle by agitating with DMF (2 x 30 s), 1:1 DMF/DCM (1 x 30 s), DCM (2 x 30 s), and 1:1 DMF/DCM (1 x 30 s). The side-chain protected amino acid (5 equivalents), HCTU or HATU (5 equivalents), and HOAt (5 equivalents) was dissolved in 15 mL of DMF. To the solution, DIPEA (8 equivalents) was added and after 1 min, the activated solution was applied to the resin and agitated for 1 h (unless otherwise noted). Coupling was repeated once, and the completion of coupling was monitored by Kaiser test. This procedure was followed by capping by agitating the resin with capping solution (90:8:2 of DMF/acetic anhydride/DIPEA) for 7 min. Subsequently, iterative deprotection, coupling, and capping steps followed. After Fmoc removal from the last coupled residue, the resin was washed and dried. Cleavage was performed by suspending the resin in cleavage cocktail (95:2.5:2.5 of trifluoroacetic acid/water/triisopropylsilane). Typically, for 1 g of resin, 25-30 mL of cleavage cocktail was used to accommodate the high swelling of the ChemMatrix resin in TFA. After 1.5 h of cleavage reaction, the resin was filtered. The resin was further washed with 2 mL of TFA, and then 10 mL of DCM. All the filtrates were evaporated by applying a stream of N₂. To the concentrated solution, 10 mL of cold diethyl ether was added to allow precipitation of the peptide. Centrifugation (10800 x g, 10 min) was performed to precipitate the peptide and discard the ether supernatant. The peptide was suspended in 1 mL of acetonitrile. Then, 2 mL of 0.1% TFA in water was added and the suspension vortexed to dissolve the peptide. The solution was frozen and lyophilized to obtain the crude peptide.

3.4.6. SPPS of Cyl_LS-Dhb2Cys with DL-MeLan (A-Ring) and DL-Lan (B-Ring)

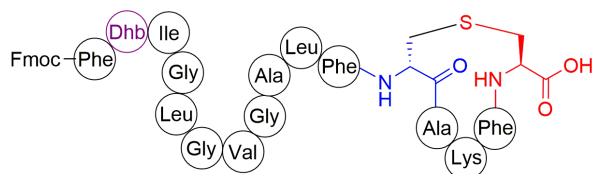


Intermediate **3.6**. Subsequent to loading compound **3.25** to the resin, the resin-substitution was found to be 0.09 mmol/g. Phe, Lys, and Ala were coupled using 0.5 mmol of side-chain protected amino acid building blocks, 0.5 mmol of HCTU, 0.5 mmol of HOAt, and 0.8 mmol of DIPEA in DMF (1 h single coupling). The alloc/allyl group was removed by adding Pd(PPh₃)₄ (0.22 mmol, 0.26 g), PhSiH₃ (1.1 mmol, 0.135 mL) in 1:1 (DMF/DCM), and agitating in N₂ for 2 h. The resin was washed with DCM (3 x 20 mL), 0.5% of sodium diethyldithiocarbamate in DMF (3 x 20 mL), DMF (3 x 20 mL), 1:1 DCM/DMF (3 x 20 mL). The Fmoc-group was removed and coupling was performed by adding PyAOP (0.5 mmol), HOAt (0.5 mmol) in DMF to the resin and agitating the resin in DMF for 5 min followed by addition of 2,4,6-collidine (1 mmol) and agitation (2 x 2.5 h). After washing and drying the resin, a little of the resin was cleaved (95:2.5:2.5 = TFA:TIS:H₂O) for 1 h and analyzed by ESI. ESI-MS calculated for C₂₄H₃₇N₆O₆S (M+H⁺) 537.24, observed 537.4. (*Notebook IX, Page 43*)



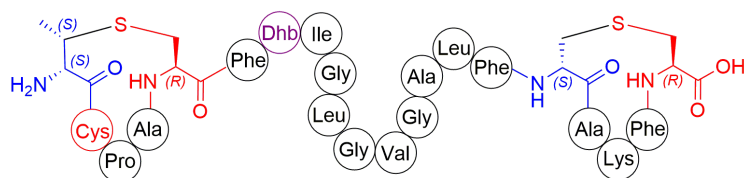
Intermediate **3.7**. The residues (from C to N terminus) Phe, Leu, Ala, Gly, Val, Gly, and Leu were coupled by the same chemistry as before. After Fmoc-deprotection, test cleavage was performed on a small amount of resin. ESI-MS calculated for C₅₇H₈₈N₁₃O₁₃S

(M+H⁺) 1194.62, observed 1194.6; calculated for C₅₇H₈₉N₁₃O₁₃S (M+2H)²⁺ 597.3, observed 597.9. (*Notebook IX, Page 43*)



Intermediate 3.8. The residue Gly was coupled, the resin was dried, and the resin was split into approximately two equal portions. Further

synthesis was performed on ca. half of the resin (~0.05 mmol). Gly was coupled for another round followed by coupling of Ile. The dipeptide Fmoc-PheDhb-OH required extensive coupling durations of 1 h and 3 h – with 0.2 mmol of amino acids and coupling agents when Kaiser test indicated incomplete coupling. Therefore, coupling was repeated with 0.3 mmol of dipeptide and coupling agents for 11 h, upon which Kaiser test indicated complete coupling. A little of the resin was cleaved and the peptide was analyzed by ESI-MS. ESI-MS calculated for C₉₃H₁₂₇N₁₇O₁₉S (M+2H)²⁺ 908.95, observed 909.0. (*Notebook IX, Page 44*)



Peptide 3.10. After Fmoc-removal, Fmoc-DL-MeLan building block with allyl/alloc protection (0.2 mmol) was

coupled using HATU (0.2 mmol), HOAt (0.2 mmol), and DIPEA (0.4 mmol) for 5 h. Kaiser test gave dark brown coloration (Kaiser test has been found to be inconclusive for N-terminal Lan/MeLan residues). Subsequent amino acids (0.5 mmol) were coupled using HATU (0.5 mmol), HOAt (0.5 mmol), and DIPEA (0.8 mmol). Ala involved double coupling (1 h, 2h). Kaiser test was clean at this stage. Pro involved single 5 h coupling. Cys(Trt) involved overnight coupling (7 h). The allyl/alloc groups were deprotected by adding Pd(PPh₃)₄ (0.2 mmol) and PhSiH₃ (1 mmol) in DMF/DCM (1:1), and agitating for 7 h. The resin was washed with DCM (3 x 20 mL), 0.5% solution of sodium diethyldithiocarbamate in DMF (3 x 20 mL), and DMF/DCM

(1:1, 3 x 20 mL). Then the Fmoc-group was removed and coupling/cyclization was performed by adding PyAOP (0.5 mmol), HOAt (0.5 mmol) in DMF and after 5 min of agitation, 2,4,6-collidine was added and the reaction was stirred (couple was performed twice for 1.5 h and 3 h). The resin was washed and dried overnight by a stream of N₂. Test cleavage followed by analysis by MALDI-TOF MS indicated product formation. The calculated m/z for C₉₆H₁₄₃N₂₂O₂₂S₃ is 2051.98, observed 2052.12. The resin (0.6 g) was cleaved and the obtained peptide was lyophilized. Peptide was purified using a Phenomenex Jupiter C₁₂, 4 μm Proteo 90 Å column with a gradient of 2% to 100% A (0.1% TFA in H₂O) in D (80% MeCN in 0.086% TFA) over 45 min (flow rate: 4 mL/min). Of the crude peptide, 46 mg was purified in 11 injections. Yield: 3 mg (partially purified material). (*Notebook IX, Page 45*)

3.4.7. Cys to Dha Elimination Reaction on Synthesized CylLs-T2C (DL-A Ring, DL-B Ring)

Synthesized and purified peptide **3.10** (236 μg) was taken in an Eppendorf tube and to the content was added acetonitrile (16 μL) and the mixture vortexed to generate a white suspension. To the suspension, 50 μL of 0.1% aqueous TFA was added to generate a clear solution. The solution was diluted with 134 μL of H₂O followed by addition of 20 μL of TCEP (10 mM stock), and 65 μL of NH₄HCO₃ (200 mM stock, pH 8.9) resulting in a solution with final pH 8.4. To the solution was added 2,5-dibromohexanedioic acid (1 mg) and then the white suspension was stirred at RT (1 h) and at 37 °C (4 h). MALDI-TOF MS of both the crude suspension and the supernatant (after centrifugation) indicated product formation (m/z calculated for C₉₆H₁₄₁N₂₂O₂₂S₂ (M+H⁺) 2018, observed 2018.47). From the reaction, sample was prepared for analytical HPLC purification to ensure the dissolution of any precipitated product, leaving the residue of unreacted 2,5-dibromohexanedioic acid. The sample preparation was as follows: The

reaction was centrifuged (16100 x g, 2 min) and the supernatant was collected. To the residue was added 16 μ L of MeCN and vortexed, followed by addition of 200 μ L of aqueous 0.1% TFA and then further vortexed. The suspension was centrifuged (16100 x g, 2 min) and the supernatant was combined with the earlier supernatant. This step was repeated twice and the combined supernatants (ca. 800 μ L) was injected onto a Hypersil gold C₄ column with a flow rate of 1 mL/min. Product eluted with R_t of 29.8 min. This reaction was performed in several sets and purified to generate the desired peptide **3.11** in sufficient quantity for bioassays. (*Notebook IX, Page 48*)

3.4.8. Mutagenesis of Cytolysin S Gene

The numeric 1 designates the first residue of the core peptide and the last residue of the leader peptide is denoted by -1. The *cyL_S* precursor gene is encoded within the multiple cloning site (MCS) 1 of pRSFDuet-1 plasmid with *cyLM* gene encoded in the MCS 2 (provided by Dr. Weixin Tang) (15). The cytolysin S mutants were generated using the following primers by QuikChange site-directed mutagenesis based on a modified protocol (38). The *cyL_S* gene in pRSF-Duet plasmid was used as a template to introduce the single point mutations. *cyL_S-T2S* was used as a template to generate *cyL_S-T2S/T1S*, and *cyL_S-T2C* was used as a template to generate *cyL_S-T2C/T7A*. (*Notebook VIII, Pages 65, 66, and Notebook IX, Pages 22, 25*)

Primer Name	Primer Sequences (5' to 3')
CyL _S _T2S_FP	CAGGCAGAAACCAGCCCGGCATGTTTTACC
CyL _S _T2S_RP	GGTAAAACATGCCGGGCTGGTTTCTGCCTG
CyL _S _T1S/T2S_FP	G TTCAGGCAGAAAGCAGCCCGGCATG
CyL _S _T1S/T2S_RP	CATGCCGGGCTGCTTTCTGCCTGAAC

CylL _s _T2C_FP	CAGGCAGAAACCTGCCCCGGCATGTTTTACC
CylL _s _T2C_RP	GGTAAAACATGCCGGGCAGGTTTCTGCCTG
CylL _s _T2C/T7A_FP	CCGGCATGTTTTGCAATTGGTCTGGGTG
CylL _s _T2C/T7A_RP	CACCCAGACCAATTGCAAAACATGCCGG

3.4.9. General Procedure for Overexpression of Cytolysin Variants

Electrocompetent *E. coli* BL21 (DE3) cells were transformed with the pRSFDuet-1 plasmid encoding cytolysin precursor peptide in MCS1 and CylM in MCS2, and the transformed cells were spread on LB + Kan (50 µg/mL) agar plate and incubated at 37 °C overnight. Cells from a single colony were used to inoculate a LB + Kan (50 µg/mL) starter culture (100 mL), which was shaken at 37 °C overnight. The starter culture was used to grow a large scale LB + Kan (50 µg/mL) culture (2 x 2.5 L) at 37 °C to OD_{600 nm} of 0.6 to 0.7. The culture was cooled in the cold room (4 °C) for 30 min and then induced with IPTG to a final concentration of 0.5 mM. The culture was then incubated at 18 °C for 17 h when OD_{600 nm} reached around 1.2. The cells were harvested by centrifugation (10,500 x g, 15 min) and the cell pellets were stored in two 50 mL tubes. One of the pellets was used to obtain the modified cytolysin peptide. The pellet was thawed on ice and LanA start buffer (compositions of LanA, LanB1, LanB2 and elution buffer is described in Section 2.4.18) was added and mixed with pipet followed by lysis by sonication (4.4 s on, 9.9 s off, 35% amplitude). The lysed cells were centrifuged (23,800 x g, 30 min) and the supernatant was filtered through 0.45 µ filters and loaded onto a Ni-His trap column pre-equilibrated with LanA start buffer. Following loading, the column was washed with 3 CV of Lan buffer1 (B1). To the cell pellet was further added LanB1 and mixed with a pipet followed by sonication (4.4 s on, 9.9 s off, 35% amplitude). The lysed cells were centrifuged (23,800 x g, 30

min) and the supernatant was filtered through 0.45 μ filters and loaded onto Ni-His trap column. Following loading the column was subsequently washed with Lan B1 (4 CV) and Lan buffer 2 (6 CV) followed by elution (3 CV). The eluted fraction was zip-tipped and analyzed by MALDI MS, which indicated the presence of the desired peptide. The eluent was desalted on C₄ SPE column and lyophilized to obtain fluffy white peptide. (*Notebook VIII, Pages 88 (Cyl_{LL}-WT), 89 (Cyl_{LS}-WT), 71 (Cyl_{LS}-Dhb2Dha), 72 (Cyl_{LS}-Dhb1Dha/Dhb2Dha), and Notebook IX, Pages 23 (Cyl_{LS}-Dhb2Cys), 26 (Cyl_{LS}-Dhb2Cys/Dhb7Ala)*)

3.5. REFERENCES

1. Coburn, P. S., and Gilmore, M. S. (2003) The *Enterococcus faecalis* cytolysin: a novel toxin active against eukaryotic and prokaryotic cells, *Cell. Microbiol.* 5, 661-669.
2. Richards, M. J. M. F., Edwards, J. R. M. S., Culver, D. H. P., Robert P. Gaynes, M. D., the, and System, N. N. I. S. (2000) Nosocomial Infections in Combined Medical-Surgical Intensive Care Units in the United States, *Infect. Control Hosp. Epidemiol.* 21, 510-515.
3. Todd, E. W. (1934) A comparative serological study of streptolysins derived from human and from animal infections, with notes on pneumococcal haemolysin, tetanolysin and staphylococcus toxin, *J. Pathol. Bacteriol.* 39, 299-321.
4. Jett, B. D., Huycke, M. M., and Gilmore, M. S. (1994) Virulence of enterococci, *Clin. Microbiol. Rev.* 7, 462-478.
5. Brock, T. D., Peacher, B., and Pierson, D. (1963) Survey of the Bacteriocins of Enterococci, *J. Bacteriol.* 86, 702-707.
6. Kobayashi, R. (1940) Studies concerning Hemolytic Streptococci. Part I. The Typing of Human Hemolytic Streptococci and their Relation to Diseases and their Distributions on Mucous Membranes., *Kitasato Arch. Exp. Med.* 17, 218-241.
7. Roelofsen, B., de Gier, J., and van Deenen, L. L. M. (1964) Binding of lipids in the red cell membrane, *J. Cell. Compar. Physio.* 63, 233-243.
8. Gilmore, M. S., Segarra, R. A., Booth, M. C., Bogie, C. P., Hall, L. R., and Clewell, D. B. (1994) Genetic structure of the *Enterococcus faecalis* plasmid pAD1-encoded cytolytic toxin system and its relationship to lantibiotic determinants, *J. Bacteriol.* 176, 7335-7344.
9. Segarra, R. A., Booth, M. C., Morales, D. A., Huycke, M. M., and Gilmore, M. S. (1991) Molecular characterization of the *Enterococcus faecalis* cytolysin activator, *Infect. Immun.* 59, 1239-1246.
10. Gilmore, M. S., Segarra, R. A., and Booth, M. C. (1990) An HlyB-Type Function Is Required for Expression of the *Enterococcus faecalis* Hemolysin/Bacteriocin, *Infect. Immun.*, 3914-3923.
11. Coburn, P. S., Hancock, L. E., Booth, M. C., and Gilmore, M. S. (1999) A Novel Means of Self-Protection, Unrelated to Toxin Activation, Confers Immunity to the Bactericidal Effects of the *Enterococcus faecalis* Cytolysin, *Infect. Immun.* 67, 3339-3347.

12. Haas, W., Shepard, B. D., and Gilmore, M. S. (2002) Two-component regulator of *Enterococcus faecalis* cytolysin responds to quorum-sensing autoinduction, *Nature* *415*, 84-87.
13. Coburn, P. S., Pillar, C. M., Jett, B. D., Haas, W., and Gilmore, M. S. (2004) *Enterococcus faecalis* Senses Target Cells and in Response Expresses Cytolysin, *Science* *306*, 2270-2272.
14. Booth, M. C., Bogie, C. P., Sahl, H.-G., Siezen, R. J., Hatter, K. L., and Gilmore, M. S. (1996) Structural analysis and proteolytic activation of *Enterococcus faecalis* cytolysin, a novel lantibiotic, *Mol. Microbiol.* *21*, 1175-1184.
15. Weixin, T., and van der Donk, W. A. (2013) The sequence of the enterococcal cytolysin imparts unusual lanthionine stereochemistry, *Nat. Chem. Biol.* *9*, 157-159.
16. Chatterjee, C., Paul, M., Xie, L., and van der Donk, W. A. (2005) Biosynthesis and mode of action of lantibiotics, *Chem. Rev.* *5*, 633-684.
17. Tang, W., Jiménez-Osés, G., Houk, K. N., and van der Donk, W. A. (2015) Substrate control in stereoselective lanthionine biosynthesis, *Nat. Chem.* *7*, 57-64.
18. Ludwick, A. G., Jelinski, L. W., Live, D., Kintanar, A., and Dumais, J. J. (1986) Association of peptide chains during Merrifield solid-phase peptide synthesis. A deuterium NMR study, *J. Am. Chem. Soc.* *108*, 6493-6496.
19. Masuda, K., Ooyama, H., Shikano, K., Kondo, K., Furumitsu, M., Iwakoshi-Ukena, E., and Ukena, K. (2015) Microwave-assisted solid-phase peptide synthesis of neurosecretory protein GL composed of 80 amino acid residues, *J. Pep. Sci.* *21*, 454-460.
20. Chalker, J. M., Gunnoo, S. B., Boutureira, O., Gerstberger, S. C., Fernandez-Gonzalez, M., Bernardes, G. J. L., Griffin, L., Hailu, H., Schofield, C. J., and Davis, B. G. (2011) Methods for converting cysteine to dehydroalanine on peptides and proteins, *Chem. Sci.* *2*, 1666-1676.
21. Becker, H., Lucas, H.-W., Maul, J., Pillai, V. N. R., Anzinger, H., and Mutter, M. (1982) Polyethyleneglycols grafted onto crosslinked polystyrenes: A new class of hydrophilic polymeric supports for peptide synthesis, *Die Makromol. Chem., Rapid Commun.* *3*, 217-223.
22. Renil, M., and Meldal, M. (1996) POEPOP and POEPS: Inert polyethylene glycol crosslinked polymeric supports for solid synthesis, *Tetrahedron Lett.* *37*, 6185-6188.
23. Rademann, J., Grøtli, M., Meldal, M., and Bock, K. (1999) SPOCC: A Resin for Solid-Phase Organic Chemistry and Enzymatic Reactions on Solid Phase, *J. Am. Chem. Soc.* *121*, 5459-5466.
24. de la Torre, B., Jakab, A., and Andreu, D. (2007) Polyethyleneglycol-Based Resins as Solid Supports for the Synthesis of Difficult or Long Peptides, *Int. J. Pep. Res. Ther.* *13*, 265-270.
25. Kates, S. A., McGuinness, B. F., Blackburn, C., Griffin, G. W., Solé, N. A., Barany, G., and Albericio, F. (1998) "High-load" polyethylene glycol-polystyrene (PEG-PS) graft supports for solid-phase synthesis, *Pept. Sci.* *47*, 365-380.
26. García-Martín, F., Quintanar-Audelo, M., García-Ramos, Y., Cruz, L. J., Gravel, C., Furic, R., Côté, S., Tulla-Puche, J., and Albericio, F. (2006) ChemMatrix, a Poly(ethylene glycol)-Based Support for the Solid-Phase Synthesis of Complex Peptides, *J. Comb. Chem.* *8*, 213-220.

27. García-Martín, F., White, P., Steinauer, R., Côté, S., Tulla-Puche, J., and Albericio, F. (2006) The synergy of ChemMatrix resin® and pseudoproline building blocks renders Rantes, a complex aggregated chemokine, *Biopolymers* 84, 566-575.
28. Eritja, R., Martin, J. P. Z., Walker, P. A., Lee, T. D., Legesse, K., Albericio, F., and Kaplan, B. E. (1987) On the use of S-t-butylsulphenyl group for protection of cysteine in solid-phase synthesis using Fmoc-amino acids., *Tetrahedron* 43, 2675-2680.
29. Lukszo, J., Patterson, D., Albericio, F., and Kates, S. (1996) 3-(1-Piperidiny)alanine formation during the preparation of C-terminal cysteine peptides with the Fmoc/t-Bu strategy, *Lett. Pept. Sci.* 3, 157-166.
30. Ross, A. C., Liu, H., Pattabiraman, V. R., and Vederas, J. C. (2009) Synthesis of the Lantibiotic Lactocin S Using Peptide Cyclizations on Solid Phase, *J. Am. Chem. Soc.* 132, 462-463.
31. Levengood, M. R., Knerr, P. J., Oman, T. J., and van der Donk, W. A. (2009) In vitro mutasynthesis of lantibiotic analogues containing nonproteinogenic amino acids, *J. Am. Chem. Soc.* 131, 12024-12025.
32. Knerr, P. J., and van der Donk, W. A. (2013) Chemical Synthesis of the Lantibiotic Lacticin 481 Reveals the Importance of Lanthionine Stereochemistry, *J. Am. Chem. Soc.* 135, 7094-7097.
33. Fukase, K., Kitazawa, M., Sano, A., Shimbo, K., Fujita, H., Horimoto, S., Wakamiya, T., and Shiba, T. (1988) Total synthesis of peptide antibiotic nisin, *Tetrahedron Lett.* 29, 795-798.
34. Liu, W., Chan, A. S. H., Liu, H., Cochrane, S. A., and Vederas, J. C. (2011) Solid Supported Chemical Syntheses of Both Components of the Lantibiotic Lacticin 3147, *J. Am. Chem. Soc.* 133, 14216-14219.
35. Knerr, P. J., and van der Donk, W. A. (2012) Chemical Synthesis and Biological Activity of Analogues of the Lantibiotic Epilancin 15X, *J. Am. Chem. Soc.* 134, 7648-7651.
36. Chen, R., and Tolbert, T. J. (2011) On-resin Convergent Synthesis of a Glycopeptide from HIV gp120 Containing a High Mannose N-linked Oligosaccharide, *Methods Mol. Biol.* 751, 343-355.
37. Peptide Tips, In http://www.anaspec.com/html/peptide_tips.html, Anaspec Inc., last accessed August 9, 2015.
38. Edelheit, O., Hanukoglu, A., and Hanukoglu, I. (2009) Simple and efficient site-directed mutagenesis using two single-primer reactions in parallel to generate mutants for protein structure-function studies, *BMC Biotechnol.* 9, 61.

CHAPTER 4. SYNTHESIS OF MICROBISPORICIN ANALOGUES

4.1. INTRODUCTION

Microbisporicin (also known as NAI-107) is a lanthipeptide produced by *Microbispora corallina* and is the most potent lantibiotic known to date (1). Microbisporicin was found to be an inhibitor of peptidoglycan biosynthesis with a different mode of action than the one exhibited by β -lactams or glycopeptides (2). Microbisporicin showed activity against *Staphylococcus aureus*, but not against the L form of the pathogen (L3751), which lacks a functional cell wall suggesting this peptide targets the peptidoglycan. In vitro biochemical studies revealed that microbisporicin inhibited the assembly of lipid II molecules from its precursor components (3). These results were further corroborated by in vivo mode of action studies where soluble peptidoglycan precursors accumulated following treatment of cells with microbisporicin. Together these results point towards microbisporicin being capable of inhibiting peptidoglycan biosynthesis.

Clinically relevant Gram-positive pathogens like methicillin-resistant *S. aureus* (MRSA) and vancomycin-resistant enterococci (VRE) are susceptible to microbisporicin (4). Microbisporicin showed superior activity (MICs \leq 0.13–4.0 $\mu\text{g/mL}$) than vancomycin and teicoplanin against *Staphylococci*, *Streptococci*, *Enterococci*, and *Lactobacilli*. The lanthipeptide was also active against anaerobic *Clostridia* (MICs \leq 0.13 $\mu\text{g/mL}$) and *Propionibacteria* (MIC \leq 0.13–4.0 $\mu\text{g/mL}$). Compared to other lanthipeptides, microbisporicin has stronger antimicrobial activity against aerobic and anaerobic Gram-positive, as well as against Gram-negative bacteria such as *Moraxella catarrhalis*, *Neisseria spp.*, and *Haemophilus influenza* (5). Furthermore, microbisporicin showed better in-vivo efficacy in mouse models of infections of *Streptococcus*

pneumonia, MRSA, and VRE compared to linezolid, vancomycin, or penicillin G (6). The in vivo pharmacodynamics of microbisporicin against various *S. aureus* strains revealed potent activity against a murine thigh infection model (7). Based on the promising potential described above, microbisporicin is currently in late preclinical-phase trials and has shown better results in treating multidrug resistant infections than linezolid and vancomycin (8).

To further understand the potent bioactivity of microbisporicin, structural characterization of this lanthipeptide was performed. The structures of microbisporicin A1 and A2 were obtained through chemical degradation and extensive NMR characterization studies (1, 4, 9). The N-terminal portion of microbisporicin (residues 1-11) exhibits high similarity to nisin. This motif has been previously shown to be important for binding the pyrophosphate moiety present in lipid II (10). The B ring in microbisporicin is the most rigid one with a β -turn, while the C ring is larger and more mobile than the N-terminal ring (9). Besides the usual post-translational modifications found in lanthipeptides, microbisporicin is the first example of a lanthipeptide containing a 5-chloro-tryptophan (ClTrp) and mono- (in A2 lanthipeptide) or bis- (in A1 lanthipeptide) hydroxy-proline (Figure 4.1) (4). The unusual post-translational modifications present in this lanthipeptide coupled with its unique antimicrobial activities suggest these modifications to be important for conferring microbisporicin's potent bioactivity.

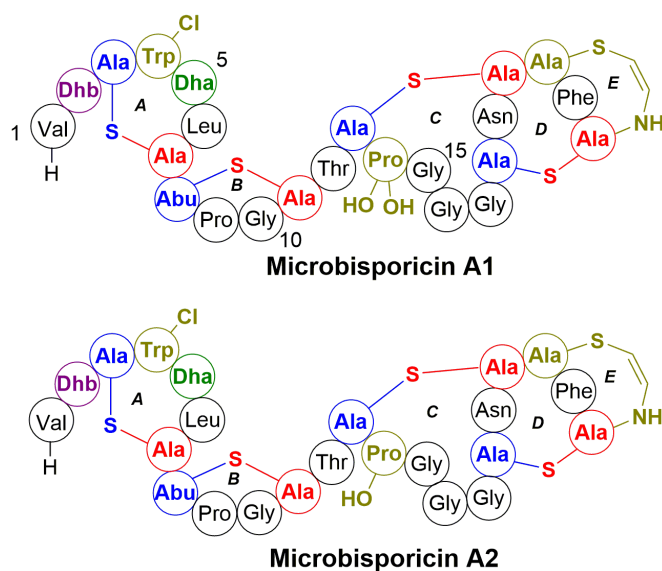


Figure 4.1. Structures of microbisporicin A1 and A2. The difference between the two peptides is in the extent of hydroxylation of Pro14. Trp4 is chlorinated and the C-terminus is characterized by *S*-[(*Z*)-2-aminovinyl]-*D*-cysteine moiety.

The biosynthetic gene cluster responsible for microbisporicin biosynthesis has been identified (*mibA*, *mibB*, *mibC*, *mibD*, *mibH*, *mibS*, *mibO*, Figure 4.2) (8). The *mibA* gene encodes the precursor peptide MibA, which is a 57-aa peptide with an N-terminal leader region covering 33 residues. The dehydratase MibB encoded by *mibB* is a homolog of the nisin dehydratase NisB, and its structure and enzymatic activity has been recently characterized (Ortega *et al.* unpublished). MibC is the lanthipeptide cyclase and shows homology to other members of its class. MibD decarboxylates the C-terminal Cys to give rise to an enethiolate moiety. Whether this enzyme also catalyzes the Michael-type addition to generate the C-terminal *S*-[(*Z*)-2-aminovinyl]-*D*-cysteine is still not clear (8). First observed among lanthipeptides, the flavin-dependent tryptophan halogenase MibH and the flavin reductase MibS coordinate to chlorinate Trp4. Another unique post-translational modification, hydroxylation of Pro14, is predicted to be carried out by MibO, a cytochrome P450 enzyme (8). The importance of the chlorination at Trp4 and hydroxylation at Pro14 was established, when the deschloro and non-hydroxylated

microbisporicin analogues, which are produced in small amounts by the producing strain, showed reduced antimicrobial activity (11). Halogenation of microbisporicin occurs within the A ring, a conserved motif present in many class I lantibiotics. Based on the importance of ClTrp for microbisporicin bioactivity and the prevalence of this A ring in class I lantibiotics, MibH might serve as an enzymatic tool to insert ClTrp in other class I lantibiotics. This strategy could enable the creation of lantibiotic analogs with improved biological activity.

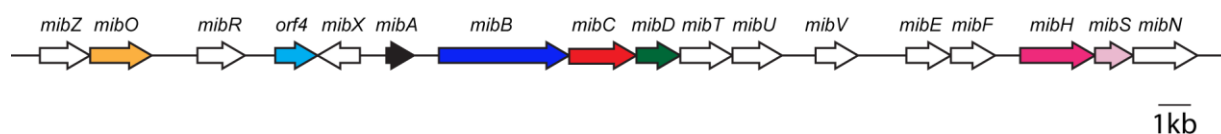


Figure 4.2. Biosynthetic gene cluster highlighting the genes responsible for the post-translational modifications in color (courtesy of Manuel Ortega, adapted from Bibb and co-workers (8)).

To achieve this objective currently the substrate specificity of the halogenase MibH is being investigated to reveal the minimum recognition motif within the precursor peptide that would still be chlorinated by MibH. Biochemical assays revealed chlorination to be leader peptide independent but require at least some of the rings since the linear MibA was not a substrate (Ortega *et al.* unpublished). However, it is still not clear what region within the core peptide is important for recognition by MibH. To address this question, halogenation assays were designed using a microbisporicin analog containing only the A and B rings.

Since the biosynthesis of microbisporicin has not yet been reconstituted *in vitro* nor in *E. coli*, chemical synthesis of the A and B rings of microbisporicin was envisioned to discern whether MibH is capable of recognizing just these two rings for efficient chlorination of Trp4 within the A ring in the synthesized peptide. The peptide sequence from residues 1 to 11 poses challenges typically associated with the synthesis of highly hydrophobic peptides. Additionally, the synthesis of Dha5 within the A ring has not been attempted earlier by Fmoc-based SPPS. In

addition, besides serving as a mechanistic probe, the chemical synthesis of rings A and B of microbisporicin allows us to access a substrate that could be used for MibH co-crystallization attempts. Truncated synthetic microbisporicin should have a more rigid framework compared to the full-length peptide, and hence could be a better substrate for binding the enzyme MibH to facilitate crystallization of the peptide-enzyme complex.

The dehydratase MibB dehydrates Ser/Thr residues in MibA via glutamylation of Ser/Thr residues followed by glutamate elimination. In our efforts to obtain co-crystal structures of the dehydratase MibB with its substrate MibA, a short peptide containing a non-hydrolyzable Ser-Glu amide was designed. Due to the flexibility of the MibA core region, attempts of obtaining co-crystal structures of MibB in complex with MibA have been unfruitful. To address this problem, I synthesized a shorter peptide containing a non-hydrolyzable Ser-Glu amide for crystallization attempts. This shorter peptide should contain a lower degree of conformational freedom and thus might be a better substrate for co-crystallization. To assess whether this peptide would be a substrate analogue for MibB, a peptide analog containing a Ser-Glu ester was also synthesized, and the extent of glutamate elimination catalyzed by MibB was assessed via mass spectrometry.

4.2. RESULTS AND DISCUSSION

4.2.1. Synthesis of the A and B Rings of Microbisporicin

The structure of the A and B ring fragment of microbisporicin contains one Lan and one MeLan crosslink, with an additional ValDhb moiety at the N-terminus (Figure 4.3). MibH chlorinates the Trp4 in the full-length modified precursor peptide.

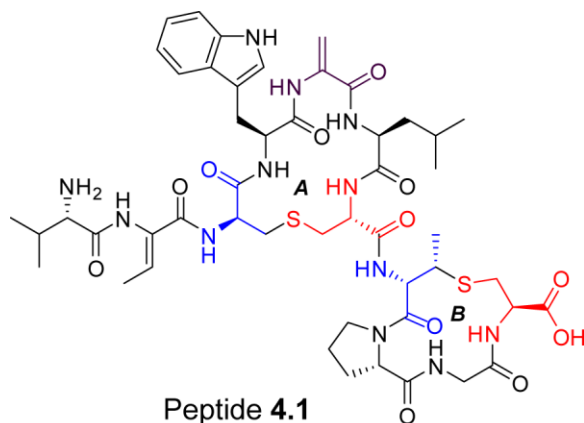
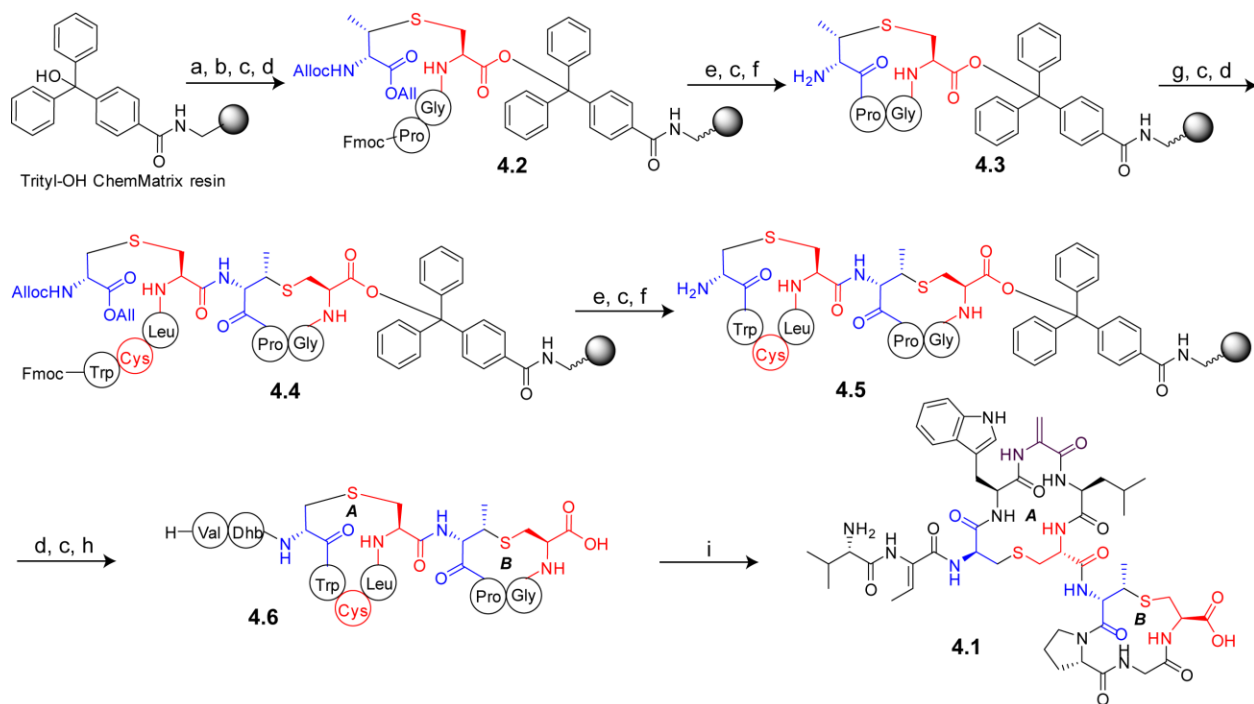


Figure 4.3. Structure of the A and B ring of deschloro-microbisporicin.

Owing to the high hydrophobicity of the target peptide, PEG-based ChemMatrix resin was employed. To prevent racemization of the C-terminal MeLan, a bulky trityl linker was used to connect the growing peptide chain to the resin. Attempts at introducing the Dha5 within the A-ring using a Fmoc-TrpDha-OH dipeptide building block did not yield the desired product. The electrophilicity of the Dha moiety and the reactivity of the free indole of Trp (primarily at C2 (12)) could lead to undesired side-reactions. Hence, a Cys residue was instead introduced in place of Dha5 as a Dha precursor. This strategy also solved the potential problem of the reactivity of indole ring in Trp as N^{α} -Fmoc- N^{in} -Boc-L-Trp was used to incorporate the Trp. After cyclization to generate the A-ring, Fmoc-ValDhb-OH dipeptide was coupled, to generate the target peptide upon final deprotection and cleavage from the resin. The peptide was purified and subjected to elimination reaction where the Cys5 was transformed to Dha5 chemo-selectively as described in chapter 3, generating the target peptide **4.1** (Scheme 4.1, Figure 4.4).



Scheme 4.1. Synthesis of peptide **4.1**. Reagents and conditions: (a) SOCl_2 ; (b) Coupling of compound **3.24**; (c) piperidine, DMF; (d) SPPS; (e) $\text{Pd}(\text{PPh}_3)_4$, PhSiH_3 , DMF, CH_2Cl_2 ; (f) PyAOP, HOAt, 2,4,6-collidine, DMF; (g) coupling of compound **3.25**; (h) cleavage from resin using 92:4:4 of TFA:H₂O:triisopropylsilane; (i) 2,5-dibromohexanediamide. Prior to cleavage from resin, all residues contained appropriate side-chain protecting groups for Fmoc SPPS.

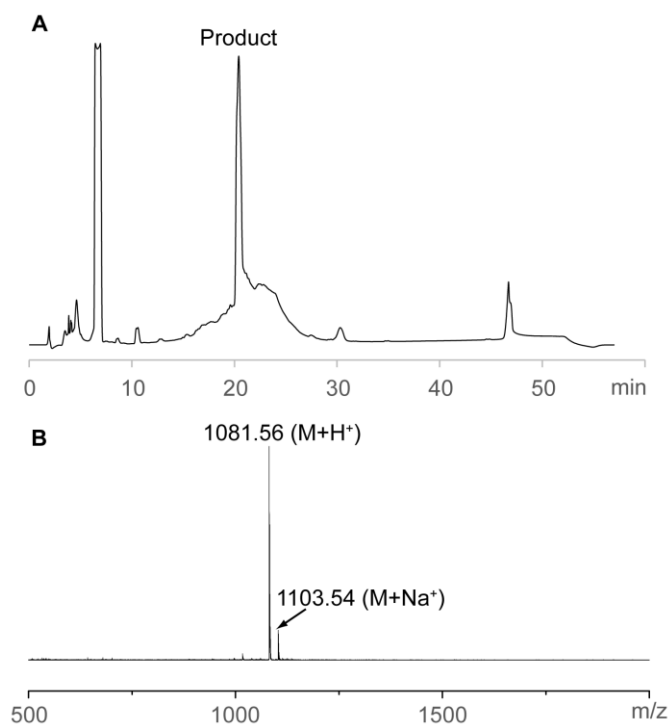


Figure 4.4. Purification and analysis of A and B ring of deschloro-microbisporicin. (A) HPLC trace of the elimination reaction. Fraction between R_t of 20.1-20.9 min contained the product. (B) MALDI-TOF MS of the product fraction.

4.2.2. Synthesis of Microbisporicin Tetrapeptide with Glutamylated Ser3 and its Analogue

The N-terminal tetrapeptide fragment of microbisporicin was synthesized on solid phase. Using orthogonal protections, peptide with glutamylated Ser linked by an ester bond was generated (Figure 4.5, Scheme 4.2).

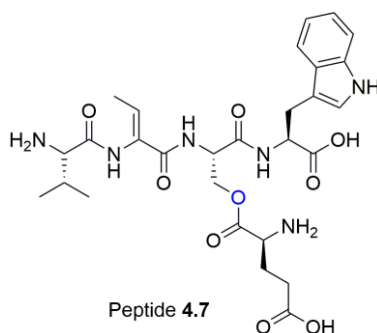
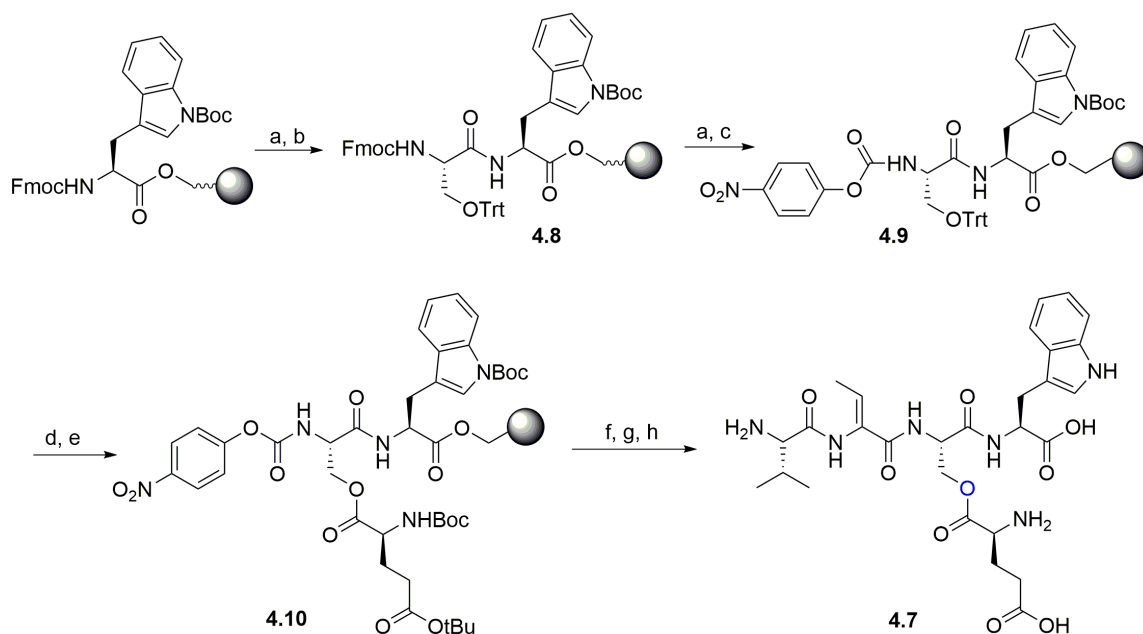


Figure 4.5. Microbisporicin tetrapeptide with glutamylated Ser3. Linear tetrapeptide fragment of the N-terminal portion of microbisporicin. The glutamate is tethered to Ser3 with an ester linkage.



Scheme 4.2. SPPS of microbisporicin tetrapeptide with ester-linked glutamylated Ser3 (peptide **3.32**). Reagents and conditions: (a) 20% piperidine in DMF (2 x 5 min) (b) Coupling of Fmoc-Ser(Trt)-OH using HCTU/DIPEA chemistry (2 h) (c) 4-nitrobenzyl chloroformate (3 equiv.), DIPEA (30 equiv.), DCM (45 min) (d) wash with TFA:TIPS:DCM (2:2.5:95.5) until filtrate is colorless (e) coupling of Boc-Glu(γ -tBu)-OH using DIC (10 equiv.), DMAP (1 equiv.) in DMF/DCM (1:9), overnight (f) SnCl₂ (6 M), HCl in diethyl ether (5 mM) in DMF (2 x 1 h) (g) coupling of compound **4.16** using DIC (4 equiv.), HOAt (4 equiv.) (h) cleavage with TFA:TIPS:H₂O (95:2.5:2.5).

Another analogue of the tetrapeptide with glutamylated Ser linked by an amide bond was also generated by SPPS (Figure 4.6, Scheme 4.3).

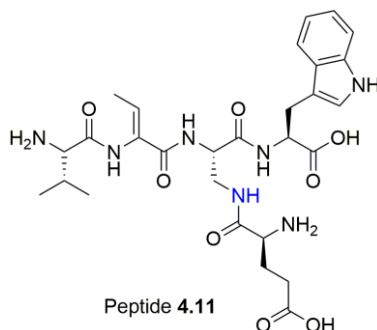
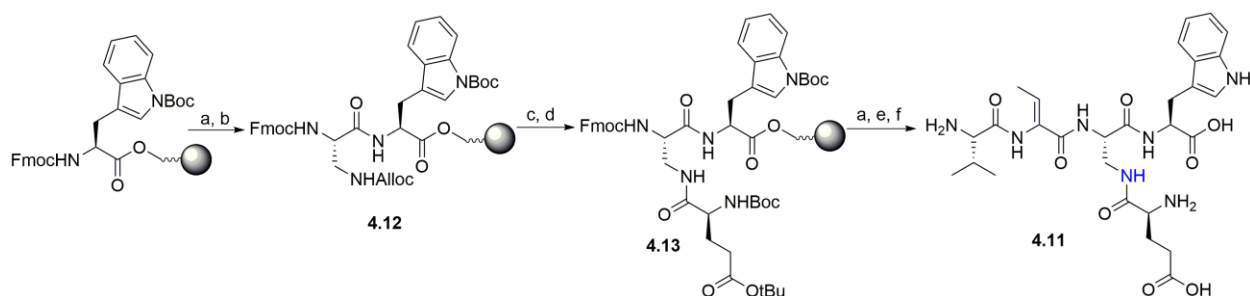


Figure 4.6. Microbisporicin tetrapeptide with glutamylated 2,3-diaminopropanoic acid. The tetrapeptide is the N-terminal portion of microbisporicin.



Scheme 4.3. SPPS of microbisporicin tetrapeptide with amide-linked glutamylated 2,3-diamino propanoic acid. Reagents and conditions: (a) 20% piperidine in DMF (b, d, e) coupling using HCTU, DIPEA (c) Pd(PPh₃)₄, PhSiH₃ (f) TFA/TIPS/H₂O (95/2.5/2.5)

4.3. CONCLUSION AND OUTLOOK

Microbisporicin is a clinically relevant lanthipeptide owing to its strong antimicrobial activity, and is currently being evaluated in preclinical trials. Part of its strong bioactivity is dependent on the unique post-translational chlorination of Trp4 and hydroxylation of Pro14. These unusual post-translational modifications were found to be independent of the presence of leader peptide. The N-terminal portion of microbisporicin core peptide containing the A and B ring shares structural similarity with other class I lanthipeptides like nisin. This A and B ring in nisin forms the motif that binds to the pyrophosphate region of lipid II. The rest of the microbisporicin core peptide has a distinct structure containing an amino-vinyl Cys moiety at the C-terminus. It is interesting to see if the halogenase MibH recognizes the common microbisporicin motif of the A and B ring and chlorinate the Trp4 within the A-ring. This would also reflect on whether MibH requires the distinct structural features of the entire microbisporicin core peptide for activity.

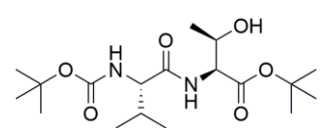
I have synthesized the N-terminal portion of microbisporicin containing rings A and B ring via solid phase to address this question. The purified peptide was subjected to enzymatic

assay with MibH (with Manuel Ortega). However, MibH failed to chlorinate the Trp4 residue in the synthetic A and B ring of microbisporicin (peptide **4.1**). Based on this result, the A and B-rings are not the sole motif for MibH recognition. This result indirectly points that the C terminus of microbisporicin is also critical for recognition and efficient chlorination of Trp4 by MibH.

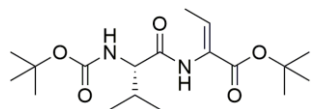
MibB is the dehydratase that glutamylates Ser/Thr residues followed by elimination. MibB did not eliminate the glutamate from the synthetic tetrapeptide **4.7** (with Manuel Ortega). Hence, a longer portion of the core peptide is required for effective binding of the substrate by the enzyme MibB.

4.4. EXPERIMENTAL

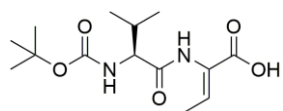
4.4.1. Synthesis of Boc-ValDhb-OH Building Block

 Compound **4.14**. L-Threonine tert-butyl ester hydrochloride (1 g, 4.72 mmol) was dissolved in DCM (24 mL) and DIPEA (1.24 mL, 7.1 mmol). To the solution, Boc-valine (1.03 g, 4.72 mmol), HOBt (0.73 g, 4.72 mmol), and EDC-HCl (0.9 g, 4.72 mmol) were added as solid. The reaction was stirred for 17 h. The reaction was washed with sat. aqueous NaHCO₃, 10% citric acid, and water. Each aqueous layer was back-extracted with DCM. The organic fractions were combined, washed with brine, dried over Na₂SO₄, filtered, and concentrated. Yield: 1.9 g (quantitative). ¹H NMR (500 MHz, CDCl₃) δ 6.55 (d, *J* = 8.8 Hz, 1H), 5.09 (d, *J* = 8.8 Hz, 1H), 4.48 (dd, *J* = 8.8, 2.8 Hz, 1H), 4.28 (qd, *J* = 6.4, 2.8 Hz, 1H), 3.92 (dd, *J* = 8.8, 6.4 Hz, 1H), 2.12 (m, 1H), 1.47 (s, 9H), 1.44 (s, 9H), 1.2 (d, *J* = 6.4 Hz, 3H), 0.99 (d, *J* = 6.8 Hz, 3H), 0.96 (d, *J* = 7.2 Hz, 3H). ¹³C NMR (125 MHz, CDCl₃)

δ 172.1, 169.6, 153.9, 82.3, 79.9, 68.3, 60.2, 57.7, 30.7, 28.2, 27.9, 19.8, 19.2, 17.9. HRMS-ESI calculated for $C_{18}H_{34}N_2O_6Na$ 397.2315, observed 397.2307. (*Notebook IX, Page 84*)



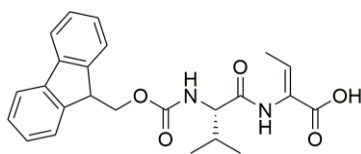
Compound **4.15**. Compound **4.14** (0.92 g, 2.46 mmol) was dissolved in DCM (30 mL) and triethylamine (0.93 mL, 6.67 mmol) was added, and the solution was chilled in an ice-bath. Methanesulfonyl chloride (0.42 mL, 5.43 mmol) was added dropwise, and the solution was stirred for 1 h, gradually warming to room temperature. The reaction was concentrated under reduced pressure, then taken up in 1,2-dichloroethane (30 mL) and DBU (1.6 mL). The reaction was heated to reflux in an oil bath (90 °C) for 4 h, and then concentrated. The residue was taken up in EtOAc, washed with 10 % citric acid, saturated aqueous $NaHCO_3$, brine, dried over Na_2SO_4 , filtered, and concentrated. The residue was purified by flash chromatography (SiO_2 , 7:1, then 4:1 hexanes/EtOAc) to generate product. Yield: 0.64 g (73%). 1H NMR (500 MHz, $CDCl_3$) δ 6.71 (q, $J = 7.2$ Hz, 1H), 5.05 (d, $J = 7.2$ Hz, 1H), 4.04 (t, $J = 7.2$ Hz, 1H), 2.22 (m, 1H), 1.74 (d, $J = 7.2$ Hz, 3H), 1.48 (s, 9H), 1.45 (s, 9H), 1.02 (d, $J = 6.8$ Hz, 3H), 0.97 (d, $J = 6.8$ Hz, 3H). ^{13}C NMR (125 MHz, $CDCl_3$) δ 169.8, 163.5, 150.8, 132.7, 81.9, 67.8, 60.4, 30.9, 28.4, 28.2, 19.5, 17.8, 14.9. (*Notebook IX, Page 85*)



Compound **4.16**. Compound **4.15** (0.1 g, 0.28 mmol) was dissolved in DCM (2.0 mL), and to the solution TFA (2.0 mL) was added, following which the reaction was stirred for 1.5 h. The reaction was concentrated under reduced pressure, the residue was repeatedly taken up in DCM, and the solution was re-concentrated to remove the remaining acid. To the resulting residue was added sodium carbonate (0.06 g, 0.56 mmol), H_2O (3 mL) and 1,4-dioxane (3 mL), and the solution was chilled in an ice-bath. Boc_2O (0.067 g, 0.31 mmol) was added portion-wise as a solid. The reaction was stirred for 20 h, gradually warming to room temperature. The reaction was diluted with H_2O and acidified to pH 2.0 with 2 M HCl.

The faintly cloudy solution was transferred to a separatory funnel along with 50 mL of EtOAc and shaken. Further 10 mL of H₂O was added to the aqueous layer, which was then extracted with EtOAc (2 x 50 mL). The combined organic layer was dried over Na₂SO₄ and concentrated on the rotary evaporator. DCM was added to transfer the content to a scintillation vial and dried in the rotary evaporator to generate a white residue. The content was further dried using a vacuum pump overnight. Yield: 0.077 g (92%). ¹H NMR (500 MHz, CDCl₃) δ 6.84 (q, *J* = 7 Hz, 1H), 3.97 (d, *J* = 6.5 Hz, 1H), 2.09 (sep, *J* = 7 Hz, 1H), 1.76 (d, *J* = 7 Hz, 3H), 1.45 (s, 9H), 1.03 (d, *J* = 7 Hz, 3H), 0.99 (d, *J* = 7 Hz, 3H). HRMS-ESI calculated for C₁₄H₂₅N₂O₅ 301.1763, observed 301.1761. (*Notebook IX, Page 39*)

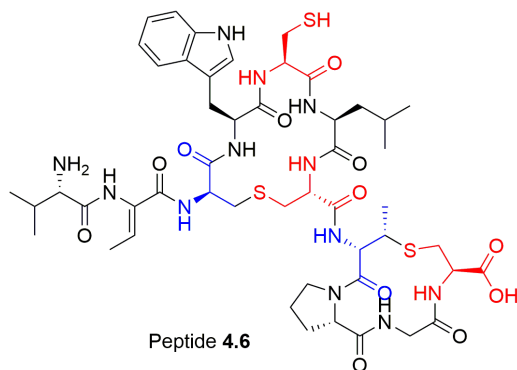
4.4.2. Synthesis of Fmoc-ValDhb-OH Building Block



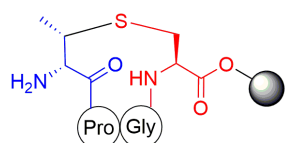
Compound **4.17**. Compound **4.15** (0.63 g, 1.77 mmol) was dissolved in DCM (5.6 mL), and to the solution TFA (5.6 mL) was added, following which the reaction was stirred for 1.5 h. The reaction was concentrated under reduced pressure, repeatedly taken up in DCM, and re-concentrated to remove the remaining acid. To the resulting residue was added sodium carbonate (0.38 g, 3.54 mmol), H₂O (17 mL) and 1,4-dioxane (17 mL), and the system was chilled in an ice-bath. Fmoc-OSu (0.6 g, 1.71 mmol) was added portion-wise as a solid. The reaction was stirred for 19 h, gradually warming to room temperature. Over time, the reaction turned from colorless to milky white. The volatile components were removed under reduced pressure, when white suspension forms. The reaction was diluted with H₂O and acidified to pH 2.0 with 2 M HCl. The aqueous suspension was extracted with EtOAc (3 x 100 mL), when cloudy organic layer forms. The organic layer was washed with brine and then concentrated to ~ 25 mL, when white cloudy precipitate formed. Excess hexanes was added (200 mL) to the suspension and the

white flocculent suspension was filtered over a Buchner funnel to yield white powder. The powder was further dried on a vacuum pump for 6 h. Yield: 0.7 g (94%). ^1H NMR (500 MHz, CDCl_3) δ 7.79 (d, $J = 7.6$ Hz, 2H), 7.68 (t, $J = 6.8$ Hz, 2H), 7.39 (t, $J = 7.2$ Hz, 2H), 7.30 (t, $J = 7.2$ Hz, 2H), 7.24 (d, $J = 8.8$ Hz, 1H), 6.84 (q, $J = 7.2$ Hz, 1H), 4.39 (d, $J = 6.8$ Hz, 1H), 4.24 (t, $J = 7.2$ Hz, 1H), 4.05 (m, 1H), 2.13 (m, 1H), 1.74 (d, $J = 7.2$ Hz, 3H), 1.04 (d, $J = 6.8$ Hz, 1H), 0.99 (d, $J = 6.8$ Hz, 1H). ^{13}C NMR (125 MHz, CDCl_3) δ 183.2, 172.2, 157.5, 144.0, 141.4, 135.3, 127.6, 127.4, 124.9, 119.7, 66.7, 61.1, 47.2, 30.8, 17.4, 12.9. HRMS-ESI calculated for $\text{C}_{24}\text{H}_{26}\text{N}_2\text{O}_5\text{Na}$ 445.1739, observed 445.1737. (*Notebook IX, Page 86*)

4.4.3. SPPS of the Deschloro-Microbisporicin A and B Rings with Cys5

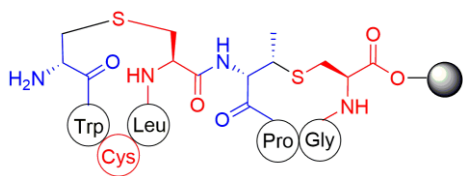


The general procedure for peptide synthesis followed was described in Section 3.4.5. HATU was used as coupling agent for most of the couplings unless otherwise stated. The coupling duration and repeats in coupling are mentioned in parenthesis. Capping was performed after coupling each Fmoc-protected amino acid residue.



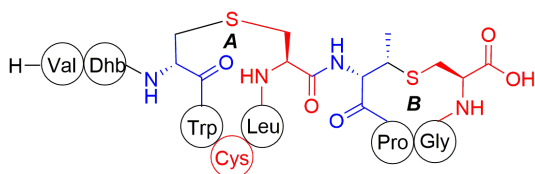
Intermediate **4.3**. Compound **3.24** was loaded onto the trityl-linked ChemMatrix resin (0.1 mmol) as follows. Compound **3.24** (0.15 mmol, 85 mg) was dissolved in 10 mL of DCM, to which DIPEA (0.75 mmol, 0.13 mL) was added, the

solution was applied to the swelled chlorinated resin, and reacted for 3 h. After washing the resin, the unreacted resin was capped by reacting with AcOH (0.5 mmol, 0.03 mL), and DIPEA (2 mmol, 0.35 mL) dissolved in DCM (10 mL) for 2 h. The resin was washed and dried. Absorbance measurement at 301 nm for a known amount to resin led to a calculated resin substitution of ~ 0.1 mmol/g. Fmoc-Gly-OH was coupled (1 h + 1 h), followed by Fmoc-Pro-OH (2 h + 2 h). Allyl/alloc groups were removed followed by Fmoc removal. Subsequent coupling was performed by adding PyAOP (0.5 mmol), and HOAt (0.5 mmol) in DMF to the resin and agitating the resin in DMF for 5 min followed by addition of 2,4,6-collidine (1 mmol) and agitation (2 x 2.5 h). After washing and drying the resin, a little of the resin was cleaved (95:2.5:2.5 = TFA:TIS:H₂O) for 1 h and analyzed by ESI. ESI-MS calculated for C₁₄H₂₃N₄O₅S 359.13 (M+H⁺), observed 359.5. (*Notebook IX, Page 93*)



Intermediate **4.5**. Half of the resin-attached intermediate was taken forward (~0.05 mmol resin). To the swelled resin, compound (DL-Lan-allyl/alloc) was coupled (11.5 h

coupling). Fmoc-Leu-OH was coupled (1.5 h + 2 h), then Fmoc-Cys(Trt)-OH (1 h + 4.5 h) was coupled, followed by coupling of Fmoc-Trp(Boc)-OH (10 h). The allyl/alloc group was removed followed by Fmoc-deprotection, and coupling with PyAOP, HOAt, and collidine to install the A ring. After washing and drying the resin, a little of the resin was cleaved (95:2.5:2.5 = TFA:TIS:H₂O) for 1 h and analyzed by ESI. ESI-MS calculated for C₄₀H₅₇N₁₀O₁₀S₃ 933.33 (M+H⁺), observed 933.5. (*Notebook IX, Page 94*)



Peptide **4.6**. To the resin-attached intermediate, Fmoc-ValDhb-OH (0.2 mmol, 85 mg) was coupled for 13 h. After washing and drying the resin, a little

of the resin was cleaved (95:2.5:2.5 = TFA:TIS:H₂O) for 1 h and analyzed by ESI. HRMS-ESI calculated for C₄₉H₇₁N₁₂O₁₂S₃ 1115.4398, observed 1115.4436. The resin was cleaved in 10 mL of TFA:TIPS:H₂O (92:4:4) for 1.5 h, and the obtained peptide was lyophilized. Peptide was purified using a Phenomenex Luna C₁₈ column with a gradient of 20% to 100% A (80% MeCN in 0.086% TFA) in D (0.1% TFA in H₂O) over 37 min (flow rate: 8 mL/min). Of the crude peptide, 14.6 mg was purified in 4 injections. Yield: ca. 1 mg. (*Notebook IX, Page 94*)

4.4.4. Synthesis of Peptide 4.1 by Cys to Dha Conversion in Peptide 4.6

Peptide **4.1**. Purified peptide **4.6** (280 µg) was split into two Eppendorf tubes and to each tube, was added acetonitrile (20 µL) and the mixture was vortexed to generate a white suspension. To the suspension, 20 µL of 0.1% aqueous TFA was added to generate a clear solution. The solution was diluted with 250 µL of H₂O followed by addition of 8 µL of TCEP (10 mM stock), and 40 µL of NH₄HCO₃ (200 mM stock, pH 8.9) resulting in a solution with final pH 8.4. To the solution in each tube was added 2,5-dibromohexanediamide (1 mg) and then the white suspension was stirred at RT (1 h) and at 37 °C (4 h). MALDI-TOF MS of the reaction indicated product formation (m/z calculated for C₄₉H₆₉N₁₂O₁₂S₂ (M+H⁺) 1081.45, observed 1081.51). The sample was prepared for analytical HPLC purification to ensure the dissolution of any precipitated product, leaving the residue of unreacted 2,5-dibromohexanediamide. The sample preparation was as follows: The reaction was centrifuged (16100 x g, 2 min) and the supernatant was collected. To the residue was added 16 µL of MeCN and the resulting mixture vortexed, followed by addition of 150 µL of aqueous 0.1% TFA, and then further vortexed. The suspension was centrifuged (16100 x g, 2 min) and the supernatant was combined with the earlier supernatant. This step was repeated again by suspending the residue with 5 µL of MeCN

and 50 μL of aqueous 0.1% TFA and centrifugation. The combined supernatants (ca. 950 μL) were injected into a Hypersil gold C_4 column and purified using a gradient of 20% A to 100% A in 45 min with a flow rate of 1 mL/min. Product eluted with R_t of 20.4 min. MALDI-TOF MS indicated the presence of clean peptide **4.1** (*Notebook IX, Page 100*).

4.4.5. SPPS of Microbisporicin Tetrapeptide with Ester-Linked Glutamylated Ser3

Peptide **4.7**. N^α -Fmoc- N^{in} -Boc-L-Trp-Wang resin (333 mg, substitution: 0.3 mmol/g) was swelled in DMF, and the Fmoc was removed. Fmoc-L-Ser(trt)-OH (0.57 g, 0.4 mmol), HCTU (0.17 g, 0.4 mmol), DIPEA (0.14 mL, 0.8 mmol), and HOAt (54 mg, 0.4 mmol) was dissolved in 5 mL of DMF and applied to the resin, which was agitated with nitrogen for 1 h to obtain resin-bound intermediate **4.8**. After Fmoc-removal, 4-nitrobenzylchloroformate (80 mg, 0.37 mmol) and DIPEA (0.5 mL, 3 mmol) was dissolved in DCM and applied to the resin while agitating for 45 min to obtain resin-bound intermediate **4.9**. The trityl-group was removed by washing thrice with 15 mL of TFA:TIPS:DCM (2:2.5:95.5). The yellow filtrate gradually turned colorless. After washing the resin further with DCM (3 x 1 min), the resin was placed in a round bottom flask. Boc-Glu(OtBu)-OH (1 mmol, 0.3 g), diisoproylcarbodiimide (1 mmol, 0.16 mL), and 4-dimethylaminopyridine (13 mg, 0.1 mmol) dissolved in 1:9 of DMF/DCM was applied to the resin and the mixture stirred overnight for 14 h. The resin was transferred back to the fritted container and filtered to obtain resin-bound intermediate **4.10**. Tin(II) chloride (5.68 g) was dissolved in 5 mL of HCl in diethyl ether (final concentration of 5 mM) in DMF. The tin(II) chloride solution was applied to the resin and sparged under nitrogen (2 x 1 h). After washing the resin with DMF and DCM, Boc-ValDhb-OH (compound **4.16**, 71 mg, 0.24 mmol), HOAt (27.2 mg, 0.2 mmol), and DIC (0.04 mL, 0.26 mmol) dissolved in 5 mL of DMF was applied to the resin and coupled for 4.5 h. After washing and drying the resin, the final cleavage was performed

using a mixture of TFA:TIPS:H₂O (95:2.5:2.5) for 1.5 h. Out of 45.5 mg of crude peptide, 25 mg was purified using a Phenomenex C₁₈ column to yield ca. 2 mg of purified peptide **4.7** (gradient: 2% A, 98% B to 100% A in 45 min, flow rate: 1 mL/min, R_t 14 min). ESI-MS calculated for C₂₈H₃₉N₆O₉ 603.27, observed 603.4.

4.4.6. SPPS of Microbisporicin Tetrapeptide with Amide-linked Glutamylated 2,3-Diamino Propanoic Acid

Peptide **4.11**. N^α-Fmoc-Nⁱⁿ-Boc-L-Trp-Wang resin (333 mg, substitution: 0.3 mmol/g) was swelled in DMF, and the Fmoc-group was removed. N^α-Fmoc-N^β-allyloxycarbonyl-L-2,3-diaminopropionic acid (123 mg, 0.3 mmol), HCTU (124 mg, 0.3 mmol), and DIPEA (0.1 mL, 0.6 mmol) was dissolved in 5 mL of DMF and reacted with the resin for 1 h to obtain resin-bound intermediate **4.12**. Allyl-group removal was carried out by reacting with Pd(PPh₃)₄ (115.6 mg, 0.1 mmol), and PhSiH₃ (0.13 mL, 1.0 mmol) dissolved in 10 mL of 1:1 DMF/DCM in the dark for 3 h. Resin was washed with DCM (3 x 10 mL), 0.5% sodium diethyldithiocarbamate in DMF (3 x 10 mL), and 1:1 DMF/DCM (3 x 10 mL). To the washed resin, Boc-Glu(OtBu)-OH (91 mg, 0.3 mmol), HCTU (124 mg, 0.3 mmol), and DIPEA (0.1 mL, 0.6 mmol) dissolved in 5 mL of DMF was added and the reaction was left for 1 h to obtain resin-bound intermediate **4.13**. After Fmoc-removal, Fmoc-ValDhb-OH (64 mg, 0.15 mmol), HCTU (62 mmol, 0.15 mmol), and DIPEA (0.05 mL, 0.3 mmol) dissolved in 5 mL of DMF was reacted with the resin for 14 h. After washing the resin, the Fmoc-group was removed. After washing and drying the resin, the final cleavage was performed using a mixture of TFA:TIPS:H₂O (95:2.5:2.5) for 1.5 h. Crude peptide (35.6 mg) was purified using a Phenomenex C₁₈ column over 9 injections to yield ca. 1.5 mg of purified peptide **4.11** (gradient: 2% A, 98% D to 100% A in 45 min, flow rate: 1 mL/min, R_t 14.7 min). ESI-MS calculated for C₂₈H₄₀N₇O₈ 602.29 (M+H⁺) observed 602.4.

4.5. REFERENCES

1. Lazzarini, A., Gastaldo, L., Candiani, G., Ciciliato, I., Losi, D., Marinelli, F., Selva, E., and Parenti, F. (2005) Antibiotic 107891, its factors A1 and A2, pharmaceutically acceptable salts and compositions, and use thereof., *International Publication Number WO 2005/014628 A, International Publication.*
2. Castiglione, F., Cavaletti, L., Losi, D., Lazzarini, A., Carrano, L., Feroggio, M., Ciciliato, I., Corti, E., Candiani, G., Marinelli, F., and Selva, E. (2007) A Novel Lantibiotic Acting on Bacterial Cell Wall Synthesis Produced by the Uncommon Actinomycete *Planomonospora* sp, *Biochemistry.* *46*, 5884-5895.
3. Münch, D., Müller, A., Schneider, T., Kohl, B., Wenzel, M., Bandow, J. E., Maffioli, S., Sosio, M., Donadio, S., Wimmer, R., and Sahl, H.-G. (2014) The Lantibiotic NAI-107 Binds to Bactoprenol-bound Cell Wall Precursors and Impairs Membrane Functions, *J. Biol. Chem.* *289*, 12063-12076.
4. Castiglione, F., Lazzarini, A., Carrano, L., Corti, E., Ciciliato, I., Gastaldo, L., Candiani, P., Losi, D., Marinelli, F., Selva, E., and Parenti, F. (2008) Determining the Structure and Mode of Action of Microbisporicin, a Potent Lantibiotic Active Against Multiresistant Pathogens, *Chem. Biol.* *15*, 22-31.
5. French, G. L. (2006) Bactericidal agents in the treatment of MRSA infections—the potential role of daptomycin, *J. Antimicrob. Chemother.* *58*, 1107-1117.
6. Jabés, D., Brunati, C., Candiani, G., Riva, S., Romanó, G., and Donadio, S. (2011) Efficacy of the New Lantibiotic NAI-107 in Experimental Infections Induced by Multidrug-Resistant Gram-Positive Pathogens, *Antimicrob. Agents Chemother.* *55*, 1671-1676.
7. Lepak, A. J., Marchillo, K., Craig, W. A., and Andes, D. R. (2015) In Vivo Pharmacokinetics and Pharmacodynamics of the Lantibiotic NAI-107 in a Neutropenic Murine Thigh Infection Model, *Antimicrob. Agents Chemother.* *59*, 1258-1264.
8. Foulston, L. C., and Bibb, M. J. (2010) Microbisporicin gene cluster reveals unusual features of lantibiotic biosynthesis in actinomycetes, *Proc. Natl. Acad. Sci. U.S.A.* *107*, 13461-13466.
9. Vasile, F., Potenza, D., Marsiglia, B., Maffioli, S., and Donadio, S. (2012) Solution structure by nuclear magnetic resonance of the two lantibiotics 97518 and NAI-107, *J. Pep. Sci.* *18*, 129-134.
10. Hsu, S.-T. D., Breukink, E., Tischenko, E., Lutters, M. A. G., de Kruijff, B., Kaptein, R., Bonvin, A. M. J. J., and van Nuland, N. A. J. (2004) The nisin-lipid II complex reveals a pyrophosphate cage that provides a blueprint for novel antibiotics, *Nat. Struct. Mol. Biol.* *11*, 963-967.
11. Maffioli, S. I., Iorio, M., Sosio, M., Monciardini, P., Gaspari, E., and Donadio, S. (2014) Characterization of the Congeners in the Lantibiotic NAI-107 Complex, *J. Nat. Prod.* *77*, 79-84.
12. Reay, A. J., Williams, T. J., and Fairlamb, I. J. S. (2015) Unified mild reaction conditions for C2-selective Pd-catalysed tryptophan arylation, including tryptophan-containing peptides, *Org. Biomol. Chem.* *13*, 8298-8309.

CHAPTER 5. SYNTHESIS TOWARDS UNDERSTANDING OF THE BIOSYNTHETIC PATHWAYS OF DEHYDROPHOS, FOSFAZINOMYCIN, AND RHIZOCTICIN^{‡‡}

5.1. INTRODUCTION

Phosphonate and phosphinate compounds are characterized by the presence of carbon phosphorus bonds (C–P in phosphonates, and either C–P–C or C–P–H in phosphinates). Phosphonates have high stability toward enzymes that hydrolyze P–O bonds in phosphate esters and anhydrides, and are stable to treatment with boiling acids or bases (3). Phosphonates structurally mimic phosphates and carboxylates, thereby competing with these native substrates for binding to enzyme active-site (4). Some phosphonates also covalently bind to and irreversibly inhibit enzymes (5). As phosphates and carboxylates are widespread in nature, the potential for harnessing phosphonates as compounds to modulate/inhibit enzyme function is vast.

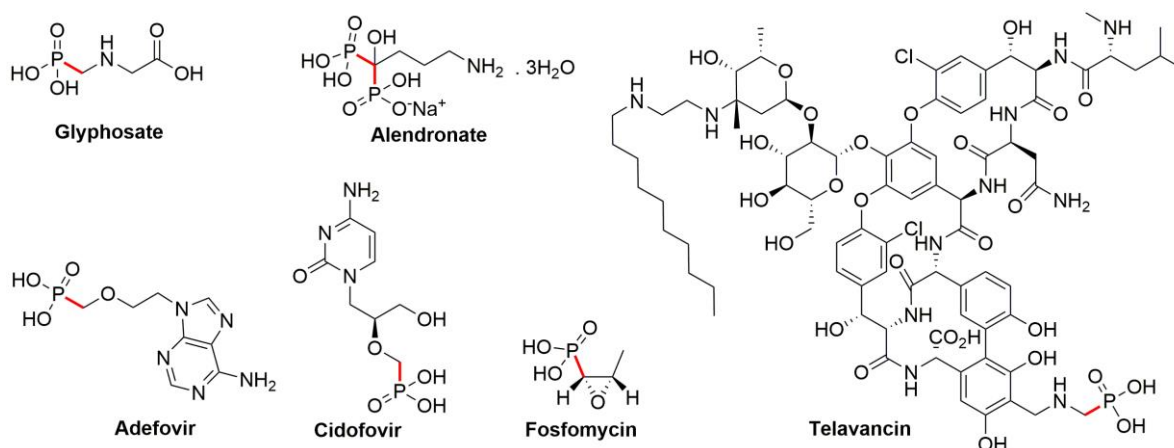


Figure 5.1. Structures of few notable phosphonate compounds. The C–P bonds are colored red.

Several natural and artificial phosphonates exhibit antifungal, herbicidal, antiparasitic, or antimicrobial properties (6). Glyphosate is a commonly used herbicide that inhibits pathways

^{‡‡} Adapted in part with permission from:

1. Bougioukou, D. J., Mukherjee, S., and van der Donk, W. A. (2013) Revisiting the biosynthesis of dehydrophos reveals a tRNA-dependent pathway, *Proc. Natl. Acad. Sci. U.S.A.* 110, 10952-10957.
2. Gao, J., Ju, K.-S., Yu, X., Velásquez, J. E., Mukherjee, S., Lee, J., Zhao, C., Evans, B. S., Doroghazi, J. R., Metcalf, W. W., and van der Donk, W. A. (2014) Use of a Phosphonate Methyltransferase in the Identification of the Fosfazinomycin Biosynthetic Gene Cluster, *Angew. Chem. Int. Ed.* 53, 1334-1337.

that are involved in the biosynthesis of aromatic amino acids in plants (7). The bisphosphonate alendronate is effective in preventing and treating osteoporosis (8). Adefovir is a reverse transcriptase inhibitor employed to treat viral infections that cause hepatitis B (9), and cidofovir is another antiviral drug that is effective in treating retinal infections that occur in some AIDS patients (10). Fosfomycin is used for treating urinary tract infections (11), and telavancin is a phosphonate analogue of vancomycin with improved ADME (absorption, distribution, metabolism, and excretion) properties (12) (Figure 5.1).

The biosynthesis of most of the phosphonates commences with the installation of the C–P bond by phosphoenol pyruvate mutase (PepM) (13-15) (Figure 5.2). The equilibrium of the reaction strongly favors the reactant phosphoenol pyruvate (PEP) over phosphonopyruvate (PnPy). The strength of the P–O bond in PEP accounts for the observed equilibrium constant ($K_{eq} = 500$, favoring PEP) (13). The thermodynamically unfavorable equilibrium is biosynthetically driven forward in most phosphonate pathways by an irreversible decarboxylation step catalyzed by phosphonopyruvate decarboxylase to generate phosphonoacetaldehyde (PnAA) (Figure 5.2, drawn in red) (16, 17). Various transformations of PnAA result in the production of multiple phosphonates. In one route, PnAA is reduced by a conserved metal and NAD(P)H dependent group III alcohol dehydrogenase (AD) to yield 2-hydroxyethylphosphonate (2-HEP), which is the common intermediate towards production of dehydrophos (18), fosfomycin (19), and phosphinothricin (20). 2-HEP is also converted to methyl phosphonate by methylphosphonate synthase, which cleaves the C–C bond in 2-HEP in an Fe(II) dependent fashion (21). PnAA can also be transaminated to yield 2-aminoethylphosphonate, which is involved in forming the polar head groups in phospholipids and phosphonoglycans (22). Finally, the rhizocticin and plumbemycin families arise from the

product of an aldol reaction between PnAA and the enolate form of pyruvate (23). The unfavorable PepM equilibrium can also be driven forward by nucleophilic addition of an acetate anion equivalent to the carbonyl group of PnPy (24). This is believed to be the committed step to the biosynthesis of FR-900098 and fosmidomycin. The compounds K-26 and I5B2 do not appear to arise from PEP (Figure 5.2, in dotted box) (25).

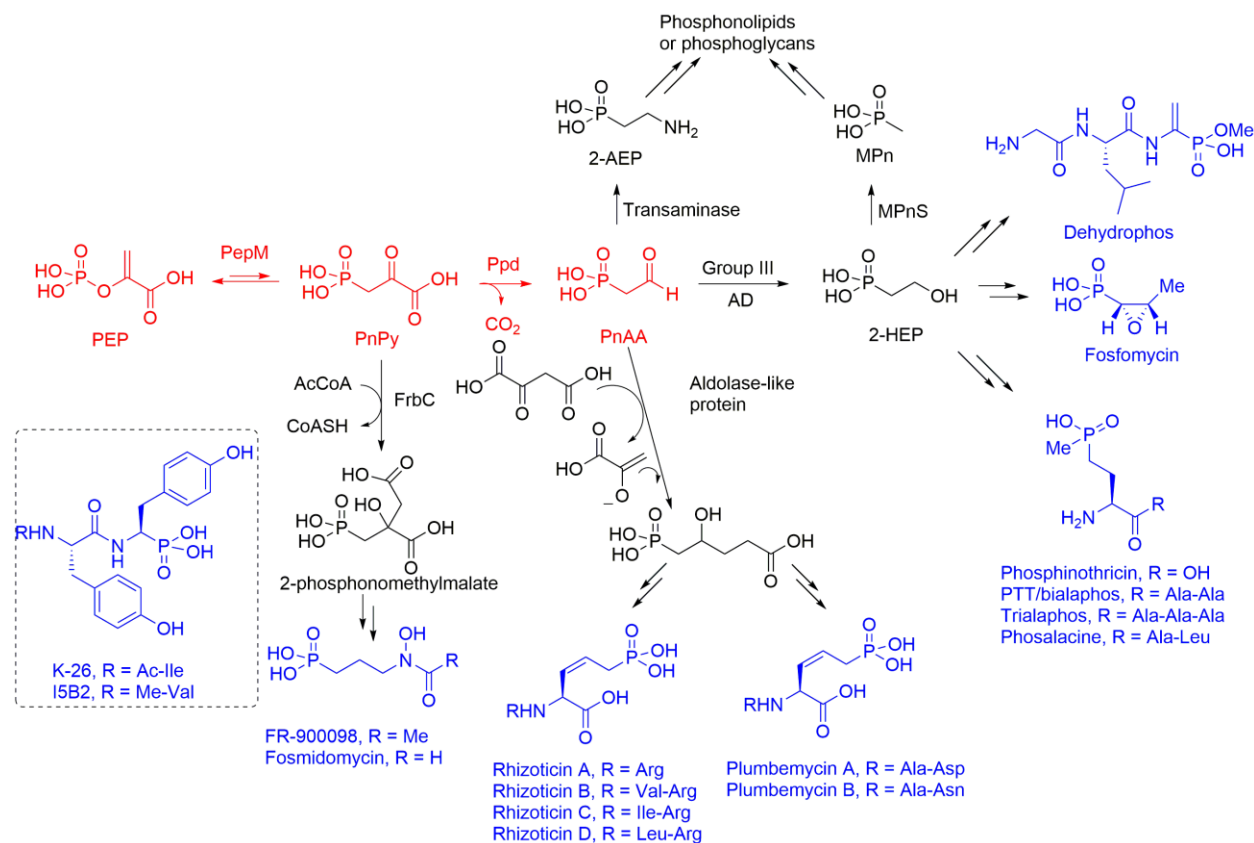


Figure 5.2. Overview of the biosynthesis of a number of phosphonate and phosphinate natural products. The equilibration of PEP and PnPy followed by irreversible generation of PnAA is conserved in most of the phosphonates, and is colored red. The phosphonate products of various biosynthetic pathways are colored blue. Adapted from Peck *et al.* (6).

5.1.1. Biosynthesis of Dehydrophos

Dehydrophos, formerly known as A53868 factor A, is a broad-spectrum antibiotic isolated from *Streptomyces luridus* (26). The structure was revised thrice, being finally corrected by comparing the NMR spectra of synthetic standards with the spectra of ¹³C and ¹⁵N labelled

dehydrophos, obtained from the producing organism (Figure 5.3A) (27). Studies on the structure-activity relationship and screening of the bioactivity of *Salmonella* mutants indicated a “Trojan-horse” type mechanism, where the peptide is required for the uptake by the membrane-bound permeases followed by the action of proteases to release the active phosphonate cargo inside the cells (28, 29). The protease mediated cleavage of dehydrophos results in the formation of 1-aminovinylphosphonate, Δ Ala(P), which tautomerizes to the corresponding imine, and finally hydrolyzes to generate methyl acetylphosphonate (MAP) (Figure 5.3B) (29). The bioactivity of dehydrophos is thought to arise from MAP, which is a potent inhibitor of pyruvate dehydrogenase (30), and bacterial 1-deoxy-D-xylulose 5-phosphate synthase (31).

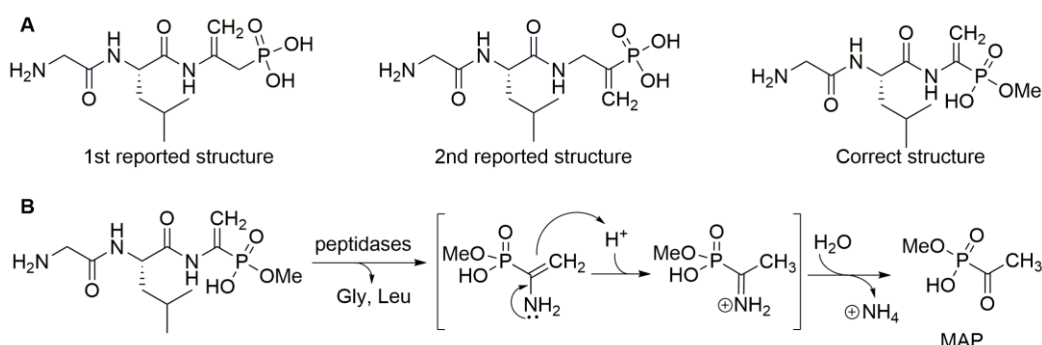


Figure 5.3. Structure of dehydrophos and its conversion into MAP. (A) The two previously reported incorrect structures as well as the correct structure of dehydrophos are shown. (B) The generation of MAP from dehydrophos by the action of peptidases followed by tautomerization and hydrolysis of the resultant imine is presented.

The early steps in the biosynthesis of dehydrophos share the common pathway employed for most phosphonates (Figure 5.4) (18), where DhpE and DhpF perform the roles of PEP mutase and decarboxylase, respectively. DhpG is an Fe(II)-dependent dehydrogenase that reduces PnAA to 2-HEP in a NADH dependent fashion. DhpA is an α -ketoglutarate-dependent non-heme iron dioxygenase responsible for the hydroxylation at C1 to generate 1, 2-dihydroxyethyl phosphonate (DHEP). The next reaction is phosphorylation of the hydroxyl group at the C2 position by DhpB, an enzyme homologous to glycerate kinase. The resultant

product, 1-hydroxy-2-phosphorylethyl phosphonate (HP-EP), is oxidized by DhpC to 1-oxo, 2-phosphorylethylphosphonate (OP-EP). The rest of the biosynthetic steps were putatively assigned (assigned steps are indicated by dotted arrows, Figure 5.4). Transamination of OP-EP was predicted to be catalyzed by DhpD, which shows homology to aspartate aminotransferases. The resulting compound, 1-amino-2-phosphorylethylphosphonate (AP-EP), also referred to as the phosphonate analogue of phosphoserine (pSer(P)), was thought to be coupled to Leu and Gly by the enzymes DhpH and DhpK. DhpH and DhpK contain putative Acyl-CoA *N*-acyltransferase domains known to catalyze peptide bond formation. Vinyl group formation was initially believed to be catalyzed by β -elimination of phosphate moiety of pSer(P) by the N-terminal portion of DhpH, followed by coupling of the resulting 1-aminovinylphosphonate (Δ Ala(P)) to Leu by the C-terminal portion of DhpH (Figures 5.4 and 5.5). The problem with this hypothesis is that Δ Ala(P) is prone to tautomerisation and subsequent hydrolysis, and hence will not be suitable for coupling to Leu, unless the putative Δ Ala(P) intermediate is tightly bound by DhpH and is well-shielded from solvent. The work described in this chapter focuses on this transformation and helps to clarify the incorporation of the vinyl moiety in dehydrophos (*I*). In addition, the Gly-L-Leu- Δ Ala(P) intermediate was proposed to be methylated by the SAM-dependent methyltransferase DhpI to complete the biosynthesis of dehydrophos (32). In this work, we showed that methylation actually occurs at an earlier step in the biosynthetic pathway (*I*).

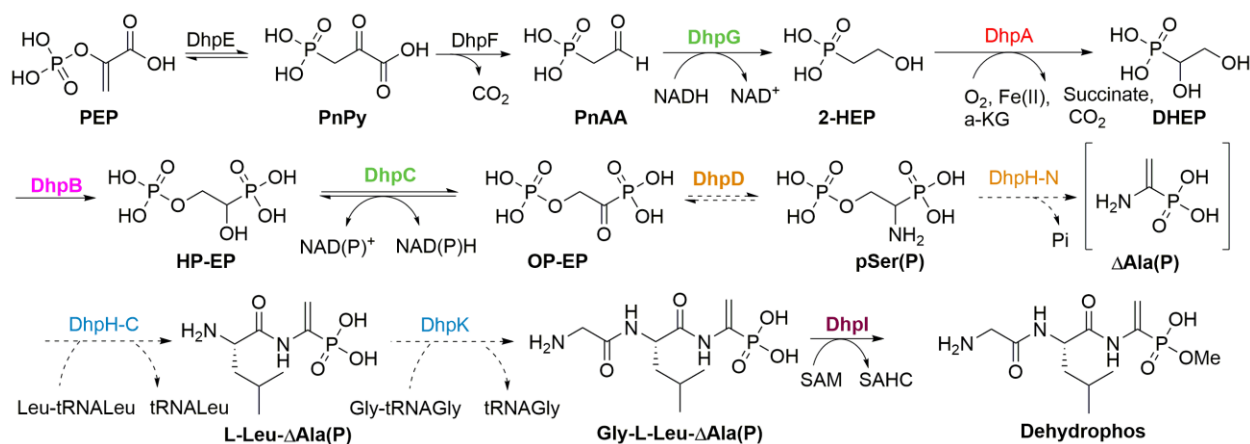


Figure 5.4. Dehydrophos biosynthetic pathway proposed earlier to this work. Established early stages (solid arrows) and predicted late stages (dotted arrows) in the biosynthesis of dehydrophos (18). Adapted from Bougioukou et al. (1).

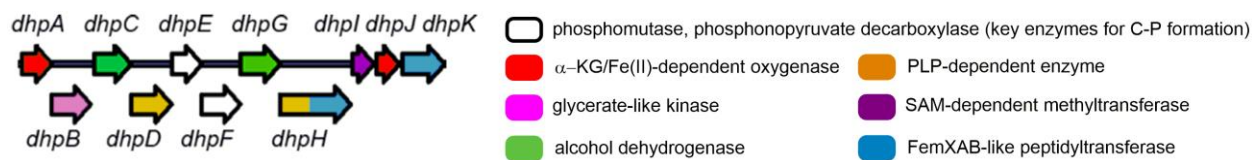


Figure 5.5. Biosynthetic gene cluster for dehydrophos production showing functional assignment of putative enzymes. Figure courtesy, Dr. Despina Bougioukou (1).

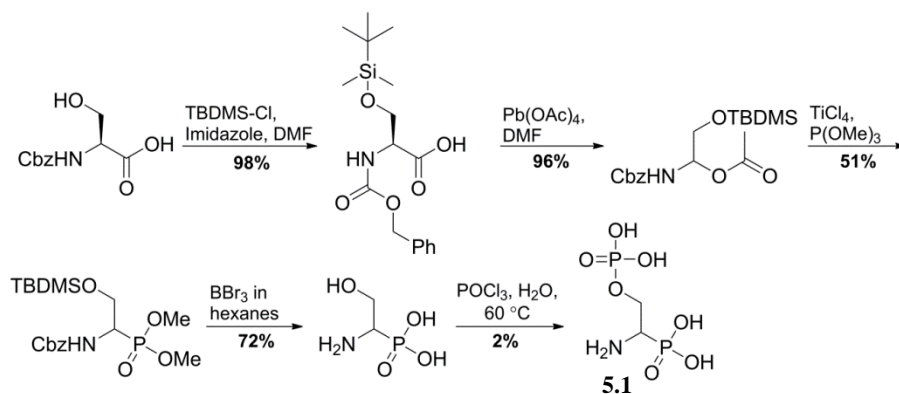
In addition to the work on dehydrophos biosynthesis, I have synthesized compounds involved in the biosynthetic pathways of fosfazinomycin and rhizocticin. In the fosfazinomycin project, the synthesized phosphonate was used to confirm the structure of a novel phosphonate product obtained from the strain, *Streptomyces sp.* WM6372. The phosphonate compound was found to be a substructure of fosfazinomycin, and conditions were developed which led to fosfazinomycin production from this strain (2). In the rhizocticin project, my efforts involved synthesizing an intermediate in the rhizocticin biosynthetic pathway. We anticipated using this intermediate to establish the activities of the putative enzymes in vitro.

5.2. RESULTS AND DISCUSSIONS

5.2.1. Dehydrophos^{§§***}

5.2.1.1. PLP-Dependent Activity of DhpD and DhpH

Based on a previous report (18), DhpD was proposed to reversibly interconvert pSer(P) and OP-EP (Figure 5.4). The formed pSer(P) was expected to undergo a β -elimination reaction catalyzed by the PLP-domain of DhpH. *Rac*-pSer(P) (compound **5.1**) was synthesized to probe these hypotheses (Scheme 5.1). Compound **5.1** was not found to be a substrate of DhpD, when used in the presence of pyruvate, oxaloacetate, or α -ketoglutarate as amino acceptors. Interestingly, incubation of compound **5.1** with His₆-DhpH or His₆-DhpH-N generated acetyl phosphonate (AP) as the only product (Figure 5.6). DhpH (or DhpH-N) is proposed to have catalyzed β -elimination of the phosphate group in pSer(P), generating Δ Ala(P), which tautomerizes to its imine form, followed by hydrolysis to generate AP. Incubation of the generated AP with DhpD and L-Ala was then shown to form L-Ala(P) (Figure 5.7).



Scheme 5.1. Synthesis of *rac*-pSer(P) starting from Cbz-L-Ser-OH. Scheme reproduced from the appendix (I).

§§ Adapted with permission from:

1. Bougioukou, D. J., Mukherjee, S., and van der Donk, W. A. (2013) Revisiting the biosynthesis of dehydrophos reveals a tRNA-dependent pathway, *Proc. Natl. Acad. Sci. U.S.A.* 110, 10952-10957.

*** I have synthesized the compounds used in this study. All other experiments were performed by Dr. Despina Bougioukou, post-doctoral researcher in the van der Donk group, Institute of Genomic Biology, UIUC.

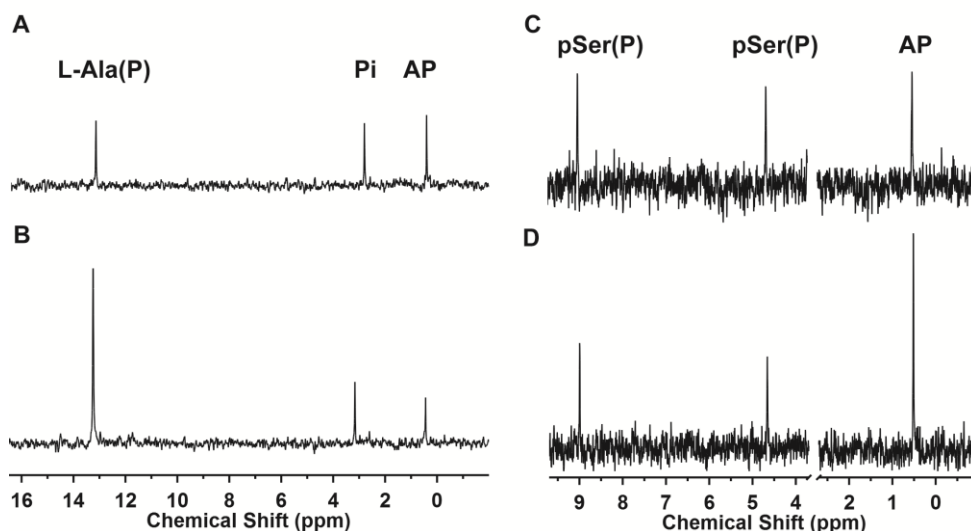


Figure 5.6. ^{31}P -NMR studies on the activities of DhpD and DhpH. (A) ^{31}P -NMR spectrum after generation of AP from L-Ala(P), when treated with DhpD in the presence of pyruvate. (B) ^{31}P -NMR spectrum after generation of L-Ala(P) from AP, when treated with DhpD in the presence of L-Ala. (C) ^{31}P -NMR showing conversion of pSer(P) to AP by DhpH. (D) ^{31}P -NMR of C spiked with standard of AP. Figure courtesy, Dr. Despina Bougioukou, IGB, UIUC (1).

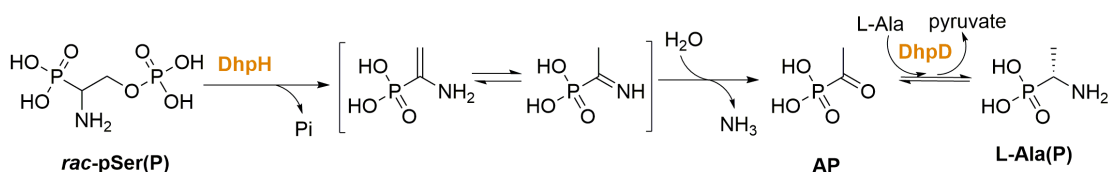
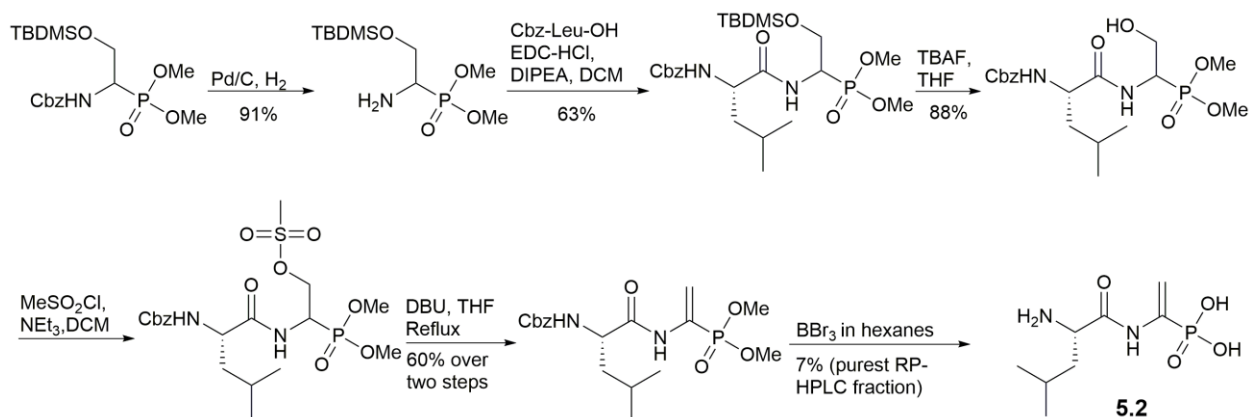


Figure 5.7. Generation of L-Ala(P) from pSer(P) using DhpH and DhpD.

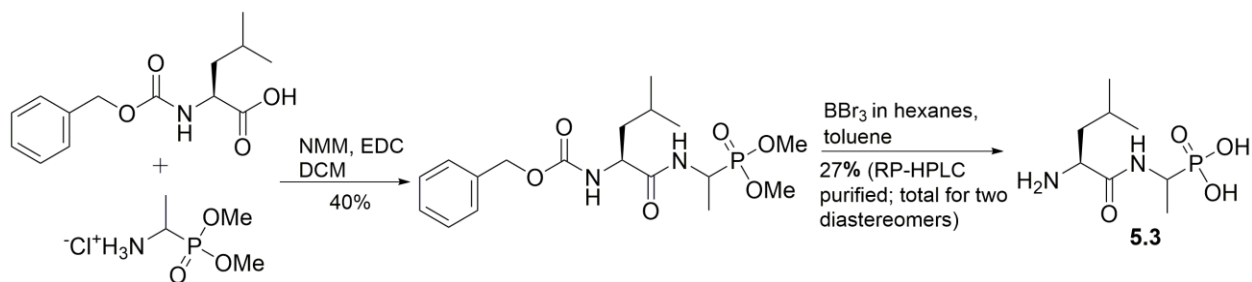
5.2.1.2. tRNA-Dependent Activity of DhpH

The full length His₆-DhpH exhibited a high A_{260}/A_{280} ratio (ca. 1.3), suggesting that nucleic acid co-purified along with the protein. The C-terminal domain of DhpH (His₆-DhpH-C) was also associated with a high A_{260}/A_{280} ratio, whereas the N-terminal domain of DhpH (His₆-DhpH-N) exhibited a lower A_{260}/A_{280} ratio of 0.7. Treatment with RNase eliminated the nucleic acids from the prepared protein, suggesting that RNA was co-purified with DhpH and DhpH-C. The isolated RNA contained leucyl-tRNA, since it was able to load L-[^{14}C (U)]-Leu in the presence of ATP and purified leucyl-tRNA synthetase (LeuRS). The hypothesis of whether DhpH can generate $\Delta\text{Ala(P)}$ from pSer(P), and subsequently catalyze reaction with L-Leu-

tRNA^{Leu} to generate L-Leu-ΔAla(P), was tested. Aminoacylated tRNA^{Leu} was generated *in situ* by LeuRS in the presence of total tRNA from *E. coli*, ATP, L-[¹⁴C(U)]-Leu, and thermostable inorganic pyrophosphatase (TIPP). This system was incubated with DhpH and compound **5.1**, and the product was monitored by a sensitive thin-layer chromatography (TLC) assay, where any product incorporating the L-[¹⁴C(U)]-Leu would show up as a radioactive spot on the TLC. No evidence of product with R_f value similar to my chemically synthesized L-Leu-ΔAla(P) (compound **5.2**, Scheme 5.2) was observed, ruling out the formation of compound **5.2** by the action of DhpH. As shown in Section 5.2.1.1, the action of DhpH-N and DhpD produced Ala(P) starting from pSer(P). We investigated whether the DhpH can generate L-[¹⁴C(U)]-Leu-Ala(P), when the same assay was set up as earlier with the addition of DhpD and L-Ala. Indeed, upon performing such an assay, the R_f value of the radioactive spot on the TLC matched with the R_f value obtained from my chemically synthesized L-Leu-Ala(P) (compound **5.3** of Scheme 5.3 and Figure 5.8). The identity of L-Leu-L-Ala(P) was confirmed based on NMR and analytical HPLC studies on the enzymatically prepared and synthetic compound **5.3** (Figure 5.9).



Scheme 5.2. Synthetic scheme for L-Leu-ΔAla(P).



Scheme 5.3. Synthetic scheme for L-Leu-Ala(P).

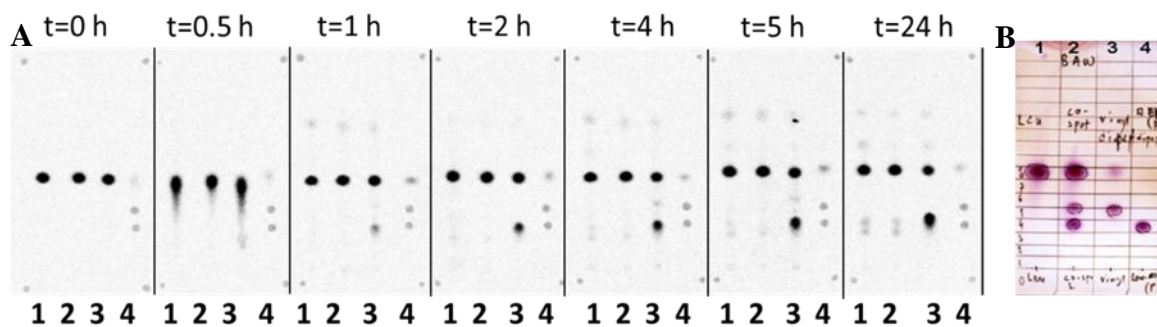


Figure 5.8. Radioactive TLC analysis of conversion of *rac*-pSer(P) to L-[¹⁴C(U)]-Leu-Ala(P) by the activity of DhpH and DhpD in a one-pot reaction. (A) Scanned phosphor imaging plate of a silica TLC sheet spotted with lane 1, DhpH, *rac*-pSer(P), L-[¹⁴C(U)]-Leu, tRNA and (re)generation components of Leu-tRNA^{Leu}; lane 2, same as in lane 1 with the addition of L-Ala; lane 3, same as in lane 1 with the addition of L-Ala and DhpD; lane 4, spots created with the R_f values obtained from synthetic L-Leu-ΔAla(P) and L-Leu-Ala(P). (B) Ninhydrin-stained TLC of lane 1, L-Leu; lane 2, L-Leu + L-Leu-ΔAla(P) + L-Leu-Ala(P); lane 3, L-Leu-ΔAla(P); lane 4, L-Leu-Ala(P). Figure courtesy, Dr. Despina Bougioukou, IGB, UIUC (1).

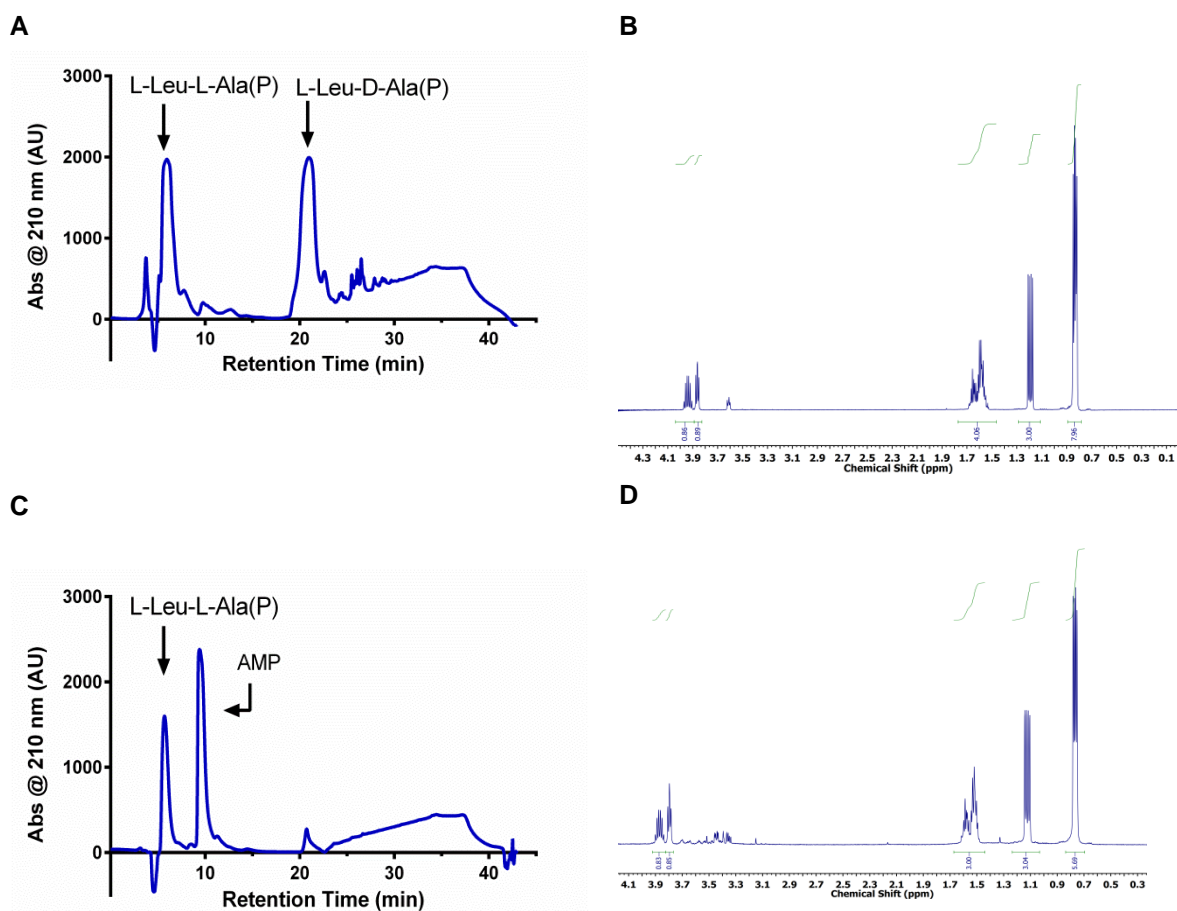


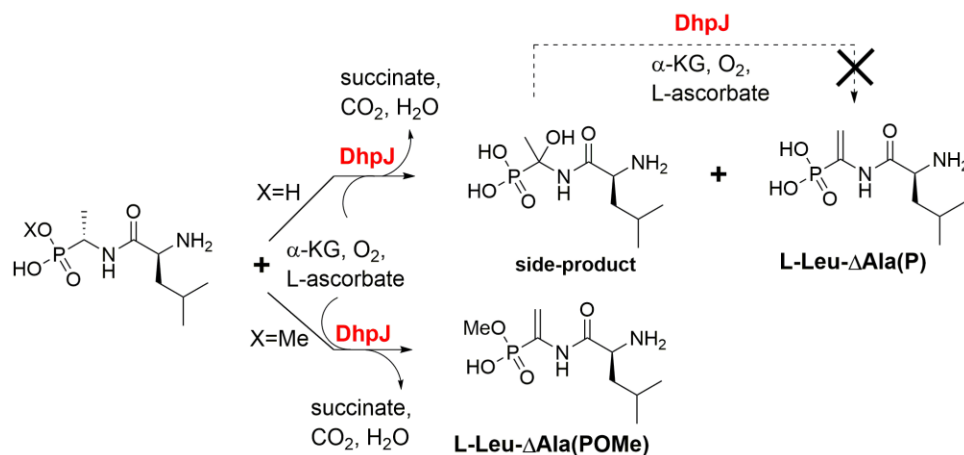
Figure 5.9. HPLC traces and ¹H NMR spectra comparing chemically and enzymatically prepared L-Leu-L-Ala(P). **A.** HPLC trace of synthetic L-Leu-(L/D)-Ala(P) **B.** ¹H NMR spectrum of HPLC fraction containing synthetic L-Leu-L-Ala(P) in D₂O. **C.** HPLC trace of enzymatically prepared L-Leu-L-Ala(P). **D.** ¹H NMR spectrum of enzymatically prepared L-Leu-L-Ala(P) in D₂O. Figure courtesy, Dr. Despina Bougioukou, IGB, UIUC (1).

5.2.1.3. Fe(II)/ α -KG/O₂-Dependent Activity of DhpJ^{†††}

As the generation of L-Leu-L-Ala(P) was established, we investigated the installation of the vinyl group in dehydrophos. Owing to solubility problems, DhpJ was expressed as a maltose binding protein (MBP) fusion protein (MBP-DhpJ). DhpJ generated L-Leu- Δ Ala(P) from L-Leu-L-Ala(P), along with a side product that is a dipeptide hydroxylated at the α -carbon of L-Ala(P).

^{†††} I have synthesized L-Leu-L-Ala(P) and L-Leu- Δ Ala(P).

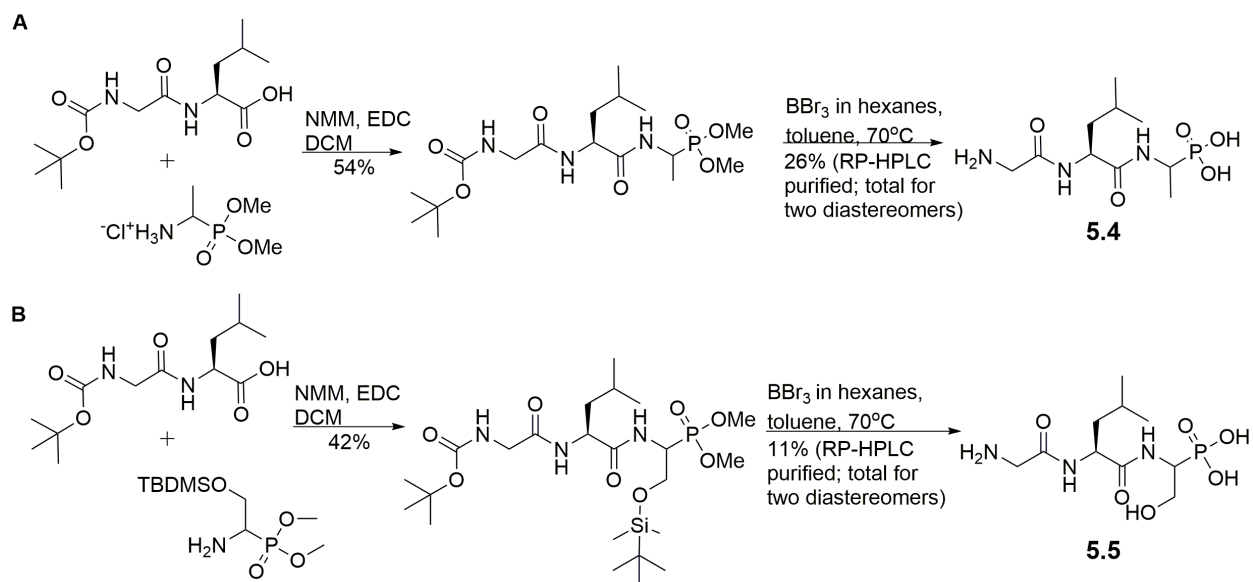
On treating the monomethylated version, L-Leu-L-Ala(POMe), only the unsaturated L-Leu- Δ Ala(POMe) was observed, suggesting that L-Leu-L-Ala(POMe) is the physiological substrate of DhpJ, and the methylation by DhpI occurs prior to the action of DhpJ.



Scheme 5.4. Representation of the activity of DhpJ where L-Leu- Δ Ala(POMe) is the sole product arising from L-Leu-L-Ala(POMe). Figure courtesy of Dr. Despina Bougioukou, IGB, UIUC (1).

5.2.1.4. Peptidyl-Transferase Activity of DhpK

Assays were performed with MBP-DhpK because of the poor solubility of DhpK. MBP-DhpK was able to catalyze the addition of Gly to the N terminus of synthetic L-Leu-Ala(P) (compound **5.3**), L-Leu- Δ Ala(P) (compound **5.2**), and methylated L-Leu- Δ Ala(POMe) in the presence of in situ generated Gly-tRNA^{Gly}. The identity of the tripeptide products was confirmed by comparing the HPLC profile and the NMR spectra with synthetic tripeptides (compounds **5.4** and **5.5**, Scheme 5.5). The HPLC traces of Gly-L-Leu-L-Ala(P) prepared enzymatically and by synthesis is shown as an example (Figure 5.10). The compounds were synthesized as diastereomers, which were separated by HPLC. The revised biosynthetic pathway is shown in Figure 5.11.



Scheme 5.5. Synthesis of phosphono-tripeptides. Scheme showing the synthesis of (A) Gly-L-Leu-Ala(P) and (B) Gly-L-Leu-Ser(P).

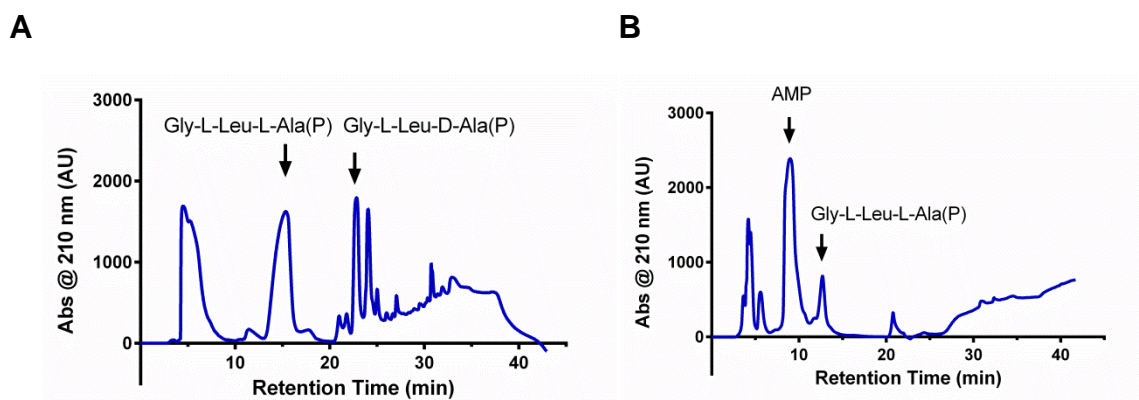


Figure 5.10. HPLC traces of Gly-L-Leu-L-Ala(P). (A) Synthetically prepared diastereomeric mixture of tripeptides. (B) Enzymatically prepared Gly-L-Leu-L-Ala(P).

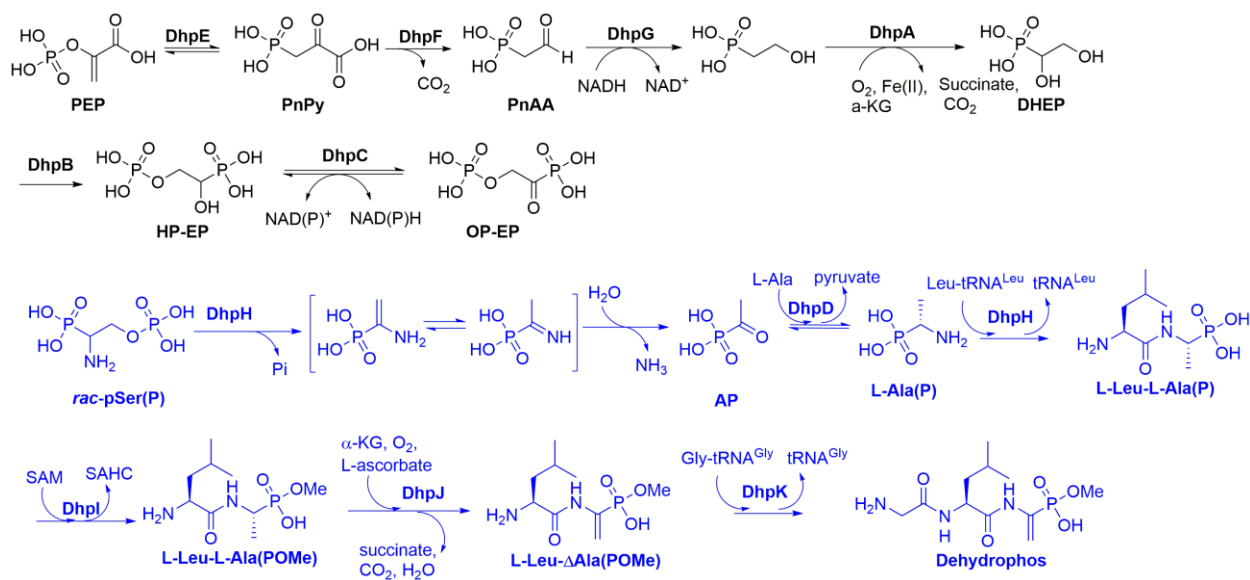


Figure 5.11. Revised biosynthesis of dehydrophos. Steps in the biosynthesis of dehydrophos established prior to this work are colored black. The steps elucidated in this current work are drawn in blue. Note that the conversion of OP-EP to pSer(P) has yet to be experimentally verified.

5.2.2. Fosfazinomycin^{###§§§}

The purification of novel phosphonates leading to their structural elucidation is a challenging task owing to their high polarity and water solubility. The substrate tolerance of the *O*-methyltransferase from the dehydrophos biosynthetic pathway, DhpI, enables it to methylate a wide range of phosphonate molecules. Using this enzyme, an assay was set up to identify and purify unknown phosphonates. A method termed as “stable isotope labelling of phosphonates in extract” (SILPE) was developed, which involved the treatment of spent media, which was suspected to contain novel phosphonates, with DhpI in the presence of a mixture of SAM and CD₃-SAM. The material was analyzed by LCMS, and phosphonates that were modified by DhpI

^{###} Adapted with permission from:

2. Gao, J., Ju, K.-S., Yu, X., Velásquez, J. E., Mukherjee, S., Lee, J., Zhao, C., Evans, B. S., Doroghazi, J. R., Metcalf, W. W., and van der Donk, W. A. (2014) Use of a Phosphonate Methyltransferase in the Identification of the Fosfazinomycin Biosynthetic Gene Cluster, *Angew. Chem. Int. Ed.* 53, 1334-1337.

^{§§§} My contribution to this project is the synthesis of compound **5.7**.

would generate two ions separated by 3.0188 Da, enabling rapid identification of phosphonate species. Using this method, two previously unknown phosphonates were identified from *Streptomyces sp.* WM6372, a strain predicted to be a phosphonate producer as it was found to encode the *pepM* gene encoding phosphoenolpyruvate mutase (Figure 5.12). The structures of these compounds were confirmed by NMR spiking experiments with chemically synthesized methyl phosphonoacetate (compound **5.6**) and 2-hydroxy-2-phosphonoacetate (compound **5.7**) (Scheme 5.6 and Figure 5.13). This strain was cultivated in various media, and the production of fosfazinomycin A and B was observed after growth in R2AS medium (Structure drawn in Figure 5.12). The biosynthetic gene cluster was putatively assigned in this study.

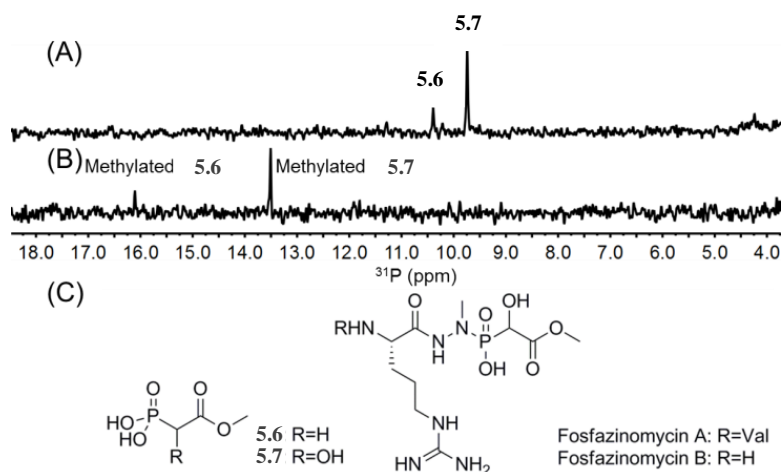
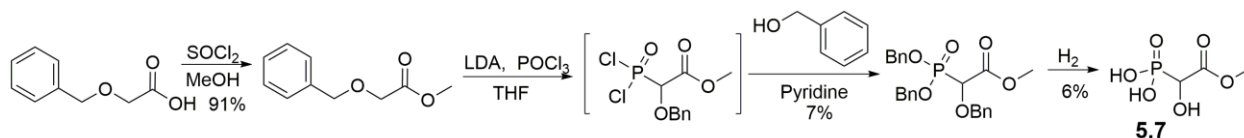


Figure 5.12. Identification of two novel phosphonates from *Streptomyces sp.* WM 6372. (A) ³¹P NMR spectra of the spent medium of *Streptomyces sp.* WM 6372, showing the region depicting phosphonates. (B) ³¹P NMR spectra of the media after treatment with DhpI and SAM. (C) Structure of phosphonates responsible for the signal in A. Also drawn are the structures of fosfazinomycin A and B. Figure courtesy of Dr. Jiangtao Gao, IGB, UIUC (2).



Scheme 5.6. Scheme showing the synthesis of compound **5.7**.

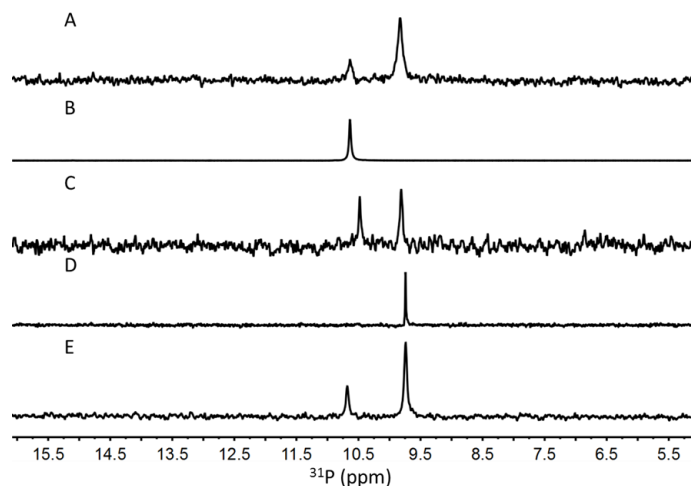


Figure 5.13. ^{31}P NMR spiking experiments to confirm identity of phosphonates produced by *Streptomyces sp.* WM 6372. (A) ^{31}P NMR of spent medium of *Streptomyces sp.* WM 6372. (B) ^{31}P NMR of synthesized compound **5.6**. (C) Spiking of A with compound **5.6**. (D) ^{31}P NMR of synthesized compound **5.7**. (E) Spiking of C with compound **5.7**. Figure courtesy of Dr. Jiangtao Gao, IGB, UIUC (2).

5.2.3. Rhizocticin

Rhizocticins are phosphonate oligopeptide antibiotics produced by *Bacillus subtilis* ATCC6633. The structures of rhizocticins were determined in 1988 (33), and were found to contain the C-terminal non-proteinogenic amino acid (*Z*)-L-2-amino-5-phosphono-3-pentenoic acid (APPA). The anti-fungal activity of rhizocticin was thought to arise due to cleavage of the molecule by host peptidases to release APPA that inhibits threonine synthase, interfering with Thr biosynthesis, and consequently blocking protein synthesis. Dr. Svetlana Borisova (post-doctoral researcher, IGB, UIUC) proposed the biosynthetic gene cluster responsible for rhizocticin production (23). The initial steps of the biosynthesis were established to generate compound **5.8**, starting from PEP. Subsequent enzymatic reactions were proposed to occur by any of three pathways, leading to rhizocticin B formation (Figure 5.14). Of the proposed routes, the third pathway is attractive, as it does not require the generation of the toxic APPA intermediate. To experimentally validate the proposed biosynthetic pathways, I synthesized the

intermediate common to pathways B and C, compound **5.9**, adapting the synthesis of similar molecules reported by Cox et al. (Scheme 5.7) (34). The reverse reaction of the aminotransferase RhiJ on compound **5.9** could potentially produce compound **5.8**, thus allowing us to investigate all three pathways. However, in experiments performed by Dr. Svetlana Borisova, which involved treatment of compound **5.9** with the enzymes putatively assigned to the rhizocticin biosynthetic pathway, no change in the starting material was observed based on ^{31}P NMR studies. The failure to observe any transformation of compound **5.9** could stem from problems with in viro reconstitution of the enzymes. Another possibility is that there are other unidentified critical components to the biosynthetic pathway.

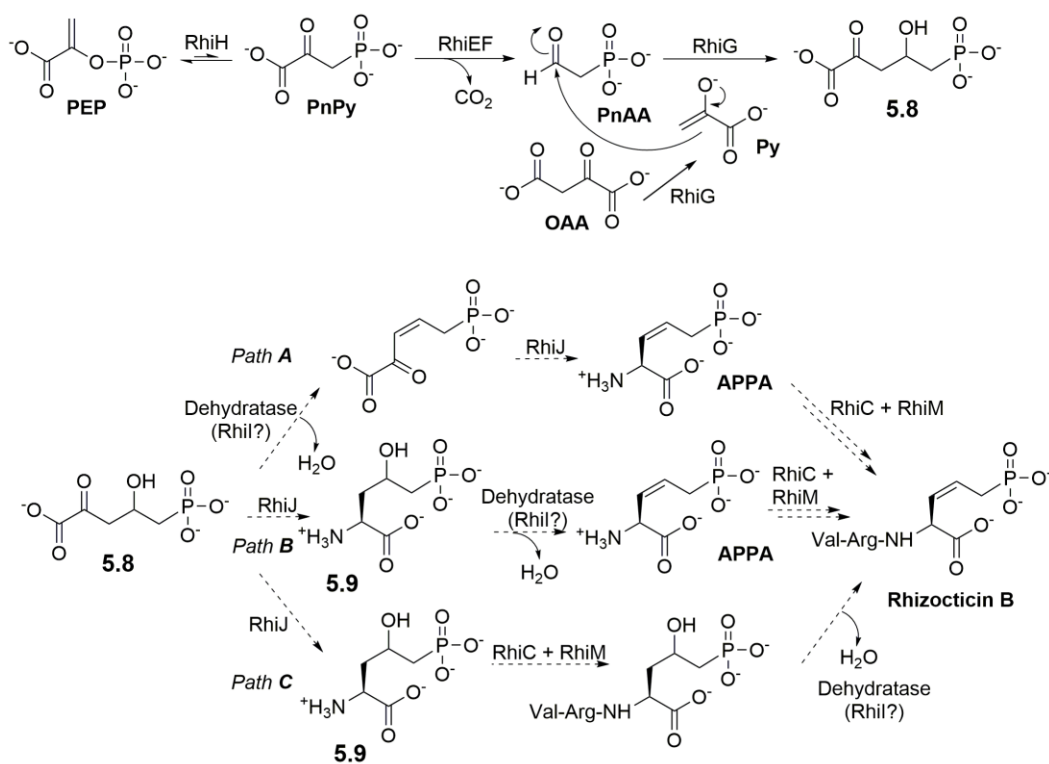
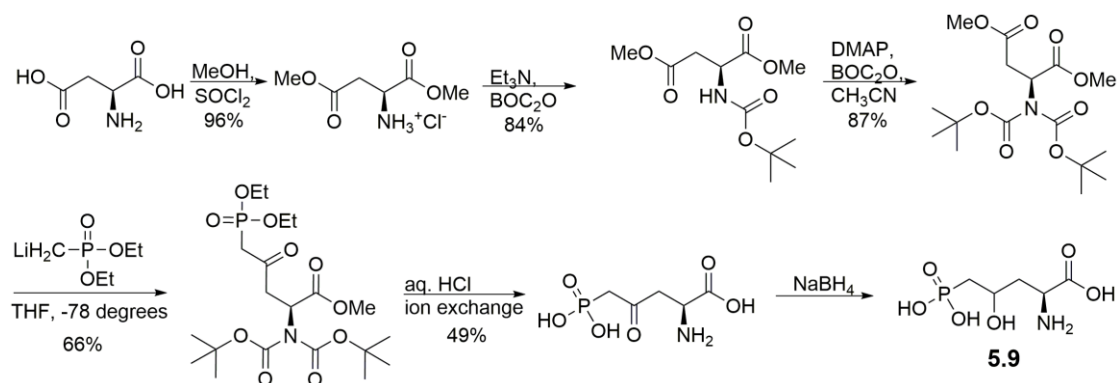


Figure 5.14. Biosynthetic pathway of rhizocticins. The established biosynthetic pathway shown connected by solid arrows, involves generation of compound **5.8** starting from PEP. Compound **5.8** was proposed to be the intermediate that could participate in one of the three pathways drawn to generate rhizocticin B. Figure adapted from Borisova et al. (23)



Scheme 5.7. Scheme for the synthesis of compound **5.9**.

5.3. CONCLUSION AND OUTLOOK

In this chapter, I have presented my collaborative efforts to understand the biosynthesis of dehydrophos, fosfazinomycin, and rhizocticin. I have synthesized substrates and intermediates that were instrumental in elucidating the late-stage biosynthesis of dehydrophos. In a series of biochemical assays performed by Dr. Despina Bougioukou (post-doctoral researcher, IGB, UIUC), many unexpected transformations were revealed during the course of this work (Figure 5.11). Acetyl phosphonate (AP) was generated by the action of the PLP-dependent N-terminal of DhpH on pSer(P). An amino group was then introduced into the resulting ketone of AP by a second PLP-dependent enzyme, DhpD, to generate L-Ala(P) – a synthetic antibiotic from Roche that was not previously thought to exist naturally. The C-terminal domain of DhpH was found to have an unprecedented activity in natural product biosynthesis, involving the coupling of an L-Leu moiety derived from L-leucyl-tRNA^{Leu} onto the L-Ala(P) intermediate to generate L-Leu-L-Ala(P). The product of this *in vitro* reaction was validated with an authentic synthetic standard. The resultant compound was then monomethylated by DhpI to yield L-Leu-L-Ala(POMe). The final steps of dehydrophos biosynthesis involved the installation of the vinyl moiety by DhpJ and the coupling of a Gly residue by DhpK. Synthetic standards were used to validate the reactivity of each of these enzymes.

Dr. Jiangtao Gao (post-doctoral researcher, IGB, UIUC) developed the SILPE method to purify and identify novel phosphonates, which involved the substrate-tolerant methyltransferase of the dehydrophos pathway, DhpI. He employed the technique to detect novel phosphonate species from *Streptomyces sp.* WM6372. I synthesized a compound that confirmed the major phosphonate product obtained from this strain. This compound was a substructure of fosfazinomycin, and conditions were achieved to obtain fosfazinomycin from the strain. My efforts in the rhizocticin pathway were to experimentally validate the late-stage biosynthetic pathway of rhizocticin, as proposed by Dr. Svetlana Borisova (post-doctoral researcher, IGB, UIUC). However, we did not observe any activity of the putative enzymes with a synthetic putative common intermediate. Further studies are required to successfully reconstitute the enzymes in vitro, and refine the biosynthetic pathway of rhizocticin.

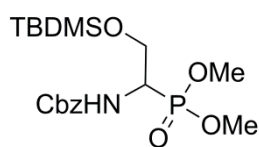
5.4. EXPERIMENTAL

5.4.1. General Procedure

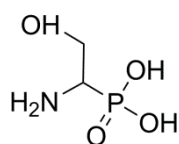
Commercially available reagents were used without further purification. All reactions were performed under nitrogen atmosphere unless otherwise noted. Reaction progress and fractions from flash chromatography purifications were monitored by thin layer chromatography (TLC) on silica-gel-coated glass plates with a F254 fluorescent indicator. Visualization was achieved by fluorescence quenching during UV irradiation, ninhydrin stain (0.5% ninhydrin in ethanol), or permanganate stain (1.5 g KMnO₄, 10 g K₂CO₃, 1.25 mL 10% NaOH in 200 mL of H₂O). Flash chromatography was performed using Silicycle SiliaFlash P60, 230-400 mesh silica gel. Cation exchange resin AG 50W-X8, hydrogen form (100-200 mesh) was purchased from Bio-Rad and used for compound purification when noted. Reversed-phase high performance liquid chromatography (RP-HPLC) was performed using an Agilent 1200 series quad pump

system equipped with a diode array detector and a G1956B mass spectrometer with a multimode-electrospray/atmospheric pressure chemical ionization (MM-ES+APCI) source. For analytical scale HPLC, a Synergi 4 μ Fusion-RP 80A column (150 x 4.6 mm, 4 μ m, Phenomenex Torrance, CA) was used with a flow rate of 0.5 mL/min (column A). For preparative HPLC, a Synergi 4 μ Fusion-RP 80A semi-preparative column (200 x 10 mm, 4 μ m, Phenomenex Torrance, CA) was used with a flow rate of 4 mL/min, (column B). Elution Gradient: 0-15 min 100 % Solvent A (0.1 % formic acid (FA) in water), 15-30 min 25 % A, 75 % solvent B (0.1 % FA in methanol), 30 to 33 min 75 % Solvent B, 38 to 43 min 100 % Solvent A. Flow: 4mL / min. Detection: @ 210 nm, 4 mL per fraction. NMR data are represented as follows: Chemical shift, multiplicity (s = singlet, d = doublet, t = triplet, q = quartet, m = multiplet and/or multiple resonance), coupling constant (if determined), integration, assignment. Mass spectrometry (except LC-MS) was performed at the University of Illinois Mass Spectrometry Center.

5.4.2. Small Molecule Synthesis

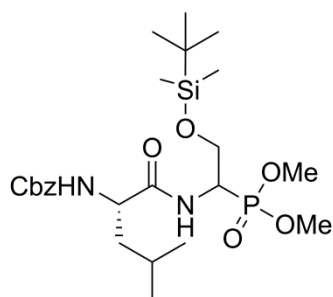


Compound **5.10**. Starting from Cbz-L-Ser-OH, compound **5.10** was synthesized in three steps following a literature procedure (28). ^1H NMR (500 MHz, CDCl_3) δ /ppm = 7.36-7.32 (m, 5H; arom), 5.27-5.25 (d, J = 10 Hz, 1H; NH), 5.13 (s, 2H; $\text{CH}_2\text{-Bn}$), 4.25-4.18 (m, 1H; H_α), 3.92-3.78 (m, 2H; H_β), 3.76 (d, J = 12.5 Hz, 3H; OCH_3), 3.74 (d, J = 12.5 Hz, 3H; OCH_3), 0.88 (s, 9H, $\text{SiC}(\text{CH}_3)_3$), 0.05 (s, 6H, $\text{Si}(\text{CH}_3)_2$). ^{31}P NMR (202 MHz, CDCl_3) δ /ppm = 26.7. MS (ESI): m/z = 418.2 ($\text{M}+\text{H}^+$). (Notebook IV, pages 11, 15, and 17)

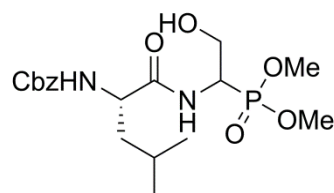


Compound **5.11**. Compound **5.10** (0.25 g, 0.6 mmol) was placed in a round bottom flask, the compound was dissolved in 9 mL of toluene, and the solution

was stirred under N₂ atmosphere and cooled on an ice-bath. To the reaction mixture, a 1 M solution of boron tribromide in hexanes (2.4 mL, 2.4 mmol) was added dropwise and the solution was stirred on an ice bath for 10 min, when a white suspension formed. The reaction flask was subsequently transferred to an oil bath preheated to 70 °C, and the solution was stirred for 5 h. The brown reaction mixture was quenched by adding 3.0 mL of dry MeOH and the reaction mixture turned nearly colorless (35). The reaction mixture was diluted by adding EtOAc (15 mL) and extracted twice with 10 mL of H₂O. The aqueous layers were back extracted with 10 mL of EtOAc and the aqueous fraction was lyophilized to generate a yellow powder. The crude mass was passed through a cation exchange column and eluted with water to obtain a final yield of 75 mg (57 %) of bromide salt of the product as white solid. (*Notebook II, page 85*)

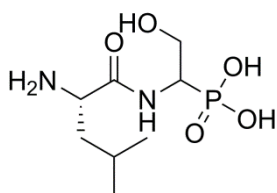


Compound **5.12**. This compound was synthesized as previously reported (28, 32). ¹H NMR (500 MHz, CDCl₃) δ/ppm = 7.38-7.30 (m, 5H; arom), 6.48 (dd, *J* = 10 Hz, 1H; NH), 5.2 (d, *J* = 10 Hz, 1H; NH), 5.11 (d, *J* = 12.5 Hz, 1H; CH₂Bn), 5.09 (d, *J* = 12.5 Hz, 1H; CH₂Bn), 4.55-4.46 (m, 1H), 4.28-4.18 (m, 1H), 4.02-3.96 (m, 1H), 3.73 (m, 6H; OCH₃), 1.68 (m, 4H), 0.95-0.93 (m, 6H; Hδ Leu), 0.89 (s, 9H; Si(CH₃)₃), 0.07 (s, 6H; Si(CH₃)₂). ³¹P NMR (202 MHz, CDCl₃) δ 26.4, 26.29 (pair of diastereomers). (*Notebook III, pages 21, 22*)



Compound **5.13**. Compound **5.12** (1.0 g, 1.88 mmol) was treated with 4 mL of 1 M TBAF solution in THF (4 mmol) with vigorous stirring under nitrogen for 45 min. The reaction mixture was diluted with 100 mL of dichloromethane (DCM) and washed with 0.1 M aqueous HCl (2×25 mL). The

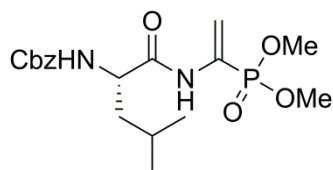
acidic layer was back extracted with 20 mL of DCM. The organic layers were collected, dried over Na₂SO₄, filtered, and concentrated. The residue was purified by flash chromatography (SiO₂) eluting with 3% MeOH in DCM to 4% MeOH in DCM to yield the desired product (0.69 g, 1.66 mmol, 88%). ¹H NMR (500 MHz, CDCl₃) δ/ppm = 7.36-7.26 (m, 5H; arom), 5.51-5.44 (m, 1H), 5.11-5.09 (m, 2H, CH₂-Bn), 4.56-4.48 (m, 1H), 4.34-4.24 (m, 1H), 3.98-3.92 (m, 1H), 3.80-3.68 (m, 6H; OCH₃), 1.71-1.62 (m, 2H), 1.58-1.51 (m, 1H), 0.99-0.89 (m, 6H; Hδ Leu). ¹³C NMR (125 MHz, CDCl₃) δ/ppm = 173, 156, 136, 128.6, 128.3, 67, 61.7, 61.4, 54, 53, 52, 42, 25, 24. ³¹P NMR (202 MHz, CDCl₃) δ/ppm = 26.2, 25.9 (pair of diastereomers). HRMS (ESI): m/z calc. for C₁₈H₂₉N₂O₇P 417.1792, found 417.1791. TLC: R_f = 0.15 (3% MeOH in DCM). (*Notebook III, page 23*)



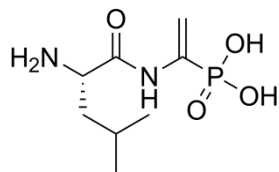
Compound **5.14**. Compound **5.13** (52.7 mg, 0.13 mmol) was dissolved in 1.7 mL of toluene and the flask was immersed in an ice-bath. To this solution, 380 μL of a 1 M solution of boron tribromide in hexanes (0.38 mmol) was added dropwise and the reaction was stirred at 0 °C for 10 min when the reaction mixture turned from colorless to white. The flask was transferred to an oil bath heated to 70 °C and the reaction was stirred for an additional 3 h, when the reaction mixture turned brown. The reaction mixture was allowed to cool to room temperature and was quenched with 2 mL of dry MeOH, when a clear brownish-black solution formed. The solution was concentrated on a rotary evaporator. The residue was diluted with 6 mL of water and extracted with 5 mL of ethyl acetate. The organic layer was back-extracted with 5 mL of water. The combined aqueous layers were collected and lyophilized to obtain crude product (60 mg). The crude product was purified by Fe-IMAC and the purest fraction was lyophilized (ca 1.6 mg). ¹H NMR δ/ppm = 4.18-4.06 (m, 1H;

H α Ser), 3.95-3.70 (m, 2H; H β Ser), 3.60- 3.48 (m, 1H; H α Leu), 1.65-1.45 (m, 3H; H β/γ Leu), 0.85-0.72 (m, 6H; H δ Leu). ^{31}P NMR (202 MHz, D $_2\text{O}$) δ/ppm = 17, 16.7 as diastereomers.

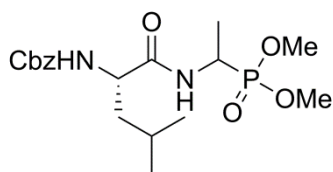
(*Notebook IV, page 5*)



Compound **5.15**. Compound **5.13** (0.15 g, 0.37 mmol) was dissolved in dry DCM (2 mL). The flask was cooled in an ice-bath, and triethylamine (0.1 mL, 0.74 mmol) and methanesulfonyl chloride (0.06 mL, 0.77 mmol) were added. The reaction mixture was allowed to warm to room temperature and stirred for 1 h and 15 min. The solvent was evaporated and ^{31}P NMR spectroscopy indicated complete conversion to the mesylated product. ^{31}P NMR (500 MHz, CDCl $_3$) δ/ppm = 22.76, 22.70 (pair of diastereomers). The mesylated product was dissolved in 5 mL of dry THF, followed by addition of diazabicycloundecene (DBU, 0.14 mL, 0.93 mmol) and the solution was refluxed for 30 min. The reaction mixture was then cooled and the solvent was evaporated. The residue was purified by flash chromatography (SiO $_2$) with 100 % EtOAc as the eluent to yield the desired product (103 mg, 0.26 mmol, 60 %). ^1H NMR (500 MHz, CDCl $_3$) δ/ppm = 7.71 (s, 1H; NH), 7.38-7.32 (m, 5H; arom), 6.73-6.64 (d, J = 42 Hz, 1H; =CH $_{\text{trans}}$), 5.65-5.61 (d, J = 19.5 Hz, 1H; =CH $_{\text{cis}}$), 5.13 (s, 2H; CH $_2$ -Bn), 4.22 (s, 1H; NH), 3.75 (d, J = 7.5 Hz, 3H; OCH $_3$), 3.73 (d, J = 7.5 Hz, 3H; OCH $_3$), 1.71-1.66 (m, 2 H; H β Leu), 1.54- 1.50 (m, 1H; H γ Leu), 0.96 (s, 6H; H δ Leu). ^{13}C NMR (125 MHz, CDCl $_3$) δ/ppm = 172, 156, 136, 129, 128.8, 128.5, 128.2, 116, 67, 54, 53.5, 41, 25, 23, 22. ^{31}P NMR (202 MHz, CDCl $_3$) δ/ppm = 15.8. HRMS (ESI) m/z calc. for C $_{18}$ H $_{27}$ N $_2$ O $_6$ P 399.1685, found 399.1686. TLC: R $_f$ = 0.5 (100 % EtOAc). (*Notebook III, page 37*)

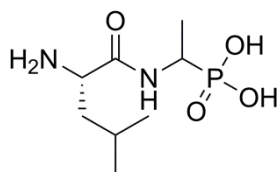


Compound **5.2**. Compound **5.15** (42.3 mg, 0.11 mmol) was dissolved in 1.6 mL of toluene and the flask was immersed in an ice bath. To the solution, a 1 M solution of BBr_3 in hexanes was added (0.32 mL, 0.32 mmol), and the flask was transferred to an oil bath heated to $70\text{ }^\circ\text{C}$ for 3 h and allowed to cool to $30\text{ }^\circ\text{C}$. The reaction mixture was quenched by addition of 2 mL of dry MeOH. The solvent was evaporated and the residue suspended in 4 mL of deionized water after which the mixture was extracted with EtOAc (2×3 mL) and the EtOAc layers were back-extracted with water (3 mL). The combined aqueous layers were lyophilized to generate crude product (~ 31.5 mg). LC-MS purification was performed using analytical HPLC (column A) to optimize the conditions for separation, after which preparative HPLC (column B) was used to purify the compound. Product was collected with $R_t=10.5$ min, which was checked by MS. The presence of product was confirmed by ^{31}P and ^1H NMR spectroscopy. ^1H NMR (500 MHz, D_2O) $\delta/\text{ppm} = 8.28$ (s, 1H; NH), 5.89-5.82 (d, $J = 35$ Hz, 1H; $=\text{CH}_{\text{trans}}$), 5.50-5.47 (d, $J = 15.5$ Hz, 1H; $=\text{CH}_{\text{cis}}$), 3.96-3.93 (t, $J = 8$ Hz, 1H; $\text{H}\alpha$ Leu), 1.69-1.53 (m, 3H; $\text{H}\beta/\gamma$ Leu), 0.82-0.79 (m, 6H; $\text{H}\delta$ Leu). ^{31}P NMR (202 MHz, CDCl_3) $\delta/\text{ppm} = 6.44$. Yield: 1.2 mg HRMS (ESI) m/z calculated for $\text{C}_{18}\text{H}_{28}\text{N}_2\text{O}_6\text{P}$ 399.1685, found 399.1686. (*Notebook III, page 39*)

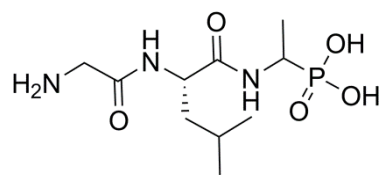


Compound **5.16**. N-Cbz-L-Leu-OH (334 mg, 1.26 mmol) was suspended in 5 mL of dry DCM. To this mixture, 1-ethyl-3-(3-dimethylaminopropyl)carbodiimide hydrochloride (EDC-HCl; 240 mg, 1.25 mmol) was added, followed by addition of dimethyl-1-aminoethyl phosphonate (194 mg, 1.02 mmol) and DIPEA (0.6 mL, 3.57 mmol); the solution was stirred at room temperature for 18 h. The reaction mixture was diluted with DCM (20 mL) and washed with 10% citric acid (10 mL), followed by sat. aqueous NaHCO_3 (10 mL), and brine (10 mL). The organic layer was

dried with Na₂SO₄, filtered, and concentrated under reduced pressure. The crude product was purified by silica gel flash chromatography and the product eluted with 3% EtOAc in hexanes (280 mg, 69%). ¹H NMR (500 MHz, CDCl₃) δ/ppm = 7.34-7.27 (m, 5H; arom), 5.10-5.05 (m, 2H, CH₂-Bn), 4.55-4.45 (m, 1H), 4.32-4.26 (m, 1H), 3.73-3.65 (m, 6H; OCH₃), 1.7-1.45 (m, 3H; Hβ/γ Leu), 1.35-1.22 (m, 3H; CH₃), 0.94-0.86 (m, 6H; Hδ Leu). ³¹P NMR (202 MHz, CDCl₃) (δ = 28.95, 28.72); product present as two diastereomers. MS (ESI): m/z = 401.4 (M+H⁺). TLC: R_f = 0.48 (10% MeOH in DCM). (*Notebook IV, page 74*)

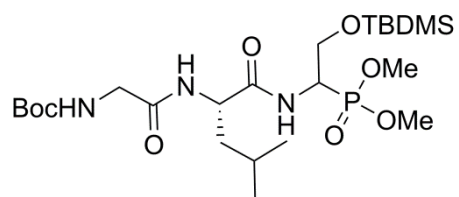


Compound **5.3**. Compound **5.16** (283 mg, 0.71 mmol) was dissolved in 9 mL of toluene and the flask was cooled in an ice-bath. To this solution, 2.1 mL of a 1 M solution of BBr₃ in hexanes (2.1 mmol) was added and the reaction was stirred for 10 min at 0 °C resulting in a yellow precipitate. The flask was placed in an oil bath maintained at 70 °C for 4.5 h. The reaction mixture was cooled and 10 mL of dry MeOH was added to quench the reaction. A clear greenish-black solution formed, which was concentrated on a rotary evaporator to remove all solvents, the residue was redissolved in 5 mL of EtOAc and extracted with H₂O (5 mL). The aqueous layer was collected in a vial and lyophilized. Crude yield: 189 mg. ¹H NMR (500 MHz, CDCl₃) δ/ppm = 4.10-3.90 (dq, *J* = 10 Hz; Hα Ala^P), 3.85-3.80 (dd, *J* = 10 Hz; Hα Leu), 1.65-1.50 (m, 3H; Hβ/γ), 1.22-1.12 (m, 3H; CH₃), 0.85-0.76 (t, 6H; Hδ Leu). ³¹P NMR (202 MHz δ = 23.45, 22.81) indicated the presence of the product as two diastereomers. HRMS (ESI) m/z calculated for C₈H₁₉N₂O₄P 239.1161, found 239.1158. The crude product (189.6 mg) was purified by RP-HPLC (column B) to yield 20 mg of each diastereomers. (*Notebook IV, page 77*)



Compound **5.4**. Gly-L-Leu-Ala(P) was synthesized from Boc-Gly-L-Leu-Ala(P) methyl ester using similar chemistry as reported previously (32). ^1H NMR (500 MHz, CDCl_3) $\delta/\text{ppm} =$

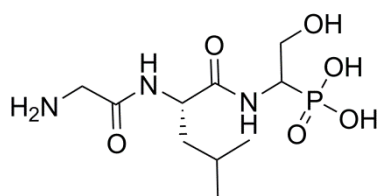
4.20-4.17 (t, $J = 5$ Hz, 1H; $\text{H}\alpha$ Leu), 4.08-4.00(m, 1H; $\text{H}\alpha$ Ala^P), 3.70-3.65 (s, 2H; $\text{H}\alpha$ Gly), 1.54-1.37 (m, 3H; $\text{H}\beta/\gamma$ Leu), 1.20-1.12 (m, 3H; $\text{H}\beta$ Ala), 0.77-0.67 (dd, $J = 5$ Hz, 6H; $\text{H}\delta$ Leu). ^{31}P NMR (202 MHz $\delta/\text{ppm} = 23.45, 22.81$) indicated the presence of product as two diastereomers. MS (ESI): $m/z = 237.1$ ($\text{M}-\text{H}^+$). The 33 mg of crude product was purified by RP HPLC (column B) to give 4 mg and 2.4 mg of the two diastereomers. (*Notebook IV, pages 21, 27*)



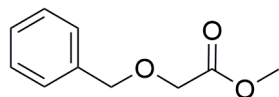
Compound **5.17**. This compound was synthesized by peptide coupling of Boc-Gly-L-Leu-OH (32) with a Ser(P) analog obtained after deprotection of the N-terminal Cbz

group of compound **5.10**. Boc-Gly-L-Leu-OH (242 mg, 0.84 mmol) was dissolved in 3 mL of dry DCM, to which dimethyl (1-amino-2-((tert-butyldimethylsilyl)oxy)ethyl)phosphonate (198.3 mg, 0.7 mmol) and N-methylmorpholine (0.12 mL, 1.09 mmol) were added. To this suspension, 1-ethyl-3-(3-dimethylaminopropyl)carbodiimide hydrochloride (EDC-HCl, 201.2 mg, 1.05 mmol) was added and the reaction was stirred for 8 h 45 min. The reaction mixture was then diluted with DCM and extracted with 10% citric acid (10 mL), sat. aqueous NaHCO_3 (20 mL), and brine (20 mL). The organic layer was dried over sodium sulfate, filtered, and concentrated. The residue was purified by silica gel flash chromatography eluting with 3% MeOH in DCM. (165 mg, 0.3 mmol, 42%). ^1H NMR (500 MHz, CDCl_3) $\delta/\text{ppm} = 6.49$ -6.45 (t, $J = 10$ Hz, 1H), 4.75-4.45 (m, 1H), 4.03-3.96 (m, 1H), 3.82-3.74 (m, 6H; OCH_3), 1.70-1.52 (m, 4H), 1.45 (s; 9H,

C(CH₃)₃ Boc), 1.02-0.96 (m, 1H), 0.96-0.91 (t, 6H, H δ Leu), 0.91-0.89 (d, 9H; SiC(CH₃)₃), 0.08 (t, 6H; Si(CH₃)₃). ³¹P NMR (202 MHz, CDCl₃) δ /ppm = 26.41, 26.27 indicated product as two diastereomers. MS(ESI) m/z: 554.2 (M+H⁺). TLC: R_f = 0.3 (10% EtOAc). (*Notebook IV, page 23*)

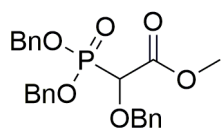


Compound **5.5**. Compound **5.17** (54.3 mg, 0.098 mmol) was dissolved in 1.5 mL of toluene and the flask was cooled in an ice bath. To this solution, 1 M BBr₃ in hexanes (0.3 mL, 3.06 equiv) was added and the reaction was stirred on an ice bath for 10 min. Then the flask was transferred to an oil bath pre-heated to 70 °C and the reaction was stirred for another 4 h. After cooling the reaction mixture to room temperature, 2 mL of dry MeOH was added to quench the reaction. The resulting clear solution was concentrated on a rotary evaporator after which the residue was taken up in EtOAc (5 mL) and extracted with water (5 mL). The aqueous layer was lyophilized (crude yield: 45.2 mg). The crude material was purified by RP-HPLC (column B) to yield two diastereomers (1.6 mg and 1.5 mg). ¹H NMR (500 MHz, CDCl₃) δ /ppm = 4.32-4.28 (m, 1H; H α Leu), 4.10-4.04 (m, 1H; H α Ser^P), 3.81-3.75 (m, 1H), 3.76-3.72 (d, 2H, H α Gly), 3.60-3.52 (m, 1H), 1.62-1.46(m, 3H, H β / γ Leu), 0.80-0.75 (dd, *J* = 5 Hz, 6H, H δ Leu). Both diastereomers had a similar ¹H NMR pattern. ³¹P NMR (202 MHz δ = 14.4, 14.7). HRMS (ESI) m/z calculated for C₁₀H₂₂N₃O₆P 312.1324, found 312.1322. (*Notebook IV, page 29*)



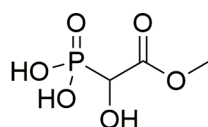
Compound **5.18**. Thionyl chloride (1.64 mL, 22.6 mmol) was added dropwise to 10 mL of dry MeOH in a round bottom flask placed in an ice bath and the reaction was stirred for 5 min. To the reaction mixture, a solution of benzyloxyacetic acid (3.13 g, 18.8 mmol) in 10 mL of dry MeOH was cannula transferred over a

period of 15 min. The reaction was allowed to warm to room temperature and was stirred under N₂ for 22 h. The reaction mixture was concentrated on a rotary evaporator and dissolved in 30 mL of dichloromethane (DCM). The solution was then extracted with 2 × 30 mL of saturated NaHCO₃ solution and 1 × 20 mL of brine. The organic layer was dried over Na₂SO₄ and concentrated on a rotary evaporator. The residue was purified by flash chromatography (SiO₂) using 100% DCM as eluent to generate product **5.18** as a colorless oil. TLC: R_f 0.61 (100% DCM). Yield: 3.1 g (91%). ¹H and ¹³C NMR data matched the reported spectra (36). (*Notebook III, page 90*)



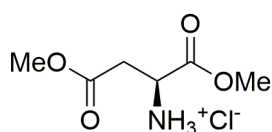
Compound **5.19**. Lithium diisopropyl amide (LDA) was generated in-situ by adding n-BuLi (6.76 mL, 10.8 mmol, 1.3 equiv.) to a solution of dry diisopropyl amine (1.76 mL, 12.5 mmol, 1.5 equiv.) in 5 mL of dry THF at -78 °C. After stirring at -78 °C for 10 min, the solution was stirred for another 10 min in an ice bath and cooled back to -78 °C. To the generated LDA, a solution of methyl benzyloxyacetate **5.18** (1.49 g, 8.3 mmol) in 5 mL of dry THF was cannula-transferred over 10 min. The reaction was stirred at -78 °C for 10 min. This reaction mixture was cannula-transferred to a solution of phosphorus oxychloride (0.78 mL, 8.3 mmol, 1 equiv.) in 5 mL of dry THF at -78 °C over a period of 15 min and allowed to stir at -78 °C for 12 h. Then, a mixture of benzyl alcohol (1.72 mL, 16.6 mmol, 2 equiv.) and pyridine (1.34 mL, 16.6 mmol, 2 equiv.) was added to the reaction mixture, which was allowed to warm to room temperature overnight while stirring. The reaction was quenched by the addition of 5 mL of water after which the reaction mixture was immediately diluted with 60 mL of ethyl acetate and washed with 20 mL of brine. The organic layer was dried over Na₂SO₄ and concentrated. The residue was purified by flash chromatography (SiO₂) using a gradient from 20% to 50% EtOAc in hexanes. This procedure had to be used three times as a result of very

closely eluting impurities to generate product **5.19**. TLC: R_f 0.38 (50% EtOAc in hexanes). Yield = 251 mg (7%). ^1H NMR (600 MHz, CDCl_3) δ /ppm = 7.31-7.28 (m, 15H), 5.1 (d, $J = 10$ Hz, 4H), 4.79-4.77 (d, $J = 10$ Hz, 1H), 4.56-4.54 (d, $J = 10$ Hz, 1H), 4.45-4.41 (d, $J = 20$ Hz, 1H), 3.73 (s, 3H). ^{13}C NMR (150 MHz, CDCl_3) δ /ppm=167.6, 136.0, 135.8, 128.0-128.6, 75.3 (d, $J=158.5$ Hz), 74.2 (d, $J=12.1$ Hz), 68.9 (d, $J=10.6$ Hz), 52.7. ^{31}P NMR (202 MHz, CDCl_3) δ /ppm = 15.96 (product). HRMS (ESI) m/z calculated for $\text{C}_{24}\text{H}_{26}\text{O}_6\text{P}$ 441.1467 ($\text{M}+\text{H}^+$), observed 441.1452. ^{31}P NMR analysis demonstrated the formation of product ($\delta = 15.9$ ppm) along with a side product ($\delta = 1.36$ ppm), which eluted with the same R_f value. The side product was identified as $\text{PO}(\text{OBn})_2\text{OMe}$ by NMR and MS analysis. (*Notebook III, pages 92, 93*)



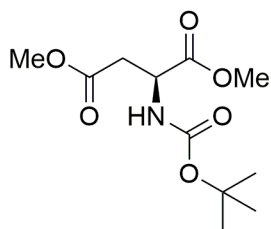
Compound **5.7**. Methyl 2-(benzyloxy)-2-(bis(benzyloxy)phosphoryl)acetate

5.19 (126.4 mg) was dissolved in 5 mL of dry MeOH in a 50 mL round bottomed flask and 10% Pd/C (54 mg) was added. The heterogeneous mixture was sparged with H_2 (1 atmosphere) for 20 min, and allowed to stir for 20 h. The reaction mixture was filtered over Celite and concentrated. ESI MS indicated mainly the presence of mono-benzyl protected product. The product from this reaction was dissolved in 5 mL of dry THF and an additional 25 mg of 5% Pd/C was added, the vessel was kept under 1 atmosphere of H_2 and stirred for 23 h. The reaction mixture was filtered over Celite. The mixture was purified by size-exclusion chromatography Sephadex LH-20 to yield the desired product **5.7** as a white power (3 mg, 6% yield). ^1H and ^{13}C NMR data matched the reported spectra as obtained from acidic hydrolysis of fosfazinomycin (37). (*Notebook III, page 95*)

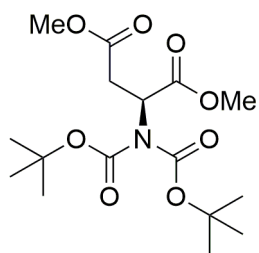


Compound **5.20**. To a stirred suspension of L-aspartic acid (2.66 g, 20 mmol) in 15 mL of dry MeOH kept chilled in an ice bath, SOCl_2 (2

mL) was added dropwise. L-Aspartic acid dissolved and the solution turned yellow. The reaction mixture was left to stir for 49 h and 10 min. Then, the reaction was concentrated under reduced pressure and a yellow oil formed. The concentrated oil was triturated with cold ether when a yellowish solid forms. The solid was transferred to a Buchner filter and repeatedly washed with cold ether to yield a white solid, which was dried overnight with a vacuum pump. Yield = 3.8 g (96%). $^1\text{H NMR}$ (400 MHz, CDCl_3) δ 8.83 (s, 2H), 4.58 (m, 1H), 3.84 (s, 3H), 3.75 (s, 3H), 3.33-3.26 (m, 2H). (*Notebook I, page 89*)

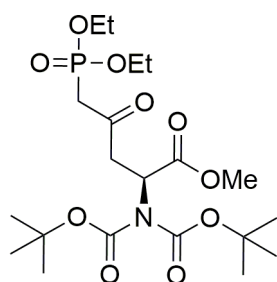


Compound **5.21**. Compound **5.20** (1.99 g, 10 mmol) was suspended in 16 mL of dry THF at room temperature. To the solution, Et_3N (1.54 mL of, 11 mmol) was added followed by addition of Boc anhydride (2.42 g, 11 mmol). The solution was stirred under N_2 for 4 h. TLC indicated the disappearance of starting material. Product appeared as a pink white creamy mass. It was evaporated in-vacuo in a rotary evaporator to give a dense pink-white residue. The residue was dissolved in 12 mL of EtOAc. The solution was washed with 12 mL of H_2O in a separatory funnel. The organic layer was dried over Na_2SO_4 and concentrated in-vacuo to yield a dry solid, which on drying with a vacuum pump overnight gave a pink-white solid. Yield = 2.56 g (84%). $^1\text{H NMR}$ (400 MHz, CDCl_3) δ = 5.5 (d, 1H), 4.58(m, 1H), 3.76(s, 3H), 3.64 (s, 3H), 3 (dd, 1H), 2.8 (dd, 1H), 1.42 (s, 9H). (*Notebook I, page 90*)

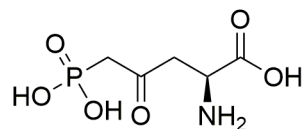


Compound **5.22**. Compound **5.21** (1.57 g, 6.03 mmol) was dissolved in 20 mL of CH_3CN . To the solution, DMAP (0.16 g, 1.29 mmol, 0.21 equ) was added, followed by Boc_2O (2.42 g, 11.1 mmol, 1.84 equiv). The clear yellow solution was allowed to stir at room temperature in N_2 for 22 h after

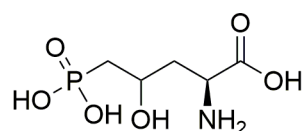
which the solution became reddish brown, which was concentrated to give a dry red solid. Crude weight: 2.19 g. The residue was purified by flash chromatography (SiO₂) to yield 1.9 g (87%) of product. R_f = 0.48 in 30 % EtOAc in hexanes. ¹H NMR (500 MHz, CDCl₃) δ = 5.42 (t, 1H), 3.76(s, 3H), 3.74 (s, 3H), 3.22 (dd, 1H), 2.78 (dd, 1H), 1.5 (s, 2H). (*Notebook II, page 27*)



Compound **5.23**. Two round bottom flasks were used, in one of which compound **5.22** (0.604 g, 1.67 mmol) was dissolved in 5.0 mL of dry DMF and stirred at -78°C under nitrogen. In the other round bottom flask, 5.0 mL of THF was added and under nitrogen, 1.2 mL of (7.4 mmol, 4.43 equiv.) of diethyl methylphosphonate was added followed by addition of 5.0 mL of 1.6 M BuLi (8 mmol, 4.8 equiv.) in hexane, and the solution was allowed to stir for 20 min. The entire content of the 2nd flask was transferred to the 1st flask by a cannula over a period of 25 min, after which the reaction mixture was allowed to stir for another 1.5 h at -78°C under nitrogen. The reaction was then quenched by adding 0.45 μL (8 mmol, 4.81 mmol) of glacial acetic acid, and the solution was allowed to come to room temperature. Then, the reaction mixture was diluted by adding ethyl acetate (30 mL) after which the solution was washed with brine in a separatory funnel. The organic layer was dried over Na₂SO₄, the solvent was evaporated by a rotary evaporator, and the residue was further dried with a vacuum pump. Crude weight = 1.45 g. The residue was purified by flash chromatography (SiO₂) using 3:2 EtOAc/petroleum ether as the eluent. R_f = 0.25 in 3:2 EtOAc/petroleum ether. Yield = 0.53 g (66 %). ¹H NMR (500 MHz, CDCl₃) δ = 5.5 (dd, 1H), 4.15 (m, 4H), 3.7 (s, 3H), 3.6 (dd, 1H), 3.25 (dd, 1H), 3.1 (dd, 1H), 2.9 (dd, 1H), 1.5 (s, 18H), 1.33 (m, 6H). ³¹P NMR (500 MHz, CDCl₃) δ = 20.57 (s, 1P). (*Notebook II, page 6*).



Compound **5.24**. Compound **5.23** (0.531 g, 1.1 mmol) was transferred to a round bottom flask with a few drops of DCM, 4.0 mL of 5 M HCl was added and the solution was refluxed for 4 h, and cooled to room temperature. The solution was extracted with ethyl acetate (3 x 20 mL). The aqueous layer containing the compound was concentrated. Crude weight = 0.25 g. ³¹P and ¹H NMR of the crude material indicated the presence of product. The product was purified by Dowex 50wx-8 resin twice. After the 2nd ion exchange chromatography, the eluents were collected into four fractions and lyophilized yielding, 8.8 mg, 17 mg, 91 mg, and 16 mg. Overall yield: 133 mg (49%). A ¹H NMR spectrum indicated the presence of product with minor side product containing a monomethyl phosphonate ester. The third fraction was carried forward for the next reaction. ¹H NMR (500 MHz, D₂O) δ 4.19-4.17 (m, 1H), 3.39-3.24 (m, 2H), 3.13-2.98 (m, 2H). ³¹P NMR (500 MHz, D₂O) δ 17.72. (*Notebook II, page 9*)



Compound **5.8**. Compound **5.24** (30 mg, 0.14 mmol) was transferred to a 10 mL round bottom flask and dissolved in 0.8 mL of milipore water, the solution was cooled to 0 °C, to which NaBH₄ was added. The solution was stirred in an ice-bath for 2 h, and quenched by adding a few drops of 1 M HCl and lyophilized. ¹H and ³¹P NMR spectra and ESI MS indicated the presence of product along with other minor impurities like mono-ethyl protected phosphonate. The product was purified by eluting thorough Dowex ion-exchange chromatography. Yield = 27.9 mg. ³¹P NMR (500 MHz, D₂O) δ 22.5. (*Notebook II, page 31*)

5.5. REFERENCES

1. Bougioukou, D. J., Mukherjee, S., and van der Donk, W. A. (2013) Revisiting the biosynthesis of dehydrophos reveals a tRNA-dependent pathway, *Proc. Natl. Acad. Sci. U.S.A.* *110*, 10952-10957.
2. Gao, J., Ju, K.-S., Yu, X., Velásquez, J. E., Mukherjee, S., Lee, J., Zhao, C., Evans, B. S., Doroghazi, J. R., Metcalf, W. W., and van der Donk, W. A. (2014) Use of a Phosphonate Methyltransferase in the Identification of the Fosfazinomycin Biosynthetic Gene Cluster, *Angew. Chem. Int. Ed.* *53*, 1334-1337.
3. Horiguchi, M. (1984) Occurrence, identification and properties of phosphonic and phosphinic acids, In *Biochemistry of Natural C-P Compounds* (Hori, T., Horiguchi, M., and Hayashi, A., Eds.), pp 24-52, Shiga, Jpn: Jpn. Assoc. Res. Biochem. C-P Compd.
4. Metcalf, W. W., and van der Donk, W. A. (2009) Biosynthesis of Phosphonic and Phosphinic Acid Natural Products, *Annu. Rev. Biochem.* *78*, 65-94.
5. Wanke, C., and Amrhein, N. (1993) Evidence that the reaction of the UDP-N-acetylglucosamine 1-carboxyvinyltransferase proceeds through the O-phosphothioacetal of pyruvic acid bound to Cys115 of the enzyme, *Eur. J. Biochem.* *218*, 861-870.
6. Peck, S. C., Gao, J., and van der Donk, W. A. (2012) Discovery and Biosynthesis of Phosphonate and Phosphinate Natural Products, In *Methods Enzymol.* (Hopwood, D. A., Ed.), pp 101-123, Academic Press.
7. Steinrücken, H. C., and Amrhein, N. (1980) The herbicide glyphosate is a potent inhibitor of 5-enolpyruvylshikimic acid-3-phosphate synthase, *Biochem. Biophys. Res. Commun.* *94*, 1207-1212.
8. Papapoulos, S. E. (1993) The role of bisphosphonates in the prevention and treatment of osteoporosis, *Am. J. Med.* *95*, S48-S52.
9. De Clercq, E., and Holy, A. (2005) Acyclic nucleoside phosphonates: a key class of antiviral drugs, *Nat. Rev. Drug Discov.* *4*, 928-940.
10. Snoeck, R., Sakuma, T., De Clercq, E., Rosenberg, I., and Holy, A. (1988) (S)-1-(3-hydroxy-2-phosphonylmethoxypropyl)cytosine, a potent and selective inhibitor of human cytomegalovirus replication, *Antimicrob. Agents Chemother.* *32*, 1839-1844.
11. Stein, G. E. (1998) Single-Dose Treatment of Acute Cystitis with Fosfomycin Tromethamine, *Ann. Pharmacother.* *32*, 215-219.
12. Leadbetter, M. R., Adams, S. M., Bazzini, B., Fatheree, P. R., Karr, D. E., Krause, K. M., Lam, B. M., Linsell, M. S., Nodwell, M. B., Pace, J. L., Quast, K., Shaw, J. P., Soriano, E., Trapp, S. G., Villena, J. D., Wu, T. X., Christensen, B. G., and Judice, J. K. (2004) Hydrophobic vancomycin derivatives with improved ADME properties: discovery of telavancin (TD-6424), *J. Antibiot. (Tokyo)*. *57*, 326-336.
13. Bowman, E., McQueney, M., Barry, R. J., and Dunaway-Mariano, D. (1988) Catalysis and thermodynamics of the phosphoenolpyruvate/phosphonopyruvate rearrangement. Entry into the phosphonate class of naturally occurring organophosphorus compounds, *J. Am. Chem. Soc.* *110*, 5575-5576.
14. Hidaka, T., Imai, S., and Seto, H. (1989) Biosynthesis mechanism of carbon-phosphorus bond formation. Isolation of carboxyphosphoenolpyruvate and its conversion to phosphinopyruvate, *J. Am. Chem. Soc.* *111*, 8012-8013.

15. Seidel, H. M., Freeman, S., Seto, H., and Knowles, J. R. (1988) Phosphonate biosynthesis: isolation of the enzyme responsible for the formation of a carbon-phosphorus bond, *Nature* 335, 457-458.
16. Barry, R. J., Bowman, E., McQueney, M., and Dunaway-Mariano, D. (1988) Elucidation of the 2-aminoethylphosphonate biosynthetic pathway in *Tetrahymena pyriformis*, *Biochem. Biophys. Res. Commun.* 153, 177-182.
17. Zhang, G., Dai, J., Lu, Z., and Dunaway-Mariano, D. (2003) The Phosphonopyruvate Decarboxylase from *Bacteroides fragilis*, *J. Biol. Chem.* 278, 41302-41308.
18. Circello, B. T., Eliot, A. C., Lee, J.-H., van der Donk, W. A., and Metcalf, W. W. (2010) Molecular Cloning and Heterologous Expression of the Dehydrophos Biosynthetic Gene Cluster, *Chem. Biol.* 17, 402-411.
19. Hidaka, T., Goda, M., Kuzuyama, T., Takei, N., Hidaka, M., and Seto, H. (1995) Cloning and nucleotide sequence of fosfomycin biosynthetic genes of *Streptomyces wedmorensis*, *Molec. Gen. Genet.* 249, 274-280.
20. Seto, H., and Kuzuyama, T. (1999) Bioactive natural products with carbon-phosphorus bonds and their biosynthesis, *Nat. Prod. Rep.* 16, 589-596.
21. Metcalf, W. W., Griffin, B. M., Cicchillo, R. M., Gao, J., Janga, S. C., Cooke, H. A., Circello, B. T., Evans, B. S., Martens-Habbena, W., Stahl, D. A., and van der Donk, W. A. (2012) Synthesis of Methylphosphonic Acid by Marine Microbes: A Source for Methane in the Aerobic Ocean, *Science* 337, 1104-1107.
22. Hilderbrand, R. L. (1983) *The Role of phosphonates in living systems*, CRC Press, Boca Raton, Fl.
23. Borisova, S. A., Circello, B. T., Zhang, J. K., van der Donk, W. A., and Metcalf, W. W. (2010) Biosynthesis of Rhizocitcins, Antifungal Phosphonate Oligopeptides Produced by *Bacillus subtilis* ATCC6633, *Chem. Biol.* 17, 28-37.
24. Eliot, A. C., Griffin, B. M., Thomas, P. M., Johannes, T. W., Kelleher, N. L., Zhao, H., and Metcalf, W. W. (2008) Cloning, Expression, and Biochemical Characterization of *Streptomyces rubellomurinus* Genes Required for Biosynthesis of Antimalarial Compound FR900098, *Chem. Biol.* 15, 765-770.
25. Ntai, I., Manier, M. L., Hachey, D. L., and Bachmann, B. O. (2005) Biosynthetic Origins of C-P Bond Containing Tripeptide K-26, *Org. Lett.* 7, 2763-2765.
26. Hunt, A. H., and Elzey, T. K. (1988) Revised Structure of A53868A, *J. Antibiot.* 41, 802.
27. Whitteck, J. T., Ni, W., Griffin, B. M., Eliot, A. C., Thomas, P. M., Kelleher, N. L., Metcalf, W. W., and van der Donk, W. A. (2007) Reassignment of the structure of the antibiotic A53868 reveals an unusual amino dehydrophosphonic acid, *Angew. Chem. Int. Ed. Engl.* 46, 9089-9092.
28. Kuemin, M., and van der Donk, W. A. (2010) Structure-activity relationships of the phosphonate antibiotic dehydrophos, *Chem. Commun.* 46, 7694-7696.
29. Circello, B. T., Miller, C. G., Lee, J.-H., van der Donk, W. A., and Metcalf, W. W. (2011) The Antibiotic Dehydrophos Is Converted to a Toxic Pyruvate Analog by Peptide Bond Cleavage in *Salmonella enterica*, *Antimicrob. Agents Chemother.* 55, 3357-3362.
30. O'Brien, T. A., Kluger, R., Pike, D. C., and Gennis, R. B. (1980) Phosphonate analogues of pyruvate. Probes of substrate binding to pyruvate oxidase and other thiamin pyrophosphate-dependent decarboxylases, *Biochim. Biophys. Acta* 613, 10-17.

31. Smith, J. M., Vierling, R. J., and Meyers, C. F. (2012) Selective inhibition of E. coli 1-deoxy-d-xylulose-5-phosphate synthase by acetylphosphonates, *Med. Chem. Commun.* 3, 65-67.
32. Lee, J.-H., Bae, B., Kuemin, M., Circello, B. T., Metcalf, W. W., Nair, S. K., and van der Donk, W. A. (2010) Characterization and structure of DhpI, a phosphonate O-methyltransferase involved in dehydrophos biosynthesis, *Proc. Natl. Acad. Sci. U.S.A.* 107, 17557-17562.
33. Rapp, C., Jung, G., Kugler, M., and Loeffler, W. (1988) Rhizocticins — New phosphono-oligopeptides with antifungal activity, *Liebigs Ann. Chem.*, 655-661.
34. Cox, R. J., Gibson, J. S., Bele, M., and Martín, M. (2002) Aspartyl Phosphonates and Phosphoramidates: The First Synthetic Inhibitors of Bacterial Aspartate-Semialdehyde Dehydrogenase, *ChemBioChem* 3, 874-886.
35. Mortier, J., Gridnev, I. D., and Guénot, P. (2000) Reactions of Phosphonates with Organohaloboranes: New Route to Molecular Borophosphonates, *Organometallics* 19, 4266-4275.
36. Desage-El Murr, M., Nowaczyk, S., Le Gall, T., and Mioskowski, C. (2006) Synthesis of Pulvinic Acid and Norbadione A Analogues by Suzuki–Miyaura Cross-Coupling of Benzylated Intermediates, *Eur. J. Org. Chem.* 2006, 1489-1498.
37. Ogita, T., Gunji, S., Fukazawa, Y., Terahara, A., Kinoshita, T., Nagaki, H., and Beppu, T. (1983) The structures of fosfazinomycins A and B, *Tetrahedron Lett.* 24, 2283-2286.